University of Sussex

Predictions in Multifield Inflation

Jonathan Frazer

Submitted for the degree of Doctor of Philosophy

University of Sussex

20th of March 2013

Declaration

I hereby declare that this thesis has not been and will not be submitted in whole or in part to another University for the award of any other degree.

Signature:

Jonathan Frazer

UNIVERSITY OF SUSSEX

Jonathan Frazer, Doctor of Philosophy

Predictions in multifield inflation

Abstract

Models of inflation with more than one active field are an important class where it is not fully understood how to compute predictions. This problem can be understood in terms of two characteristics of these models: the sensitivity to initial conditions and the superhorizon evolution of the primordial density perturbation ζ. This thesis seeks to make significant progress in understanding how to overcome these two issues.

To track the superhorizon evolution of ζ in general requires numerical techniques. By extending the transport method first proposed by Mulryne, Seery and Wesley, here, a computationally efficient and highly versatile method for computing the statistics of ζ is developed. The increased efficiency and versatility allows models that were previously unaccessible to be studied.

Utilising this new capability two models are explored. A new toy model of inflation in the Landscape and a 6-field D-brane model of inflation first proposed by Agarwal, Bean, McAllister, and Xu. The nature of these models allows for a statistical analysis of inflationary realisations to be performed. We conclude that the fundamental ability to constrain models of this kind is determined by the scale of features in the potential. We also show the D-brane model is under considerable pressure from current observations of the spectral index and may be ruled out by future observations.

Finally, I show that there exists a class of models for which the probability distribution of observables may be computed analytically. I show the peak of the density function is largely dominated by the geometry of the potential and comparatively insensitive to the distribution of initial conditions. I argue that this characteristic should be expected in a broader range of models and for such models, it is possible to make robust predictions.

Acknowledgements

I feel deeply honoured to have been given the opportunity to do research. I love my work and my life in general and I have many people to thank for this privilege.

I am hugely grateful for the guidance provided by my supervisor Andrew Liddle over the course of my Ph.D. He has been everything I ever hoped for in a supervisor. His ability to see the bigger picture and his approach to problems is a wonderful thing to behold.

I owe enormous thanks to David Seery. David showed me a very different side to research which I had not encountered before, yet now I find it hard to imagine how I would have progressed without it. His kindness, support and patience has been of central importance in developing my technical ability. Being given the opportunity to see the way he does calculations and his approach to projects is something I value immensely.

The ability to encourage and inspire others is a quality I hold with the highest regard. I think every encounter with both David and Andrew has left me feeling more able and more enthusiastic to work. There are many many others I would also like to thank for affecting me in a similar way. I would like to thank all my colleagues and collaborators and in particular, Gemma Anderson, Albert Asawaroengchai, Chris Byrnes, Joe Elliston, Kevin Falls, Antony Lewis, Edouard Marchais, David Mulryne, Donough Regan and Phil Rooney for many enjoyable discussions, their help, support and friendship. I would also like to thank a number of people, many of which I have not (yet) met but am nevertheless exceedingly grateful for their exciting papers, brilliant talks and their presence in the physics community. A few names I would particularly like to single out are Nima Arkani-Hamed, Neil Barnaby, Frank Berkshire, Cliff Burgess, Georgi Dvali, Richard Easther, Stephen Hawking, Tom Kibble, David Lyth, Joao Magueijo, Juan Maldacena, Liam McAllister, Hiranya Peiris, Leonard Susskind, Max Tegmark, Henry Tye, David Wands and Steven Weinberg.

I am quite sure that my love of physics and my attitude to research has significant routes in my education. I was exceedingly lucky to have Miguel Cruz as my physics teacher and Liam Bauress teaching me mathematics. I would like to thank Miguel for giving little care

to the syllabus and instead encouraging discussion and curiosity through experiment. It was thanks to Liam that I first found joy in mathematics. His deep love of mathematics and physics was infectious to the point that I don't think it is an understatement to say he changed the course of my life.

I want to acknowledge Mafalda Dias. It is hard to express the impact she has on my life. That which means most to me I have her to thank for. Her presence brings colour, warmth and peace. She is my source of creativity and love.

Finally I would like to thank my parents John and Julia Frazer. For our home, for every opportunity you have ever given me, for your endless support, understanding and love. For showing me what it means to create something and for showing me how to pursue the things I love, I dedicate this thesis to you.

Contents

Introduction

0.1 Prelude

Observations of the Cosmic Microwave Background (CMB) have provided significant evidence in favour of an inflationary phase taking place in the very early stages of the Universe. As well as providing an elegant solution to a number of important problems with the standard model of cosmology, inflation also predicts the existence of small temperature fluctuations in the CMB which have now been observed and shown to be in striking agreement. As such, inflation has emerged as the leading candidate to describe the early stages of the universe and the origin of structure.

With a number of high precision observational projects underway and more planned for the future, it is clear we live in an exciting time. More than refining the standard model of cosmology, by constraining our description of the early universe when it was both hot and dense, we are constraining particle physics at energies that will never be achieved by terrestrial experiments.

At present, the best means of constraining models of inflation is via the statistics of the primordial curvature perturbation ζ. It is therefore essential that we understand how to compute these statistics to a high precision for any model we wish to confront with observation. For the simplest models of inflation, where inflation is driven by a single scalar field with canonical kinetic terms, the method for computing ζ is well understood and so models of this kind are straightforward to constrain. However as our understanding of particle physics has evolved, so have models of inflation and it is no longer clear that the simplest models are the ones best motivated from the perspective of fundamental physics. A broad class of models well motivated by our current knowledge of string theory, is the class where inflation is driven by more than one scalar field. In these models the inflationary dynamics can be much richer than in models with just a single field and hence computing the prediction for ζ is considerably more complex. The subject of this thesis is to address

this issue.

In order to compute the prediction for ζ in multifield models of inflation, broadly speaking, two challenges must be overcome.

The first challenge is that unlike a single field model of inflation where there is only one possible inflationary trajectory, a given multifield model permits an infinite number of inflationary trajectories. In principle, each inflationary trajectory gives rise to a different outcome for ζ and hence the prediction of the model is not a set of single values for observable quantities such as the power spectrum, spectral index, running, etc. but a multivariate probability distribution. The ability to constrain a multifield model is therefore not just limited by the accuracy of observations but also by the model itself. It is of critical importance we learn how to handle this characteristic.

This challenge is made substantially more problematic when considering inflation in the context of the Multiverse. The Multiverse picture of string theory predicts a landscape potential for the effective theory of inflation, consisting of many, possibly hundreds, of scalar fields and a very large number of metastable vacua.

The second challenge is perhaps less formidable than the first but nevertheless crucial if multifield models of inflation are to be confronted with observation. In a single field model of inflation ζ is conserved on superhorizon scales but this is not the case for multifield models. In a multifield model ζ can continue to evolve throughout the duration of inflation and in some cases even through reheating. It is therefore essential to find a method of tracking this evolution.

The superhorizon evolution of ζ is the result of the richer inflationary dynamics made possible by the presence of more than one active field. A natural question to ask is if this will give rise to some kind of signature – some observable characteristic not possible to generate in a single field model of inflation. The search for inflationary signatures is central to the idea of constraining models. The most famous signature of multifield inflation is the possible creation of a non-Gaussian ζ distribution of the local type. This type of deviation from Gaussianity is parameterised by the amplitude $f_{\rm NL}$, which if observed to be non-zero, rules out all the simplest models of inflation.

This thesis seeks to address these issues and does so in the following way: In collaboration with Andrew Liddle, the first two papers study a toy model of inflation in the landscape. Using standard cosmological perturbation theory, the first paper tracks the evolution of quantities relating to the two-point function of ζ for an ensemble of inflationary realisations. This paper introduces the model and performs a first attempt at analysing

the range of inflationary behaviour capable within the model and its consequences for observable quantities.

The second paper performs a considerably more thorough analysis. By abandoning the use of standard perturbation theory in favour of the transport method, the significant increase in computational efficiency enables a much larger ensemble to be studied and for a broad range of model parameters. We also extend the analysis to include the evolution of $f_{\rm NL}$.

The aim of these papers is two-fold. By studying the superhorizon evolution of ζ for a large number of trajectories we can gain some insight on the relation between inflationary dynamics and evolution of the ζ statistics. The second objective is to study how features of the potential affect the distribution of observables quantities, i.e what characteristics of the potential affect the ability to constrain the model.

The third paper came from a collaboration with David Seery, David Mulryne and Raquel Ribeiro and is about the transport method. As can be seen in the second paper, the transport method was initially proposed as a computationally efficient method for computing the superhorizon evolution of ζ but was only applicable to models satisfying the slow-roll conditions. In this paper we substantially extend the method's capability as well as making clear its relation to other methods in the literature. We also explain the equivalence of the separate universe assumption to geometrical optics in field space and hence provide a set of intuitive tools for understanding superhorizon evolution. Some of these tools were already made use of in the second paper.

The fourth paper is the result of a collaboration with Andrew Liddle and Mafalda Dias. We study a 6-field model of D-brane inflation, where contributions from the bulk are modelled by spherical harmonics with random coefficients. The approach taken in this paper is similar to that of the first two but this time the model is much more sophisticated. By performing this analysis we were able to compute the distribution for the spectral index and show that it was in mild tension with results from WMAP 7 and that it may be possible to rule out the model with future data.

In the final paper of this thesis I return to the problem of computing the distribution of observables but I take a very different approach to that taken in the other papers. The other models under investigation in this work are constructed with some contributions to the potential receiving random coefficients. The key question to address with such models is how these random coefficients give rise to different inflationary realisations and hence what is the range of values of observables generated by the model. For simpler models

containing a single minimum one can do somewhat better. In such models the main issue is the sensitivity to initial conditions. In the final paper of this thesis I show that for a particular class of models of this kind it is possible to compute the probability distribution for observables analytically. I show that the distribution function will in general be highly predictive and that this characteristic should be common to a much broader class of models than those studied in the paper.

0.2 The universe is homogeneous on large scales

Current observations are in striking agreement with the standard model of cosmology but it is straightforward to show that if the expansion history of the universe is dominated by familiar matter alone, then there is a serious issue. This point will be discussed in some detail but do to so, first it is necessary to mention some of the standard assumptions which are required in order to make an account of this expansion history. This section is largely a summary of discussions that can be found in Refs. [1–4] to which the reader is referred for more detailed discussion.

0.2.1 Basic ingredients

The Cosmological Principle states that on large scales the universe is both homogenous and isotropic. If this is true then the universe may be described by a time-ordered sequence of homogeneous and isotropic three-dimensional slices. There are only three types of space that respect these symmetries:

Flat space. This has the Euclidean metric

$$dl^2 = dx^2 = \delta_{ij} dx^i dx^j \tag{1}$$

A sphere embedded in four-dimensional Euclidean space. This has the metric

$$dl^2 = dx^2 + dz^2, \qquad z^2 + x^2 = a^2, \tag{2}$$

where a is the radius of the 3-sphere.

A hyperbolic sphere embedded in four-dimensional Euclidean space. This has the metric

$$dl^2 = dx^2 - dz^2, \qquad z^2 - x^2 = a^2, \tag{3}$$

where a^2 is a positive constant. The induced metrics on the three surfaces of the latter two metrics inherit the symmetries of the four-dimensional line element.

Moving into polar coordinates, under a suitable rescaling of the radial direction these three metrics may be expressed as

$$dl^2 = a^2 \left[d\chi^2 + S(\chi)^2 d\Omega \right], \tag{4}$$

where Ω is the angular coordinates $d\Omega = d\theta^2 + \sin^2\theta d\phi$ and

$$S(\chi) \equiv \begin{cases} \sinh\chi & \text{hyperbolic sphere} \\ \chi & \text{Euclidean space} \\ \sin\chi & \text{sphere} \end{cases}. \tag{5}$$

The space-time metric follows immediately. Simply by including time and making a an arbitrary function of time t, one obtains the Robertson–Walker metric

$$ds^2 = dt^2 + a(t) \left[d\chi^2 + S(\chi)^2 d\Omega \right]. \tag{6}$$

An equation determining the form of $a(t)$ may be obtained from Einstein's equation

$$R_{\mu\nu} = T_{\mu\nu} - \frac{1}{2} g_{\mu\nu} T \tag{7}$$

Where $R_{\mu\nu}$ is the Ricci tensor, $g_{\mu\nu}$ is the metric, $T_{\mu\nu}$ is the stress-energy tensor and T is its trace. By imposing the Robertson–Walker metric and modelling matter and energy by a perfect fluid, one obtains the Friedmann equation

$$3H^2 = \rho, \tag{8}$$

where ρ energy density of the universe and

$$H \equiv \frac{\dot{a}}{a} \tag{9}$$

is the Hubble parameter. To make contact with the known matter constituents one more equation is required. This is the conservation of energy equation $\nabla_\mu T^\mu_0 = 0$, where ∇_μ represents covariant differentiation with respect to space-time coordinates. Taking an equation of state relating the pressure p to the energy density ρ to be of the form

$$p = (\gamma - 1)\rho, \tag{10}$$

where γ is a constant, the conservation of energy equation becomes

$$\frac{\dot{\rho}}{\rho} = -3\gamma H. \tag{11}$$

There are three types of perfect fluid relevant to cosmic history, matter, radiation, and the vacuum. Each has a different value for γ. Any non-relativistic particle is simply referred to as matter and has essentially zero pressure and so $\gamma = 1$. Radiation refers to relativistic particles. The equation of state of any relativistic particle should be indistinguishable from that of photons and hence the equation of state can be obtained from the energy-momentum tensor for electromagnetism. This is traceless due to conformal symmetry and so $\gamma = 4/3$. Finally, Lorentz invariance implies the vacuum energy is proportional to the metric and hence $\gamma = 0$.

With these equations to hand we are now able to discuss the causal structure of the universe and it is here that one encounters what is arguably the most serious problem with the standard model of cosmology.

0.2.2 The horizon problem

Since photons travel along null geodesics $ds^2 = 0$, a particularly simple picture of the problem presents its self if the metric in Eq. (6) is expressed in terms of conformal time

$$\tau = \int \frac{dt}{a(t)}. \tag{12}$$

Under the assumption that the universe is isotropic, without loss of generality we can neglect the angular coordinates and consider only the radial direction. The Robertson–Walker metric written in terms of conformal time then becomes

$$ds^2 = a(\tau)\left[d\tau^2 - d\chi^2\right]. \tag{13}$$

and so light rays form straight lines at 45° in the $\tau - \chi$ plane

$$\chi(\tau) = \pm\tau + \text{const.} \tag{14}$$

We can relate the comoving horizon to the expansion history. First express the comoving horizon as

$$\chi_{\rm h}(\tau) = \Delta\tau = \int_{a_{\rm i}}^{a} (aH)^{-1} d\ln a, \tag{15}$$

where $a_{\rm i} \equiv 0$ is the initial singularity and $(aH)^{-1}$ is the comoving Hubble radius. Then by integrating the conservation of energy equation (11) to get

$$(aH)^{-1} = c\, a^{\frac{3}{2}\gamma - 1}, \tag{16}$$

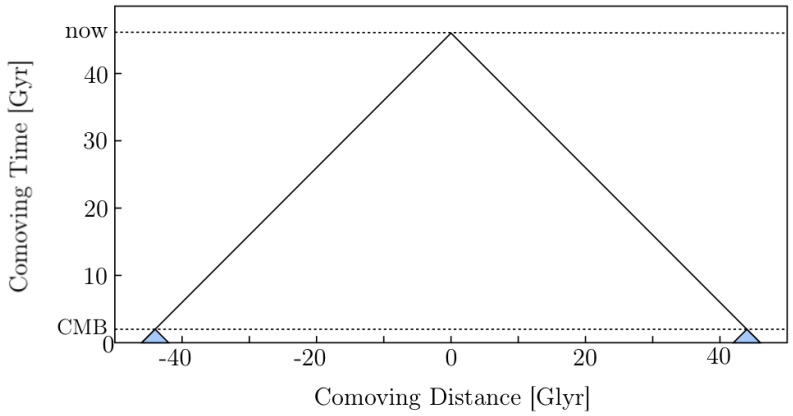

Figure 1: The horizon problem of the standard model of cosmology. There exist regions of the CMB whose past light cones do not overlap and yet are observed to have the same temperature to a high accuracy.

where c is a constant, we can substitute this into Eq. (15) to obtain

$$\chi_{\rm h} = \Delta\tau = \frac{2c}{3\gamma - 2}\left[a^{\frac{3}{2}\gamma-1} - a_i^{\frac{3}{2}\gamma-1}\right]. \tag{17}$$

This is the problem. Both matter and radiation satisfy what is known as the strong energy condition (SEC), $3\gamma - 2 > 0$. If the expansion history is determined by perfect fluids satisfying the SEC alone then the comoving time between now and the initial singularity is finite.

$$\tau_i = \frac{2c}{3\gamma - 2}a_i^{\frac{3}{2}\gamma-1} = 0 \quad \text{if} \quad \gamma > \frac{2}{3}. \tag{18}$$

If this is the case, then how is the homogeneity of the CMB justified? As illustrated in Fig. 1, the finite time between the initial singularity and decoupling means that, as we view the CMB on the sky, two regions separated by more than a certain angle (this angle turns out to be about 2.3°) will be causally disconnected.

To express the problem slightly differently we can rewrite the equation for the particle horizon in terms of the Hubble sphere

$$\chi_{\rm h}(t) = \frac{2c}{3\gamma - 2}(aH)^{-1} \quad \text{if} \quad \gamma > \frac{2}{3}. \tag{19}$$

This equation is particularly helpful as it unites two conceptually different horizons. Two events separated by a distance greater than $\chi_{\rm h}$ can never have communicated with each other, whereas the Hubble radius is the distance over which particles can travel in one expansion time and so, if two events are separated by a distance greater than the Hubble radius, it means they can not communicate now.

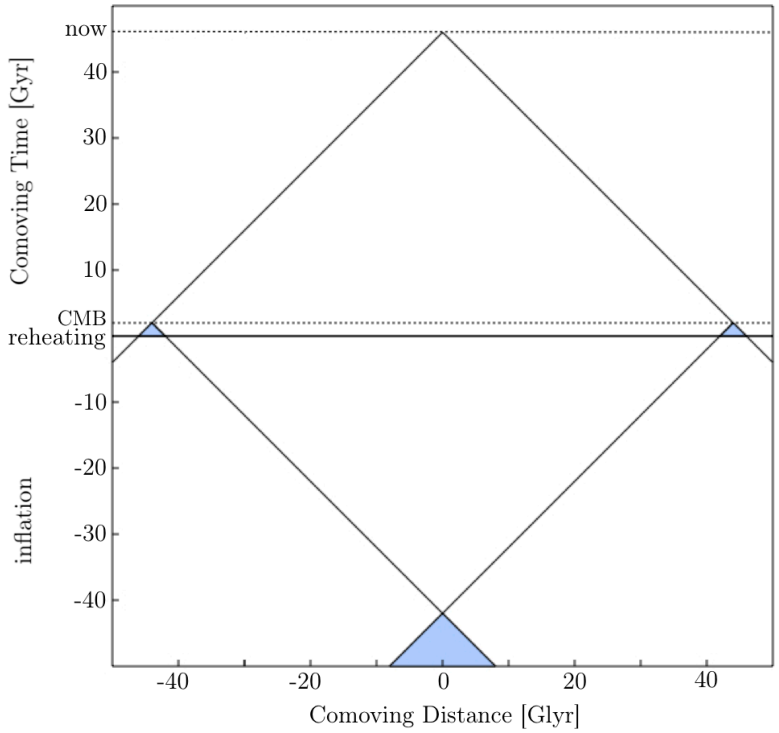

Figure 2: The horizon problem is solved if a period dominated by a fluid violating the SEC took place prior to decoupling. Expansion dominated by a fluid violating the SEC means that there is no longer a finite conformal time between decoupling and the initial singularity. With our choice of normalisation this means conformal time can go to negative values and hence the past light cones of all observed points on the CMB overlap.

0.2.3 A possible solution

Given the above the discussion, the solution to this problem may be defined in two equivalent ways: A mechanism to extend the conformal time between the initial singularly and decoupling must be found. If this time difference can be made sufficiently large, such that the past light-cones of all locations of the observed CMB overlap, then there is no longer a problem. Equivalently, if we can find a mechanism that enables scales entering the Hubble sphere now to have been inside the Hubble sphere some time in the past, then there is no longer a problem.

One solution is to postulate an era dominated by a fluid violating the strong energy condition. This gives the required causal structure since

$$\tau_i = \frac{2c}{3\gamma - 2} a_i^{\frac{3}{2}\gamma - 1} = -\infty \quad \text{if} \quad \gamma < \frac{2}{3}. \tag{20}$$

So if such a period lasts sufficiently long, since the conformal time can go to negative values, as shown in Fig. 2, all areas of the CMB turn out to be causally connected.

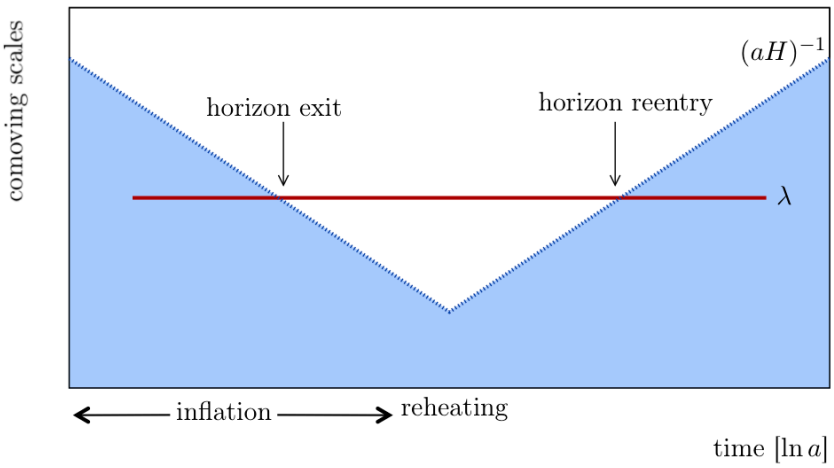

Figure 3: The horizon problem of the standard model is solved if a period where the comoving Hubble sphere decreases took place prior to decoupling. The dotted blue line separates scales inside the Hubble sphere (blue region) from regions outside the Hubble sphere (white region). A given scale λ that has only recently entered the Hubble sphere can still have been in causal contact in the past provided an era where the Hubble sphere shrinks took place.

According to Eq. (16), postulating a violation of the SEC is equivalent to postulating a period of decreasing Hubble radius. This is perhaps a more intuitive way of visualising the solution. Consider some scale of cosmological interest which has only recently entered the Hubble radius. If the era of expanding Hubble radius was preceded by an era of shrinking radius, then such a scale can have been inside the Hubble radius at some point in the past. This postulated phase of shrinking Hubble radius is what is usually referred as inflation and is the subject of this thesis.

Probably the most straightforward way to achieve inflation is by a positive vacuum energy [5], which as discussed above has an equation of state $\gamma = 0$. However, classically such a phase would never end. Quantum mechanically, the mechanism could be terminated by tunnelling but this turns out to be in disagreement with observation. In what follows, the next simplest option will be discussed [6–8]. There are of course other mechanisms though. Some can be understood as a relatively straightforward extension of the slow-roll single scalar field model that will be introduced here. Other interesting alternatives however are more distinct yet are not discussed in this work.

The action for a single scalar field is

$$S_\phi = \int d^4x\sqrt{-g}\mathcal{L}(\phi, \partial_\mu\phi) \tag{21}$$

where $g = \det g_{\mu\nu}$ and

$$\mathcal{L}(\phi, \partial_\mu\phi) = \frac{1}{2}\partial_\mu\phi\partial^\mu\phi - V(\phi). \tag{22}$$

Varying the action with respect to ϕ gives the Klein–Gordon equation

$$\Box\phi + \frac{dV}{d\phi} = 0, \tag{23}$$

where $\Box\phi = \frac{1}{\sqrt{-g}}\partial_\mu(\sqrt{-g}g^{\mu\nu}\partial_\nu\phi)$ is the D'Alembertian operator acting on ϕ. Imposing homogeneity implies that the background field ϕ can only be a function of time and not of spatial coordinates and so the Klein–Gordon equation becomes

$$\ddot{\phi} + 3H\dot{\phi} + \frac{dV}{d\phi} = 0, \tag{24}$$

where here and throughout the rest of this thesis, reduced Planck units are used, $8\pi G = c = \hbar = M_{\rm pl} = 1$.Varying the action with respect to the metric gives the stress energy tensor, which under homogeneity gives

$$\rho_\phi = \frac{1}{2}\dot{\phi}^2 + V \tag{25}$$

$$p_\phi = \frac{1}{2}\dot{\phi}^2 - V. \tag{26}$$

Substituting this equation for ρ_ϕ into the Friedmann equation we can then see how the field affects the expansion history

$$3H^2 = \frac{1}{2}\dot{\phi}^2 + V. \tag{27}$$

The question now is what forms of $V(\phi)$ give rise to inflation. Recalling the definition of inflation as a period where the Hubble radius is decreasing, it is straightforward to derive a couple of constraints:

$$\frac{d}{dt}(aH)^{-1} = -\frac{\dot{a}H + a\dot{H}}{(aH)^2} = -\frac{1}{a}(1-\epsilon) \tag{28}$$

where

$$\epsilon \equiv \frac{\dot{H}}{H^2} \tag{29}$$

and so inflation requires $\epsilon < 1$. Also, inflation needs to persist for a sufficiently long time, which requires that the fractional change per Hubble volume is small

$$\eta \equiv \frac{|\dot{\epsilon}|}{H\epsilon}. \tag{30}$$

Applying these constraints to the Klein–Gordon equation (24) and Friedmann equation (27), one can obtain approximate analogous parameters constraining the form of the potential. Denoting differentiation with respect to the field with a prime $'$, inflation occurs when

$$\epsilon_V \equiv \frac{1}{2}\left(\frac{V'}{V}\right)^2 \ll 1, \tag{31}$$

$$|\eta_V| \equiv \frac{|V''|}{V} \ll 1. \tag{32}$$

0.3 The Universe has structure

Our existence is proof that the universe is not perfectly homogenous. Even the CMB, whose remarkable homogeneity resulted in the postulation of a whole new cosmic era, dominated by exotic matter, actually has minute temperature fluctuations. Arguably the greatest success of inflation, and a major reason for why it has become the leading candidate for a description of the early universe, is its ability to predict these fluctuations to a high accuracy [9–16].

A beautiful consequence of a shrinking Hubble radius is that the zero-point fluctuations of the inflaton field become cosmologically relevant. It is the fact that we can essentially observe fossils of microphysical processes in the early universe, that makes studying the CMB such a central tool in cosmology and a promising probe of particle physics.

0.3.1 Classical Perturbations

To understand the origin of the temperature fluctuations observed in the CMB one must study perturbations to the background evolution. Assuming only scaler perturbations to the metric, the perturbed Robertson–Walker metric may be written as

$$ds^2 = a^2(\tau)\left\{(1+2\Psi)d\tau^2 - 2B_i dx^i d\tau - \left[(1-2\Phi)\delta_{ij} + 2E_{ij}\right]dx_i dx_j\right\}. \tag{33}$$

where $\Psi(\tau, x)$ is the lapse, $B_i(\tau, x)$ is the shift, $\Phi(\tau, x)$ is the spatial curvature perturbation and $E_{ij}(x, \tau)$ is the spatial shear. However, not all of these perturbations are physical. Consider a gauge transformation of the form

$$x^\mu \to x^{\mu'} = x^\mu + \xi^\mu = x^\mu + (\xi^0, \xi_i). \tag{34}$$

We see there are four functional degrees of freedom in the perturbations to the metric and two gauge functions (ξ^0, ξ_i) so by the correct choice of gauge it is possible to set two of the functional degrees of freedom to zero. Considering a gauge transformation to the perturbed field $\delta\phi \to \delta\phi + \dot{\phi}\xi^0$, it is possible to derive a gauge invariant quantity

$$v = \delta\phi + \dot{\phi}\frac{\Phi}{\mathcal{H}}, \tag{35}$$

where for this section dots represent derivatives with respect to conformal time and $\mathcal{H} = \frac{da}{d\tau}/a$ has the same form as the Hubble parameter but for conformal time. This is the

famous Mukhanov–Sasaki variable. A convenient choice when considering perturbations during inflation therefore is the flat gauge,

$$\Phi = E = 0, \tag{36}$$

and so $v = \delta\phi$. Substituting $\phi \to \phi + \delta\phi$ and the perturbed metric into Eq. (23) we get

$$\ddot{\delta\phi} + 2\mathcal{H}\dot{\delta\phi} - (\nabla^2 - a^2V'')\delta\phi = (\dot{\Psi} - \nabla^2 B)\dot{\phi} - 2a^2V'\Psi. \tag{37}$$

Einstein's equations provide constraints such that Ψ and B may be expressed solely in terms of $\delta\phi$ and background quantities. Rather remarkably, after implementing these constraints, and making the substitution

$$f \equiv a\delta\phi \quad (= av), \tag{38}$$

it is possible to obtain, without use of slow-roll approximations, a surprisingly simple equation of motion for $\delta\phi$. This is the Mukhanov–Sasaki equation

$$\ddot{f} + \left(k^2 - \frac{\ddot{z}}{z}\right) f = 0, \tag{39}$$

where $z \equiv a\dot{\phi}/\mathcal{H}$.

To quantise the theory we will need the momentum conjugate to f_k so as to be able to construct commutation relations. There are a number of ways of finding an expression for the momenta. A simple method is to realise that the Mukhanov–Sasaki equation is the equation of motion for a collection of harmonic oscillators with frequencies

$$\omega_k^2(\tau) \equiv k^2 - \frac{\ddot{z}}{z} \tag{40}$$

and so the quadratic action takes the form

$$S_f = \frac{A}{2}\int d\tau d^3k \left[\dot{f}_k^2 - \omega_k^2(\tau) f_k^2\right] \tag{41}$$

and hence

$$\pi_k \equiv \frac{\partial\mathcal{L}}{\partial\dot{f}_k} = A\dot{f}_k. \tag{42}$$

All that is required is to fix the normalisation constant A. This can be done by considering the subhorizon limit $k \gtrsim \mathcal{H}$ where the mixing with metric perturbations is negligible and hence the equation of motion simplifies to

$$\ddot{\delta\phi} + 2\mathcal{H}\dot{\delta\phi} - \nabla^2\delta\phi = 0, \tag{43}$$

which has the quadratic action

$$S_{k\gg\mathcal{H}} = \frac{1}{2}\int d\tau d^3x a^2 \left[(\dot{\delta\phi})^2 - (\nabla\delta\phi)^2\right] \tag{44}$$

which to be consistent with the full action requires $A = 1$.

0.3.2 Quantisation

To quantise f the standard procedure is analogous to that of the harmonic oscillator – Promote the field f and its momentum conjugate to quantum operators $\hat{f}$ and $\hat{\pi}$ and write the perturbation as a superposition of creation and annihilation operator

$$\hat{f}(\tau, x) = \int \frac{d^3k}{(2\pi)^{3/2}} \left[f_k(\tau)\hat{a}_k e^{ik.x} + f_k^*(\tau)\hat{a}_k^\dagger e^{-ik.x} \right], \tag{45}$$

where $\hat{f}$ and $\hat{\pi}$ satisfy the equal-time commutation relations

$$[\hat{f}(\tau, x), \hat{\pi}(\tau, y)] = i\delta(x - y) \tag{46}$$

$$[\hat{f}(\tau, x), \hat{f}(\tau, y)] = [\hat{\pi}(\tau, x), \hat{\pi}(\tau, y)] = 0, \tag{47}$$

and hence the creation and annihilation operators respect

$$[\hat{a}_k, \hat{a}_{k'}^\dagger] = \delta(k - k') \tag{48}$$

$$[\hat{a}_k, \hat{a}_{k'}] = [\hat{a}_k^\dagger, \hat{a}_{k'}^\dagger] = 0. \tag{49}$$

There is a well motivated choice for the vacuum state known as the Bunch–Davies vacuum. At early times all modes of interest were deep inside the horizon and so we can choose to solve the Mukhanov–Sasaki equation in this limit where the modes have time-independent frequencies

$$\ddot{f}_k + k^2 f_k = 0. \tag{50}$$

i.e. the initial conditions are that of a free field in Minkowski space.

$$\lim_{\tau \to -\infty} f_k(\tau) = \frac{1}{\sqrt{2k}} e^{-ik\tau} \tag{51}$$

As mentioned, it seems difficult to obtain a general solution to the Mukhanov–Sasaki equation, but it is possible to obtain an analytical solution for the case of $H = \text{const}$, namely for pure de Sitter expansion, which for many models is a good approximation. For de Sitter space, the Mukhanov–Sasaki equation is

$$\ddot{f} + \left(k^2 - \frac{2}{\tau^2} \right) f = 0, \tag{52}$$

which for Bunch–Davies initial conditions has the solution

$$f_k(\tau) = \frac{e^{-ik\tau}}{\sqrt{2k}} \left(1 - \frac{i}{k\tau} \right). \tag{53}$$

At this stage it is now possible to calculate the effect of quantum fluctuations

$$\langle 0|\hat{f}_k^\dagger \hat{f}_{k'}|0\rangle = |f|^2\delta(k-k') = P_f(k)\delta(k-k'). \tag{54}$$

We are interested in effects on scales leaving the horizon $k\tau \to 0$ and so

$$\lim_{k\tau\to 0} P_f = \frac{1}{2k^3}\frac{1}{\tau^2} = \frac{1}{2k^3}(aH)^2. \tag{55}$$

An exceedingly important quantity for observation, and indeed the central quantity of interest in this thesis, is the curvature perturbation ζ, since for reasons that will be discussed in due course, for single field models of inflation, it is conserved on superhorizon scales. By observation of this variable it is possible to know about the state of the universe during inflation without detailed knowledge of the history in between. In the flat gauge the curvature perturbation is related to the field perturbation by

$$\zeta = -\frac{\mathcal{H}}{\dot{\phi}}\delta\phi \tag{56}$$

and so $\zeta = -\frac{f}{z}$. Importantly, we can relate the power spectrum of ζ to the fluctuations during inflation by

$$P_\zeta(k) = \frac{1}{z^2}P_f. \tag{57}$$

Evaluated at horizon crossing $k = aH$ this is purely a function of k

$$P_\zeta(k) = \frac{1}{4k^3}\frac{H^2}{\epsilon}\bigg|_{k=aH}. \tag{58}$$

It is by observation of this quantity that it is possible to test inflation. It is by studying the details of this power spectrum that it is hoped we can probe particle physics at energy scales that may never again occur in the history of the universe.

0.3.3 Conservation of ζ on superhorizon scales

As mentioned one of the key characteristics of ζ as an observable is that it ceases to evolve on superhorizon scales. Since this is an important point for every paper included in this thesis, it is probably worth discussing this in a little more detail.

The proof by Weinberg [17] that ζ is conserved in the large wavelength limit is quite long and technical so is not included here. Instead we describe the separate universe argument as given by Wands et al [18].

The key concept is that superhorizon sized patches of space will evolve independently of one another. One can understand ζ as parameterising the local rescaling of the scale factor relative to the background evolution

$$a(t,x) = a(t)e^{\zeta(t,x)} \tag{59}$$

and so considering the evolution of spatial patches smoothed on these scales, one essentially wishes to compute the difference in the expansion of these patches. When there is only one field ϕ acting as the inflaton, the energy density and pressure are a unique function of ϕ and so the expansion of each patch is also a unique function of that field. In other words, since there are only adiabatic perturbations present, each patch undergoes identical evolution up to a time shift. In this situation, constant density surfaces differ by a fixed expansion and hence ζ is conserved.

When there is more than one field, as will be the case for all work done in this thesis, in addition to adiabatic perturbations, isocurvature perturbations are also present. This means that constant density slicings are no longer simply related by a time shift. Remembering that under the slow-roll approximation, the energy density is well approximated by the "altitude" on the potential; when there is more than one field, two regions of space may have equal energy density at some stage, but if the field constituents are different, then they will undergo distinct field space evolution resulting in the expansion being different in each region. This means that in order to compute ζ one must track this superhorizon evolution. How this can be achieved and its effect on specific observables is one of the central topics of the papers included in this thesis. For this reason further discussion will be left for later chapters.

One approach to learning about inflation is to strive to make model independent statements; essentially seeking to place constraints on the effective Lagrangian via observations of ζ. The generality of such an approach is highly appealing but progress can be slow. Another way is to take a "top down" approach and try to study inflation by deriving it from fundamental theory. This ultimately is the goal of inflation; to achieve a foundation in fundamental theory thereby providing a means of confronting this theory with observation. Unfortunately any prospect of achieving such a goal is a long way off and at present it is difficult to say anything concrete about inflation from a top down perspective. Nevertheless attempts at such an approach have already proven to be exceedingly useful. Trying to connect inflation with something more fundamental highlights conceptual issues of inflation that may not be apparent without considering explicit models. One issue I find

particularly troubling is the idea that there can be an intrinsic and significant uncertainty in the prediction for observables for a given model. This uncertainty is manifest in all multifield models of inflation and in the context of string theory this problem is particularly acute. For this reason, I now turn to the discussion of inflation in string theory as a means of introducing this topic.

0.4 There may be more than one universe

Historically it has been hoped that fundamental theory will provide a unique description of reality. Specifically it was thought that such a theory would contain a unique description of the early universe and hence of inflation, if it occurred.

To date, the leading candidate for such a fundamental theory is string (or M) theory. However, string theory has not turned out to be what was first envisaged. Rather than giving a single theory of reality, as will be discussed in more detail in what follows, string theory has emerged as being more like a continuum of theories. The question then is how is this to be interpreted. Some would argue that reality still corresponds to a unique theory which must somehow be selected from this larger mathematical framework. From this point of view, assuming inflation is correct, the ability to derive a description of inflation from string theory simply awaits further developments of the underlying theory.

However there is another interpretation. An increasingly popular picture of string theory is that it gives rise to what is often referred to as the string landscape. If this picture is to be taken seriously then the implications for inflation are profound. Such a picture calls for a very different approach to studying inflation. Conversely, an interesting question is whether or not inflation may be used to test this model. Indeed, currently the question of whether or not such a theory can be tested at all is an open question. It seems that inflation may be one approach to shedding light on this issue.

This section is a non-technical review of the basic ideas of inflation in string theory and particularly in the context of the string landscape. It is important to emphasise that the subject of this thesis is not to derive models of inflation from string theory, however ideas relating to the landscape are explored in the earlier papers of this thesis and even when not being discussed directly, the possible existence of a landscape will affect many of the key results of this work. It is also important to bear in mind that the discussion in

this section is highly speculative. Despite this, I feel it is important that this discussion is raised.

0.4.1 Basic inflationary mechanisms in string theory

It is interesting to note that substantial challenges have had to be overcome to achieve inflation in a string motivated setup. The phrase "string motivated" is used here rather than "derived" because significant leaps of faith need to be made in order to achieve a setup with any kind of analytic control. Nevertheless, it is clear that these stringy examples represent significant progress and bring with them valuable lessons.

We observe 3 spatial dimensions and time but string theory requires 11 dimensions. To achieve the $(3+1)$-dimensions we observe the other dimensions must be compactified. There is a continuum of ways of achieving this, where the parameters distinguishing compactifications are synonymously referred to as the moduli. These moduli describe things like the size and shape of the compactified space and appear as scalar fields in the low energy effective field theory. The central issue in trying to construct a string model of inflation is the ability to obtain a successful stabilisation of moduli. For instance, a typical $4d$ effective potential obtained by compactification in type IIB string theory takes the form [19]

$$V(\varphi,\rho,\phi) \sim e^{\sqrt{2\varphi}-\sqrt{6\rho}}\tilde{V}(\phi), \tag{60}$$

where φ and ρ are canonically normalised scalar fields representing the dilaton and volume of the compactified space respectively and ϕ represents all other fields. In principle $\tilde{V}(\phi)$ can drive inflation but the steep potential experienced by φ and ρ push them to arbitrarily large values and hence the radius of the compactified space rapidly expands meaning that the $4d$ space decompactifies to $10D$. In the last decade there has been significant developments in finding ways of obtaining stable compactifications. It is this progress which has allowed for the currently existing models of string inflation to be developed and it is the limitations of the methods used which stifle further progress.

Once a stable compactification is achieved, broadly speaking there are two types of commonly studied string inflation. Inflation driven by the moduli fields themselves, and inflation driven by the motion of branes in the compactification.

Specific examples of moduli inflation in general require considerable fine tuning but have the appealing characteristic of not requiring any additional ingredients beyond those

which go into obtaining a stable compactification. Furthermore, all permit chaotic inflation and hence provide a mechanism for bringing about the right initial conditions for inflation to take place. The significance of this fine tuning will be discussed in due course as will chaotic inflation.

String theory permits the existence of extended d-dimentional objects referred to as branes. In d-brane inflation, the inflaton in the effective $4d$ action actually represents the physical separation of a pair, or stack of branes. These models require carefully constructed configurations of branes moving in what are only semi-realistic compactifications and so it is hard to see how such models could be considered in any sense a natural setup. That said, they have proved incredibly valuable. As an example, d-brane inflation can involve dynamics that are drastically different to the slow-roll scenario described in the previous section. This has been particularly educational in the context of the search for inflationary signatures.

0.4.2 The inflationary landscape of string theory

The currently known methods for stabilising moduli may severely limit our ability to construct explicit models but the construction of such models is not the only way to make progress. Clearly significant development of these techniques is sorely needed but nevertheless a very interesting trend seems to have emerged. Modern approaches to compactifying the extra dimensions seem to give rise to an abundance of scalar fields. These include, but are not exclusively, the moduli fields; for the purposes of this discussion they may all be treated equally.

The fields are not in general associated with any symmetry of the theory and so varying a field will in general give rise to a change in potential energy. In this work it is assumed that the low energy properties of string theory may be well approximated by field theory such that in this context we can simply picture the existence of some number of scalar fields and a potential. We cannot assume a great deal about the couplings of these fields but it seems reasonable to assume that the potential will be complicated – a multidimensional landscape with multiple hills and valleys.

Before proceeding it should be noted that even at this stage the picture presented may be the wrong interpretation. What is well established is the existence of a large class of models with cosmological constant that may be tuned by varying fluxes [20]. What is less

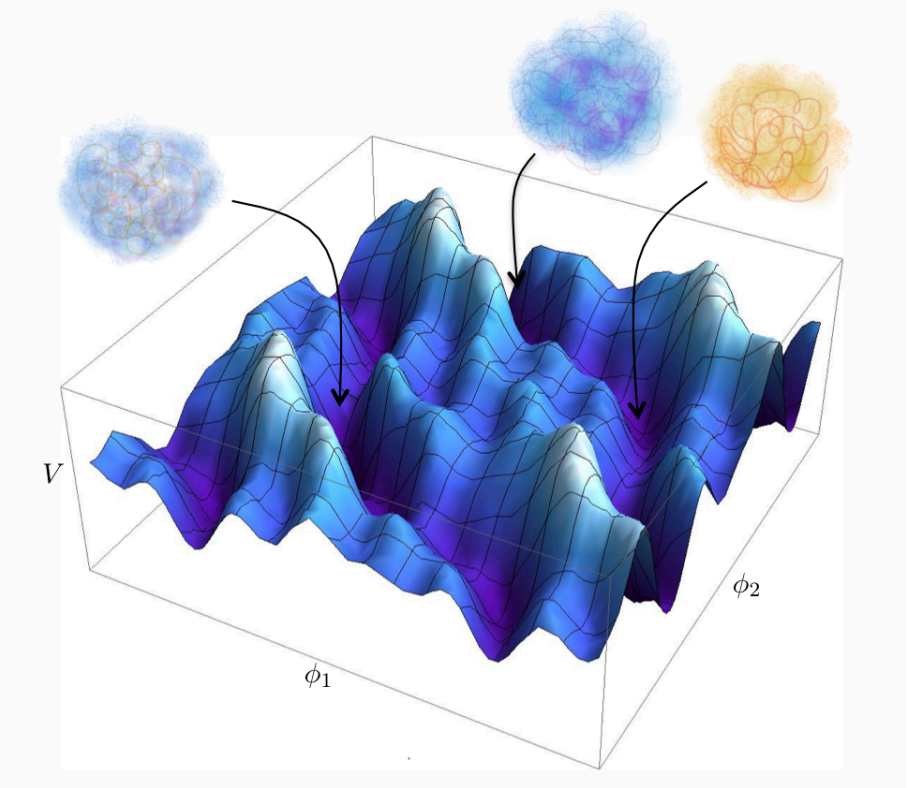

Figure 4: The string landscape picture comes about by the existence of moduli space. There is no explicit symmetry and so varying a moduli field ϕ gives rise to a change in energy V. A given location in moduli space correspond to a specific compactification of the extra dimensions. Our observable universe requires stabilised moduli and so must be located in a suitable minimum, somewhere in this landscape. The "scribbles" represent different stable compactifications of the extra dimensions located at the minima of V

clear is whether this gives rise to a single low energy effective field theory with a potential possessing many minima, or rather, many different effective field theories with different potentials. This distinction will be returned to in due course. For now, it will be assumed that a single low energy effective field theory exists with some complicated potential.

As illustrated in Fig. 4, different minima in this potential correspond to different stable compactifications. Each minimum with positive energy will give rise to regions of space undergoing de Sitter expansion, where "fundamental constants" such as the charge of the electron etc. will be different.

In the landscape picture, the thought is that all of these regions of the potential are actually realised in space-time, and give rise to what is often referred to as the multiverse. Minima with larger energy will give rise to space undergoing more rapid expansion than a minimum with lower energy. We should therefore expect that the vast majority of space-time is drastically different to our observable patch. From time to time, regions of

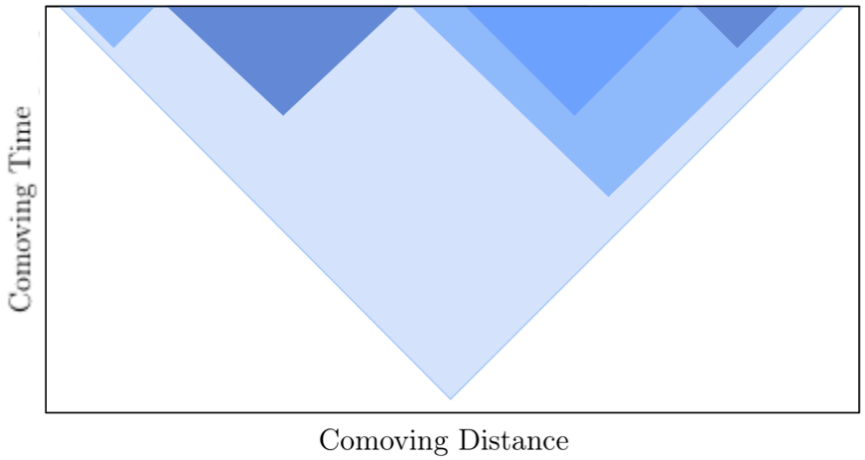

Figure 5: Conformal diagram of how the string landscape gives rise to bubbles. The different shades of blue represent different vacua in the landscape. Regions of space in the parent vacuum (lighter blue) can can tunnel to another vacuum (darker blue).

this larger space-time will quantum tunnel to another minimum in the landscape and will thereby undergo a different expansion or, if the minimum is at negative energy, collapse. If the energy of the new vacuum is sufficiently close to zero, that region may turn out to resemble our observable patch. We should therefore picture something like Fig. 5, bubbles or "verses" which may or may not be similar to our observable patch, causally disconnected as a result of being separated an inflationary region of space-time.

0.4.3 Predictions in the landscape

One might ask the question of whether we should care about distinguishing between string theory giving rise to many causally disconnected verses described by different regions of the potential of one effective field theory, or string theory giving rise to many different effective field theories. Especially given that at present neither picture allows us to explicitly compute anything. One important distinction is that the landscape comes with some powerful conceptual tools that are not obviously applicable in the non-landscape picture. These tools may allow for more progress to be made despite our ignorance and so, although it is hard to constrain string theory with our current understanding, there is a small hope that it may be possible to test the existence of the landscape.

The key difference is that in the landscape picture different vacuum states are dynamically related. This means that there is the possibility of an attractor solution – a mechanism for preferring some vacua over others, which may provide a solution to fine

tuning arguments. For instance, a consequence of being able to move from one vacuum state to another is that it provides an obvious means of anthropic selection.

There are a number of values we observe in nature, such as the charge of the electron, the number of spatial dimensions, the value of the cosmological constant etc. which we have no explanation but if their values were very different, life could not exist. This observation has given rise to what is known as the weak anthropic principle, "The conditions an observer observes must allow for an observer to exist to observe them". With regard to the landscape, all this means is that we only need to worry about regions of the landscape which are capable of sustaining life. Or to take things from another perspective, provided there exists a diverse range of conditions in the landscape, then there is an answer of sorts for why we observe such apparently fine tuned values. Exactly how much one can extract from such a line of reasoning is fraught with controversy. One must tread carefully in the vicinity of tautologies. However, in the context of the landscape it clearly acts as an additional selection factor to any dynamical effects and so in that sense it is an important consideration.

A famous example of the use of anthropic reasoning in the context of the landscape is in determining the small value of the cosmological constant. It is well known that from the perspective of quantum field theory, every known contribution to the cosmological constant is much larger in magnitude than the observed value, and so it seems miraculous that they should cancel against each other to such a high precision. To date, one of the most compelling explanations of the small value is the anthropic argument. In the original proposal by Weinberg [21], he argued that if all other parameters remained constant and the cosmological constant was much larger, then structure formation would be inhibited and if it was larger in magnitude but negative, then our universe would collapse before life would have time to evolve. The string landscape provides a setting in which it makes sense to use such an argument. It is expected that there is an enormous number of vacua (an often quoted number is 10^{500}) where for sensible estimates of the range of allowed vacuum energies the spectrum is dense. Provided the spectrum is sufficiently dense, the conclusion is that our observed vacuum energy should be a random value drawn from this spectrum but truncated at the anthropic bounds.

This provides a rather striking solution[1] to the cosmological constant problem but perhaps it is possible to do even better. If one can make more precise estimates of the

[1]The term "solution" is used loosely here. There is ongoing debate over the merit of such an approach and in any case the argument has been refined considerably since Weinberg's original proposal.

distribution of vacua, then this is one way it may be possible to confront the landscape with observation!

The ability to go beyond anthropic bounds and actually try and compute probability distributions clearly requires a number of significant developments. However, even without detailed knowledge of the string landscape, it may be possible to make significant progress. Many of the important challenges, at this stage, are problems of statistics, which can be worked on independently of detailed knowledge of the landscape. Indeed, as already alluded to, some of these problems are not only applicable to the string landscape, but to a number of much simpler effective field theories as well.

One such problem which has received considerable attention is what is known as the measure problem. The issue here is that according to the string landscape, we live in an infinite universe containing an infinite number of bubble verses, each of which is infinite. Borrowing the description of Ref. [22], in order to make a prediction, one is essentially asking to compare the relative probability p_1/p_2 of seeing one observable over another. This can be found by counting the number of times N each occur

$$\frac{p_1}{p_2} = \frac{N_1}{N_2}. \tag{61}$$

The problem for making a prediction in the landscape is that both the numerator and denominator are infinite and so the ratio is ill-defined. With a choice of measure one can regulate this divergence but since the answer is sensitive to this choice, one can not make a prediction until the correct measure is identified.

0.5 Overview of the papers

Having introduced some basic ideas we are now suitably equipped to discuss some of the concepts directly relating to the papers of this thesis.

A central feature of the previous section is that string theory seems to point towards there being an abundance of scalar fields. At present string theory does not tell us a great deal about the nature of these fields but the very idea that inflation may have been driven by not one but many fields, already begs a number of questions. This work is primarily interested in one particular question

How does one compute predictions when there is more than one field?

As already mentioned, regardless of the underlying theory, there are two characteristics which make multiple field inflation different from the single field case. One trait is that ζ is not conserved on superhorizon scales. The second trait is that multifield models are sensitive to initial conditions in a way that single field models are not.

The superhorizon evolution of ζ can be computed in a number of ways. However, in general, it is necessary to use numerical techniques which for complicated models possessing multiple fields can quickly become very computationally expensive. Furthermore, some techniques can be a bit of a "black box"; one can compute the superhorizon evolution, but it is not necessarily straightforward to trace the source of this evolution. This is particularly problematic in the search for signatures. An important question is whether or not multifield inflation can be distinguished from single field inflation. To address this question necessarily requires a deep understanding of the generation of perturbations and so one requires not one, but a number of tools for studying these perturbations,[2] each providing a new perspective on the issue.

A theme that runs throughout all these papers is the pursuit of a more intuitive understanding of the generation of perturbations. This is done in two ways: By studying a large number of inflationary realisations, we start to get a better understanding of the types of behaviour that can occur, then equipped with this better understanding, an improved technique for computing the perturbations is developed; improved in the sense of being computationally more efficient as well as providing a new geometrical picture of the underlying dynamics. This in turn is used to further study inflationary realisations.

The problem with initial conditions is less well understood and how best to handle it seems to depend on the model in question.[3] In this work two approaches are taken:

One approach is heavily influenced by the landscape. If the potential is complicated and possesses many minima, then it seems that the best way to progress is with an inherently statistical approach. Little was known about models of this kind when this work began and so, as is apparent in the first two papers, it was sensible to start out by taking a highly explorative approach. In work done in collaboration with Andrew Liddle, we constructed a toy model of inflation in the landscape and explored how random realisations of the

[2] *"...every theoretical physicist who is any good knows six or seven different theoretical representations for exactly the same physics"* [23].

[3] It should also be noted that relatively little work in the literature seeks to address this issue and so this work may in some sense be considered early steps in trying to rectify the situation.

potential gave rise to different inflationary outcomes. Familiarising ourselves with the landscape, the goals of our exploration crystallised – it seems the best way to approach such systems is by looking for emergent simplicity. As pointed out in Ref. [24], this is a well known phenomena in random matrix theory and one can hope for something similar to occur in the inflationary landscape. Understanding such behaviour, it seems, would be a promising approach to understanding the predictive capability of models of this kind.

In the final paper of this work, inflation in the vicinity of a single minimum was considered. Working with models of this kind allowed for a very different approach to be taken. Here it seems one can understand the predictive capabilities of the model in terms of the existence of dynamical attractors. The existence of such attractors, by definition, reduces the sensitivity to initial conditions, and hence it can be possible to make robust predictions even without knowledge of the measure.

By addressing these aspects of multifield inflation and inflation in landscape-like potentials it seems we can make substantial progress in understanding the relationship between details of the theory and the ability to make predictions. After the papers this discussion will be returned to.

References

[1] Steven Weinberg. “Cosmology”. In: (2008) (cit. on p. 4).

[2] David H. Lyth and Andrew R. Liddle. “The primordial density perturbation: Cosmology, inflation and the origin of structure”. In: (2009) (cit. on p. 4).

[3] Sean M. Carroll. “Spacetime and geometry: An introduction to general relativity”. In: (2004) (cit. on p. 4).

[4] Daniel Baumann. “The Physics of Inflation: A Course for Graduate Students in Particle Physics and Cosmology”. In: (2011) (cit. on p. 4).

[5] Alan H. Guth. “The Inflationary Universe: A Possible Solution to the Horizon and Flatness Problems”. In: *Phys.Rev.* D23 (1981), pp. 347–356 (cit. on p. 9).

[6] Andrei D. Linde. “Scalar Field Fluctuations in Expanding Universe and the New Inflationary Universe Scenario”. In: *Phys.Lett.* B116 (1982), p. 335 (cit. on p. 9).

[7] Andrei D. Linde. “A New Inflationary Universe Scenario: A Possible Solution of the Horizon, Flatness, Homogeneity, Isotropy and Primordial Monopole Problems”. In: *Phys.Lett.* B108 (1982), pp. 389–393 (cit. on p. 9).

[8] Andreas Albrecht and Paul J. Steinhardt. “Cosmology for Grand Unified Theories with Radiatively Induced Symmetry Breaking”. In: *Phys.Rev.Lett.* 48 (1982), pp. 1220–1223 (cit. on p. 9).

[9] S.W. Hawking. “The Development of Irregularities in a Single Bubble Inflationary Universe”. In: *Phys.Lett.* B115 (1982), p. 295 (cit. on p. 11).

[10] Alexei A. Starobinsky. “Dynamics of Phase Transition in the New Inflationary Universe Scenario and Generation of Perturbations”. In: *Phys.Lett.* B117 (1982), pp. 175–178 (cit. on p. 11).

[11] James M. Bardeen, Paul J. Steinhardt and Michael S. Turner. “Spontaneous Creation of Almost Scale - Free Density Perturbations in an Inflationary Universe”. In: *Phys.Rev.* D28 (1983), p. 679 (cit. on p. 11).

[12] Alan H. Guth and S.Y. Pi. “Fluctuations in the New Inflationary Universe”. In: *Phys.Rev.Lett.* 49 (1982), pp. 1110–1113 (cit. on p. 11).

[13] S.W. Hawking and I.G. Moss. “FLUCTUATIONS IN THE INFLATIONARY UNIVERSE”. In: *Nucl.Phys.* B224 (1983), p. 180 (cit. on p. 11).

[14] Viatcheslav F. Mukhanov. "Gravitational Instability of the Universe Filled with a Scalar Field". In: *JETP Lett.* 41 (1985), pp. 493–496 (cit. on p. 11).

[15] Viatcheslav F. Mukhanov and G.V. Chibisov. "Quantum Fluctuation and Nonsingular Universe. (In Russian)". In: *JETP Lett.* 33 (1981), pp. 532–535 (cit. on p. 11).

[16] Misao Sasaki. "Large Scale Quantum Fluctuations in the Inflationary Universe". In: *Prog.Theor.Phys.* 76 (1986), p. 1036 (cit. on p. 11).

[17] Steven Weinberg. "Adiabatic modes in cosmology". In: *Phys.Rev.* D67 (2003), p. 123504. arXiv:astro-ph/0302326 [astro-ph] (cit. on p. 14).

[18] David Wands et al. "A New approach to the evolution of cosmological perturbations on large scales". In: *Phys.Rev.* D62 (2000), p. 043527. arXiv:astro-ph/0003278 [astro-ph] (cit. on p. 14).

[19] Andrei D. Linde. "Inflationary Cosmology". In: *Lect.Notes Phys.* 738 (2008), pp. 1–54. arXiv:0705.0164 [hep-th] (cit. on p. 17).

[20] Tom Banks. "The Top 10^{500} Reasons Not to Believe in the Landscape". In: (2012). arXiv:1208.5715 [hep-th] (cit. on p. 18).

[21] Steven Weinberg. "Anthropic Bound on the Cosmological Constant". In: *Phys.Rev.Lett.* 59 (1987), p. 2607 (cit. on p. 21).

[22] Ben Freivogel. "Making predictions in the multiverse". In: *Class.Quant.Grav.* 28 (2011), p. 204007. arXiv:1105.0244 [hep-th] (cit. on p. 22).

[23] Richard Feynman. *The character of physical law.* laurel. MIT Press, 1995 (cit. on p. 23).

[24] Nishant Agarwal et al. "Universality in D-brane Inflation". In: *JCAP* 1109 (2011), p. 002. arXiv:1103.2775 [astro-ph.CO] (cit. on p. 24).

Paper 1

Exploring a string-like landscape

Jonathan Frazer and Andrew Liddle

We explore inflationary trajectories within randomly-generated two-dimensional potentials, considered as a toy model of the string landscape. Both the background and perturbation equations are solved numerically, the latter using the two-field formalism of Peterson and Tegmark which fully incorporates the effect of isocurvature perturbations. Sufficient inflation is a rare event, occurring for only roughly one in 10^5 potentials. For models generating sufficient inflation, we find that the majority of runs satisfy current constraints from WMAP. The scalar spectral index is less than 1 in all runs. The tensor-to-scalar ratio is below the current limit, while typically large enough to be detected by next-generation CMB experiments and perhaps also by Planck. In many cases the inflationary consistency equation is broken by the effect of isocurvature modes.

1.1 Introduction

Historically researchers have hoped that there is a fundamental physical theory uniquely describing what we observe. More than that, many have hoped that it has a signature allowing us to distinguish it from any other theory we might have imagined along the way. While string theory may or may not be the answer to all our questions, what is exciting is that for the first time it gives us a theory that might be (see ref. [1] for a nice review of string theory in cosmology). But string theory has surprised those who work with it time and time again. First there was one string theory, then there were five, then it turned out there was a continuum of theories [2, 3]!

How are we to interpret this? Susskind coined the term *landscape* [3]. He described what he called the megaverse (now more commonly referred to as the multiverse), where in the low-energy approximation, different regions may be characterized by the values of a large number of scalar fields. The consequence of this is that we have some very complicated potential $V(\phi_1, ..., \phi_D)$, with a very large number of minima, each corresponding to a different metastable vacuum energy. This implies that instead of trying to predict the values of observables, we should be trying to predict probability distributions.

An early study of the possible consequences of this landscape picture for inflation was carried out by Tegmark [4], who generated a large number of random one-dimensional potentials and explored the inflationary outcomes. However a one-dimensional approach gives a very limited view as compared to the possible dynamics of the landscape, in particular limiting the effect of the choice of initial conditions and restricting the observable outcome to adiabatic perturbations. In this article we take further steps towards a more realistic rendition of the landscape, while remaining quite rudimentary, by carrying out a similar analysis in a two-dimensional field space. This broadens the effect of initial conditions, as there are now a family of possible trajectories passing through each point in field space, and permits isocurvature perturbations which can modify the form of the late-time adiabatic spectrum. Our aim is to characterize the spread of observational predictions for such models. In future work we will extend further to a D-dimensional landscape, which adds computational complexity but no new issues of principle, unlike the extension from one to two dimensions.

1.2 Approach

1.2.1 Where we intend to explore

Ideally we would like to explore the landscape potential $V(\phi_1, ..., \phi_D)$ directly but sadly the explicit form is currently unknown. So to be getting on with we construct an artificial potential. The hope is we can explore how certain characteristics expected to be manifest in the true potential give rise to a probability distribution for observables. Adapting the approach taken in ref. [4], we define a potential

$$V(\phi_1, .., \phi_D) = m_{\rm v}^4 f\left(\frac{\phi_1}{m_{\rm h_1}}, .., \frac{\phi_D}{m_{\rm h_D}}\right), \tag{1.1}$$

	Single Feld	Two-Field	Multi-field
Motivation	All that inflation asks for	Richer behaviour yet still simple	Natural consequence of many fundamental theories
Surfaces	Maxima, Minima, Slopes	Maxima, Minima, Saddles, Valleys, Ridges	Maxima, Minima, Saddles, Valleys, Ridges
Perturbations	Curvature	Curvature and Isocurvature	Curvature and Isocurvature
Issues	Requires very flat potentials that may be hard to realize in fundamental theory	Initial Conditions	Initial conditions

Table 1.1: Summary of some of the differences between single scalar field models and more scalar fields.

where f is a well-behaved dimensionless function and $m_{\rm v}$ and $m_{\rm h_i}$, $(i \in 1..D)$, are the characteristic vertical and horizontal mass scales. Ultimately $m_{\rm v}$ is to be adjusted to give the correct amplitude of observed perturbations. Adjusting this mass does not affect anything other than the distribution of vacuum energies, so for now we will not concern ourselves with it.

In ref. [4] the case where $D = 1$ was extensively investigated. We wish to move to higher D as it allows for a broader range of behaviour, particularly isocurvature perturbations which will be one of the main focuses of this paper. In this paper we only take the step of increasing D from 1 to 2; however we believe this is the biggest step as there are no further qualitative differences to go beyond $D = 2$. We reserve analysis of that case to future work.[1] Table 1.1 summarizes some of the changes as the number of scalar fields is increased.

To construct our landscape, following an approach similar to ref. [4] we use a random function of the form

$$f(x, y) = \sum_{j=1}^{m} \sum_{k=1}^{n} \left[a_{j,k} \cos\left(jx + ky\right) + b_{j,k} \sin\left(jx + ky\right) \right] \tag{1.2}$$

where in practice we truncate the series at the values $m = n = 5$ and the Fourier coeffi-

[1] An exception may be the distribution of the vacua, which changes in an interesting way both classically and particularly with regard to tunnelling [5–7] .

cients $a_{j,k}$, $b_{j,k}$ are independent Gaussian random variables with zero mean and standard deviation

$$\sigma = e^{-(j^2+k^2)/2n}, \tag{1.3}$$

With this form, the potentials we simulate are periodic with periodicity scale $2\pi m_{\mathrm{h_i}}$, and we can only expect reasonable results if the evolution spans a distance in the x–y plane less than the periodicity of the function. For our choice of the horizontal mass $m_{\mathrm{h_i}}$, which we are about to discuss, the periodicity is large enough to have no effect.

The precise form of our potential clearly has no theoretical motivation and as such we are free to tinker with it as we please. We are interested in how features of the landscape affect the evolution of the power spectrum and observables, so what we need to consider is on what scale these features occur. If any, it is this quality of our landscape which should be motivated by fundamental theory. Our choice of potential allows us to adjust this in three ways; the truncation number, the standard deviation of the Fourier coefficients, and the choice of $m_{\mathrm{h_i}}$. The truncation number and tuning of the standard deviation are specific to our potential, but the mass scale is a rather more general feature of potentials. Thus, to try and focus on this sense of scale, we fix the deviation and truncation number as stated above and discuss our options in terms of adjusting the horizontal mass with respect to some reference mass, taken to be the reduced Planck mass M_{Pl}. If we think of features in the landscape as being anything that can cause a change in direction of the inflationary trajectory, then we are essentially asking how many of these features we expect the trajectory to encounter during an evolution giving rise to a sufficiently large number of e-folds of inflation. There are many interesting mass scales that we will not be attempting to explore here, but crudely speaking they fall into four categories:

$m_{\mathrm{h_i}} \gg M_{\mathrm{Pl}}$**:** This mass choice is poorly motivated by theory but was nonetheless explored as one of many cases for single scalar field in ref. [4]. More generally speaking, this case corresponds to a trajectory on a nearly flat, almost featureless potential. The advantage of this is that it is highly predictive since all trajectories look pretty much the same and in the single-field case can readily be in agreement with observation. Also, it is easy to get lots of inflation.

$m_{\mathrm{h_i}} \ll M_{\mathrm{Pl}}$**:** This mass choice corresponds to something akin to an egg box.[2] The main issue with this choice is that it becomes difficult to achieve sufficient inflation without

[2] Allowing a high truncation number when $m_{\mathrm{h_i}} \gtrsim M_{\mathrm{Pl}}$ introduces small-scale power into the potential to similar effect.

getting eternal inflation, since the trajectory will almost always roll straight into a minimum. That said, one might imagine that if the number of scalar fields was sufficiently large then the chance of getting sufficient inflation would increase. This is a particularly important effect if tunnelling is taken into consideration [5–7], but to keep things simple we will not be doing so in this paper.

$m_{\mathrm{h_i}} \ll M_{\mathrm{Pl}}$ **and** $m_{\mathrm{h_j}} \gg M_{\mathrm{Pl}}$**:** While our choice of potential would require additional terms to investigate this scenario, we are referring to the sort of case where there is more than one kinematically significant scale. An example of this kind of situation was investigated in refs. [8, 9]. The setup they considered could be imagined as a sort of multi-dimensional version of a board with nails stuck in it. The trajectory has a slow-roll drift velocity with what the authors describe as a brownian motion imposed on top of this. Depending on the scales involved, this could lead to interesting features in the power spectra and, for a given suitable background evolution, the extra distance covered due to the random motion will increase the number of e-folds.

$m_{\mathrm{h_i}} \sim M_{\mathrm{Pl}}$**:** Finally we have the beginners' ski slope, an example of which is shown in Fig. 1.1. This is what we will be investigating. There are no jumps and the features are gentle so an advanced skier or snowboarder would probably be rather bored in our landscape, but for inflation we feel this is an interesting scale on which to begin our exploration. This mass scale is well motivated by theory and it also gives rise to quite a broad range of behaviour, since in order to obtain a sufficient number of e-folds of inflation, the trajectory generally has to take a non-straight path. The downside is that the broad range of behaviour will make the model less predictive but then again, it is interesting to see how robust the values of certain parameters are under such variations. Also, while the variability in a two scalar field model may be large, one can easily imagine that the deviation might decrease as more scalar fields are introduced. This tendency was seen in ref. [10] for Nflation models with random initial conditions on many uncoupled fields.

1.2.2 How we explore it

As we discussed, any model of inflation where the potential has multiple minima predicts a probability distribution for the cosmological parameters. We wish to compute this dis-

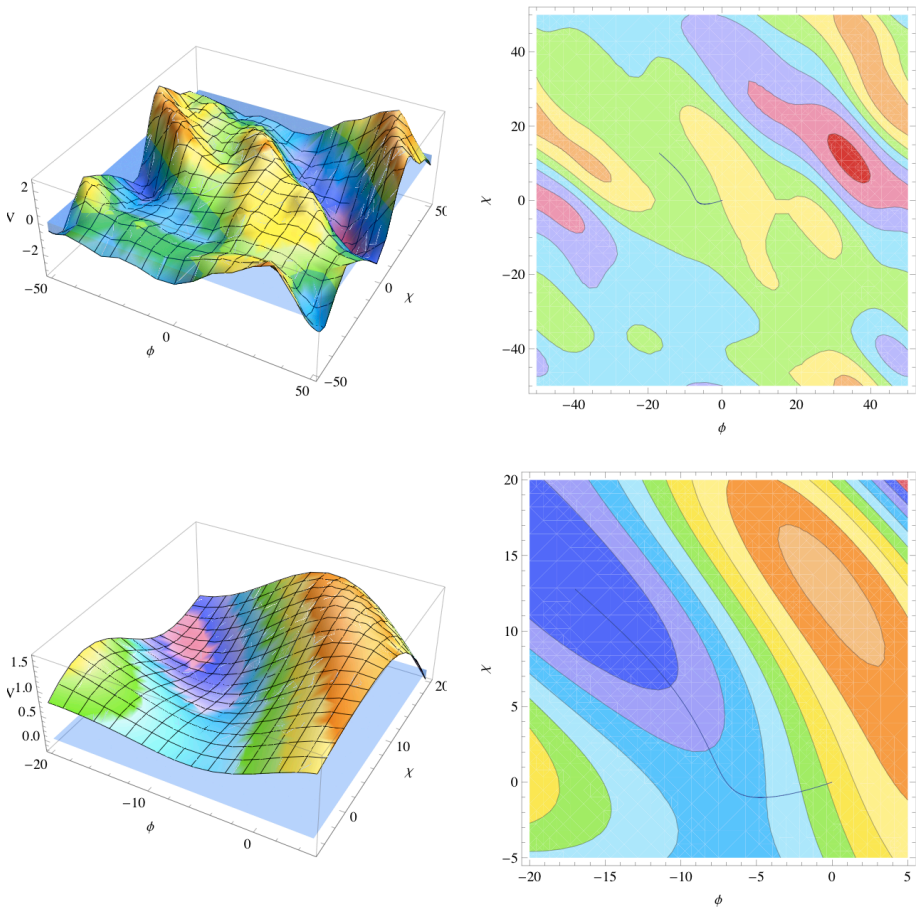

Figure 1.1: An example of our landscape, shown on two scales together with the trajectory taken during inflation. The first scale corresponds to the periodicity of the function, and the second shows the features relevant to the inflationary trajectory. The "water level" indicates the height of the minima determining the vacuum energy. We see this is very close to $V = 0$; this, together with the fact that this trajectory gives a sufficient number of e-folds of inflation (in this case $N = 173$), means that we have an anthropically suitable bubble universe.

tribution for the potential described above. To do this we perform essentially the same experiment that was performed in ref. [4]:

1. Generate a random potential $V(\phi)$ and start at $\phi = (0, 0)$.
2. If $V(0, 0) < 0$ then reject model, otherwise evolve to find the field trajectory.
3. If model gets stuck in eternal inflation, reject.
4. Once the model stops inflating, if the number of e-folds of inflation $N < 60$ we reject as insufficient inflation occurred. Otherwise find the local minimum to calculate ρ_{vac}, and if $\rho_{\text{vac}} < 0$, reject. If $N \geq 60$ and $\rho_{\text{vac}} \geq 0$, calculate observables.
5. Repeat many times to obtain a statistical sample.

6. (Change some assumptions and do it all again.)

We start the evolution at $V(0,0)$ for practical purposes. Instead of viewing this as starting at the same position in many different potentials, since the statistics of our landscape are invariant under translation, one could equally view this as starting at random positions in one infinite potential. An alternative choice of initial conditions would be to start only at maxima. This relates to the choice of measure, a problem we will discuss shortly but which in reality is an issue well beyond the scope of this paper. Step 2 is there since it would make no sense to do otherwise; generally we are not interested in the statistics of initial conditions that don't give rise to regions of space. Step 3 rejects trajectories that get stuck in minima that lead to eternal inflation. We will not be considering tunnelling in this paper, so once again we give no statistical weighting.

Step 4 describes what we do when we finally do encounter a potentially viable trajectory. The rejections that take place here are more debatable since they are essentially anthropic rejections. In ref. [11] it was shown that anthropic arguments place an incredibly strong bound on the vacuum energy. This was and still is a very important result and the realization that it sits so naturally with string theory is more than a little exciting. We do not explore this idea in our current work; indeed we ignore it since the extremely narrow permitted range for the present vacuum energy is not computationally accessible. Instead we place only an approximate lower bound, rejecting universes with a negative vacuum energy on the grounds that they will recollapse shortly after inflation ends. Technically very slightly negative vacuum energies are anthropically acceptable but this does not affect what we are interested in here. Rejecting inflation of less than 60 e-folds comes from arguing that this is a requirement for the formation of galaxies on a smooth cosmological background [4]. Steps 5 and 6 follow trivially.

In constructing our experiment in this way we have inadvertently chosen a measure. We do not wish to go into it in any depth here but it is important to realize that what is known as *The Measure Problem* [4, 12–17] directly affects this work. If we subscribe to Bayesian statistics then one can describe the current situation as follows: Define $P(U)$ to be the probability of finding yourself in a particular region of space-time where inflation has ended which we now define as a bubble universe U, from now on simply referred to as a universe. Then define $P(O)$ to be the probability of making an observation O in any bubble universe. What one defines as an observation changes the results dramatically. One could simply decide observation meant finding protons for instance. Here, observation

corresponds to an observer measuring a particular set of cosmological parameters. The conditional probability of making an observation O in a universe U is $P(O|U)$, called the likelihood. Meanwhile, the probability that we are in a universe U given that we have the observation O is $P(U|O)$, called the posterior probability. Bayes' theorem then gives us

$$P(U|O) = \frac{P(O|U)P(U)}{P(O)}. \tag{1.4}$$

Our experiment essentially makes an attempt at calculating $P(O)$ but this can be written as

$$P(O) = \int_M P(O|U)P(U)dU \tag{1.5}$$

where M is the multiverse, and dU is the measure. So as you can see we have issues. The probability of making an observation O given U is where anthropic arguments come in. For example, the probability of making an observation in a universe that can't form galaxies is, we guess, not very high. We also have the problem of counting infinities and this is the measure problem. We have possibly an infinite number of universes, infinite in extent and yet we need to count the probability of making observations in them. We do not wish to discuss this in any detail but we need to remember that our experiment, for the time being, uses a measure where initial conditions are weighted equally (step 1) to start with but then we give zero weighting to universes that are invalid on anthropic grounds (step 4).

1.3 Calculating observables

In this section we lay down the theoretical framework involved in calculating observables. Much of this section follows ref. [18], which gives an extremely thorough and comprehensive review of how to make two-field model calculations. We therefore only give a summary of the calculations involved, operating in a simplified setting where we assume the fields are canonically normalized and working to lowest order in the perturbations (since the effect of higher-order terms would be much smaller than the uncertainty of our overall implementation). First we introduce the unperturbed equations. In the context of our work these are the equations used to perform the experiment described in the previous section. Next we move on to the background kinematics. These will prove invaluable in our attempts to understand what aspects of the potential are important in affecting observables

and how these characteristics extend to a larger number of scalar fields. We then move on to the perturbed equations which finally lead us to calculating observables. We use reduced Planck units ($M_{\rm Pl} = 1$) throughout and the vector notation $\phi = (\phi_1, .., \phi_D)$. In practice we will often simply have $\phi = (\phi_1, \phi_2)$ but where it will be helpful in later discussion, we write down explicitly how this extends to D scalar fields.

1.3.1 Background equations

We take the background spacetime to be flat, $(3+1)$-dimensional, homogeneous and isotropic and thus described by the Robertson–Walker metric,

$$ds^2 = -dt^2 + a^2(t)\left[dx^2 + dy^2 + dz^2\right], \tag{1.6}$$

where $a(t)$ is the scale factor. We are investigating inflation driven by D scalar fields with canonical kinetic terms. The non-gravitational part of the action is

$$S = \int \left[-\frac{1}{2}\sum_{i=1}^{D} \partial^\mu \phi_i \partial_\mu \phi_i - V(\phi_1, .., \phi_D)\right] \sqrt{-g}\, d^4x, \tag{1.7}$$

and thus we have the standard field equation

$$\ddot{\phi} + 3H\dot{\phi} + \nabla^\dagger V = 0, \tag{1.8}$$

where H is the Hubble parameter, whose dynamics are found from the $(0,0)$ component of Einstein's equations,

$$3H^2 = \rho. \tag{1.9}$$

From eq. (1.7) we also obtain

$$\rho = \frac{1}{2}|\dot{\phi}|^2 + V \quad , \quad P = \frac{1}{2}|\dot{\phi}|^2 - V \tag{1.10}$$

and so eq. (1.9) becomes

$$3H^2 = \frac{1}{2}|\dot{\phi}|^2 + V. \tag{1.11}$$

Working in terms of comoving time t is not particularly convenient for our current work. Instead it is much more helpful to make the transformation

$$dN \equiv H dt, \tag{1.12}$$

where N is the logarithmic growth of the scale factor and represents the number of e-foldings of inflation. Using N is useful since it is directly related to observables; it also

simplifies all the equations and renders them dimensionless, thus making it simpler to compare the relative size of terms. From now on we will use the notation

$$' \equiv \frac{d}{dN} \tag{1.13}$$

to represent differentiation with respect to N.

To further simplify the equations we introduce the slow-roll parameter

$$\epsilon \equiv -\frac{\dot{H}}{H^2}. \tag{1.14}$$

Inflation ends when $\ddot{a} \leq 0 \iff \epsilon \geq 1$. If we combine the field equation (1.8) with the comoving time derivative of eq. (1.11) we see that the slow-roll parameter can also be interpreted in terms of the field speed;

$$v \equiv |\phi'| = \sqrt{2\epsilon}. \tag{1.15}$$

Making the transformation given in eq. (1.12) and substituting eq. (1.14), the field and Friedman equations simplify to

$$\phi' + \nabla^\dagger \ln V = -\frac{\phi''}{3-\epsilon} \tag{1.16}$$

and

$$H^2 = \frac{V}{3-\epsilon} \tag{1.17}$$

respectively.

Equation (1.16) together with eq. (1.14) give the evolution of the fields. To solve them we need to provide initial conditions. We choose these to be $\phi = (0, 0)$ and $\phi' = (-V_{,\phi_1}/V, -V_{,\phi_2}/V)$.

1.3.2 Relating kinematics to the potential via the slow-roll slow-turn approximations

This subsection is predominantly a summary of ref. [18], although our case is simpler in that we are only concerned with canonical kinetic terms. We also make the extension to a larger number of scalar fields a little more explicit.

We wish eventually to investigate the evolution of perturbations. As summarized in Table 1.1, when there is only one scalar field, the only type of perturbation that exists is density perturbations, generated by perturbing the field along the trajectory. When

there are more scalar fields however, for every extra scalar field there is another direction perpendicular to the trajectory in which perturbations can also arise. The perturbations perpendicular to the trajectory correspond to isocurvature perturbations but these in turn can fuel the evolution of the density perturbations. Decomposing the perturbations in this way leads us to introduce a new basis. If we think of the old basis as $B = \{e_1, .., e_D\}$ where e_1 points in the direction ϕ_1, e_2 points in the direction ϕ_2 and so on, then we can think of the new basis $K = \{e_\parallel, e_{\perp_1}, .., e_{\perp_{D-1}}\}$ as a rotation of the old basis such that the first basis vector now points along the trajectory and we label it $e_\parallel$. The other basis vectors will then point perpendicular to the the trajectory and we label them $e_{\perp_i}$. We refer to this as the *kinematic basis*[3] and we denote the components of a general vector $\mathbf{A}$ and matrix M as, for instance

$$A_\parallel = e_\parallel \cdot \mathbf{A} \quad , \quad M_{\parallel\perp_i} = e_\parallel^\dagger M e_{\perp_i}. \tag{1.18}$$

Using the kinematic basis we can now introduce the slow-roll slow-turn (SRST) approximations. There is more than one way to interpret the well-known single-field slow-roll approximations and as discussed in ref. [18], this affects how the slow-roll approximations generalize to multiple scalar fields. With regard to how slow-roll extends, probably the minimal requirement is to say:

- Expansion is nearly exponential.
- Deviation from this expansion changes slowly.

If we take this as our definition then our slow-roll conditions become

$$\epsilon = \frac{1}{2}v^2 \ll 1 \quad , \quad \left|\frac{\phi_\parallel''}{v}\right| \ll 1. \tag{1.19}$$

Although these are sufficient to guarantee the above requirements, it is helpful to have a slow-turn approximation which we define as

$$\left|\frac{\phi_{\perp_i}''}{v}\right| \ll 1. \tag{1.20}$$

There are $D-1$ of these slow-turn conditions and violation of any one of these conditions would render the trajectory no longer slowly turning, so one might prefer to instead write

$$\frac{1}{D-1}\left|\frac{\phi_\perp{}''}{v}\right| \ll 1, \tag{1.21}$$

[3]For a fully kinematic basis, one could also define one of the perpendicular fields such that the direction of the turning of the field is entirely along it, but we choose not to do that here since our basis will make it clearer how to extend our statistics to D fields.

but for our purpose we find the former more useful. If the field is both slowly rolling and slowly turning we say it satisfies SRST.

Returning to eq. (1.16) we see that the left-hand side represents deviations from the SRST limit and so under SRST conditions we can write

$$\phi' \simeq -\nabla^\dagger \ln V \tag{1.22}$$

and the Friedman equation becomes

$$3H^2 \simeq V. \tag{1.23}$$

When trying to understand how various features of the potential affect observables, sometimes it is nice to interpret things in terms of the kinematics of the scalar field and at other times perhaps it is better to look directly at the underlying geometry. For this reason, amongst others, it is helpful to be able to approximately jump from one approach to the other. Direct from eq. (1.22) we have

$$\epsilon \simeq \frac{1}{2}|\nabla^\dagger \ln V|^2 \tag{1.24}$$

and differentiating eq. (1.22) one obtains

$$\phi'' \simeq -M\nabla^\dagger \ln V, \tag{1.25}$$

where M is the Hessian of $\ln V$, otherwise known as the mass matrix,

$$M \equiv \nabla^\dagger \nabla \ln V. \tag{1.26}$$

We therefore arrive at approximations relating the kinematic quantities directly to the potential:

$$\left(\frac{\phi''_\parallel}{v}\right) \simeq -M_{\parallel\parallel}, \tag{1.27}$$

termed the speed-up rate, and

$$\left(\frac{\phi''_{\perp_i}}{v}\right) \simeq \left|M_{\parallel\perp_i}\right|, \tag{1.28}$$

known as the i-th component turn rate.

We don't look at the second-order equations here but we refer the reader to ref. [18] should they need them.

1.3.3 The perturbed equations

Continuing to adopt the same approach as that chosen in ref. [18] it can be shown that by using a multifield version of the Mukhanov–Sasaki variable [19], the field perturbations decouple from perturbations in the metric and thus we are able to focus solely on the curvature and isocurvature perturbations. The evolution of the field perturbations can be found by perturbing the equation of motion for the background. The standard result in Fourier space is

$$\delta\ddot{\phi} + 3H\delta\dot{\phi} + \left(\frac{k}{a}\right)^2 \delta\phi = -\left[\nabla^\dagger\nabla V - \left(3 - \frac{\dot{H}}{H^2}\right)\dot{\phi}\dot{\phi}^\dagger - \frac{1}{H}\ddot{\phi}\dot{\phi}^\dagger - \frac{1}{H}\dot{\phi}\ddot{\phi}^\dagger\right]\delta\phi, \quad (1.29)$$

where k is the comoving wavenumber. Substituting Eqs. (1.12), (1.14) and (1.16) one eventually reaches

$$\frac{1}{3-\epsilon}\delta\phi'' + \delta\phi' + \left(\frac{k^2}{a^2V}\right)\delta\phi = -\left[M + \frac{\phi''\phi''^\dagger}{(3-\epsilon)^2}\right]\delta\phi \quad (1.30)$$

and we see that mode evolution is primarily governed by the mass matrix with small corrections.

Rotating to the kinematic basis, we can separate eq. (1.30) to find evolution equations for the adiabatic ($\delta\phi_\parallel$) and entropy modes ($\delta\phi_\perp$). Starting with the adiabatic mode, projecting in the $e_\parallel$ direction, then solving the resulting equation in the super-horizon limit $(k/aH)^2 \ll 1$, one finds that the growing super-horizon adiabatic modes are described by

$$\delta\phi'_\parallel = \left(\frac{\phi''_\parallel}{v}\right)\delta\phi_\parallel + 2\sum_i^{D-1}\left(\frac{\phi''_{\perp_i}}{v}\right)\delta\phi_{\perp_i}, \quad (1.31)$$

or equivalently

$$\left(\frac{\delta\phi_\parallel}{v}\right)' = +2\sum_i^{D-1}\left(\frac{\phi''_{\perp_i}}{v^2}\right)\delta\phi_{\perp_i}, \quad (1.32)$$

or when SRST holds

$$\delta\phi'_\parallel \simeq M_{\parallel\parallel}\delta\phi_\parallel - 2\sum_i^{D-1} M_{\parallel\perp_i}\delta\phi_{\perp_i}. \quad (1.33)$$

So we see that the evolution of adiabatic modes can be inferred directly from the background kinematics. The first term of eq. (1.31) tells us that the faster the speed-up rate, the faster the evolution of the mode. The second term tells us about the sourcing of the adiabatic modes from the entropy modes. We see that for a given size of entropy mode, the faster the turn rate, the more the adiabatic mode will be sourced by that entropy mode. For our experiment we will see there is a distribution associated with the likelihood

of encountering a given turn rate. This means that as we extend to a larger number of scalar fields, it becomes increasingly likely that the fuelling from entropy modes will be a significant effect.

Following the same procedure for the entropy modes we find that

$$\frac{\delta\phi''_{\perp_i}}{3-\epsilon} + \delta\phi'_{\perp_i} = -\mu_{\perp_i}\frac{\delta\phi_{\perp_i}}{v}, \tag{1.34}$$

where μ_i is the effective entropy mass

$$\mu_{\perp_i} \equiv M_{\perp_i\perp_i} + \frac{9-\epsilon}{(3-\epsilon)^2}\left(\frac{\phi''_{\perp_i}}{v}\right)^2 \tag{1.35}$$

and so is well approximated by $\mu_{\perp_i} \simeq M_{\perp_i\perp_i}$. The great news here is that eq. (1.34) tells us that each of the entropy modes evolves independently of the others. This means we can find their amplitude and determine the evolution of adiabatic modes without solving a massive set of fully coupled equations. We also see that the evolution of a given entropy mode is dominated by the curvature of the log of the potential along that entropic direction. This makes sense intuitively as when the curvature is positive, a given trajectory is stable in the sense that a perturbed trajectory will be redirected back onto the background trajectory. Conversely, when the curvature is negative, the trajectory is dispersive and perturbations will evolve, fuelling the growth of that entropy mode.

From here we are in a position to discuss curvature and isocurvature perturbations. The curvature perturbation represents the perturbation in the curvature of constant-time hypersurfaces. In the comoving gauge we have the gauge-invariant quantity, R, which during inflation can be shown to be

$$R = \frac{\delta\phi_\parallel}{v}. \tag{1.36}$$

Isocurvature perturbations represent relative fluctuations in the different fields that leave the total curvature unchanged and hence are related to entropy perturbations, here defined as[4]

$$S_i \equiv \frac{\delta\phi_{\perp_i}}{v}. \tag{1.37}$$

Using eq. (1.32) then gives us

$$R' = +2\sum_i^{D-1}\left(\frac{\phi''_{\perp_i}}{v}\right)S_i \tag{1.38}$$

[4]This definition, following refs. [18, 20], is chosen so that the isocurvature mode typically has the same amplitude as the adiabatic one at horizon crossing, and differs from the alternative convention where the isocurvature perturbations are normalized like massless field perturbations.

	$M_{\|\|\|} > 0$	$M_{\|\|\|} < 0$
$M_{\perp\perp} > 0$	Playoff	Damping
$M_{\perp\perp} < 0$	Fueling	Playoff

Table 1.2: Origins of evolution of isocurvature modes.

and so we see that the super-horizon evolution of the density perturbation is independent of the speed-up rate; instead it depends on the sum of the isocurvature perturbations, each multiplied by their corresponding turn rate. We also see that when there is no turn rate (in any of the directions), the single-field result that the density perturbation is conserved on super-horizon scales is recovered.

For the isocurvature perturbations we use the approach of ref. [20] and parameterize the isocurvature modes as

$$S_i' = \beta_i S_i. \tag{1.39}$$

We then find that β can be well approximated in the SRST limit as

$$\beta_i \simeq M_{\|\|\|} - M_{\perp_i\perp_i} \tag{1.40}$$

So interpreting this from the geometrical point of view we see that the evolution of a given set of isocurvature modes depends on the integral of the difference between the curvature along the adiabatic and entropic directions in a very intuitive manner. As summarized in Table 1.2, negative curvature in the adiabatic direction and positive curvature in the entropic direction corresponds to maximum damping of isocurvature modes, while positive curvature in the adiabatic direction and negative curvature in the entropic direction corresponds to maximum fuelling.

Plugging eq. (1.39) into eq. (1.38) we have the result

$$R \simeq R_* + \sum_i^{D-1} \int_{N_*}^{N} 2\frac{\phi_{\perp_i}''}{v} e^{\int_{N_*}^{\tilde{N}} M_{\|\|\|} - M_{\perp_i\perp_i} d\tilde{\tilde{N}}} d\tilde{N}. \tag{1.41}$$

and the total isocurvature perturbation S is given by

$$S = \sum_i^{D-1} S_i \simeq \sum_i^{D-1} S_{*i} e^{\int_{N_*}^{N} M_{\|\|\|} - M_{\perp_i\perp_i} d\tilde{N}}, \tag{1.42}$$

where $*$ denotes that a given quantity is to be evaluated at horizon crossing. Continuing

with the approach of ref. [20] it will be helpful to rewrite eqs. (1.41) and (1.42) as

$$\begin{pmatrix} R \\ S_1 \\ \vdots \\ S_{D-1} \end{pmatrix} = \begin{pmatrix} 1 & T_{RS_1} & \cdots & T_{RS_{D-1}} \\ 0 & T_{SS_1} & & \\ \vdots & & \ddots & \\ 0 & & & T_{SS_{D-1}} \end{pmatrix} \begin{pmatrix} R_* \\ S_{1*} \\ \vdots \\ S_{D-1*} \end{pmatrix} \tag{1.43}$$

where the transfer functions T_{RS_i} and T_{SS_i} are given by

$$T_{RS_i}(N_*, N) \equiv \int_{N_*}^{N} 2\frac{\phi''_{\perp_i}}{v} S_i(N_*, \tilde{N}) d\tilde{N}. \tag{1.44}$$

and

$$T_{SS_i}(N_*, N) \equiv e^{\int_{N_*}^{N} M_{\parallel\parallel} - M_{\perp_i \perp_i} d\tilde{N}} \tag{1.45}$$

respectively. To reduce computational effort we substitute the approximation of eq. (1.28) when calculating T_{RS} (1.44). In the cases we tested we found this approximation to be more than satisfactory.

1.3.4 Power spectra and cosmological parameters

We are now finally ready to discuss the evolution of the power spectra. For a general quantity $\mathcal{X}$, the power spectra and cross spectra are defined as

$$P_{\mathcal{X}} \delta^3(\mathbf{k} - \tilde{\mathbf{k}}) \equiv \frac{k^3}{2\pi^2} \langle \mathcal{X}(\mathbf{k}), \mathcal{X}^\dagger(\tilde{\mathbf{k}}) \rangle \tag{1.46}$$

and

$$C_{\mathcal{X}\mathcal{Y}} \delta^3(\mathbf{k} - \tilde{\mathbf{k}}) \equiv \frac{k^3}{2\pi^2} \langle \mathcal{X}(\mathbf{k}), \mathcal{Y}^\dagger(\tilde{\mathbf{k}}) \rangle \tag{1.47}$$

respectively. We do not go into details here but quantizing and solving the perturbed equations (see e.g. ref. [18]) leads us to

$$P_{R_*} \simeq \left(\frac{H_*}{2\pi}\right)^2 \frac{1}{2\epsilon_*} \left[1 + 2(C-1)\epsilon - 2C M_{\parallel\parallel}\right]_*, \tag{1.48}$$

$$P_{S_{i*}} \simeq \left(\frac{H_*}{2\pi}\right)^2 \frac{1}{2\epsilon_*} \left[1 + 2(C-1)\epsilon - 2C M_{\perp\perp}\right]_* \tag{1.49}$$

and

$$C_{RS_{i*}} \simeq \left(\frac{H_*}{2\pi}\right)^2 \frac{1}{2\epsilon_*} \left[-2C M_{\parallel\perp_i}\right]_* \tag{1.50}$$

where $C = 2 - \ln 2 - \gamma \approx 0.7296$ and γ is the Euler–Mascheroni constant. For future use we also introduce the tensor power spectrum which takes the usual form

$$P_{T_*} \simeq 8 \left(\frac{H_*}{2\pi}\right)^2 \left[1 + 2(C-1)\epsilon\right]_*, \tag{1.51}$$

which is conserved for super-horizon modes. We used the above second-order expressions in our computation but as one would expect, there would have been almost no difference had we used first-order approximations.

Applying the transfer matrix eq. (1.43) we finally arrive at one of our most important destinations, namely the power spectra at the end of inflation

$$P_R = P_{R_*} + \sum_i^{D-1} \left(2T_{RS_i} C_{RS_{i*}} + T^2_{RS_i} P_{S_{i*}}\right), \tag{1.52}$$

$$P_S = \sum_i^{D-1} P_{S_i} = \sum_i^{D-1} T^2_{SS_i} P_{S_{i*}} \tag{1.53}$$

and

$$C_{RS_i} = T_{SS_i} C_{RS_{i*}} + T_{RS_i} T_{SS_i} P_{S_{i*}}. \tag{1.54}$$

We see most of our previous comments on super-horizon evolution apply in much the same way to the power spectra. It is now also easy to see one of the reasons why we chose to break our exploration down into two stages. The interesting super-horizon behaviour predominantly comes from the transfer functions. We have seen that the super-horizon modes associated with entropy perturbation evolve independently of one another, each separately affecting the evolution of the adiabatic power spectrum. This means that by making a statistical analysis of one set of entropy perturbations, we can easily see how the statistics will generalize to a larger number of scalar fields.

Now that we finally have the power spectra the hard work is over. From here it is straightforward to find approximations for what we consider the key observables, namely the tensor-to-scalar ratio, spectral indices, and the running. We will evaluate these 55 e-foldings before the end of inflation, taken to be the time that the observed scales crossed the horizon during inflation. We call this the pivot scale N_{pivot}. All observable quantities are henceforth assumed evaluated at this scale.

The tensor-to-scalar ratio r is defined as the ratio of the tensor power spectrum eq. (1.51) to the scalar (curvature) power spectrum eq. (1.52)

$$r \equiv \frac{P_T}{P_R}. \tag{1.55}$$

Note that since the tensor power spectrum is conserved on super-horizon scales, the single-field result provides an upper bound for the multi-field case. We define the spectral index of a power spectrum $P_{\mathcal{X}}$ as

$$n_{\mathcal{X}} \equiv \frac{d \ln P_{\mathcal{X}}}{d \ln k}. \tag{1.56}$$

Note however that the common definition of the scalar spectral index is related to this definition by

$$n_{\rm s} = 1 + n_R. \tag{1.57}$$

We find calculating T_{RS} to be computationally demanding so in practice when calculating the spectral index we do the following:

$$\begin{aligned} \frac{d\ln P_{\mathcal{X}}}{d\ln k} &\simeq \frac{\ln P_{\mathcal{X}}(N_{\rm pivot}+\frac{\Delta N}{2}) - \ln P_{\mathcal{X}}(N_{\rm pivot}-\frac{\Delta N}{2})}{\Delta N}; \\ &\simeq \ln\frac{P_{\mathcal{X}}(N_{\rm pivot}) + P_{\mathcal{X}}(N_{\rm pivot}+1)}{P_{\mathcal{X}}(N_{\rm pivot}-1) + P_{\mathcal{X}}(N_{\rm pivot})}. \end{aligned} \tag{1.58}$$

The running of the spectral index $\alpha_{\mathcal{X}}$ is a straightforward extension of the spectral index, defined as

$$\alpha_{\mathcal{X}} \equiv \frac{dn_{\mathcal{X}}}{d\ln k}, \tag{1.59}$$

and hence we approximate it using the same technique,

$$\frac{dn_{\mathcal{X}}}{d\ln k} \simeq n_{\mathcal{X}}\left(N_{\rm pivot}+1/2\right) - n_{\mathcal{X}}\left(N_{\rm pivot}-1/2\right). \tag{1.60}$$

The minimum number of computations of T_{RS} required to obtain the running in this way is three, which is why we take averages when calculating the spectral index.

We do not consider non-gaussianity in this paper. A methodology for computing it within the same formalism has now been given in ref. [21]; however, as for instance shown in that paper, it would typically be expected to be small in these types of models.

1.4 Findings

1.4.1 Two scalar fields

We performed 5×10^6 runs and obtained 75 successful outcomes in terms of sufficient inflation achieved without subsequent collapse. Table 2.2 summarizes some of the mean values accumulated and shows that our model is in good agreement with observation in all parameters so far tested. Figure 1.2 shows histograms of the curvature spectral index and tensor-to-scalar ratio, a histogram of the number of e-folds and a plot of r against $n_{\rm s}$, colour-coded with the number of e-folds. The last plot also shows the present observational limits from a data compilation including WMAP7 results [22].

Quantity	Result	Observed	Agreement
n_R	-0.06 ± 0.02	-0.027 ± 0.014	Y
α_R	-0.0003 ± 0.0009	-0.022 ± 0.020	Y
$n_{\rm iso}$	0.001 ± 0.13	N/A	N/A
$\alpha_{\rm iso}$	-0.02 ± 0.22	N/A	N/A
r	0.05 ± 0.03	< 0.24 (95% c.l.)	Y
T_{SS}	0.06 ± 0.43	N/A	N/A
T_{RS}	0.8 ± 0.9	N/A	N/A

Table 1.3: Some cosmological parameter constraints.

Planck hopes to measure the tensor-to-scalar ratio with an accuracy of a few hundredths, hence has discovery potential if it is of order 0.1 or so. For this reason it is interesting to note that of the universes not already rejected by the $n_{\rm s}$–r plot, there seems to be a preference for universes with larger r. We also note that all large e-fold universes (green points) lie within the 95% confidence limit and only a couple of blue points are rejected, but more data are needed to conclude whether or not large e-fold universes are favoured within our model. We find this potential trend quite intriguing since it is easy to conceive of measures which give strong weighting to universes with a large number of e-folds, but will not pursue this further in this paper.

We need to clarify what *agreement* actually means in this context. Both the observed data and the results of our experiment are given in terms of a distribution of values for the observables. As it happens, the statistical spread of each is comparable at present, with a substantial area of overlap; one can therefore conclude that there is a good chance of a single realization from our model giving predictions in accord with the observations. If a model data point lies outside the range observed, then it simply indicates that we do not live in that universe and such data would not necessarily act against the model. Future observations hope to home in on a single value for each observable to ever increasing accuracy, which will clearly soon have higher precision than our model predictions. Provided the observationally-favoured region remains within the envelope predicted by the model, however, such higher-precision measurements will not in themselves be able to argue against the model, at least without further model refinements for instance around the choice of measure and anthropic arguments. At this point we then must invoke the Copernican principle over this remaining anthropically reduced landscape and say we expect to

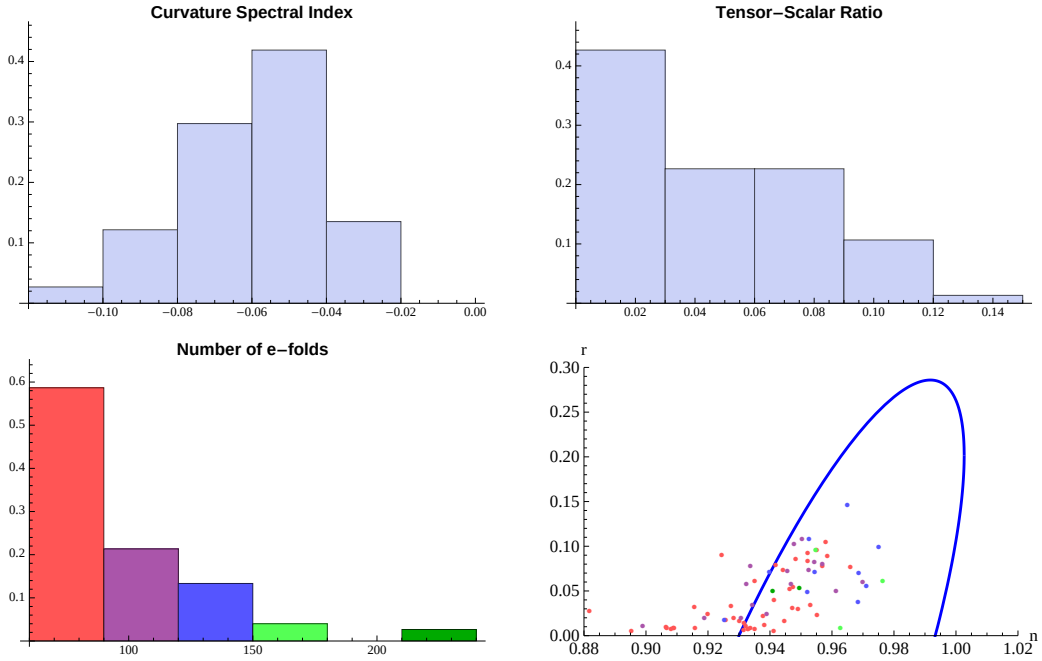

Figure 1.2: Histograms of the curvature spectral index, tensor-to-scalar ratio, and e-folds, plus a plot of the tensor-to-scalar ratio against the spectral index where the points have been colour-coded according to the number of e-folds. The blue line on the n_s–r plot is the 95% confidence contour from WMAP+BAO+H_0.

observe values according to the statistics of the model distribution. It is in this sense that we say our results are in agreement with observation.

The histogram of e-folds, Fig. 1.2, shows that the number of universes drops off rapidly with the number of e-folds. We rejected universes with less than 60 e-folds of inflation but in the process of doing so we found that sufficient inflation was a very rare process, testing millions of universes to find tens of candidates. This is not a new result for "stringy" models. For instance ref. [23] investigated one of the most rigorously derived inflationary models from string theory, namely brane–anti-brane inflation, and found much the same thing, while ref. [24] found the same result for tunnelling landscape models. For our model though this is of no concern at all. We are not worried about what proportion of field space allows for anthropically suitable conditions, only that there exists *some* proportion.

Moving on to the results of the calculations done in the previous section, we look at the role played by isocurvature perturbations in modifying the adiabatic perturbations from their horizon-crossing value. Figure 1.3 confirms that the curvature power spectrum always increases, and for a non-negligible proportion of the time the fractional change is very large. Looking at the histograms for the transfer functions we see that the isocurvature perturbations are an important source, since at horizon exit they are of the same order as

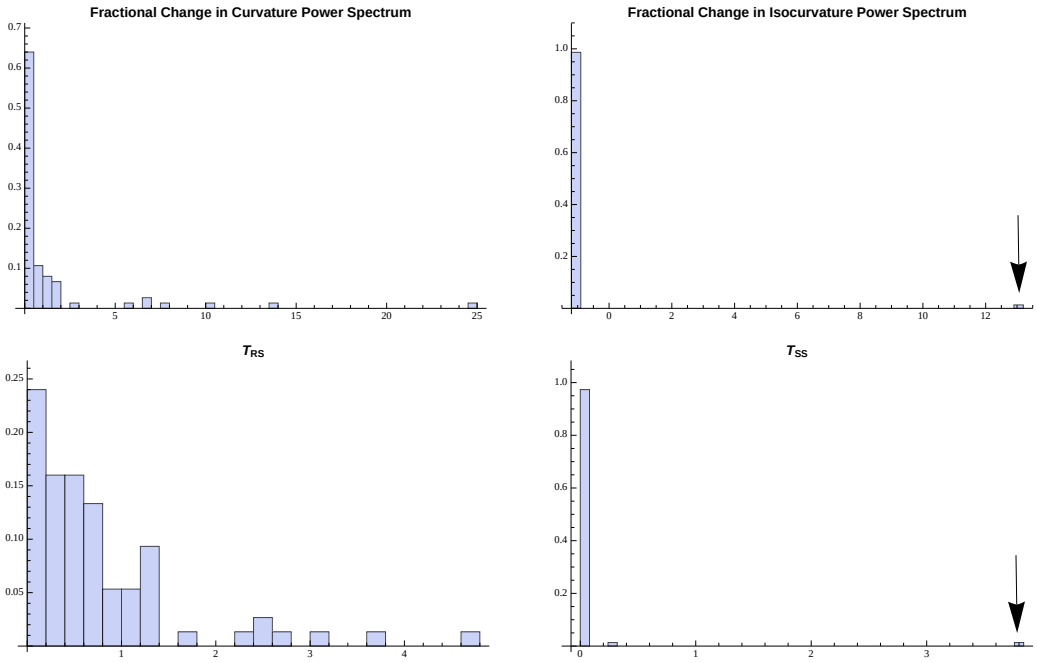

Figure 1.3: Histograms of the fractional change in the curvature and isocurvature power spectra accompanied by histograms for the transfer functions. Arrows indicate Universe 1832942.

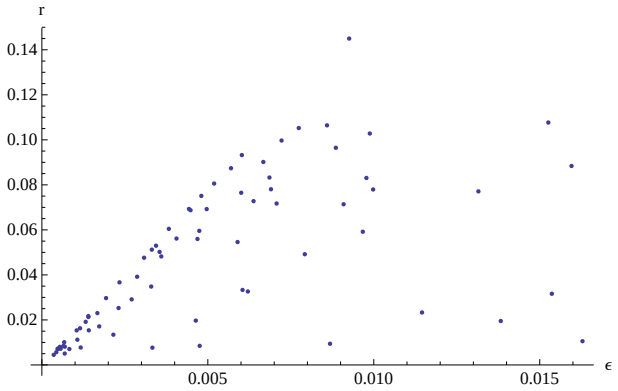

Figure 1.4: Plot of r against ϵ, demonstrating the consistency relation $r = -8n_{\rm T} = 16\epsilon$ becoming an inequality.

the curvature power spectrum and it is not particularly uncommon for T_{RS} to be significant or even greater than one.

One consequence of the super-horizon fuelling of adiabatic perturbations is that we have explicit violation of the consistency relation, as demonstrated in the plot of r against ϵ in Fig. 1.4 (the tensor spectral index in these models is given by $n_{\rm T} = -2\epsilon$ as usual). Substituting eqs. (1.51) and (1.52) into eq. (1.55), we have

$$r = \frac{16\epsilon}{1 + 4CT_{RS}\phi_\perp''/v + T_{RS}^2}. \tag{1.61}$$

So we see we have a line of points corresponding to $r = 16\epsilon$ as in the single scalar field case but with many points dropping below the line where T_{RS} and the turn rate have

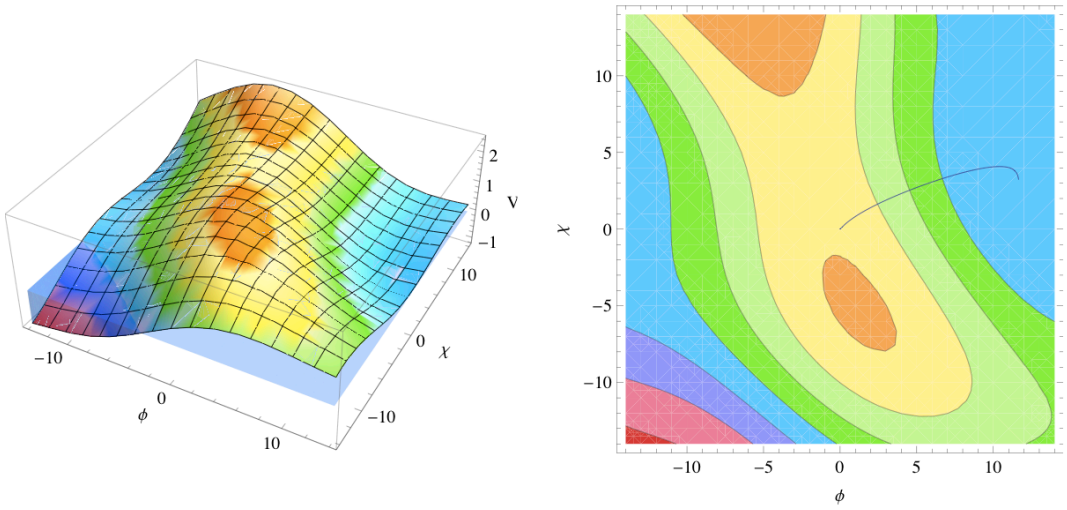

Figure 1.5: Example potential giving rise to $T_{RS} = 3.6$, and the corresponding evolution in the ϕ–χ plane.

suppressed the value of r. Hence the relation becomes an inequality when there are extra degrees of freedom, as first described in ref. [25].

As an example of the sort of situation that can give rise to large T_{RS} values we include Fig. 1.5. As mentioned earlier, generally the dominant effect is the turn rate and while there are a number of types of trajectory that lead to large T_{RS}, in this case we see that it is the cumulative effect of a fairly continuously curved trajectory spiralling its way to a minimum.

As pointed out in ref. [1] (see refs. [22, 26–30] for primary references), the CMB places strong observational constraints against the existence of isocurvature perturbations. As such, any multi-field model must either generate no isocurvature perturbations at horizon exit, or must find a way to make them disappear after horizon exit but before horizon entry. Our model falls nicely into the second category. Fig. 1.3 shows that the transfer function T_{SS} consistently causes the isocurvature power spectrum to go to zero after horizon exit (except in one case which we will discuss in a moment). Referring back to eq. (1.45) and Table 1.2, we see that pure damping occurs when $M_{|||} < 0$ and $M_{\perp\perp} > 0$; we find that this scenario is typically the case, an example of which is shown in Fig. 1.6. This result is not particularly surprising since one consequence of our choice of measure is that hilltop inflation is a very rare process, thus most inflation scenarios occur in the vicinity of a minimum. In such cases, at least to some extent the trajectory will be moving towards that minimum. We then have that perpendicular curvature will usually be positive and since the minimum must be very close to $V = 0$, the log of the potential will have negative

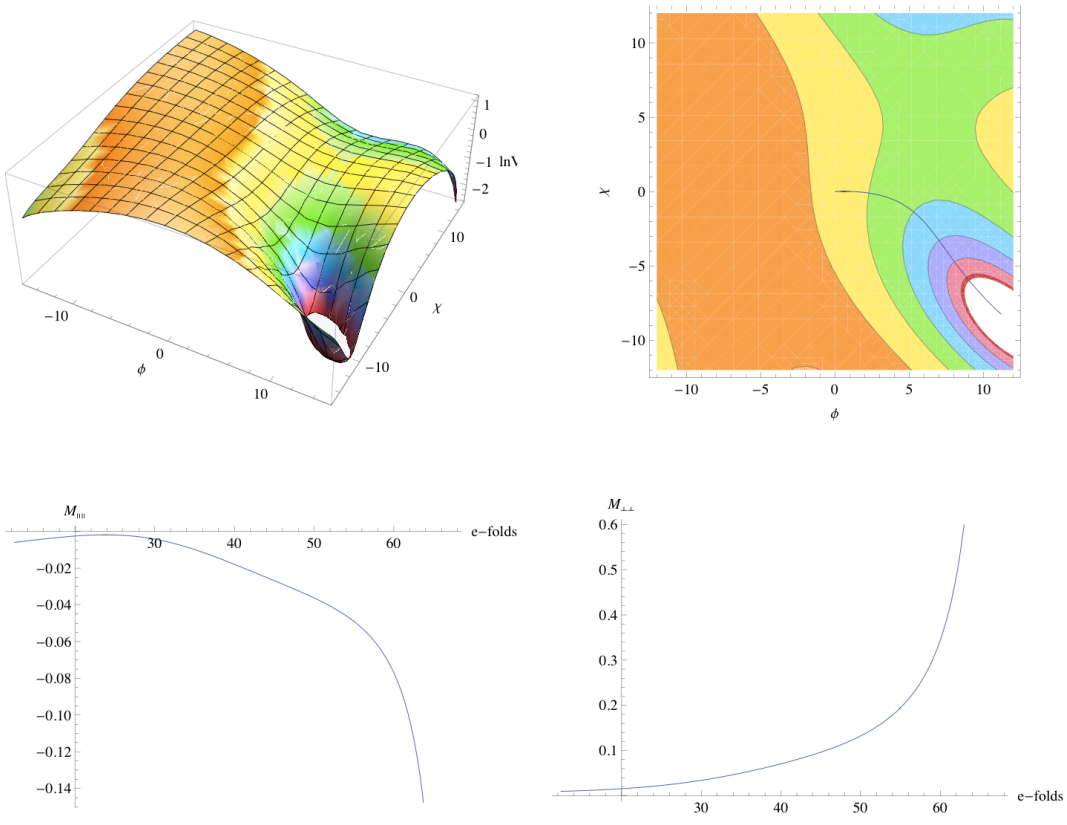

Figure 1.6: Example plot of $\ln V$, the trajectory, and the relevant mass matrix components, showing why T_{SS} tends to be so small.

curvature in the direction of motion.

1.4.2 The curious case of Universe 1832942

Figure 1.3 shows one dramatic exception to the damping of the isocurvature perturbations just described. In one case the isocurvature perturbations were actually fuelled rather than damped. Fig. 1.7 shows plots of the potential, its logarithm, the trajectory, and a plot of the parallel and perpendicular components of the mass matrix near the end of inflation for this case which we call Universe 1832942. Remembering Table 1.2, we see that for the majority of the evolution the isocurvature perturbations are damped but near the end of the evolution the trajectory overshoots the minimum causing a sharp reversal in direction as it reaches the far side of the valley. As the trajectory goes through this sharp turn at low V the arguments above reverse, but we see that the dominant effect in this case seems to be the change in curvature as the trajectory traverses the minimum.

We have severe violation of SRST so our calculations of observables are no longer reli-

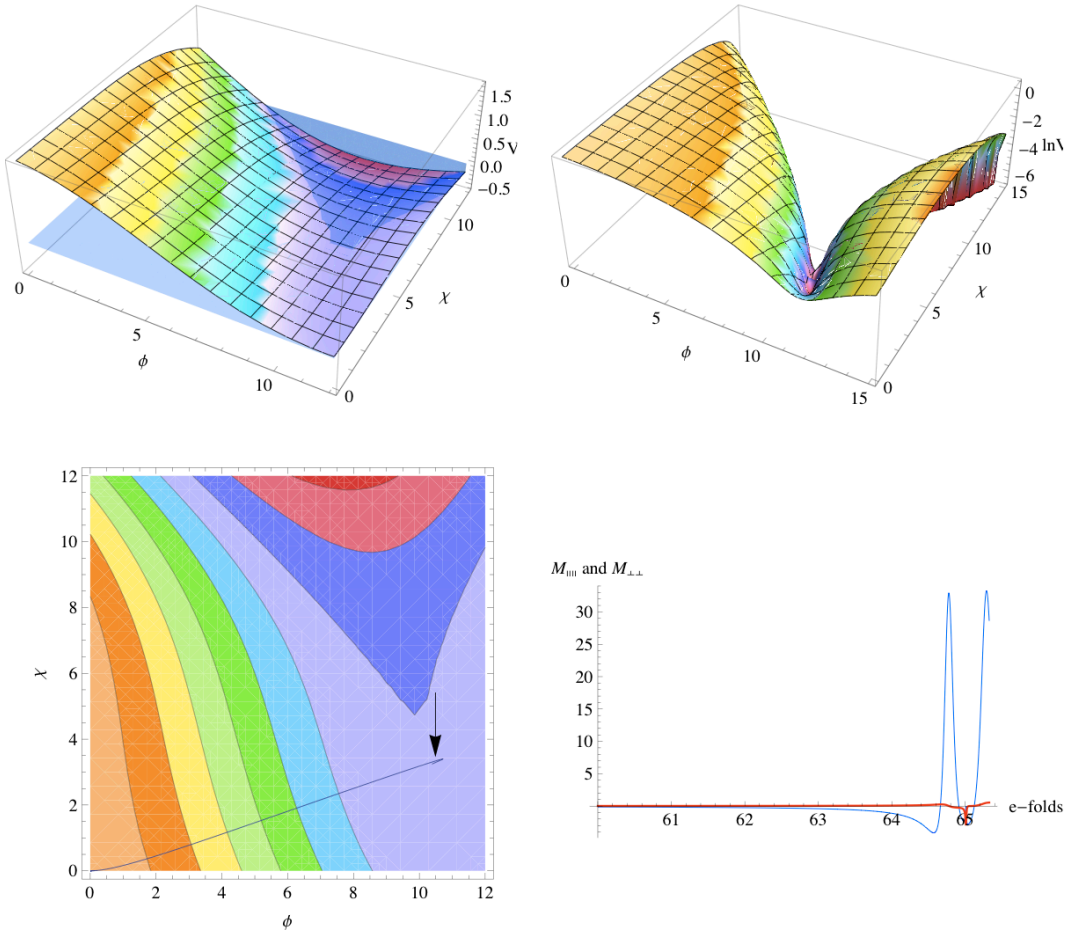

Figure 1.7: Plots of the potential, log of the potential, trajectory and relevant components of the mass matrix ($M_{||||}$ is blue, $M_{\perp\perp}$ is red) for the one case we found, Universe 1832942, where the isocurvature perturbations were fuelled rather than going to zero. The arrow indicates where the trajectory turns back on itself.

able, but we find the values $n_{\rm s} = 0.94$ and $r = 0.005$, with the low r value resulting from a significant evolution of the power spectrum after horizon exit of 108%. We see that Universe 1832942 sits within the 95% confidence contour of Fig. 1.2, but we remind the reader that this confidence limit does not take surviving isocurvature modes into consideration.

1.4.3 How will observables change with D?

As was mentioned at the beginning of this paper, we feel much of the phenomenology of a D scalar field landscape is manifest with just two scalar fields. This is true in terms of the types of phenomena that exist, but can we make any comments on how the values of observables might change with D?

The short answer is no. From a statistical standpoint we know that the mean values

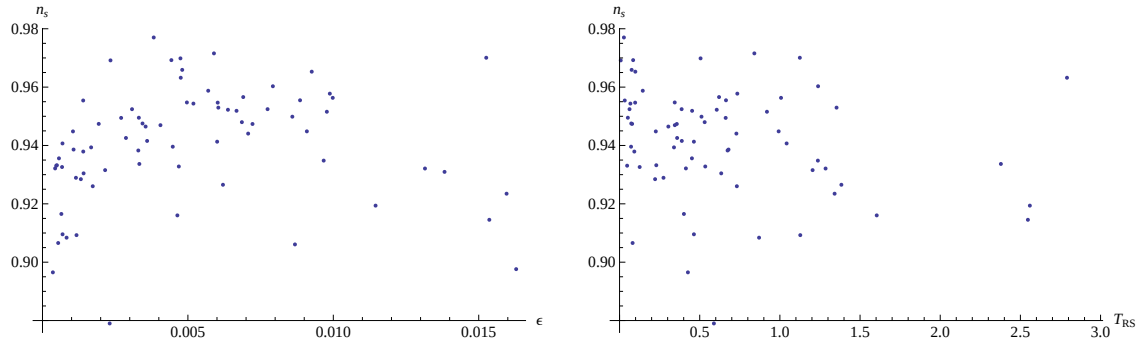

Figure 1.8: Correlations of $n_{\rm s}$ with ϵ and T_{RS}.

of ϵ and T_{RS} will both increase with D, so one might think that parameters such as $n_{\rm s}$ and r could tend to some value as a result of one parameter coming to dominate. This may well be true but how so is not obvious. The lack of any strong correlation in Fig. 1.8 for $n_{\rm s}$ with respect to ϵ or T_{RS} leads us to think that predicting how $n_{\rm s}$ will change with D is non-trivial. That said, there is an important distinction between how ϵ and T_{RS} will change with D. T_{RS} is unbounded, in that as you increase D you just get an increasing sum of T_{RS_i} terms; this has both a cumulative effect and increases the statistical chance of encountering a large T_{RS_i}. The value of ϵ in contrast is capped, if for no other reason because inflation will end if ϵ is too large, but it may not ever even increase that much.

There are a number of examples in the literature where a large number of scaler fields can actually lead to a decrease in ϵ, one example being assisted inflation [31]. So for cases where the absolute values of ϵ and T_{RS} are important we can hazard a guess and say that for sufficiently large D eventually the dominant effect will be T_{RS}. This is the case for the tensor-to-scalar ratio and remembering Fig. 1.4 and eq. (1.61) we would thus expect increasingly severe violation of the consistency relation, with a suppression of r as we move to higher D. We will investigate this as part of a future study of the D-dimensional case.

1.5 Discussion

We have investigated the properties of inflationary trajectories in a toy-model landscape with two scalar fields, in which we fully track the effects of isocurvature perturbations. We have focussed on the well-motivated case where the variations in the potential correspond to masses of the order of $M_{\rm Pl}$. Trajectories with sufficient inflation are rare, with one

successful run per roughly 10^5 randomly generated potentials, but the successful runs are typically in good accord with observational constraints on the perturbations, mostly lying within the region of the n_s–r plane delineated by the WMAP+BAO+H_0 95% confidence contour.

We find that isocurvature perturbations naturally go to zero after horizon exit. This is a direct result of the typical geometry of the landscape in the vicinity of an inflationary trajectory. For isocurvature perturbations to not go to zero one requires an unstable trajectory, which happened only in one of our successful realizations. Nevertheless, in many cases the isocurvature perturbations have a lasting consequence as we find significant fueling of the adiabatic perturbations from the entropy perturbations to be a fairly common occurrence. Because of this, we find that the tensor-to-scalar amplitude often lies below the level that would be predicted by the single-field consistency equation. One might speculate that this effect is likely to become more prominent as the number of scalar fields is increased, both from a statistical standpoint and as a purely cumulative effect, since such evolution is closely linked with turns in the trajectory. We plan to investigate this dependence in future work.

While our work significantly extends previous comparable analyses in the literature, such as ref. [4], it nevertheless remains rudimentary and many further steps are needed if it is to become more realistic, beyond the issue of the number of scalar fields. Most pressing is a proper treatment of the way the measure problem affects our work, particularly in combination with anthropic selection. At the moment we have largely ignored this and obtained results which are based on a uniform distribution of initial conditions, rather than as drawn from random late-time observers. It would be reasonable to believe that this would typically enhance the likelihood that our Universe emerged from the vicinity of a hilltop region, as those are the regions which subsequently undergo the most inflation.

References

[1] C.P. Burgess. "Lectures on Cosmic Inflation and its Potential Stringy Realizations". In: *Class.Quant.Grav.* 24 (2007), S795. arXiv:0708.2865 [hep-th] (cit. on pp. 27, 48).

[2] Petr Horava and Edward Witten. "Heterotic and type I string dynamics from eleven-dimensions". In: *Nucl.Phys.* B460 (1996), pp. 506–524. arXiv:hep-th/9510209 [hep-th] (cit. on p. 27).

[3] Leonard Susskind. "The Anthropic landscape of string theory". In: (2003). arXiv:hep-th/0302219 [hep-th] (cit. on pp. 27, 28).

[4] Max Tegmark. "What does inflation really predict?" In: *JCAP* 0504 (2005), p. 001. arXiv:astro-ph/0410281 [astro-ph] (cit. on pp. 28–30, 32, 33, 52).

[5] Amir Aazami and Richard Easther. "Cosmology from random multifield potentials". In: *JCAP* 0603 (2006), p. 013. arXiv:hep-th/0512050 [hep-th] (cit. on pp. 29, 31).

[6] Sash Sarangi, Gary Shiu and Benjamin Shlaer. "Rapid Tunneling and Percolation in the Landscape". In: *Int.J.Mod.Phys.* A24 (2009), pp. 741–788. arXiv:0708.4375 [hep-th] (cit. on pp. 29, 31).

[7] S.-H. Henry Tye. "A New view of the cosmic landscape". In: (2006). arXiv:hep-th/0611148 [hep-th] (cit. on pp. 29, 31).

[8] S.-H. Henry Tye, Jiajun Xu and Yang Zhang. "Multi-field Inflation with a Random Potential". In: *JCAP* 0904 (2009), p. 018. arXiv:0812.1944 [hep-th] (cit. on p. 31).

[9] S.-H. Henry Tye and Jiajun Xu. "A Meandering Inflaton". In: *Phys.Lett.* B683 (2010), pp. 326–330. arXiv:0910.0849 [hep-th] (cit. on p. 31).

[10] Soo A Kim and Andrew R Liddle. "Nflation: multi-field inflationary dynamics and perturbations". In: *Phys.Rev.* D74 (2006), p. 023513. arXiv:astro-ph/0605604 [astro-ph] (cit. on p. 31).

[11] Steven Weinberg. "Anthropic Bound on the Cosmological Constant". In: *Phys.Rev.Lett.* 59 (1987), p. 2607 (cit. on p. 33).

[12] Jason Kumar. "A Review of distributions on the string landscape". In: *Int.J.Mod.Phys.* A21 (2006), pp. 3441–3472. arXiv:hep-th/0601053 [hep-th] (cit. on p. 33).

[13] Alexander Vilenkin. "A Measure of the multiverse". In: *J.Phys.* A40 (2007), p. 6777. arXiv:hep-th/0609193 [hep-th] (cit. on p. 33).

[14] Raphael Bousso. "Precision cosmology and the landscape". In: (2006). arXiv:hep-th/0610211 [hep-th] (cit. on p. 33).

[15] Delia Schwartz-Perlov and Alexander Vilenkin. "Measures for a Transdimensional Multiverse". In: *JCAP* 1006 (2010), p. 024. arXiv:1004.4567 [hep-th] (cit. on p. 33).

[16] Raphael Bousso et al. "Boundary definition of a multiverse measure". In: *Phys.Rev.* D82 (2010), p. 125032. arXiv:1005.2783 [hep-th] (cit. on p. 33).

[17] Andrei Linde and Mahdiyar Noorbala. "Measure Problem for Eternal and Non-Eternal Inflation". In: *JCAP* 1009 (2010), p. 008. arXiv:1006.2170 [hep-th] (cit. on p. 33).

[18] Courtney M. Peterson and Max Tegmark. "Testing Two-Field Inflation". In: *Phys.Rev.* D83 (2011), p. 023522. arXiv:1005.4056 [astro-ph.CO] (cit. on pp. 34, 36–40, 42).

[19] Viatcheslav F. Mukhanov, H.A. Feldman and Robert H. Brandenberger. "Theory of cosmological perturbations. Part 1. Classical perturbations. Part 2. Quantum theory of perturbations. Part 3. Extensions". In: *Phys.Rept.* 215 (1992), pp. 203–333 (cit. on p. 39).

[20] David Wands et al. "An Observational test of two-field inflation". In: *Phys.Rev.* D66 (2002), p. 043520. arXiv:astro-ph/0205253 [astro-ph] (cit. on pp. 40–42).

[21] Courtney M. Peterson and Max Tegmark. "Non-Gaussianity in Two-Field Inflation". In: *Phys.Rev.* D84 (2011), p. 023520. arXiv:1011.6675 [astro-ph.CO] (cit. on p. 44).

[22] E. Komatsu et al. "Seven-Year Wilkinson Microwave Anisotropy Probe (WMAP) Observations: Cosmological Interpretation". In: *Astrophys.J.Suppl.* 192 (2011), p. 18. arXiv:1001.4538 [astro-ph.CO] (cit. on pp. 44, 48).

[23] Loison Hoi and James M. Cline. "How Delicate is Brane-Antibrane Inflation?" In: *Phys.Rev.* D79 (2009), p. 083537. arXiv:0810.1303 [hep-th] (cit. on p. 46).

[24] Ben Freivogel et al. "Observational consequences of a landscape". In: *JHEP* 0603 (2006), p. 039. arXiv:hep-th/0505232 [hep-th] (cit. on p. 46).

[25] Misao Sasaki and Ewan D. Stewart. "A General analytic formula for the spectral index of the density perturbations produced during inflation". In: *Prog.Theor.Phys.* 95 (1996), pp. 71–78. arXiv:astro-ph/9507001 (cit. on p. 48).

[26] Patrick Crotty et al. “Bounds on isocurvature perturbations from CMB and LSS data”. In: *Phys.Rev.Lett.* 91 (2003), p. 171301. arXiv:astro-ph/0306286 [astro-ph] (cit. on p. 48).

[27] K. Moodley et al. “Constraints on isocurvature models from the WMAP first-year data”. In: *Phys.Rev.* D70 (2004), p. 103520. arXiv:astro-ph/0407304 [astro-ph] (cit. on p. 48).

[28] David Parkinson et al. “Testing for double inflation with WMAP”. In: *Phys.Rev.* D71 (2005), p. 063524. arXiv:astro-ph/0409071 [astro-ph] (cit. on p. 48).

[29] Maria Beltran et al. “Bounds on CDM and neutrino isocurvature perturbations from CMB and LSS data”. In: *Phys.Rev.* D70 (2004), p. 103530. arXiv:astro-ph/0409326 [astro-ph] (cit. on p. 48).

[30] Hannu Kurki-Suonio, Vesa Muhonen and Jussi Valiviita. “Correlated primordial perturbations in light of CMB and LSS data”. In: *Phys.Rev.* D71 (2005), p. 063005. arXiv:astro-ph/0412439 [astro-ph] (cit. on p. 48).

[31] Andrew R. Liddle, Anupam Mazumdar and Franz E. Schunck. “Assisted inflation”. In: *Phys.Rev.* D58 (1998), p. 061301. arXiv:astro-ph/9804177 [astro-ph] (cit. on p. 51).

Paper 2

Multi-field inflation with random potentials: field dimension, feature scale and non-Gaussianity

Jonathan Frazer and Andrew Liddle

We explore the super-horizon evolution of the two-point and three-point correlation functions of the primordial density perturbation in randomly-generated multi-field potentials. We use the Transport method to evolve perturbations and give full evolutionary histories for observables. Identifying the separate universe assumption as being analogous to a geometrical description of light rays, we give an expression for the width of the bundle, thereby allowing us to monitor evolution towards the adiabatic limit, as well as providing a useful means of understanding the behaviour in $f_{\rm NL}$. Finally, viewing our random potential as a toy model of inflation in the string landscape, we build distributions for observables by evolving trajectories for a large number of realisations of the potential and comment on the prospects for testing such models. We find the distributions for observables to be insensitive to the number of fields over the range 2 to 6, but that these distributions are highly sensitive to the scale of features in the potential. Most sensitive to the scale of features is the spectral index, with more than an order of magnitude increase in the dispersion of predictions over the range of feature scales investigated. Least sensitive was the non-Gaussianity parameter $f_{\rm NL}$, which was consistently small; we found no examples of realisations whose non-Gaussianity is capable of being observed by any planned experiment.

2.1 Why random potentials?

2.1.1 First reason

With the prospect of improved data from the Planck mission fast approaching, there has been a lot of interest in finding inflationary models exhibiting specific observable footprints. Large non-Gaussianity signals peaking at various shapes is one example, another being features in the primordial power spectrum. While this is a crucial step towards understanding what observables are specific to a particular model, often the set-up can be somewhat contrived and to gain understanding as to whether such behaviour is a general feature of the model, one may need to invoke Monte Carlo techniques. In such a situation it may be helpful to employ some element of 'randomness' at the level of the construction of the model.

For example, a popular model of inflation coming from string theory is Dirac–Born–Infeld inflation. The Lagrangian describing DBI-inflation is

$$\mathcal{L} = -T(\phi)\sqrt{1 - \frac{2X}{T(\phi)}} + T(\phi) - V(\phi), \tag{2.1}$$

where $X = -\frac{1}{2}g_{\mu\nu}\partial^\mu\phi\partial^\nu\phi$ and $T(\phi)$ is the brane tension. If the D3-brane velocity approaches its limiting speed

$$1 - \frac{2X}{T(\phi)} \to 0, \tag{2.2}$$

then a period of inflation can occur. This model has interesting observational consequences as the sound speed can become small and hence, since $f_{\rm NL}^{\rm (eq)} \sim 1/c_{\rm s}^2$, lead to large equilateral $f_{\rm NL}^{\rm (eq)}$. However the above Lagrangian also admits inflation by other means. In Ref. [1] a rather sophisticated model of brane inflation was investigated, where to simulate the effect of the bulk in different compactifications, random coefficients were used. In this set-up, conditions for DBI inflation were never encountered; instead inflection-point slow-roll inflation was vastly more common. We therefore see that while the DBI effect certainly gives an interesting observational footprint, there is no reason to believe this is a generic feature of brane models of inflation.[1]

[1] As pointed out in Ref. [1], this result is not conclusive since, rather importantly, their investigation did not go all the way to the tip of the throat. Nevertheless we feel this example illustrates the point in hand.

2.1.2 Second reason

On a more ambitious note, string theory seems to predict the existence of a landscape [2, 3], where, in the low-energy approximation, different regions may be characterised by the values of a large number of scalar fields. The consequence of this is that we have some very complicated potential $V(\phi_1, ..., \phi_d)$ with a large number of minima each corresponding to a different metastable vacuum energy. This implies that instead of trying to predict the values of observables, we should be trying to predict probability distributions for them. Indeed, as we will now discuss, this is the case not just for string theory but for any model with multiple light fields.

Most work on the consequences of a landscape has focussed on the measure problem (see Ref. [4] for a recent overview) but if the observational consequences of such a model are ever to be understood, then there are other challenges to contend with. In order for a landscape model (any model where the scalar potential has more than one minimum, or for the purposes of this discussion, even just one minimum but multiple fields) to be predictive, three questions need to be addressed:

1. *What are the statistical properties of the landscape*
2. *What are the selection effects from cosmological dynamics*
3. *What are the anthropic selection effects*

The measure problem relates to the question of handling the numerous infinities which turn up. Taking the example of slow-roll inflation,[2] any model of multi-field inflation suffers from an uncountably infinite set of choices for initial conditions. In general one needs to assume that, one way or another, at some point our region of spacetime experienced field values displaced from our local minimum. This corresponds to a single realisation of initial conditions (plus quantum scatter) that gave an anthropically suitable inflationary trajectory, which subsequently found its way to our local minimum. In order to make predictions we need to ask what proportion of the whole universe finds itself in this situation, i.e. what proportion of an infinite space finds itself in one of an infinite set of initial conditions. The ratio is ill-defined without a measure.

[2] Most discussion in this area focuses on the scenario of inflation coming from tunnelling between metastable vacua but as we discuss here, the problem is much more general than that, affecting even the most pedestrian of inflationary set-ups.

However overcoming this formidable task is not the end of it. Even with a solution to this measure problem we are still left with a considerable challenge. A solution to this issue is likely not to give us a specific set of initial conditions for a given model but a probability distribution for them. If all we can hope for is a statistical description of initial conditions, then in turn we only have a statistical description of inflationary trajectories and so, rather than calculating single values for observables, we should be calculating their distributions! The shape of these distributions will in part be determined by the model. This last point can, at least in some respects, be studied in its own right without a detailed knowledge of the string landscape or the measure problem. In this paper we take inspiration from the string landscape and study characteristics of these distributions in the context of a potential with multiple fields, containing a large number of vacua.

An early study of the possible consequences of this landscape picture for slow-roll inflation was carried out by Tegmark [5], who generated a large number of random one-dimensional potentials and explored the inflationary outcomes. In Ref. [6] we extended this to two fields to investigate the effect of entropy modes on super-horizon evolution. As already mentioned, in Ref. [1] a similar analysis was done for a six-field brane inflation model with random terms arising in the contribution coming from the bulk, where although the super-horizon effects were not analysed, both reassuringly and rather excitingly, qualitatively similar emergent behaviour was identified to that found in Ref. [6]. In this paper we further extend our work in Ref. [6] to a larger number of fields and a broader range of potentials, as well as obtaining results for the non-Gaussianity $f_{\rm NL}$. The aim is to gain insight into the origin and limits of emergent behaviour.

2.2 Architecture

2.2.1 Not the most general Fourier series

We construct our potential following an approach similar to Refs. [5, 6]. We use a random function of the form

$$V(\phi) = m_{\rm v}^4 \sum_{1<k_i<k_{\rm max}} \left[a_{\mathbf{k}} \cos\left(\frac{\mathbf{k}.\phi}{m_{\rm h}}\right) + b_{\mathbf{k}} \sin\left(\frac{\mathbf{k}.\phi}{m_{\rm h}}\right)\right] \tag{2.3}$$

where ϕ is the vector ϕ_i with i running from 1 to d, as is the vector $\mathbf{k}$ and $m_{\rm v}$ and $m_{\rm h}$ are the vertical and horizontal masses respectively. The summation in k_i means d summations take

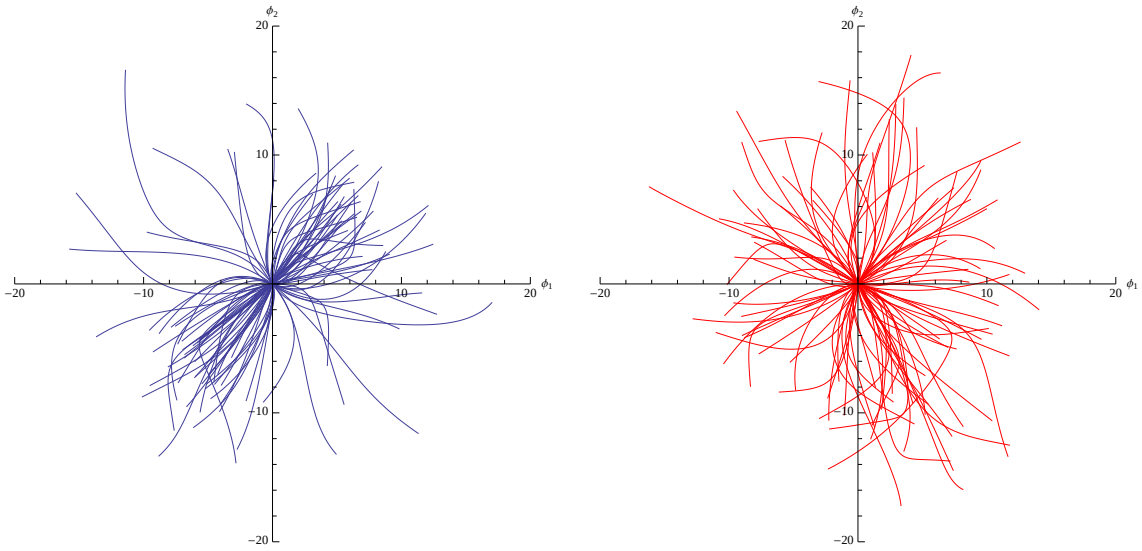

Figure 2.1: Example trajectories for our potential (blue) and Fourier series (red) for two-field model with $k_{\rm max} = 3$.

place where in each case the summation runs from $k_i = 1$ to $k_i = k_{\rm max}$. The amplitudes $a_{\mathbf{k}} \equiv a_{k_1,\ldots,k_d}$ are independent Gaussian random variables with zero mean and standard deviation

$$\sigma = e^{-\mathbf{k}.\mathbf{k}/k_{\rm max}\, d}, \tag{2.4}$$

Due to computational limitations we cannot make $k_{\rm max}$ sufficiently large to see the effect of the central limit theorem come into play. So rather than having a variance of order unity, we control the variance in the above manner. While this is a helpful thing to do computationally, one needs to bear this in mind when considering principles of effective field theory. We will return to this discussion shortly.

The potentials we simulate are periodic with periodicity scale $2\pi m_{\rm h}$, and we can only expect reasonable results if the field trajectory spans a distance in field space less than the periodicity of the random function. This turns out to always be the case.

Note that summing the potential this way means we are not using the most general Fourier series. As shown in Fig. 2.1, by restricting the summations over each k_i to non-negative values we sacrifice statistical d-spherical symmetry but in doing so we are able to build an observationally indistinguishable potential out of a fraction of the number of terms (see Table 2.1 for the number of terms in the series for various d and $k_{\rm max}$ values).

	Our Potential						Fourier Series					
Fields d	2	2	4	4	6	6	2	2	4	4	6	6
$k_{\max}$	3	5	3	5	3	5	3	5	3	5	3	5
# of terms	18	50	162	1250	1458	31250	98	242	4802	29282	235298	many

Table 2.1: Summary of how the number of terms in the potential changes with the truncation $k_{\max}$ and number of fields d for Fourier series potential and our reduced version.

2.2.2 Experiment-specific considerations

As discussed, any model of inflation where the potential has multiple minima predicts a probability distribution for the cosmological parameters. We wish to compute this distribution for various potentials of the above form. To do this we perform the same experiment as that performed in Refs. [5, 6]:

1. Generate a random potential $V(\phi)$. Start at $\phi = (0, 0)$ with initial field velocity set by the slow-roll condition.
2. If $V(0, 0) < 0$ then reject model, otherwise evolve to find the field trajectory.
3. If model gets stuck in eternal inflation, reject.
4. Once the model stops inflating, if the number of e-folds of inflation $N < 60$ we reject as insufficient inflation occurred, otherwise calculate observables.
5. Repeat steps 1-4 many times to obtain a statistical sample.
6. (Change some assumptions and do it all again.)

Note that due to our potential being statistically invariant under translation, generating multiple realisations of the potential and starting at the origin is equivalent to taking a single realisation and scanning over initial conditions. If we abandoned the slow-roll condition for the initial velocity there would be additional degrees of freedom, but we have tested that these have no impact by carrying out runs with zero initial velocity.

In Ref. [6], taking the final minimum as the ultimate vacuum energy, to give an approximately anthropically suitable solution [7] we had an additional cut stipulating the final vacuum energy must be positive to avoid subsequent collapse. This, in conjunction with the rejection of eternally inflating vacua, was found to be an extremely severe cut, in some cases reducing the proportion of otherwise viable solutions from 0.06 to more like

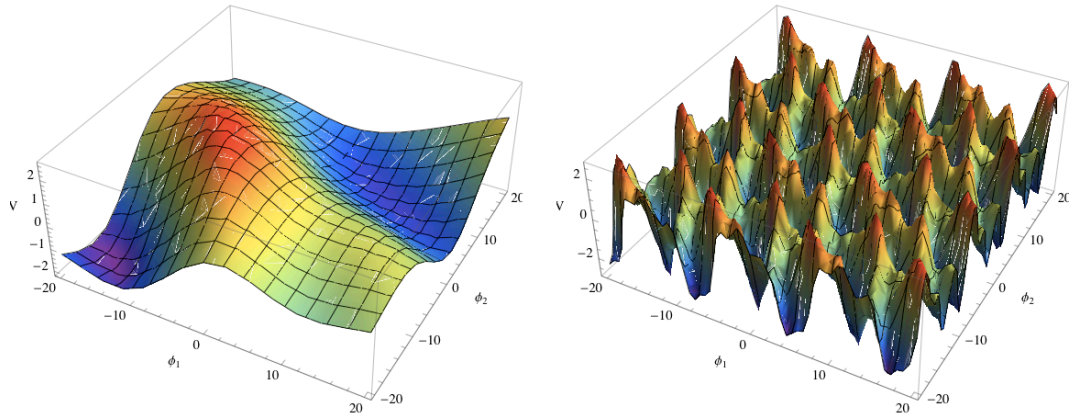

Figure 2.2: Example of two-field potentials with $m_{\rm h} = 15.8\, M_{\rm Pl}$ and $m_{\rm h} = 2.0\, M_{\rm Pl}$ respectively.

2×10^{-5}. In this paper we abandon this cut, to enable us to explore more featured potentials which would not otherwise be computationally accessible. We found this to be of little consequence for observables. An explanation for this is that the two models may differ only in the nature of the post-inflationary evolution of the trajectory, which has no effect on the evolution of observable quantities.

The other consideration regarding the experimental set-up is at what value to set the vertical and horizontal mass scales $m_{\rm v}$ and $m_{\rm h}$. The vertical mass has little dynamical impact and only affects the amplitude of the observed power spectrum by a factor and not other observables. For this reason, rather than fixing $m_{\rm v}$ we adjust it on a case-by-case basis such that the amplitude at horizon exit is $P_\zeta^* = 2 \times 10^{-5}$.

The horizontal mass $m_{\rm h}$ is more interesting. As previously discussed, motivated by the aim of minimising the number of terms in the potential for a given dynamical behaviour, the random coefficients are chosen in such a way as to make the potential essentially insensitive to truncation. This set-up means that $m_{\rm h}$ is our key parameter in adjusting how featured the potential is. As the examples in Fig. 2.2 show, adjusting the scale of features affects the length scale $\Delta\phi$ of the inflationary distance in field space. We will discuss motivation from theory for this length scale next, but it is important we understand its implications for predictability and thus we shall be showing results for a range of $m_{\rm h}$ values.

2.2.3 Basic considerations from effective field theory

Generally one expects that the inflationary potential can be well described by an effective theory containing non-renormalizable contributions coming from integrating out massive fields.[3] For instance, for a single-field model one can write

$$V(\phi) = V_0 + \frac{1}{2}m^2\phi^2 + M\phi^3 + \frac{1}{4}\lambda\phi^4 + \sum_{d=5}^{\infty}\lambda_d M_{\rm Pl}^4\left(\frac{\phi}{M_{\rm Pl}}\right)^d, \tag{2.5}$$

where the terms in the summation are non-renormalizable. One expects the masses in the summation to be at or even well below the Planck mass as, in analogy to the argument from W–W scattering for a Higgs around 1 TeV, there needs to be something to unitarize graviton–graviton scattering. There is no good reason to assume the inflaton does not couple to these extra degrees of freedom. To do so is to make a strong assumption about quantum gravity which is hard to justify, and thus we expect $\lambda_d \sim 1$. If we categorise inflation models as large field, $|\Delta\phi| \gg M_{\rm pl}$, medium field $|\Delta\phi| \sim M_{\rm pl}$ and small field $|\Delta\phi| \ll M_{\rm pl}$, then this sort of reasoning indicates small and perhaps medium field models should be considered more realistic as terms in the summation are suppressed, while to have a large-field model, one needs to justify additional symmetries to protect the flatness of the potential against the otherwise increasingly large series contributions. Crudely speaking we can think of our choice of $m_{\rm h}$ as corresponding to a decision on what energy scales we are integrating out.

Finally, we would like to consider the number of fields to be included in the model. Historically a lot of focus has been given to single-field models simply because they are the most basic inflationary set-up, but this is not what is best motivated from the field theory perspective. As already mentioned, a single-field model occurs when one degree of freedom is much lighter than all the others. This means one can integrate out the other degrees of freedom provided they are sufficiently massive, but there is no good reason to believe this is necessarily the case. For example, in string theory the contributing massive fields include stabilised moduli. Work on flux compactifications is still very much in development but typically masses correspond to around the Hubble scale. This strongly motivates models with tens if not hundreds of active fields [10].

It therefore seems quite reasonable to model the final inflationary phase in a landscape

[3] Discussion along these lines can be found in Ref. [8] and of course Ref. [9] but we would particularly like to thank Liam McAllister and Sam Rogerson for very helpful clarifications and additional comments on this matter.

as a truncated d-field Fourier series with random coefficients, provided we are dealing with small- to medium-field models. However, for computational reasons we are forced to work with something less realistic. Ideally we would work with more fields, and push to smaller field excursions than we will be working with. For the purposes of our investigation we will at times be working with inflationary trajectories that are not particularly well motivated as genuine models of inflation, yet we still find them to be quite informative when it comes to understanding inflationary dynamics.

2.3 The Transport equations

In this paper, we improve on our previous work [6] by calculating the perturbations using the Transport method of Mulryne et al. [11, 12]. This gives improved computational efficiency for the power spectrum, while still including all isocurvature effects, and additionally allows us to compute the non-Gaussianity parameter $f_{\rm NL}$. We compared results from this method with the geometric approach (see Ref. [13–15] for early work in this area; see Ref. [16–18] for some more recent work) used in our previous paper [6], and they were found to agree for all models tested, as well as giving the same distributions of observables when tested on our landscape model.

With regard to calculating $f_{\rm NL}$, compared to other methods (for instance Ref. [19–22]), the Transport approach has the benefit of being computationally more efficient, as well providing a new means of understanding contributions to $f_{\rm NL}$ by having explicit source terms. Equivalent to all other methods in the literature (including cosmological perturbation theory), it is simply an implementation of the separate universe assumption, but instead of evolving many perturbed trajectories, as is done in the popular δN approach [19–26], one evolves probability distributions.

What follows is largely a summary of the work done in Refs. [11, 12]. We focus on explicitly showing how the Transport formalism is implemented for a general d-field model of inflation and refer the reader to Refs. [11, 12] for the details.

2.3.1 Moments of ζ

In calculating the statistical properties of the curvature perturbation we invoke the separate universe assumption and consider a collection of space-time volumes whose mutual scatter will ultimately determine the microwave background anisotropy on a given scale. Each space-time volume follows a slightly different trajectory in field space, whose position at a given time we label ϕ^*, the scatter of which is determined by the vacuum fluctuations at horizon exit. Here and in what follows the superscript "$*$" indicates that the quantity is evaluated on a spatially-flat hypersurface. If we know the distribution $P(\phi^*)$ then, among other things, we can study the statistical properties of the deviation of these trajectories from their expectation value Φ, $\delta\phi_i^* = \phi_i^* - \Phi_i^*$, where i indexes the components of the trajectory ϕ, namely the species of light scalar fields. The two-point correlations among the $\delta\phi_i$ are expressed by the covariance matrix $\Sigma(t)$, where

$$\Sigma_{ij} \equiv \langle \delta\phi_i \delta\phi_j \rangle \tag{2.6}$$

and the third moment is given by

$$\alpha_{ijk} \equiv \langle \delta\phi_i \delta\phi_j \delta\phi_k \rangle \tag{2.7}$$

The covariance matrix, third moment and centroid Φ are all functions of time, but in our notation we will be suppressing the explicit time dependence.

A consequence of the separate universe assumption [23–26] is that the curvature perturbation ζ evaluated at some time $t = t_c$ is equivalent on large scales to the perturbation of the number of e-foldings $N(t_c, t_*, x)$ from an initial flat hypersurface at $t = t_*$, to a final uniform-density hypersurface at $t = t_c$,

$$\zeta(t_c, x) \simeq \delta N(t_c, t_*, x) \equiv N(t_c, t_*, x) - N(t_c, t_*) \tag{2.8}$$

where

$$N(t_c, t_*) \equiv \int_*^c H dt. \tag{2.9}$$

Expanding δN in termschap2 of the initial field perturbations to second order, one obtains

$$\zeta(t_c, x) = \delta N(t_c, t_*, x) = N_{,i}\delta\phi_i^* + \frac{1}{2}N_{,ij}(\delta\phi_i\delta\phi_j - \langle \delta\phi_i\delta\phi_j \rangle)^*, \tag{2.10}$$

where repeated indices should be summed over, and $N_{,i}$, $N_{,ij}$ represent first and second derivatives of the number of e-folds with respect to the fields ϕ_i^*. We remind the reader that it is necessary to subtract the correlation function in the second term. This is because

one can interpret the covariance matrix as the contribution from disconnected diagrams which gives the vacuum energy. In Fourier space one only considers connected diagrams from the outset and thus the subtraction is already implicitly taken care of.

Combining Eq. (2.6) and Eq. (2.7) with Eq. (2.10) we get expressions for the two- and three-point functions in terms of the moments of $P(\phi^*)$. The two-point function is

$$\langle\zeta\zeta\rangle = N_{,i}N_{,j}\Sigma_{ij}. \tag{2.11}$$

It is useful to decompose the three-point function as

$$\langle\zeta\zeta\zeta\rangle = \langle\zeta\zeta\zeta\rangle_1 + \langle\zeta\zeta\zeta\rangle_2, \tag{2.12}$$

where

$$\langle\zeta\zeta\zeta\rangle_1 = N_{,i}N_{,j}N_{,k}\alpha_{ijk}, \tag{2.13}$$

and

$$\langle\zeta\zeta\zeta\rangle_2 = \frac{3}{2}N_{,i}N_{,j}N_{,km}\left[\Sigma_{ik}\Sigma_{jm} + \Sigma_{im}\Sigma_{jk}\right]. \tag{2.14}$$

Eq. (2.13) is the intrinsic non-linearity among the fields, while Eq. (2.14) encodes the non-Gaussianity resulting from the gauge transformation to ζ; as one evolves from one flat hypersurface to another, turns in the trajectory will contribute to the non-Gaussianity. This, as well as any non-Gaussianity present at horizon exit, is what is encapsulated in Eq. (2.13). However, this super-horizon evolution also causes the hypersurface of constant density to change and so the gauge transformation from the flat hypersurface to the coinciding surface of constant density also contributes to the non-Gaussianity and this contribution is taken into account in Eq. (2.14).

2.3.2 Derivatives of N

From Eq. (2.13) and Eq. (2.14), it is clear that in order to calculate moments of the power spectrum we need a method for calculating derivatives of N. In general when using the δN technique it is difficult or impossible to find an analytic expression for the derivatives of N. It is therefore necessary to run the background field equations many times from perturbatively different initial conditions, stopping at some value for H which is the same for all the runs. One then calculates the derivatives of N with respect to the initial conditions. In using the Transport equations, however, this process is replaced by solving a set of coupled ordinary differential equations. Instead of taking the surfaces "$*$" and

"c" to be at horizon crossing and time of evaluation[4] respectively, instead the surfaces are taken to be infinitesimally separated and the transport equations evolve the field values at horizon crossing forward to the time of evaluation. The upshot of this is two-fold. As we will see, the use of ordinary differential equations to evolve the moments of the field perturbations allows us to see the source of super-horizon evolution and hence the various contributions to $f_{\rm NL}$. The second and more immediate benefit to our current discussion is that we can find a general expression for the derivatives of N. To leading order in slow-roll, for a given species "i", the number of e-folds N between the flat hypersurface and a comoving hypersurface is given by

$$N(t_c, t_*) \equiv -\int_{\phi^*}^{\phi^c} \frac{V}{V_{,i}} d\phi_i \,, \qquad \text{no sum on } i \,. \tag{2.15}$$

and so if the two surfaces are infinitesimally separated, then we can write

$$dN = \left[\left(\frac{V}{V_{,i}}\right)^* - \left(\frac{V}{V_{,j}}\right)^c \frac{\partial \phi_j^c}{\partial \phi_i^*}\right] d\phi_i^* . \tag{2.16}$$

To handle $\partial\phi_j^c/\partial\phi_i^*$ the method used in Refs. [22, 27] for sum-separable potentials is also now applicable and we introduce $d-1$ integrals of the form

$$C_i \equiv -\int \frac{d\phi_i}{V_{,i}} + \int \frac{d\phi_{i+1}}{V_{,i+1}}, \tag{2.17}$$

where in this case $i = 1 \ldots d-1$. these integrals enable us to write

$$d\phi_i^c = \frac{\partial \phi_i^c}{\partial C_j} \frac{\partial C_j}{\partial \phi_k^*} d\phi_k^* \tag{2.18}$$

which after some algebra gives the expression

$$\frac{\partial \phi_i^c}{\partial \phi_j^*} = -\left(\frac{V}{V_{,j}}\right)^* \left(\frac{V_{,i}}{V}\right)^c \left(\frac{V_{,j}^c}{V_{,k}^c V_{,k}^c} - \delta_{ij}\right) \tag{2.19}$$

Hence we find

$$N_{,i} = \left(\frac{V}{V_{,i}}\right)^* \left(\frac{V_{,i}^2}{V_{,k} V_{,k}}\right)^c , \qquad \text{no sum on } i \tag{2.20}$$

and

$$N_{,ij} = \frac{V_{,i}V_{,j}}{V_{,k}V_{,k}} + \frac{VV_{,ij}}{V_{,k}V_{,k}} - \frac{2VV_{,ik}V_{,k}V_{,j}}{(V_{,k}V_{,k})^2} - \frac{2VV_{,jk}V_{,k}V_{,i}}{(V_{,k}V_{,k})^2} + \frac{2VV_{,i}V_{,k}V_{,kl}V_{,l}V_{,j}}{(V_{,k}V_{,k})^3}, \tag{2.21}$$

where in Eq. (3.72) the limit $c \to *$ has been taken.

[4] Time of evaluation is often taken to be the end of inflation but with regard to calculating observables, any time after isocurvature modes have decayed away will give the same result. A problem arises when isocurvature modes are still present at the end of inflation. In this case the power spectrum will continue to evolve and without a model of reheating this renders the model non-predictive. We will return to this in greater detail later on.

2.3.3 Transporting the moments

Finally, we need a method for evolving the moments of the scalar perturbations. The probability distribution $P(\phi^*)$ is conserved and so, as described by the standard continuity equation, the rate of change of P is given by the divergence of the current,

$$\frac{\partial P}{\partial N} + \frac{\partial (u_i P)}{\partial \phi_i} = 0, \tag{2.22}$$

where $u_i \equiv \phi_i'$ is the field velocity and primes represent differentiation with respect to the number of e-folds N. The key achievement of Ref. [11] was to develop a method for extracting the evolution equations of the moments of P from the continuity equation. In Ref. [12] an alternative method was introduced, generalising to any number of fields on arbitrary slicing. We do not go into the techniques here; instead we just quote the resulting evolution equations for the centroid, variance and skew which collectively we refer to as the Transport equations,

$$\Phi_i' = \phi_i' + \frac{1}{2} u_{i,mn} \Sigma_{mn} + \dots \,, \tag{2.23}$$

$$\Sigma_{ij}' = u_{i,m}\Sigma_{mj} + u_{j,m}\Sigma_{mi} + \frac{1}{2} u_{i,mn}\alpha_{jmn} + \frac{1}{2} u_{j,mn}\alpha_{imn} + \dots \,, \tag{2.24}$$

$$\alpha_{ijk}' = u_{i,m}\alpha_{mjk} + u_{i,mn}\Sigma_{jm}\Sigma_{kn} + (\text{cyclic } i \to j \to k) + \cdots \,. \tag{2.25}$$

The equation for the centroid Eq. (2.23) says that the mean field value evolves as the velocity of the fields but can be affected by evolution of the wings of the distribution. The evolution equations for the variance and skew, as one might guess from the continuity equation Eq. (2.22), give evolution as the divergence of the field velocity but now also with source terms coming from the other moments.

2.3.4 Cross-sections of the bundle

As will be discussed in more detail in due course, an important consideration in our analysis will be whether or not evolution of observables is still taking place at the time of evaluation. Evolution stops when the trajectory becomes effectively single field [28]. This is to say the trajectory has reduced to a caustic [29], so for this reason we would like a description for the evolution of the cross-section of the perturbed trajectories. Such a description has recently been developed in Ref. [30], to which we refer the reader for more detailed discussion. For simplicity we only describe the broad concept here and quote results that will be needed in future discussion.

Cross-sections within the bundle are focused, sheared and rotated by the flow. These distortions can be characterised by the evolution of connecting vectors describing the displacement between nearby trajectories in the bundle. If δx_i is an infinitesimal connecting vector, then assuming $u_{i,j}$ is sufficiently smooth, δx_i is transported as

$$\delta x_i' = \delta x_j \frac{\partial u_i}{\partial \phi_j} \tag{2.26}$$

It follows that changes in the cross-section of the bundle can be determined in terms of the expansion tensor $u_{i,j}$. We can decompose this in terms of a dilation $\theta = \operatorname{tr} u_{i,j}$, a traceless symmetric shear σ_{ij}, and a traceless antisymmetric twist ω_{ij},

$$u_{i,j} \equiv \frac{\theta}{d}\delta_{ij} + \sigma_{ij} + \omega_{ij} \tag{2.27}$$

Dilation describes a rigid rescaling of δx_i by $1+\theta$, representing a global tendency of the trajectories to focus or defocus. The shear encapsulates the tendency for some trajectories to flow faster than others while conserving the cross-sectional area of the bundle. The twist represents a rotation of the bundle with preserved volume, such as the tendency of trajectories to braid. The dilation, shear and twist act as sources for one another and so one expects a bundle will typically exhibit all of these behaviours at some point.

We refer the reader to Ref. [30] for a more formal description of this formalism and its applications, but for the purposes of this paper all we need is the result that the focussing of the bundle is given by

$$\Theta(H, H_0) = \exp\left[\frac{1}{d}\int_{H_0}^{H} \theta(h) dh\right]. \tag{2.28}$$

2.4 Findings

Having set up our models and the machinery necessary to compute the observables, we now proceed to our results. The principal variables of interest to vary are the number of fields d and the horizontal mass scale m_{h}. Large values of the latter correspond to relatively smooth potentials, and small values to heavily featured potentials. We refer to individual realizations giving sufficient inflation as 'verses'.

We discuss our results in the following sequence:

1. Dynamical properties of trajectories.

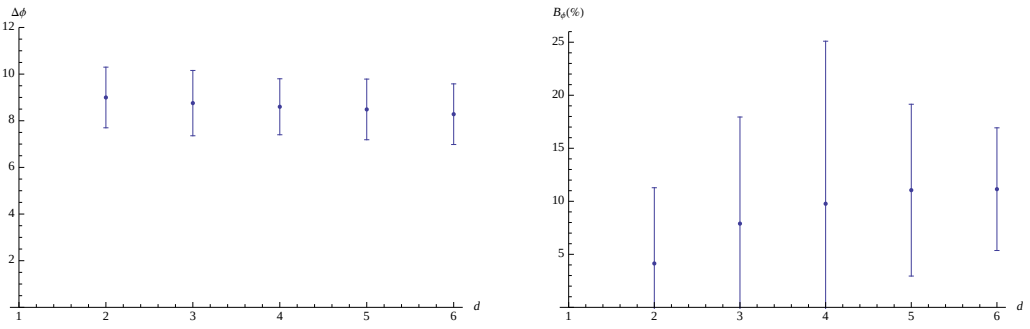

Figure 2.3: How the mean $\Delta\phi$ and percentage increase in $\Delta\phi$ due to bending of the trajectory changes with the number of fields, for $m_{\rm h} = 15\,M_{\rm Pl}$. The bars show how the standard deviation of these quantities changes over this range.

2. Perturbation evolution along individual trajectories.

3. Distribution of observables over ensembles of trajectories.

2.4.1 Trajectory dynamics

Minimal d dependence Fig. 2.3 summarises the qualitative behaviour found during our exploration of the properties of multi-field trajectories. We see that $\Delta\phi$, the length of the trajectory in field space, and B_ϕ, the percentage increase in $\Delta\phi$ due to turns in the trajectory, defined as

$$B_\phi \equiv 100\frac{\Delta\phi - \sqrt{\phi^{\rm end}\cdot\phi^{\rm end} - \phi^*\cdot\phi^*}}{\Delta\phi} \tag{2.29}$$

show only a mild sensitivity to the number of fields. In fact, for all observables and inflationary parameters we looked at, the sensitivity to changing the number of fields was small over the range $d = 2$ to $d = 6$ compared to the spread of results. This was true even for the relatively predictive large-field case of $m_{\rm h} = 15\,M_{\rm Pl}$. Least sensitive of all, we found no change whatsoever in the distribution of slow-roll parameters at horizon crossing with $\epsilon^* = 0.002 \pm 0.002$ and $\eta^* = 0.0012 \pm 0.0004$.

e-fold distributions One instance where we did find sensitivity to d was in the e-fold distributions, where we saw a decrease in the proportion of trajectories with more than 60 e-folds from 0.08 for two fields down to 0.01 for six fields. Fig. 2.3 hints at a tendency for trajectories to become shorter and more curved as the number of fields increases. So given that the trajectory will seek the route of steepest descent, it appears that for our model,

increasing the number of fields increases the chance of the trajectory encountering a slope sufficiently steep to kill inflation.

In Refs. [1, 31] slightly different parameterisations of the inflationary region of the potential were used to show the probability of obtaining a given number of e-folds of inflation was

$$P(N) \propto \frac{1}{N^{\alpha}}, \tag{2.30}$$

where $\alpha = 4$ and $\alpha = 3$ were found respectively. Bearing Eq. (2.5) in mind, it seems reasonable that Eq. (2.30) might apply more generally and indeed we find it to be a good fit to our e-fold distributions, with α increasing as the potential becomes more featured from $\alpha = 2$ through to $\alpha = 5$ over the range of $m_{\rm h}$ we investigated. To illustrate the implication of this, consider the popular idea that inflation was preceded by a tunnelling event. Using the (perhaps somewhat arbitrary) values of Ref. [31], we place an anthropic lower bound on the number of e-folds at 59.5 coming from structure formation and an observational lower bound at $N = 62$ on the curvature from tunnelling. Then for $\alpha = 2$, the probability of the model achieving sufficient inflation to be in agreement with observation is roughly 92%, while for $\alpha = 5$ it is more like 81%. However, remember we are working in the range of $\Delta\phi$ which is not best motivated theoretically. While not accessible with the techniques used here, our results lead us to expect that for small-field models, α should be larger. This has the potential to cause tension with observation, as by $\alpha = 18$ the chance of finding ourselves in the observed universe falls to 49%, i.e a typical observer would expect to see evidence of curvature.

2.4.2 Perturbation evolution: $P_{\zeta\zeta}$, $f_{\rm NL}$ and the adiabatic limit

Having seen that our model is insensitive to the number of light fields, for simplicity we only give results for two-field potentials in the remaining sections of this paper, focussing mainly on the dependence on the feature scale of the potential. But we would like to emphasise that the results hold more generally.

$P_{\zeta\zeta}$ and Θ

The key difference between single-field and multi-field inflation is that the latter admits evolution of the power spectrum on super-horizon scales. This means that in order to make a prediction from multi-field inflation one needs to know the full evolutionary history up

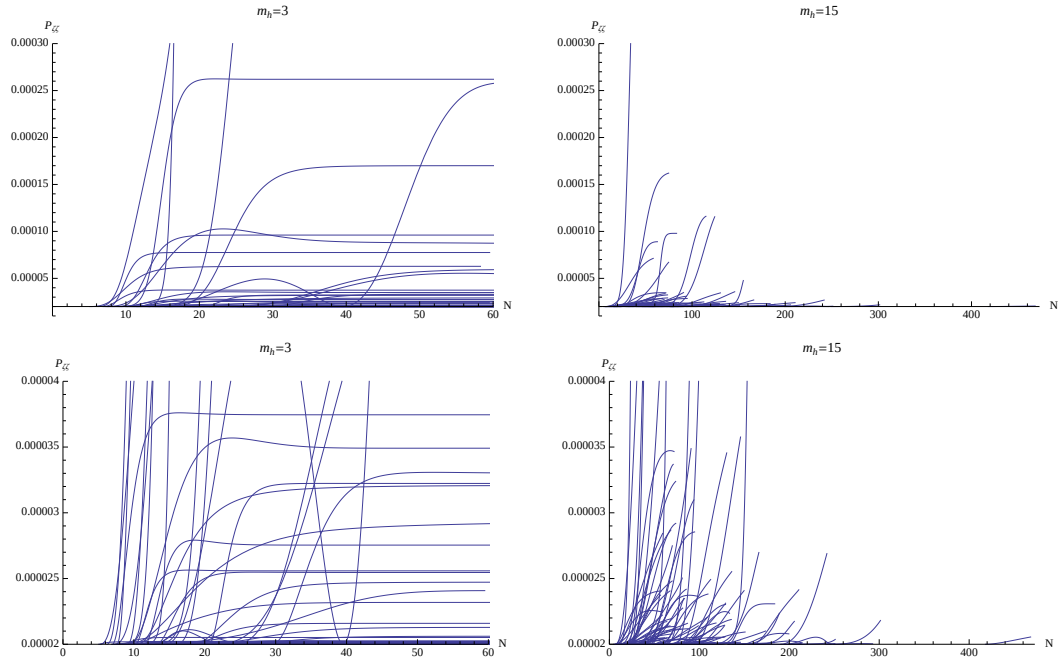

Figure 2.4: Example plots showing the super-horizon evolution of the power spectrum for modes exiting 55 e-folds before the end of inflation. $m_{\rm h} = 3M_{\rm Pl}$ corresponds to a highly-featured potential, and in all such cases evolution stops long before the end of inflation. $m_{\rm h} = 15M_{\rm Pl}$ is a comparatively smooth landscape, and then a significant proportion of verses are still evolving at the end of inflation. In almost all cases evolution is monotonic but not always.

until the model becomes effectively single field, i.e. the adiabatic limit is reached [28, 29]. Once this happens the power spectrum stops evolving and one can evaluate observable quantities at a subsequent time of one's pleasing. The problem is that there is no guarantee that such an adiabatic limit will be reached before the end of inflation, and if this is not the case making a prediction requires knowledge of reheating and so forth.

As can be seen in Figs. 2.4, 2.5 and 2.6, the ability to reach the adiabatic limit, where the perturbation on a given scale becomes constant, is strongly dependent on how featured the landscape is. For the more featured landscapes such as $m_{\rm h} = 3\,M_{\rm Pl}$, we found the adiabatic limit was reached in all cases (even the trajectories disappearing off the top of the plots), while for the smoother landscapes like $m_{\rm h} = 15M_{\rm Pl}$ the proportion of trajectories achieving this clearly drops significantly.

There is a very intuitive reason for why this should be the case. Rewriting Eq. (4.42) in terms of e-folds N we find

$$\Theta(N, N_*) = \exp\left[-\frac{1}{d}\int_{N_*}^{N}(3\epsilon - 2\bar{\eta} + \mathrm{tr}\, M_{ij})dN\right] \tag{2.31}$$

where M_{ij} is the Hessian of $\ln V$ and $\bar{\eta}$ is the generalised slow-roll parameter

$$\bar{\eta} \equiv \frac{V_{,i}V_{,j}V_{,ij}}{VV_{,k}V_{,k}} \tag{2.32}$$

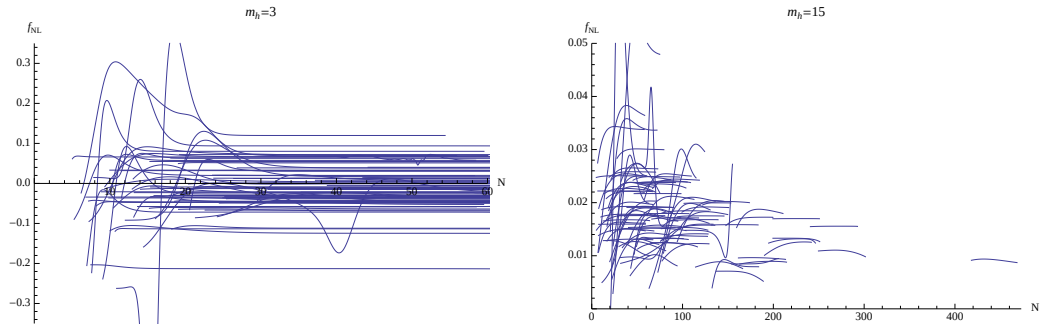

Figure 2.5: Example plots showing the super-horizon evolution of $f_{\rm NL}$ for modes exiting 55 e-folds before the end of inflation. Again we see that for the more featured landscape evolution stops early on, while for the smoother example, evolution often continues to the end of inflation.

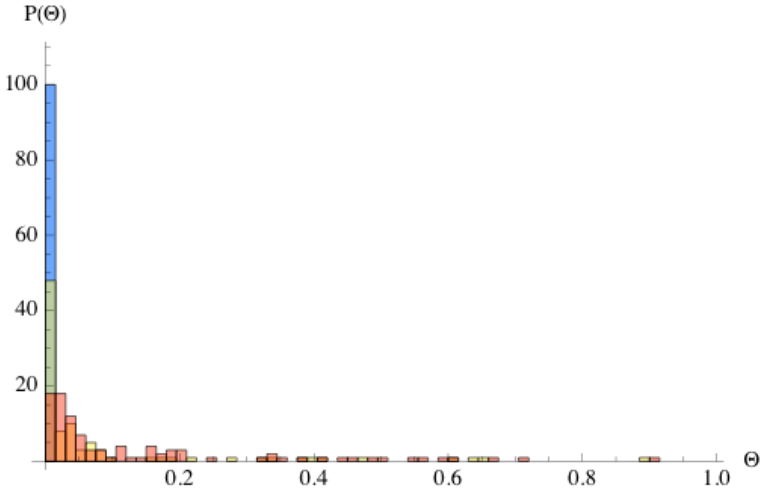

Figure 2.6: Θ at the end of inflation for $m_{\rm h} = 3\,M_{\rm Pl}$ (blue), $m_{\rm h} = 9\,M_{\rm Pl}$ (yellow) and $m_{\rm h} = 15\,M_{\rm Pl}$ (red). All trajectories essentially reach a caustic in the most featured example, less for $m_{\rm h} = 9\,M_{\rm Pl}$ and least for the smoothest landscape $m_{\rm h} = 15\,M_{\rm Pl}$.

We therefore see that in a valley, strong focussing will occur, while on a ridge or a hilltop the bundle will dilate. With this picture it is quite easy to see why we should expect evolution as seen in Fig. 2.4. The treacherous landscape of $m_{\rm h} = 3\,M_{\rm Pl}$ typically gives exactly the conditions required for a very strong focusing, while in contrast the comparatively mild, undulating meadows of $m_{\rm h} = 15\,M_{\rm Pl}$ give very little incentive for trajectories to focus to a caustic.

$f_{\rm NL}$ is always small

Much of this kind of discussion carries over to understanding the results of Fig. 2.5. First and foremost it should be noted there was not a single example of a trajectory that gave sufficient non-Gaussianity to be detected by any future planned experiment. Methods to get around this disappointingly generic feature of multi-field inflation were recently

addressed in Ref. [29] and the special case of sum-separable potentials was also discussed in Refs. [18, 32]. In the case of sum-separable hilltop potentials which reach an adiabatic limit during inflation, what is known as the horizon-crossing approximation [33] gives a good estimate of the final value for $f_{\rm NL}$.

$$f_{\rm NL} \approx -\frac{5}{6}\frac{V''_\phi}{V_\phi}\bigg|_* , \tag{2.33}$$

where in this instance ϕ represents one or at most a few fields where N_i is large. From this we see that provided there are enough fields to keep η small, with the right initial conditions, a ridge can give rise to a large $f_{\rm NL}$.

What we find in our analysis is that the problem of obtaining a large $f_{\rm NL}$ is made particularly acute by the need to obtain sufficient inflation. When we have a very smooth landscape, sufficient inflation is easily achieved but the lack of features means there is nothing to give rise to a large $f_{\rm NL}$. On the other hand, when the potential is very featured, it is difficult to start close enough to a ridge to get a large $f_{\rm NL}$ without falling off it, thereby killing inflation. In some models, such as axion N-flation [34], a sufficiently large number of fields can make it possible to overcome this problem [35, 36], as the large damping term makes it easier to be close to a ridge without falling off too soon. For our model, while we do not have the computational power to explore this possibility, with enough fields we would expect to see some examples with a large $f_{\rm NL}$, but they would constitute only a very small proportion. This is because if many fields have a large $N_{,i}$, their contributions to $f_{\rm NL}$ will, through a manifestation of the central limit theorem, cause $f_{\rm NL}$ to be vanishing in the limit of many contributing fields. Thus on average we would always expect $f_{\rm NL}$ to be small.

Trends in $f_{\rm NL}$ evolution

While we found no examples of large $f_{\rm NL}$ we did find a very diverse range of behaviour. This diversity is indicative of why detection would be such a powerful constraint on models. That said we did find some common trends. Fig. 2.7 shows two examples of evolution of $f_{\rm NL}$ together with the corresponding evolution in the width of the bundle. We chose these two examples, Verse 113147 and Verse 253911, in particular as each shows characteristics that were common to most trajectories, but also demonstrate that counter examples were found.

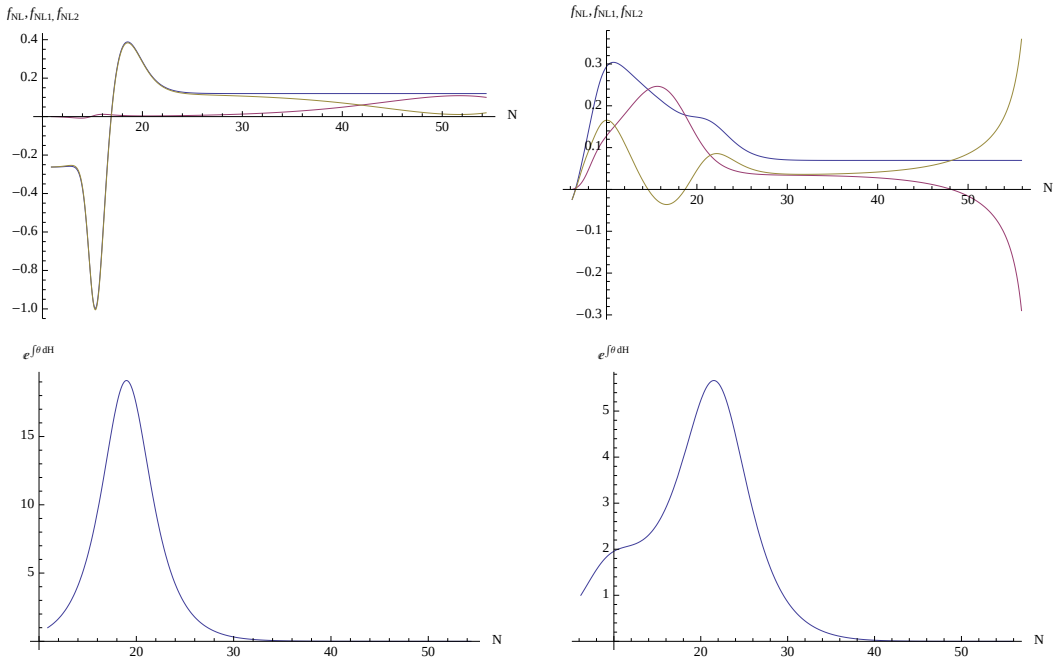

Figure 2.7: Plots of Verse 113147 (left) and Verse 253911 (right) showing very distinctive $f_{\rm NL}$ evolution. In the plots on the top row, $f_{\rm NL}$ is blue, the intrinsic component, $f_{\rm NL1}$, is red and the gauge contribution, $f_{\rm NL2}$, is yellow. The bottom row gives the corresponding evolution in the bundle width.

The gauge contribution determines the peak Analogous to Eq. (2.13) and Eq. (2.14) we can define non-Gaussianity parameters

$$f_{\rm NL1} \equiv \frac{5}{18}\frac{\langle\zeta\zeta\zeta\rangle_1}{\langle\zeta\zeta\rangle^2} \quad , \quad f_{\rm NL1} \equiv \frac{5}{18}\frac{\langle\zeta\zeta\zeta\rangle_2}{\langle\zeta\zeta\rangle^2} \tag{2.34}$$

such that $f_{\rm NL} = f_{\rm NL1} + f_{\rm NL2}$ and $f_{\rm NL1}$ is the intrinsic contribution and $f_{\rm NL2}$ the gauge contribution to $f_{\rm NL}$. As is particularly well demonstrated by Verse 113147, in all examples we found $f_{\rm NL2}$ determined any peaks in $f_{\rm NL}$. Typically it was the case that the intrinsic non-Gaussianity played a highly subdominant role in the feature, but we did find the exception that is Verse 253911 which clearly received an important contribution from the intrinsic part. In Ref. [11] it was noted that for the double quadratic potential and quadratic exponential potential this behaviour was present. Here we show this characteristic applies much more generally.

$f_{\rm NL}$ grows when the bundle dilates Features in $f_{\rm NL}$ occur whenever Θ grows. This seems very reasonable since at this point the perturbed trajectories will be exploring different parts of the potential. Typically the peak in $f_{\rm NL}$ occurred very close to the time of the peak in Θ but again, Verse 253911 shows this need not be the case precisely. We see features in $f_{\rm NL2}$ are intimately related to features in θ. We attribute this to common terms involving $V_{,ij}$.

Asymptotic behaviour of $f_{\rm NL}$ is not straightforward A result that continues to elude us is a simple way of understanding what the final value of $f_{\rm NL}$ in the adiabatic limit will be. For sum-separable hilltop potentials, the horizon-crossing approximation works well, but for more general potentials there is no equivalent. As the examples in Fig. 2.7 show, the asymptotic value can be reached in dramatically different manners. Worse still is the fact that in the adiabatic limit the intrinsic and gauge transformations need not settle to constant values. This indicates that a different set of parameters should be considered if we are to make progress with this question.

2.4.3 Interlude: The Lyth bound

Before moving on to discuss distributions of observables, we would like to take a brief moment to discuss the relation between field trajectories and the tensor-to-scalar ratio, as it will be helpful to bear in mind in the subsequent discussion.

Taking $N_{\rm CMB}$ to be the number of e-folds between when fluctuations on CMB scales left the horizon and the end of inflation, we can obtain a d-field version of the Lyth bound by writing

$$N_{\rm CMB} = \int_{\phi_{\rm CMB}}^{\phi_{\rm end}} \frac{1}{\sqrt{2\epsilon}} d\phi_{\parallel}, \tag{2.35}$$

where we are integrating along the field trajectory. If we assume ϵ is either constant or increasing over this period, then we have

$$2\epsilon < \frac{\Delta\phi}{N_{\rm CMB}}\,. \tag{2.36}$$

For single field inflation $r = 16\epsilon$ but when there are more fields the curvature perturbation evolves on super-horizon scales, suppressing r and so $r < 16\epsilon$ [6]. We therefore see that the Lyth bound remains essentially the same for multi-field models as in the single-field case

$$r < 16\epsilon < 0.03 \left(\frac{55}{N_{\rm CMB}}\right)^2 \left(\frac{\Delta\phi}{M_{\rm Pl}}\right)^2 \tag{2.37}$$

Planck hopes to measure the tensor-to-scalar ratio with an accuracy of a few hundredths, hence has discovery potential if it is of order 0.1 or so. Comparing the Lyth bound with the discussion in section 2.2.3 we therefore see that a detection would exclude practically all small- and medium-field models if only one field is admitted.[5] However as

[5] In principle one can evade this bound even in the single-field case by breaking the assumption that ϵ is monotonically increasing, though in practice this is rather difficult to achieve [37].

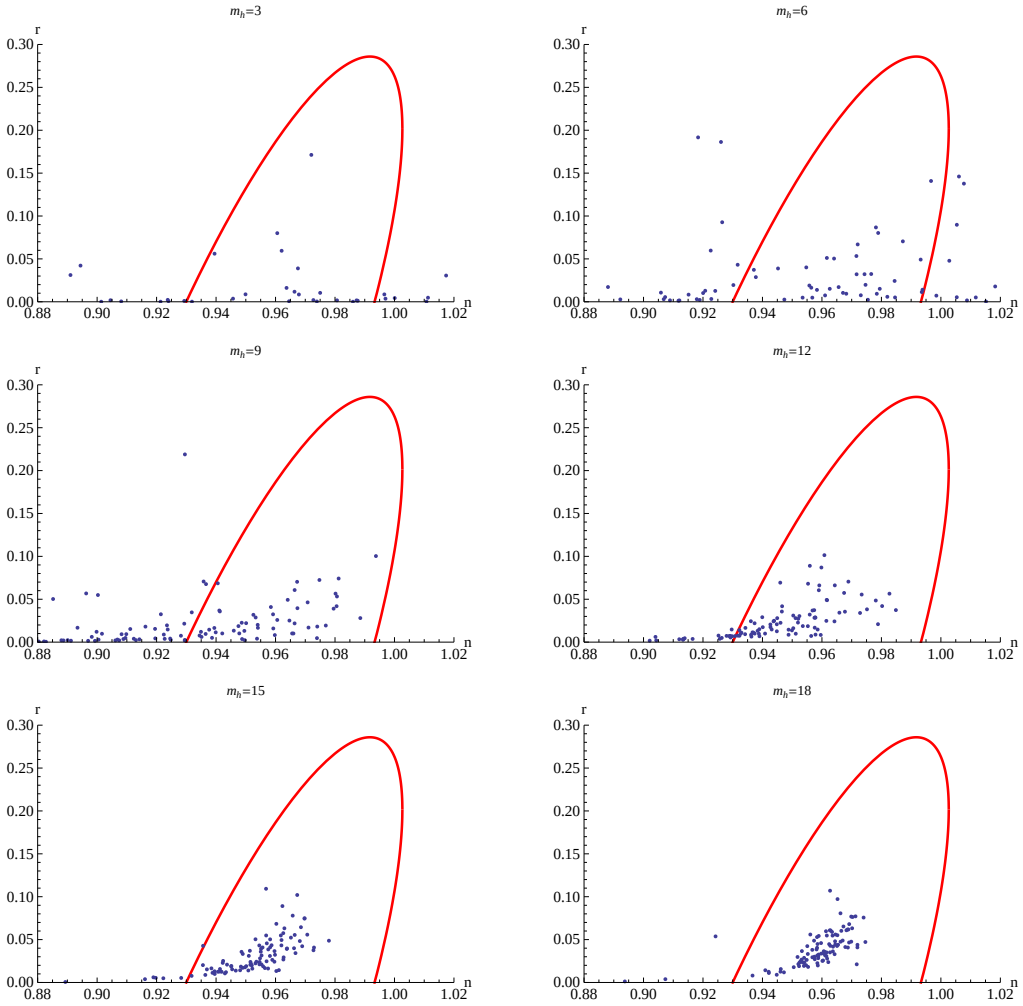

Figure 2.8: n–r plots for a range of $m_{\rm h}$, beginning with the more featured potentials. The curve shows the WMAP7+all 95% confidence limit [38].

previously discussed, multi-field models are strongly motivated by fundamental theory. If we consider the extreme case of sum-separable potentials then the discussion of Section 2.2.3 requires each $\Delta\phi_i \ll M_{\rm Pl}$ but there is no restriction on the number of fields contributing during inflation; this was for instance the motivation of the N-flation proposal [34]. Therefore, if we are to stay in the field theory favoured regime of small-field models, a detection of r would place a lower bound on the number of fields! Rewriting Eq. (2.37) in a more suggestive form we have

$$r < 0.03d \left(\frac{55}{N_{\rm CMB}}\right)^2 \frac{\Delta\phi_i \Delta\phi_i}{M_{\rm Pl}^2}\,. \tag{2.38}$$

$m_{\rm h}(M_{\rm Pl})$	$\Delta\phi$	$B_\phi(\%)$	n	r, 95% conf.	$f_{\rm NL}$
3	4.3 ± 1.7	17 ± 18	1.03 ± 0.15	0.036, $r < 0.1981$	-0.008 ± 0.078
6	7.6 ± 1.8	16 ± 18	0.93 ± 0.07	0.036, $r < 0.172$	0.029 ± 0.034
9	8.4 ± 1.8	10 ± 13	0.93 ± 0.03	0.023, $r < 0.081$	0.028 ± 0.022
12	8.6 ± 1.4	5 ± 7	0.94 ± 0.02	0.024, $r < 0.066$	0.022 ± 0.010
15	9.0 ± 1.3	4 ± 7	0.95 ± 0.01	0.032, $r < 0.074$	0.018 ± 0.007
18	9.2 ± 1.2	4 ± 9	0.96 ± 0.02	0.039, $r < 0.079$	0.016 ± 0.009

Table 2.2: Table of the mean distance in field space travelled in the last 55 e-fold of inflation for a given $m_{\rm h}$, B_ϕ, the mean percentage increase coming from bends in the trajectory, and corresponding results for observables.

2.4.4 Distribution of observables: n and r

Fig. 2.8 shows our findings for n and r at the end of inflation, also summarised in Table 2.2. As the landscape becomes more featured the viable trajectories become shorter and increasingly bendy. The Lyth bound tells us the distance travelled in field space places an upper bound on the tensor-to-scalar ratio. Furthermore, bends in the trajectory cause super-horizon evolution of the curvature power spectrum, while the tensor power spectrum is conserved, and so as Fig. 2.8 shows, we see an increasingly strong suppression in r as we move to lower $m_{\rm h}$.

As summarised in Fig. 2.6, a less featured potential reduces the chance of trajectories reaching their adiabatic limit. It is noteworthy that, despite this, the plots of the n–r plane for $m_{\rm h} = 15\,M_{\rm Pl}$ and $m_{\rm h} = 18\,M_{\rm Pl}$ show remarkable consistency for n and r at the end of inflation. This might lead one to think that the super-horizon evolution is having negligible effect, but if we take the example of $m_{\rm h} = 15\,M_{\rm Pl}$, as Table 2.2 shows, the mean increase in the field trajectory from turning is only 4%, yet if we assumed a single-field approximation was valid we would obtain $n = 0.98 \pm 0.01$ which is significantly different from the actual result of 0.95 ± 0.01. If nothing else, these results show one should be exceedingly careful when making single-field approximations. Fig. 2.9 compares distributions for the spectral index with those obtained using a single-field approximation.

The central concern regarding the possible existence of a landscape is whether or not such a model can be tested. As we have mentioned, a key challenge is the measure problem, another being our very limited understanding of fundamental theory. Once these problems are better understood though, we will still be left with distributions for observ-

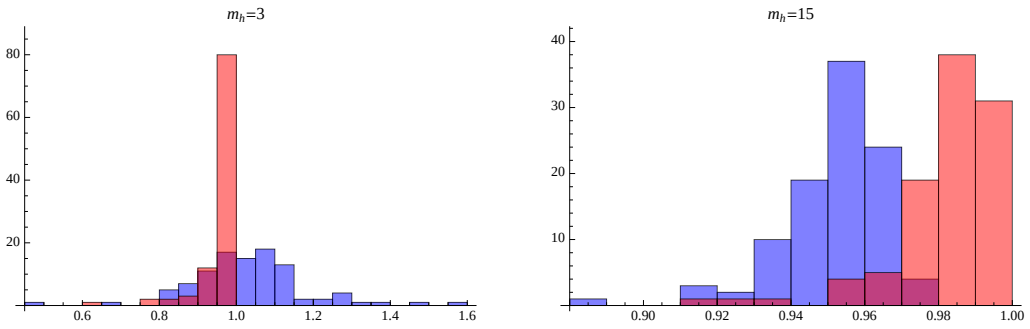

Figure 2.9: Example plots comparing spectral index as obtained using single-field approximation (red) and as calculated taking evolution up to the end of inflation into account (blue).

able quantities. No matter how well developed our understanding, it seems reasonable to assume that at some level our ability to make predictions will be fundamentally limited by the details of the theory. Our toy landscape illustrates this in a very explicit way. In a sense $m_{\rm h}$ gives a way of quantifying the complexity of each landscape. For our model, we see the spread of results for the spectral index dramatically increases as we move to more featured landscapes, while for the tensor-to-scalar ratio the spreading is considerably less dramatic due to a suppression coming from the inevitable decrease in the length of the field trajectory $\Delta\phi$. As we have seen $f_{\rm NL}$ by contrast remains consistently small.

2.5 Conclusions

We explored inflationary dynamics in randomly-generated potentials as well as the consequences for super-horizon evolution of perturbations. We found this exploration to be interesting primarily on two fronts.

First, by exploring a very large number of inflationary trajectories, we encountered a wide range of super-horizon evolution behaviour for $P_{\zeta\zeta}$ and $f_{\rm NL}$. The benefit of this was that it became easy to see what characteristics are generic and which are not. We found that peaks in $f_{\rm NL}$ tend to be determined by the gauge contribution but behaviour was rather more broad in the adiabatic limit, showing few trends. Understanding of non-Gaussianity is still in rapid development and so exploration of this kind can be very helpful in gaining insight in how to progress towards something more concrete such as Ref. [30].

We also found that keeping track of the easy-to-compute bundle width was extremely informative. By following how Θ changes along the trajectory, we were generally able

to understand what qualities of the potential gave rise to super-horizon evolution. In particular, we found that peaks in $f_{\rm NL}$ occur during regions of the potential that give rise to a dilation of the bundle. However, a more quantitative description awaits future development. We emphasise that in order to make predictions in any multi-field model, one needs to perform an equivalent analysis to ensure no evolution is taking place at the time of evaluation. We found that as the mean length of the field trajectory in field space increased, the chances of reaching an adiabatic limit drastically decreased, rendering the larger field models essentially non-predictive without a model of reheating.

Second, we looked at how varying the scale of features and the number of light fields affected the ensembles produced for a given parameter. We found that landscapes where the mean length of the field trajectory was large typically gave results consistent with current observational data (despite not necessarily reaching their adiabatic limit). However for more featured landscapes where the mean field trajectory was smaller, the spread in the spectral index increased significantly. The spread in the tensor-to-scalar ratio did not increase so dramatically. This can be understood in terms of the Lyth bound which places an upper bound on the tensor-to-scalar ratio according to the length of the field trajectory. We found varying the number of fields between 2 and 6 to have negligible effect on the distributions for observables. Amongst all trajectories we found no examples of detectably large non-Gaussianity. In absence of motivation for why we would be an atypical observer, this result is sufficiently strong to conclude that an observation of local-type non-Gaussianity by Planck would rule out models of this kind.

References

[1] Nishant Agarwal et al. "Universality in D-brane Inflation". In: *JCAP* 1109 (2011), p. 002. arXiv:1103.2775 [astro-ph.CO] (cit. on pp. 57, 59, 71).

[2] Petr Horava and Edward Witten. "Heterotic and type I string dynamics from eleven-dimensions". In: *Nucl.Phys.* B460 (1996), pp. 506–524. arXiv:hep-th/9510209 [hep-th] (cit. on p. 58).

[3] Leonard Susskind. "The Anthropic landscape of string theory". In: (2003). arXiv:hep-th/0302219 [hep-th] (cit. on p. 58).

[4] Ben Freivogel. "Making predictions in the multiverse". In: *Class.Quant.Grav.* 28 (2011), p. 204007. arXiv:1105.0244 [hep-th] (cit. on p. 58).

[5] Max Tegmark. "What does inflation really predict?" In: *JCAP* 0504 (2005), p. 001. arXiv:astro-ph/0410281 [astro-ph] (cit. on pp. 59, 61).

[6] Jonathan Frazer and Andrew R. Liddle. "Exploring a string-like landscape". In: *JCAP* 1102 (2011), p. 026. arXiv:1101.1619 [astro-ph.CO] (cit. on pp. 59, 61, 64, 76).

[7] Steven Weinberg. "Anthropic Bound on the Cosmological Constant". In: *Phys.Rev.Lett.* 59 (1987), p. 2607 (cit. on p. 61).

[8] Daniel Baumann and Liam McAllister. "Advances in Inflation in String Theory". In: *Ann.Rev.Nucl.Part.Sci.* 59 (2009), pp. 67–94. arXiv:0901.0265 [hep-th] (cit. on p. 63).

[9] David H. Lyth. "What would we learn by detecting a gravitational wave signal in the cosmic microwave background anisotropy?" In: *Phys.Rev.Lett.* 78 (1997), pp. 1861–1863. arXiv:hep-ph/9606387 [hep-ph] (cit. on p. 63).

[10] C.P. Burgess and Liam McAllister. "Challenges for String Cosmology". In: *Class.Quant.Grav.* 28 (2011), p. 204002. arXiv:1108.2660 [hep-th] (cit. on p. 63).

[11] David J. Mulryne, David Seery and Daniel Wesley. "Moment transport equations for non-Gaussianity". In: *JCAP* 1001 (2010), p. 024. arXiv:0909.2256 [astro-ph.CO] (cit. on pp. 64, 68, 75).

[12] David J. Mulryne, David Seery and Daniel Wesley. "Moment transport equations for the primordial curvature perturbation". In: *JCAP* 1104 (2011), p. 030. arXiv:1008.3159 [astro-ph.CO] (cit. on pp. 64, 68).

[13] Christopher Gordon et al. "Adiabatic and entropy perturbations from inflation". In: *Phys.Rev.* D63 (2001), p. 023506. arXiv:astro-ph/0009131 [astro-ph] (cit. on p. 64).

[14] S. Groot Nibbelink and B.J.W. van Tent. "Scalar perturbations during multiple field slow-roll inflation". In: *Class.Quant.Grav.* 19 (2002), pp. 613–640. arXiv:hep-ph/0107272 [hep-ph] (cit. on p. 64).

[15] S. Groot Nibbelink and B.J.W. van Tent. "Density perturbations arising from multiple field slow roll inflation". In: (2000). arXiv:hep-ph/0011325 [hep-ph] (cit. on p. 64).

[16] Courtney M. Peterson and Max Tegmark. "Non-Gaussianity in Two-Field Inflation". In: *Phys.Rev.* D84 (2011), p. 023520. arXiv:1011.6675 [astro-ph.CO] (cit. on p. 64).

[17] Courtney M. Peterson and Max Tegmark. "Testing Two-Field Inflation". In: *Phys.Rev.* D83 (2011), p. 023522. arXiv:1005.4056 [astro-ph.CO] (cit. on p. 64).

[18] Yuki Watanabe. "δ N versus covariant perturbative approach to non-Gaussianity outside the horizon in multifield inflation". In: *Phys.Rev.* D85 (2012), p. 103505. arXiv:1110.2462 [astro-ph.CO] (cit. on pp. 64, 74).

[19] David Wands. "Local non-Gaussianity from inflation". In: *Class.Quant.Grav.* 27 (2010), p. 124002. arXiv:1004.0818 [astro-ph.CO] (cit. on p. 64).

[20] David Langlois, Filippo Vernizzi and David Wands. "Non-linear isocurvature perturbations and non-Gaussianities". In: *JCAP* 0812 (2008), p. 004. arXiv:0809.4646 [astro-ph] (cit. on p. 64).

[21] Christian T. Byrnes and David Wands. "Curvature and isocurvature perturbations from two-field inflation in a slow-roll expansion". In: *Phys.Rev.* D74 (2006), p. 043529. arXiv:astro-ph/0605679 [astro-ph] (cit. on p. 64).

[22] Filippo Vernizzi and David Wands. "Non-gaussianities in two-field inflation". In: *JCAP* 0605 (2006), p. 019. arXiv:astro-ph/0603799 [astro-ph] (cit. on pp. 64, 67).

[23] Alexei A. Starobinsky. "Multicomponent de Sitter (Inflationary) Stages and the Generation of Perturbations". In: *JETP Lett.* 42 (1985), pp. 152–155 (cit. on pp. 64, 65).

[24] D. H. Lyth. "Large Scale Energy Density Perturbations and Inflation". In: *Phys.Rev.* D31 (1985), pp. 1792–1798 (cit. on pp. 64, 65).

[25] Misao Sasaki and Ewan D. Stewart. "A General analytic formula for the spectral index of the density perturbations produced during inflation". In: *Prog.Theor.Phys.* 95 (1996), pp. 71–78. arXiv:astro-ph/9507001 (cit. on pp. 64, 65).

[26] David H. Lyth and Yeinzon Rodríguez. "The inflationary prediction for primordial non-gaussianity". In: *Phys.Rev.Lett.* 95 (2005), p. 121302. arXiv:astro-ph/0504045 (cit. on pp. 64, 65).

[27] Thorsten Battefeld and Richard Easther. "Non-Gaussianities in Multi-field Inflation". In: *JCAP* 0703 (2007), p. 020. arXiv:astro-ph/0610296 [astro-ph] (cit. on p. 67).

[28] Juan García-Bellido and David Wands. "Metric perturbations in two field inflation". In: *Phys.Rev.* D53 (1996), pp. 5437–5445. arXiv:astro-ph/9511029 [astro-ph] (cit. on pp. 68, 72).

[29] Joseph Elliston et al. "Evolution of fNL to the adiabatic limit". In: *JCAP* 1111 (2011), p. 005. arXiv:1106.2153 [astro-ph.CO] (cit. on pp. 68, 72, 74).

[30] David Seery et al. "Inflationary perturbation theory is geometrical optics in phase space". In: *JCAP* 1209 (2012), p. 010. arXiv:1203.2635 [astro-ph.CO] (cit. on pp. 68, 69, 79).

[31] Ben Freivogel et al. "Observational consequences of a landscape". In: *JHEP* 0603 (2006), p. 039. arXiv:hep-th/0505232 [hep-th] (cit. on p. 71).

[32] Joel Meyers and Navin Sivanandam. "Non-Gaussianities in Multifield Inflation: Superhorizon Evolution, Adiabaticity, and the Fate of fnl". In: *Phys.Rev.* D83 (2011), p. 103517. arXiv:1011.4934 [astro-ph.CO] (cit. on p. 74).

[33] Soo A. Kim and Andrew R. Liddle. "Nflation: Non-Gaussianity in the horizon-crossing approximation". In: *Phys.Rev.* D74 (2006), p. 063522. arXiv:astro-ph/0608186 [astro-ph] (cit. on p. 74).

[34] S. Dimopoulos et al. "N-flation". In: *JCAP* 0808 (2008), p. 003. arXiv:hep-th/0507205 [hep-th] (cit. on pp. 74, 77).

[35] Soo A. Kim, Andrew R. Liddle and David Seery. "Non-gaussianity in axion Nflation models". In: *Phys.Rev.Lett.* 105 (2010), p. 181302. arXiv:1005.4410 [astro-ph.CO] (cit. on p. 74).

[36] Soo A. Kim, Andrew R. Liddle and David Seery. "Non-gaussianity in axion N-flation models: detailed predictions and mass spectra". In: *Phys.Rev.* D85 (2012), p. 023532. arXiv:1108.2944 [astro-ph.CO] (cit. on p. 74).

[37] Shaun Hotchkiss, Anupam Mazumdar and Seshadri Nadathur. "Observable gravitational waves from inflation with small field excursions". In: *JCAP* 1202 (2012), p. 008. arXiv:1110.5389 [astro-ph.CO] (cit. on p. 76).

[38] E. Komatsu et al. "Seven-Year Wilkinson Microwave Anisotropy Probe (WMAP) Observations: Cosmological Interpretation". In: *Astrophys.J.Suppl.* 192 (2011), p. 18. arXiv:1001.4538 [astro-ph.CO] (cit. on p. 77).

Paper 3

Inflationary perturbation theory is geometrical optics in phase space

David Seery, David J. Mulryne, Jonathan Frazer, and Raquel H. Ribeiro

A pressing problem in comparing inflationary models with observation is the accurate calculation of correlation functions. One approach is to evolve them using ordinary differential equations ("transport equations"), analogous to the Schwinger–Dyson hierarchy of *in–out* quantum field theory. We extend this approach to the complete set of momentum space correlation functions. A formal solution can be obtained using raytracing techniques adapted from geometrical optics. We reformulate inflationary perturbation theory in this language, and show that raytracing reproduces the familiar "δN" Taylor expansion. Our method produces ordinary differential equations which allow the Taylor coefficients to be computed efficiently. We use raytracing methods to express the gauge transformation between field fluctuations and the curvature perturbation, ζ, in geometrical terms. Using these results we give a compact expression for the nonlinear gauge-transform part of $f_{\rm NL}$ in terms of the principal curvatures of uniform energy-density hypersurfaces in field space.

3.1 Introduction

Our current theories of the early universe are stochastic. They do not predict a definite *state* today: rather, their predictions are statistical. To compare these predictions with observation it must usually be supposed that we are in some sense typical. This brings two challenges. First, what is typical under some circumstances may be atypical under

others. Therefore we must be precise about the type of observer of which we are a typical representative. This leads to the "measure problem," about which we have nothing new to say. In this paper we are concerned with the second challenge: after fixing a class of observers, to estimate the observables typically measured by its members.

Inflation is the most common early-universe paradigm for which we would like to compute observables. In this context we usually take ourselves to be ordinary observers of the fluctuations produced on approach to a fixed vacuum. The challenge is to calculate the typical stochastic properties of these fluctuations.

The most important fluctuation generated by inflation is the primordial density perturbation, ζ. Correlations in the temperature and polarization anisotropies of the microwave background are inherited from ζ and provide a clean probe of its statistical character. Therefore, both present-day constraints [1] and the imminent arrival of high quality microwave-background data [2, 3] make accurate estimates of its statistical properties a pressing issue. Meanwhile, large surveys of the cosmological density field will provide information about its properties on complementary, smaller scales [4]. To compare this abundance of data to models we require an efficient tool with which to estimate the n-point functions $\langle\zeta^n\rangle$.

Taking ζ to be synthesized from the fluctuation of one or more light scalar fields during an inflationary era, several computational schemes exist which enable the n-point functions to be studied. Many of these schemes employ some variant of the *separate universe picture* [5–10]. Taking H to be the Hubble parameter, this asserts that—when smoothed on some physical scale, L, much larger than the horizon scale, so that $L/H^{-1} \gg 1$—the average evolution of each L-sized patch can be computed using the *background* equations of motion and initial conditions taken from smoothed quantities local to the patch. Working from a Taylor expansion in the initial conditions for each patch, Lyth & Rodríguez showed how this assumption could be turned into a practical algorithm for calculating correlation functions [11]. This "δN method" has become the most popular way to explore the predictions of specific models, both analytically and numerically, and has developed a large literature of its own. The principal difficulty arises when calculating the coefficients of the Taylor expansion, sometimes called the "δN coefficients." We shall discuss this difficulty in §3.4.2.

Alternative approaches exist. Rigopoulos, Shellard & van Tent [12, 13] evolved each correlation function using a Langevin equation. Yokoyama, Suyama & Tanaka [14–16] decomposed each δN coefficient into components which could be computed using ordinary differential equations. Later, a systematic method to obtain 'transport' equations for the

entire hierarchy of correlation functions (rather than simply the δN coefficients) was introduced [17, 18]. A more longstanding approach uses the methods of traditional cosmological perturbation theory ("CPT") to produce "transfer matrices" [19]. This has recently been revived by a number of authors [20–26]. Numerical approaches have been employed by Lehners & Renaux-Petel [27], Ringeval [28, 29], and Huston & Malik [30, 31].

The relationship of these different methods to each other has not always been clear. Nor is it always obvious how to relate the approximations employed by each technique. In this paper we study the connections between many of these approaches using the formalism of Elliston et al. [32]. This is a statistical interpretation of the separate universe picture. In what follows we briefly summarize the construction. (See also Ref. [17, 18].)

The separate universe approximation as statistical mechanics.—Fix a large spacetime box of comoving side μ containing the region of interest. The scale μ should be much larger than the separate universe scale, requiring $\mu \gg L$, but not superexponentially larger [33–35]. After smoothing on the scale L, the fields within the large box pick out an ensemble or cloud of $N \sim (\mu/L)^3$ points in the classical phase space. The condition that μ/L is not *superexponentially* large means that the typical diameter of the cloud will be roughly of order the quantum scatter $\langle \delta\phi^2 \rangle^{1/2} \sim H$. Because N is still large, $N \gg 1$, it is convenient to describe the ensemble by an occupation probability ρ on phase space.[1] The correlation functions of ζ on the scale L are then determined by the classical statistical mechanics of this ensemble, which is encoded in the Boltzmann equation.

In familiar applications of statistical mechanics, the evolution of the ensemble may be complicated. Small-scale interactions scatter members of the cloud between orbits on phase space, represented by the collisional term in the Boltzmann equation. However, the separate universe assumption requires causality to suppress those interactions which would be required for scattering between orbits. Therefore the evolution is trivial. Each point in phase space is assigned an occupation probability by the initial conditions, which is conserved along its orbit. All that is required is a mapping of initial conditions to the final state, which is obtained by carrying the initial conditions along the phase space flow generated by the underlying theory. It follows that the Boltzmann equation can be

[1] To be certain that we are estimating only the observables measured by a typical observer living within a single terminal vacuum, we should demand that ρ has support only on points whose orbits eventually converge in some neighbourhood of that vacuum. This requires that all horizon volumes reheat almost surely in the same minimum. If some horizon volumes reheat in different minima then the resulting correlation functions are not measurable by a local observer who sees only a single vacuum.

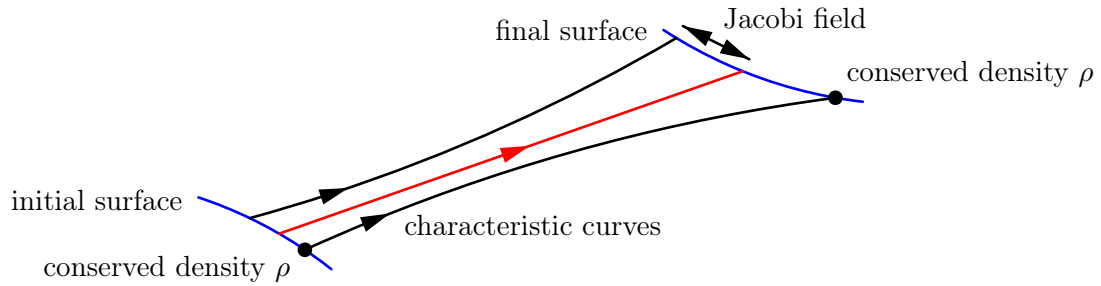

Figure 3.1: Jacobi fields. Characteristic curves are labelled by arrows, and the red characteristic is the fiducial curve. A conserved probability density is dragged along the flow. At any point, the Jacobi fields span the space infinitesimal displacements to neighbouring characteristics.

integrated using the method of characteristics.

A similar conclusion applies to the correlation functions of interest, $\langle \zeta^n \rangle$. These probe information about the distribution function over the cloud, giving a weighted average over many characteristics. Alternatively, if the cloud has only a small phase-space diameter, we can exchange information about the entire set of characteristics for the details of a *single* fiducial characteristic and a description of how nearby characteristics separate from it. In differential geometry this description is provided by the apparatus of Jacobi fields; see Fig. 3.1. We shall see that the differing implementations of the separate universe approximation can be understood as alternative methods to compute these Jacobi fields.

In applications we are frequently interested in correlation functions associated with mixed scales, rather than a single scale L. To do so we construct multiple ensembles associated with different smoothing scales. The separate universe approximation couples the evolution of all these ensembles in a specific way, which we describe in §4.4.

Outline.—In this paper we develop and refine the statistical-mechanical interpretation of the separate universe picture summarized above. Because the final distribution of occupation probabilities is an *image* generated by dragging along the phase space flow, it can be calculated in precisely the same way that geometrical optics enables us to calculate the image generated by a source of light rays. In §3.2 we show that, at least within the slow-roll approximation, this parallel is exact; the scalar field equation can be interpreted as the eikonal equation for a light ray in a medium with varying refractive index—or equivalently as Huygens' equation for a wavefront.

In §§3.2.3–3.2.4 we introduce the idea of Jacobi fields and explore their connection with the "adiabatic limit," in which all isocurvature modes decay and the curvature perturbation becomes conserved. Such limits are important because an inflationary model is predictive *on its own* only if the flow enters such a region [32, 36–39]. Jacobi fields are familiar from

the description of congruences of light rays in general relativity [40, 41]. In this case, as shown in Fig. 3.1, they describe fluctuations between the L-sized patches which make up the ensemble. Their evolution enables the adiabatic and isocurvature modes to be tracked. In particular, decay of isocurvature modes means decay of the corresponding Jacobi fields, which occurs when the bundle of trajectories undergoes focusing.

In §4.4 we use these ideas to develop evolution ("transport") equations for each correlation function, and in §3.4 we show that the Jacobi fields can be used to formally integrate the system of transport equations. This gives a practical method to identify regions where the flow becomes adiabatic. The analysis can begin from either the separate universe principle or traditional cosmological perturbation theory. As a by-product, our formal solution demonstrates that the transport equations are equivalent to the Taylor expansion algorithm introduced by Lyth & Rodríguez.

In §3.4.2 we use this solution to derive a closed set of differential equations for the Taylor coefficients, and in §3.4.3 we explain how the transport equations can be manipulated to obtain evolution equations for the coefficients of each momentum "shape". These shapes will be an important diagnostic tool when comparing inflationary models to observation [42, 43]. Together with the transport hierarchy of §4.4, the equations of §§3.4.2–3.4.3 represent the principal results of this paper. Either set can be used to obtain the correlation functions of a given theory, and we discuss their comparative advantages.

In §3.4.4 we give more a more general discussion of the relationship between the transport equations and other formulations of perturbation theory.

In §4.4.3 we specialize to the slow-roll approximation and use ray-tracing methods to derive the gauge transformation between field fluctuations and the curvature perturbation, ζ. As a result, we obtain the gauge transformation in terms of geometrical quantities—in particular, the extrinsic curvature of constant density hypersurfaces. We separate the gauge contribution to $f_{\rm NL}$ into a number of effects, corresponding to these geometrical quantities. For some models, we show that the largest of these can be attributed to a strong *relative* enhancement of the power in isocurvature fluctuations. We briefly discuss what conclusions can be drawn regarding the asymptotic magnitude of $|f_{\rm NL}|$.

Finally, we provide a brief summary of our results in §5.5.

Notation and conventions.—We use units in which $c = \hbar = 1$, and work in terms of the reduced Planck mass, $M_{\rm P}^{-2} = 8\pi G$. We use a number of index conventions which are introduced in the text. See especially the paragraph *Index convention* on p. 94, and the

discussion of primed indices below Eq. (3.32) on p. 105.

3.2 Geometrical optics in phase space

Throughout this paper, our discussion will apply to an inflationary phase which can be described by a collection of canonical scalar fields ϕ_α coupled to Einstein gravity. We initially use Greek labels α, β, ..., to label the different species of fields. The action for this system is

$$S = \frac{1}{2}\int \mathrm{d}^4x\, \sqrt{-g}\left(M_{\mathrm{P}}^2 R - \partial_a\phi_\alpha\partial^a\phi_\alpha - 2V\right), \tag{3.1}$$

where $V = V(\phi^\alpha)$ is an interaction potential depending only on the scalar fields, and indices a, b, ..., run over space time dimensions. We take the background geometry to be flat Friedmann–Robertson–Walker with scale factor $a(t)$.

3.2.1 Slow-roll approximation: rays on field space

In this subsection we impose the slow-roll approximation. This requires $\epsilon = -\dot{H}/H^2 \ll 1$ where $H = \dot{a}/a$ is the Hubble parameter. We introduce an ϵ-parameter for each species of light field,

$$\epsilon_\alpha \equiv \frac{1}{2M_{\mathrm{P}}^2}\frac{\dot{\phi}_\alpha^2}{H^2}, \tag{3.2}$$

in terms of which one can write $\epsilon = \sum_\alpha \epsilon_\alpha$. The slow-roll approximation therefore entails $\epsilon_\alpha \ll 1$.

Huygens' equation.—Combining (3.2) and the field equation for ϕ_α, and making use of the slow-roll approximation, we find

$$\frac{\mathrm{d}\phi_\alpha}{\mathrm{d}N} = \pm M_{\mathrm{P}}\sqrt{2\epsilon_\alpha} = -M_{\mathrm{P}}^2\partial_\alpha \ln V, \tag{3.3}$$

where $\mathrm{d}N \equiv \mathrm{d}\ln a$ measures the number of e-foldings of expansion experienced along the trajectory, and ∂_α denotes a partial derivative with respect to ϕ_α. Eq. (3.3) constrains the canonical momenta $\sim \dot{\phi}_\alpha$ to lie on a submanifold of the classical phase space coordinatized by the fields ϕ_α. This simplification is a consequence of the slow-roll approximation. In a theory with M scalar fields, it implies that we may work with the simpler M-dimensional field space instead of the full $2M$-dimensional phase space. This is convenient, although when we later abandon the slow-roll approximation we will have to return to phase space.

In what follows we often rewrite (3.3) in the form

$$\frac{\mathrm{d}\phi_\alpha}{\mathrm{d}N} = u_\alpha, \quad \text{where } u_\alpha \equiv -M_{\mathrm{P}}^2 \partial_\alpha f \text{ and } f \equiv \ln \frac{V}{V_*}, \tag{3.4}$$

and interpret the solution $\phi_\alpha(N)$ as an integral curve of the vector field u_α, parametrized by N. The scale V_* is arbitrary. Since f is a gradient, these integral curves correspond to pure potential flow.[2]

The unit vector parallel to u_α is

$$\hat{n}_\alpha \equiv \frac{u_\alpha}{M_{\mathrm{P}}\nu}, \tag{3.5}$$

where we have defined

$$\nu \equiv \sqrt{2\epsilon}. \tag{3.6}$$

It follows that the arc length along an integral curve, labelled s and measured using a flat Euclidean metric on field space, satisfies $\mathrm{d}s = M_{\mathrm{P}}\nu\,\mathrm{d}N$. Reparametrizing each curve in terms of s, the flow equation (3.4) can be rewritten

$$\nu \frac{\mathrm{d}\phi_\alpha}{\mathrm{d}s} = -M_{\mathrm{P}} \partial_\alpha \ln V = \partial_\alpha S, \tag{3.7}$$

where $S \equiv -M_{\mathrm{P}} f$ is Hamilton's characteristic function. Eq. (3.7) is *Huygens' equation*. Under the assumptions of geometrical optics, it describes the propagation of a light ray in a medium of spatially varying refractive index ν.

Snell's law.—We conclude that the inflationary trajectories in field space are precisely the light rays of geometrical optics, for which Huygens' equation can be thought of as a generalization of the Ibn Sahl or Snell–Descartes law. The wavefronts correspond to level sets of the characteristic function S and are therefore equipotentials, or surfaces of constant energy density in field space. Each light ray is locally orthogonal to these surfaces, so the vector $\hat{n}_\alpha$ is locally the unit vector normal to a surface of constant energy density.

When slow-roll is a good approximation ν is small, $\nu \ll 1$, and increases to $\nu \sim \mathrm{O}(1)$ near the end of inflation.

3.2.2 Rays on phase space

In some circumstances the slow-roll approximation is not available. This may be the case during inflation if slow-roll is temporarily violated—perhaps during a turn in field space, to be studied in §3.5.2—or on approach to the end of inflation, where $\epsilon \sim 1$.

[2]Since $\mathrm{d}f/\mathrm{d}N = u_\alpha \partial_\alpha f = -\|u_\alpha\|^2/M_{\mathrm{P}}^2$, it follows that f is monotone decreasing along each integral curve. Therefore one may loosely think of f as a Lyapunov function (or Morse function) for the flow.

In such cases we must return to the full second-order field equation, which cannot be written in the form of Eq. (3.3). To obtain an analogue of geometrical optics one must pass to a Hamiltonian formalism. We define

$$p_\alpha = \frac{\mathrm{d}\phi_\alpha}{\mathrm{d}N}. \tag{3.8}$$

This plays the role of Huygens' equation for ϕ_α. In terms of p_α, the scalar field equation becomes

$$\frac{\mathrm{d}p_\alpha}{\mathrm{d}N} = [\epsilon(p) - 3]p_\alpha - \frac{V_\alpha(\phi)}{H(\phi,p)^2}. \tag{3.9}$$

We must also rewrite ϵ and H in terms of p_α, obtaining

$$\epsilon(p) \equiv -\frac{\dot{H}}{H^2} = \frac{p_\alpha p_\alpha}{2M_{\mathrm{P}}^2} \tag{3.10a}$$

$$H(\phi,p)^2 M_{\mathrm{P}}^2 = \frac{V(\phi)}{3-\epsilon(p)}. \tag{3.10b}$$

Note that ϵ is purely a function of p_α, whereas H is a function of both ϕ_α and p_α.

Eqs. (3.8)–(3.9) show that, beyond slow-roll, the *precise* analogy with Huygens' equation is lost. Although these equations define a congruence of rays in phase space, it is not possible to find a characteristic function S so that these rays are everywhere orthogonal to equipotentials of S. Such a function would have to satisfy $\partial_{\phi_\alpha} S = p_\alpha$, and therefore $S = p_\alpha\phi_\alpha + g(p)$ for arbitrary g. Unfortunately, there is no choice for g which reproduces the right-hand side of Eq. (3.9).

The majority of our analysis requires only the first-order evolution equations (3.8)–(3.9), and at this level the formalism we develop will apply to evolution in phase space without imposing slow-roll. For that purpose it is convenient to combine ϕ_α and p_α into a single phase-space coordinate. We continue to write this ϕ_α, with the understanding that α now ranges over the $2M$ dimensions of phase space. The velocity vector is likewise u_α.

3.2.3 Jacobi fields and beam cross-sections

To proceed, we must carry the initial distribution of occupation probabilities along the flow, forming the "image" distribution of interest. In optical language, our task is to understand how images generated from a source of light rays are distorted by passage through a medium.

It was explained above that the typical spacing between arbitrarily selected members of the ensemble should be roughly of order the quantum scatter, $\sigma \sim \langle\delta\phi^2\rangle^{1/2}$. Because

$\sigma/M_{\rm P} \sim 10^{-5} \ll 1$, this is small in comparison with the natural scale $M_{\rm P}$. Therefore the orbits traversed by the cloud trace out a narrowly-collimated spray or "bundle" of light rays in phase space. In canonical models of inflation, setting initial conditions near horizon-crossing will make the initial profile close to Gaussian [44]. Therefore the evolution of the ensemble is similar to the evolution of tightly-focused Gaussian laser beam propagating in an optical cavity.

Connecting vectors.—Cross-sections within the laser beam may be focused, sheared or rotated by refraction. These possibilities are familiar from the study of weak gravitational lensing.

To obtain a quantitative description we slice the laser beam open, generating a cross-section. The precise slicing is arbitrary. For applications to inflation we will often slice along surfaces of fixed energy density, or after a fixed number of e-folds. Distortions of the cross section can be studied if we know how an arbitrary basis is transported from slice to slice. In general relativity this would be Fermi-Walker transport [40].

Jacobi used this method to study geodesic deviation on Riemannian manifolds. For this reason an infinitesimal vector propagated along the beam is called a *Jacobi field*. Taking $\delta\phi_\alpha$ to be such a field and the flow vector u_α to be sufficiently smooth, it will be transported by the equation

$$\frac{{\rm d}\delta\phi_\alpha}{{\rm d}N} = \delta\phi_\beta \partial_\beta u_\alpha = u_{\alpha\beta}\delta\phi_\beta. \tag{3.11}$$

The quantity $u_{\alpha\beta} \equiv \partial_\beta u_\alpha$ is the *expansion tensor*. It can be expanded in terms of a dilation $\theta = {\rm tr}\, u_{\alpha\beta}$, a traceless symmetric shear $\sigma_{\alpha\beta}$ and an antisymmetric twist $\omega_{\alpha\beta}$,

$$u_{\alpha\beta} \equiv \frac{\theta}{d}\delta_{\alpha\beta} + \sigma_{\alpha\beta} + \omega_{\alpha\beta}, \tag{3.12}$$

where $d = M$ for flows on field space, or $d = 2M$ if we do not impose the slow-roll approximation and work on the full phase space. In either case $\delta_{\alpha\beta}$ is the Kronecker δ.

Optical scalars.—Dilation describes rigid, isotropic rescaling of $\delta\phi_\alpha$ by $1+\theta$. It represents a global tendency of the light rays to focus or defocus. The shear $\sigma_{\alpha\beta}$ is a symmetric square matrix and can therefore be diagonalized, yielding d eigenvalues $\xi_{\boldsymbol{i}}$ and corresponding eigenvectors $s_{\alpha,\boldsymbol{i}}$ representing the principal shear directions (here $\boldsymbol{i}$ is a label taking values $1, \ldots, d$; see §3.5.2). The shear describes a rescaling of the component of the connecting vector in the direction $s_{\alpha,\boldsymbol{i}}$ by a factor $1 + \xi_{\boldsymbol{i}}$. Tracelessness of $\sigma_{\alpha\beta}$ implies $\sum_{\boldsymbol{i}} \xi_{\boldsymbol{i}} = 0$, so expansion in one direction must be accompanied by contraction in another. Therefore shear preserves cross-sectional area. Finally, the twist $\omega_{\alpha\beta}$ describes a rigid volume-preserving

rotation of $\delta\phi_\alpha$, representing a tendency of neighbouring trajectories to rotate around each other.

It is useful to define σ^2 to satisfy

$$\sigma^2 \equiv \frac{1}{2}\sigma_{\alpha\beta}\sigma_{\alpha\beta}. \tag{3.13}$$

Imposing the slow-roll approximation and working on field space, the flow is orthogonal to equipotentials of Hamilton's characteristic function. Therefore it is a pure potential flow, for which $\omega_{\alpha\beta} = 0$. On the full phase space this property is lost and the twist can be non-zero. In such cases it is helpful to define $2\omega^2 = \omega_{\alpha\beta}\omega_{\alpha\beta}$. Together, θ, σ^2 and ω^2 comprise the optical scalars introduced by Sachs and Penrose [45, 46].

van Vleck matrix.—Eq. (3.11) has a well-known formal solution in terms of an ordered exponential [47]. This method was used Rigopoulos, Shellard & van Tent [48, 49], and later by Yokoyama et al. [14]. It yields an explicit (but formal) expression for transport of any Jacobi field along the beam,

$$\delta\phi_\alpha(N) = \Gamma_{\alpha\beta}(N, N_0)\delta\phi_\beta(N_0), \tag{3.14}$$

where $\delta\phi_\beta(N_0)$ is the Jacobi field on some initial slice $N = N_0$. Eq. (3.14) describes the evolution of this Jacobi field at any later time N. The matrix $\Gamma_{\alpha\beta}(N, N_0)$ satisfies

$$\Gamma_{\alpha\beta}(N, N_0) \equiv \mathcal{P}\exp\int_{N_0}^{N} u_{\alpha\beta}(N')\,dN', \tag{3.15}$$

where the path-ordering operator $\mathcal{P}$ rewrites its argument with early times on the right-hand side, and later times on the left. We will occasionally refer to $\Gamma_{\alpha\beta}$ as the propagator matrix. It is closely related to a Wilson line.

Index convention.—Eq. (3.15) can be simplified with the aid of an index convention. Up to this point we have been labelling field-space indices using Greek symbols α, β, etc. To avoid writing the time of evaluation explicitly, we adopt the convention that Greek indices denote evaluation at the late time of interest, N. Latin indices i, j, etc., denote evaluation at the early time N_0. Therefore Γ can be written as a mixed index object, $\Gamma_{\alpha i}$.

Eq. (3.14) immediately implies

$$\Gamma_{\alpha i} = \frac{\partial\phi_\alpha}{\partial\phi_i}, \tag{3.16}$$

and endows this derivative with a geometric interpretation. It plays an important role in the Lyth–Rodríguez implementation of the separate universe approximation [11], where it appears due to a Taylor expansion in the initial conditions local to each L-sized patch. In

this formulation, one often projects on to equipotential surfaces in field space. We define $h_{\alpha\beta} = \partial\phi^c_\alpha/\partial\phi_\beta$ to obtain

$$\frac{\partial\phi^c_\alpha}{\partial\phi_i} = h_{\alpha\beta}\Gamma_{\beta i}. \tag{3.17}$$

The notation 'c' indicates that $\mathrm{d}\phi^c_\alpha$ can be thought of as the variation of a field ϕ^c_α defined on a fixed comoving *spacetime* hypersurface [50–52]. It follows from geometrical aguments that $h_{\alpha\beta} = \delta_{\alpha\beta} - \hat{n}_\alpha\hat{n}_\beta$, where $\hat{n}_\alpha$ is the unit normal to phase-space slices of constant potential energy, defined in (3.5). The tensor $h_{\alpha\beta}$ is the induced metric (or "first fundamental form") on these surfaces. Eq. (3.17) shows that choice of gauge is associated with projection onto an appropriate hypersurface in phase space. Moreover, Eqs. (3.16)–(3.17) show that partial derivatives with respect to ϕ_i are associated with propagation of Jacobi fields along the bundle.

Caustics.—The matrix $\Gamma_{\alpha i}$ appears whenever it is necessary to track the distortion of a line element along a flow, and has applications in fluid dynamics, general relativity and elsewhere [40, 53]. DeWitt–Morette observed that, considered as a matrix of Jacobi fields, Eq. (3.16) was related to the inverse of the van Vleck matrix, introduced in the construction of semiclassical ("WKB") approximations to the path integral [54–56].[3] We define

$$\Gamma^{-1}_{i\alpha} = \delta_{i\beta}\,\mathcal{P}\exp\left(-\int_{N_0}^{N} u_{\beta\alpha}(N')\,dN'\right). \tag{3.18}$$

The van Vleck matrix is $\Delta_{i\alpha} \equiv (N - N_0)^d\Gamma^{-1}_{i\alpha}$, and has a well-known interpretation in geometrical optics as a measure of focusing or defocusing: in particular, $|\det\Delta| \to \infty$ at a *caustic*, where light rays converge. Since $(N - N_0)$ is nonzero for $N \neq N_0$, a singularity in the van Vleck determinant implies a singularity in $\det\Gamma^{-1}$. Applying (4.20), we conclude

$$\frac{1}{\det\Gamma^{-1}} = \det\Gamma \equiv \Theta(N, N_0) = \exp\int_{N_0}^{N}\theta(N')\,dN'. \tag{3.19}$$

Therefore $\Theta \to 0$ at a caustic. This happens after finitely many e-folds only if $\theta \to -\infty$ during the flow. Otherwise, Θ is decreasing in regions where θ is negative, with large

[3] In DeWitt–Morette [54] the proof is ascribed to B.S. DeWitt. DeWitt–Morette noted that the relation between Jacobi fields and variation of a general solution of the field equations with respect to its constants of integration had been known to Jacobi (ultimately leading to his development of what is now Hamilton–Jacobi theory), and suggested that this technique could be used to simplify the long calculations which arise when solving Jacobi's equation. Applied to inflationary correlation functions, the history has been reversed: the variational formulae came first, in the form of the Lyth–Rodríguez algorithm. This often leads to simple analytic results, as DeWitt–Morette foresaw. But, as we explain in §3.4.2, this method is unsuited to numerical implementation, because of the small numerical tolerances required to reliably determine variation with respect to the initial conditions. It is preferable to solve an *ordinary* differential equation, such as Jacobi's equation (3.11) or (3.26).

negative θ implying strong focusing. Large positive θ implies strong defocusing. More generally the propagator matrix can be rewritten in terms of Θ, giving

$$\Gamma_{\alpha i} = \Theta(N, N_0)^{1/M}\, \mathcal{P} \exp\left(\int_{N_0}^{N} (\sigma + \omega)_{\alpha\beta}(N')\, dN'\right) \delta_{\beta i}. \tag{3.20}$$

The ordered exponential has determinant unity and therefore does not change the cross-sectional area of the bundle.

3.2.4 Adiabatic limit

Caustics have an important interpretation in the flows describing an inflationary model. If the bundle of trajectories has finite cross section, then the ensemble contains members which are evolving along multiple phase space trajectories. These are the eponymous "separate universes" with their individual initial conditions.

Under these circumstances one or more isocurvature modes exist. These are connecting vectors which relate the different ϕ_α within the bundle which all lie on a surface of fixed energy density, say Σ_ρ. Their number is determined by the rank of $h_{\alpha\beta}\Gamma_{\beta i}$. In the special case where the bundle cross-section decays to a point, there is a unique intersection between the bundle and Σ_ρ. Therefore $h_{\alpha\beta}\Gamma_{\beta i}$ has rank zero and all isocurvature modes disappear. In this limit, each member of the ensemble traverses the same orbit, differing from the others only by its relative position, which corresponds to the adiabatic mode, ζ. It follows that, when the cross-section collapses to a point, the fluctuations become purely adiabatic. Elliston et al. [32] described this as an 'adiabatic limit'. After this limit has been reached ζ is conserved [57, 58].

Flows which reach an adiabatic limit during inflation are no more or less likely—or natural—from the viewpoint of fundamental physics. But flows reaching an adiabatic limit *are* more predictive, because a perturbation in the purely adiabatic mode remains adiabatic long after inflation ends [59, 60], even during epochs for which we are ignorant of the relevant physics. Contrariwise, if any isocurvature modes remain then members of the ensemble may rearrange their relative positions until these modes decay. This possibility was emphasized by Meyers & Sivanandam [61, 62]; see also Ref. [32]. If the flow does not reach an adiabatic limit during inflation then the model is not predictive until we supply a prescription for the post-inflationary era, and observational predictions can depend on this choice.

Trivial, adiabatic and nonadiabatic caustics.—The outcome of this discussion is that approach to an adiabatic limit can be associated with convergence to a caustic. An early discussion of this principle, phrased almost precisely in these terms, was given by Wands & García-Bellido [38]. We conclude that $\Theta \to 0$ is a necessary condition for an adiabatic limit to occur, but as we now explain it is not sufficient.[4] A caustic can be classified by the number of dimensions lost by the flow, or equivalently the number of null eigenvalues of the propagator $\Gamma_{\alpha i}$ at the caustic. An adiabatic limit is the special case where $\Gamma_{\alpha i}$ retains a *single* non-null eigenvalue, but $h_{\alpha\beta}\Gamma_{\beta i}$ has *no* non-null eigenvalues. We describe caustics which satisfy this condition as *adiabatic*.

Eq. (3.20) shows that, were the integrated shear and twist to remain bounded while $\Theta \to 0$, then $\Gamma_{\alpha i} \to 0$. In this case no perturbations would survive, and we describe the caustic as *trivial*. An example is the case where $u_{\alpha\beta}$ is pure dilation. But barring an accurate cancellation of this kind, at least some component of $(\sigma+\omega)_{\alpha\beta}$ will typically scale proportionally to θ on approach to the caustic.[5]

Shear opposes focusing.—If the perturbations are not to vanish completely, then some *anisotropic* effect of shear and twist must oppose the isotropic contraction due to $\Theta \to 0$.

First suppose the twist is negligible. We assume that the eigenvectors of σ stabilize in the vicinity of the caustic. If the shear has some number of positive eigenvalues λ_i for which λ_i/θ has a finite, nonzero limit, then perturbations may survive in the subspace spanned by their corresponding eigenvalues. Tracelessless of σ implies that at least one eigenvalue must be negative, and perturbations in the subspace spanned by the corresponding eigenvectors will disappear. Hence, at least one dimension will be lost by the flow. In practice it is often simpler to work directly with the eigenvalues of the expansion tensor $u_{\alpha\beta}$.

If more than one eigenvalue of σ is positive, then perturbations may survive in a two- or higher dimensional subspace. In this case the caustic does not describe approach to an adiabatic limit, and we call it *nonadiabatic*. To obtain predictions for observable quantities the evolution must be continued. In practice this would require introduction

[4] One may have some reservations about this conclusion, because it seems to violate the Liouville theorem which guarantees conservation of phase-space volume. However, it should be remembered that the *canonical* phase space coordinate to which Liouville's theorem applies are not the field-space position and momenta which we are using. In particular, the canonical momenta will typically include powers of the scale factor a.

[5] In principle $u_{\alpha\beta}$ could contain off-diagonal terms which grow *faster* than the diagonal terms, and therefore θ. In this case there could be a subspace of growing perturbations. If the growth is exponential this usually signals an instability, and the formalism we are describing becomes invalid.

of a reduced phase space describing only the surviving perturbations. The flow can then be followed in this reduced phase space until a further focusing event occurs. This may itself be an adiabatic limit, or might simply describe further reduction in the phase space. One should continue in this way until an adiabatic limit is finally achieved. An example of this behaviour could occur soon after the onset of slow-roll inflation. In the early stages, independent fluctuations in the field velocities survive. But when slow-roll is a good approximation these will be exponentially suppressed, making Θ become very small. One should therefore replace the full description by a reduced phase space which includes only field perturbations. In doing so one arrives at the field-space description of slow-roll inflation given in §3.2.1.

Twist opposes focusing.—In slow-roll inflation, which we discuss in §3.2.5 below, a diverging shear is the only mechanism by which perturbations can survive on approach to a caustic. Where the twist is non-zero, which occurs when we do not impose the slow-roll approximation, more possibilities exist. Ultimately these must be addressed, to describe approach to an adiabatic limit when slow-roll is no longer a good approximation, but we defer this discussion for future work.

3.2.5 Focusing in the slow-roll approximation

In this subsection we give a more detailed discussion of the approach to a caustic during an era of slow-roll inflation.

Raychaudhuri equations.—Parametrizing each trajectory by e-folding number N, Eq. (3.4) constitutes an autonomous dynamical system. Therefore a derivative along the flow can be written $d/\mathrm{d}N = u_\alpha \partial_\alpha$. In the absence of a nontrivial field-space metric all derivatives commute, and therefore $[\partial_\gamma, \partial_\beta] u_\alpha = 0$. Contracting with u_γ and rearranging terms, one finds

$$\frac{\mathrm{d}u_{\alpha\beta}}{\mathrm{d}N} = \partial_\beta a_\alpha - u_{\alpha\gamma} u_{\gamma\beta}, \tag{3.21}$$

where a_α is the acceleration vector, defined by $a_\alpha = \mathrm{d}u_\alpha/\mathrm{d}N = u_\beta \partial_\beta u_\alpha$. For a potential flow, this can be simplified; comparison with Eq. (3.4) shows that

$$a_\alpha = \frac{M_{\mathrm{P}}^2}{2} \partial_\alpha \nu^2, \tag{3.22}$$

where, as above, ν is the local refractive index.

The evolution equations for the dilation and shear can be written

$$\frac{\mathrm{d}\theta}{\mathrm{d}N} = M_{\mathrm{P}}^2\mathcal{H} - \frac{\theta^2}{M} - 2\sigma^2 \tag{3.23}$$

$$\frac{\mathrm{d}\sigma_{\alpha\beta}}{\mathrm{d}N} = M_{\mathrm{P}}^2\Big(\mathcal{H}_{\alpha\beta} - \frac{\mathcal{H}}{M}\delta_{\alpha\beta}\Big) - \frac{2\theta}{M}\sigma_{\alpha\beta} - \Big(\sigma_{\alpha\gamma}\sigma_{\gamma\beta} - \frac{2\sigma^2}{M}\delta_{\alpha\beta}\Big). \tag{3.24}$$

These are commonly known as the Raychaudhuri equations. An equation for the evolution of the twist could be found in the same way, but is not needed in the slow-roll approximation.

We have defined $\mathcal{H}_{\alpha\beta}$ to be the Hessian of ν^2,

$$\mathcal{H}_{\alpha\beta} \equiv \frac{1}{2}\partial_\alpha\partial_\beta\nu^2, \tag{3.25}$$

and $\mathcal{H}$ is its trace. Because the Hessian measures the local curvature of a function, one can regard $\mathcal{H}_{\alpha\beta}$ as a measure of the curvature of surfaces of constant refractive index in field space.

Jacobi equation.—Eq. (3.11) shows that Jacobi fields oriented along eigenvectors of $u_{\alpha\beta}$ with positive eigenvalues grow, whereas those oriented along eigenvectors with negative eigenvalues decay.

We can find an alternative description in terms of the refractive index ν. Taking a derivative of (3.11) along the flow and using the Raychaudhuri equations to eliminate derivatives of the dilation and shear yields the Jacobi equation,[6]

$$\frac{\mathrm{d}^2\delta\phi_\alpha}{\mathrm{d}N^2} = M_{\mathrm{P}}^2\mathcal{H}_{\alpha\beta}\delta\phi_\beta. \tag{3.26}$$

It follows that the behaviour of the Jacobi fields is determined by the curvature of ν^2, considered as a function in field space. (Note this is related to, but not the same as, the curvature of surfaces of constant ν.) Qualitatively, Jacobi fields oriented along eigenvectors of $\mathcal{H}_{\alpha\beta}$ with negative eigenvalues—directions of negative curvature—will have quasi-trigonometric solutions. These will pass through zero, corresponding to the collapse of some Jacobi fields to zero length. Fields oriented along eigenvectors with positive eigenvalues will have exponential solutions. Unless the initial conditions are precisely adjusted, these will typically grow.

Focusing theorem.—By adapting the geodesic focusing theorem of general relativity [40] we can determine the circumstances under which focusing will occur after finitely many

[6] When using Jacobi fields to study geodesic deviation on a Riemannian manifold, this equation takes the form $\delta\ddot{\phi}_\alpha = -R_{\alpha\hat{n}\beta\hat{n}}\delta\phi_\beta$, where $R_{\alpha\hat{n}\beta\hat{n}} = \hat{n}^\rho\hat{n}^\sigma R_{\alpha\rho\beta\sigma}$ is a component of the Riemann curvature projected along the tangent to the geodesic.

e-folds. Pick a point on the flow where the expansion is negative, with value $\theta_\star < 0$. Inspection of (3.23) shows that, if $\mathcal{H} < 0$, then $\theta \to -\infty$ within $\Delta N = M/|\theta_\star|$ e-folds, where M is the dimension of field space. Any point where $\theta = -\infty$ is a caustic, because on arrival at this point $\Theta = 0$.

Since Morse's lemma implies that $\mathcal{H}$ is negative in a neighbourhood of any local maximum of the refractive index, $\nu^2 = 2\epsilon$, one might hope to associate such local maxima with terminal points for inflation at which an adiabatic limit would be nearly achieved.

However, the conditions of the focusing theorem are not satisfied for typical potentials. More usually the slow-roll approximation forces all fields to settle into a terminal vacuum increasingly slowly, requiring an infinite number of e-folds to reach $\Theta = 0$. Moreover, in practical examples the slow-roll approximation will break down and inflation will terminate long before the caustic is reached. Therefore we should *not* expect to achieve precisely $\Theta = 0$ during inflation. Nevertheless, a model may be sufficiently predictive if the flow spends enough e-folds in a region of large negative θ that Θ is exponentially suppressed before inflation ends.

In simple potentials it is often clear when ζ ceases to evolve. But for more complicated potentials the situation may not be so clear. Within the slow-roll approximation, this discussion shows that $\Theta \gtrsim 1$ can be taken as a clear indication that isocurvature modes are still present. Their future decay is likely to influence ζ and the outcome of any calculation which terminates with $\Theta \gtrsim 1$ should not be considered a prediction for observable quantities. Conversely, $\Theta \ll 1$ is an indication that some decay of isocurvature modes has taken place. The precise nature of the decay must be deduced from the behaviour of the shear and twist. If perturbations survive only in a one-dimensional subspace than we can infer that the isocurvature modes have decayed to the point that ζ will be approximately conserved.

Example: quadratic Nflation.—We illustrate these ideas using the quadratic approximation to Nflation [63–66]. The potential is

$$V = \sum_\alpha \frac{1}{2} m_\alpha^2 \phi_\alpha^2. \tag{3.27}$$

This model is of interest in its own right, but also describes the approach to a generic stable minimum after suitable choice of field space coordinates. We suppose that there is at least a modest hierarchy among the masses, and order these so that $m_\alpha < m_\beta$ if $\alpha < \beta$. The most massive field will settle into its minimum first, followed by the next most massive field. Therefore approach to the final minimum will be described by a trajectory

on which only ϕ_1 is dynamical, with all other ϕ_α approximately zero. We describe this as the "inflow" trajectory.

On the inflow trajectory, the dilation satisfies

$$\theta^{\text{inf}} \approx -2\frac{M_{\text{P}}^2}{\phi_1^2}\left(\sum_{\alpha\geq 2}\frac{m_\alpha^2}{m_1^2} - 1\right). \tag{3.28}$$

The minimum $\phi_1 = 0$ is a caustic, but as discussed above it cannot be reached after finitely many e-folds (within the slow-roll approximation). The expansion tensor satisfies

$$u_{\alpha\beta}^{\text{inf}} \approx \begin{pmatrix} 2\frac{M_{\text{P}}^2}{\phi_1^2} & & & \\ & \ddots & & \\ & & -2\frac{m_\alpha^2}{m_1^2}\frac{M_{\text{P}}^2}{\phi_1^2} & \\ & & & \ddots \end{pmatrix}. \tag{3.29}$$

This has one positive eigenvalue and the rest negative, so we expect it will correspond to an adiabatic limit.

The $(1,1)$ component of Γ^{inf} diverges near the caustic. This does not signal an instability, but only that $\delta\phi_1$ grows at precisely the required rate to give constant $\zeta \sim (H/\dot{\phi}_1)\delta\phi_1$.

Ordered exponentials such as (3.15) satisfy a composition property, allowing the integral over the inflationary trajectory to be broken in two. (See Fig. 3.2.) The first component is an integral from the initial point until the onset of the inflow trajectory. We take this to occur at $\phi_1 = \phi_1^*$, and choose ϕ_1^* so that (3.29) is a good approximation there. The propagator at this point is $\Gamma_{\alpha i}^*$. It is a complicated weighted average over the trajectory, and cannot usually be calculated analytically. The second component is an integral over the inflow trajectory, which we denote $\Gamma_{\alpha\beta}^{\text{inf}}$. Therefore $\Gamma_{\alpha i} = (\Gamma^{\text{inf}}\Gamma^*)_{\alpha i}$. The inflow part can be computed from (3.29),

$$\Gamma^{\text{inf}} \approx \begin{pmatrix} \frac{\phi_1^*}{\phi_1} & & & \\ & \ddots & & \\ & & \left(\frac{\phi_1}{\phi_1^*}\right)^{m_\alpha^2/m_1^2} & \\ & & & \ddots \end{pmatrix}. \tag{3.30}$$

Except perhaps for special choices of initial conditions, Eq. (3.30) gives rank $r = 1$ at the caustic. Therefore this is an example of an adiabatic caustic.

In more general circumstances, it may be necessary to diagonalize $u_{\alpha\beta}^{\text{inf}}$ before integrating over the inflow trajectory. This is reminiscent of the introduction of scaling operators in

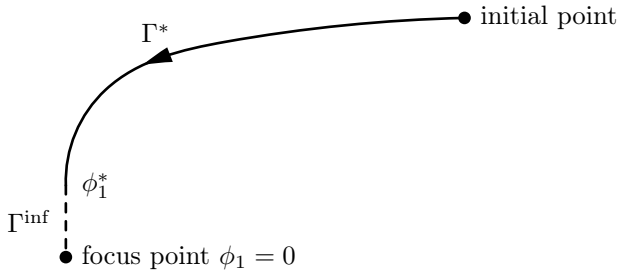

Figure 3.2: Decomposition of propagator along an inflationary trajectory. Trajectories flowing into the minimum from most initial points join an "inflow trajectory" (represented by a dashed line) at $\phi_1 = \phi_1^*$. The precise location of the junction is initial-condition dependent. The inflow trajectory sinks into the caustic, which here is a focus point, giving nearly-universal behaviour in the final stages of approach. This parallels the discussion of universality in critical phenomena; however, here, the universal region is often physically inaccessible because the slow-roll approximation breaks down in the vicinity of the focus point. The remaining part of the trajectory (represented by a solid line) is non-universal, and typically cannot be calculated analytically.

a renormalization-group framework. Indeed, the entire analysis, and the emergence of rational but non-integer power-law scaling near the caustic, parallels a renormalization group analysis in the neighbourhood of a fixed point [67]; compare also Eq. (79) of Vernizzi & Wands [50].

Focusing in double quadratic model.—Away from the inflow trajectory it is usually necessary to proceed numerically. In Fig. 3.3 we show the evolution of the focusing parameters in the well-studied model of double quadratic inflation [36, 37, 39, 48–50, 68, 69]. The potential is $V = m_1^2\phi_1^2/2 + m_2^2\phi_2^2/2$. We choose the mass ratio $m_1/m_2 = 9$ and set initial conditions $\phi_1 = 8.2M_{\rm P}$ and $\phi_2 = 12.9M_{\rm P}$.

Initially the evolution is mostly in the ϕ_2 direction. When ϕ_2 reaches the vicinity of its minimum there is a turn in field-space, which generates a spike in $f_{\rm NL}$. After the turn, the inflow trajectory is reached along the ϕ_1 direction.

This evolution is reflected in the evolution of the bundle. Initially $\theta > 0$ and the cross-section slowly dilates. It reaches a maximum at roughly three times the original cross-sectional area. After the turn, θ rapidly drops to a negative value, and thereafter diverges exponentially to $-\infty$. Therefore the bundle-cross section very rapidly diminishes to almost zero cross-sectional area. This corresponds to an approximate caustic, and leads to an adiabatic limit.

Eventually the divergence in θ would be cut off by a breakdown of the slow-roll approximation, but for typical parameter choices Θ will already be exponentially small at this point.

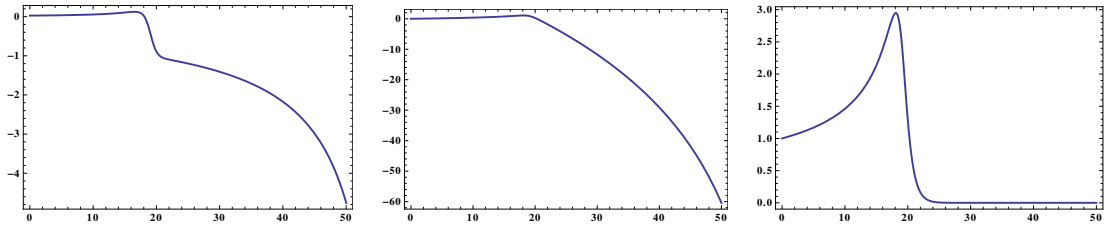

(a) Dilation θ **(b)** Integrated dilation $\int \theta \, \mathrm{d}N$ **(c)** Focusing $\Theta = \mathrm{e}^{\int \theta \, \mathrm{d}N}$

Figure 3.3: Dilation, integrated dilation and focusing parameters in the double quadratic inflation model $V = \frac{1}{2}m_1^2\phi_1^2 + \frac{1}{2}m_2^2\phi_2^2$. The mass ratio is $m_1/m_2 = 9$, and the initial conditions are $\phi_1 = 8.2M_\mathrm{P}$, $\phi_2 = 12.9M_\mathrm{P}$. All plots are against the e-folding number N, measured from horizon exit of the mode in question.

Example: axion-quadratic model.—Elliston et al. [32] introduced an approximation to the hilltop region of axion N-flation [65, 66]. The Hubble rate is dominantly supported by many axions in the quadratic region of their potential, and can be approximated by a single field. A few axions remain in the vicinity of the hilltop, where their contribution to H is negligible but their contribution to the three- and higher n-point functions in the adiabatic limit is large.

The potential is $V = m^2\phi^2/2 + \Lambda^4(1 - \cos 2\pi\chi/f)$. We set $\Lambda^4 = 25m^2f^2/4\pi^2$ and choose $f = M_\mathrm{P}$. In Fig. 3.4 we show the evolution for initial conditions $\phi = 16M_\mathrm{P}$ and $\chi = (f/2 - 0.001)M_\mathrm{P}$.

The evolution is similar to the double quadratic model. Initially θ is positive and the cross-sectional area grows. At its peak, it is more than 200 times the original cross-section. Eventually ϕ approaches its minimum and the Hubble friction decreases to the point that χ can evolve. It rolls away from the hilltop, eventually ending inflation. During this phase θ switches sign, ultimately diverging exponentially to $-\infty$. Therefore we approach an adiabatic limit. However, Fig. 3.4c shows that the rate of approach is quite slow. The cross-section decays softly, and by the end of inflation $\Theta \sim 10^{-3}$. Therefore an approximate adiabatic limit is reached and we can expect the observables to be roughly conserved through the post-inflationary evolution.

3.3 Transport equations

We now apply these ideas to obtain evolution (or "transport") equations for the correlation functions in a fixed, comoving spacetime volume. In this section our analysis will be general,

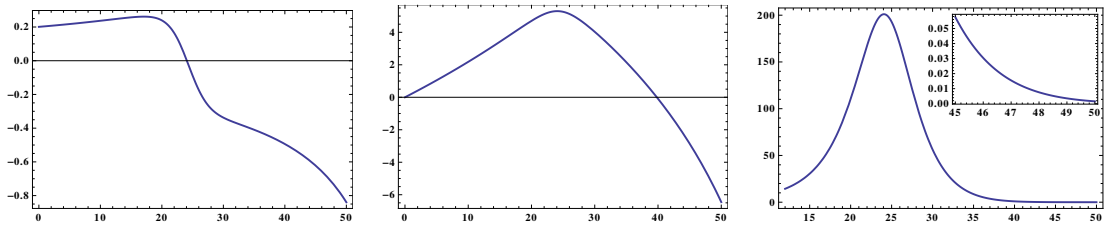

(a) Dilation θ **(b)** Integrated dilation $\int \theta \, \mathrm{d}N$ **(c)** Focusing $\Theta = \mathrm{e}^{\int \theta \, \mathrm{d}N}$

Figure 3.4: Dilation, integrated dilation and focusing parameters in the axion-quadratic model $V = \frac{1}{2}m^2\phi^2 + \Lambda^4(1 - \cos 2\pi\chi/f)$. We have set $\Lambda^4 = 25m^2f^2/4\pi^2$ and $f = M_{\mathrm{P}}$. The initial conditions are $\phi = 16M_{\mathrm{P}}$, $\chi = (f/2 - 0.001)M_{\mathrm{P}}$. In (c), the inset panel shows the evolution of Θ near the end of inflation. All plots are against the e-folding number N, measured from horizon exit of the mode in question.

and can be applied to any perturbations whose evolution equations can be expressed in the form of Eq. (3.32). If necessary this can be achieved as described in §3.2 by passing to a Hamiltonian framework. It follows that the transport of correlation functions is most naturally expressed in phase space.

Connecting vectors.—Consider the set-up described in §3.1, in which a comoving spacetime region of size μ is smoothed into separate universes of size L. Pick any one of these L-sized regions, which we take to be at spatial position $\boldsymbol{x}$. The separate universe approximation asserts that the evolution of the smoothed fields in this region is given by the flow equation (3.4). We denote the difference between these values and those in some other region, located at position $\boldsymbol{x} + \boldsymbol{r}$, by $\delta\phi_\alpha(\boldsymbol{r})$. This is a connecting vector in the sense of Eq. (3.11). Taylor expanding u_α, the corresponding deviation equation is

$$\frac{\mathrm{d}\delta\phi_\alpha(\boldsymbol{r})}{\mathrm{d}N} = u_{\alpha\beta}[\phi(\boldsymbol{x})]\delta\phi_\beta(\boldsymbol{r}) + \frac{1}{2}u_{\alpha\beta\gamma}[\phi(\boldsymbol{x})]\left\{\delta\phi_\beta(\boldsymbol{r})\delta\phi_\gamma(\boldsymbol{r}) - \langle\delta\phi_\beta(\boldsymbol{r})\delta\phi_\gamma(\boldsymbol{r})\rangle\right\} + \cdots . \tag{3.31}$$

We assume $\langle\delta\phi_\alpha(\boldsymbol{r})\rangle = 0$ and have subtracted a zero-mode to preserve this throughout the motion.[7] The tensor $u_{\alpha\beta}$ was defined in (3.11), and $u_{\alpha\beta\gamma} \equiv \partial_\gamma u_{\alpha\beta}$. We describe them, together with higher-index counterparts obtained by further differentiation, as u-tensors. They inherit a dependence on $\boldsymbol{x}$ through evaluation at $\phi_\alpha = \phi_\alpha(\boldsymbol{x})$. After transformation to Fourier space, the subtractions in Eq. (4.19) correspond to discarding disconnected correlation functions. Therefore statistical properties of the ensemble do not depend on our choice of fiducial point.

[7] In the language of Feynman diagrams, this would correspond to removing contributions arising from disconnected pieces. This procedure is routine in applications of the separate universe principle.

If μ/L is not superexponentially large, we can typically expect $|\delta\phi_\alpha(\boldsymbol{r})|$ to be small and slowly varying. In Fourier space, this implies that $\delta\phi_\alpha(\boldsymbol{r})$ is constructed from only a few soft, infrared modes which we label $\boldsymbol{k}$. The remaining modes have been integrated out in the smoothing process used to obtain this effective, separate-universe description. Working explicitly in terms of these modes, Eq. (4.19) yields a connecting vector and deviation equation for each combination of species and $\boldsymbol{k}$-mode[8]

$$\frac{\mathrm{d}\delta\phi_{\alpha'}}{\mathrm{d}N} = u_{\alpha'\beta'}(\boldsymbol{x})\delta\phi_{\beta'} + \frac{1}{2}u_{\alpha'\beta'\gamma'}(\boldsymbol{x})\left\{\delta\phi_{\beta'}\delta\phi_{\gamma'} - \langle\delta\phi_{\beta'}\delta\phi_{\gamma'}\rangle\right\} + \cdots . \tag{3.32}$$

Eq. (3.32) has been written in an abbreviated "de Witt" notation, in which the primed, compound index α' carries *both* an unprimed species (or "flavour") label α and a momentum $\boldsymbol{k}_\alpha$. Contraction over primed indices implies summation over the flavour label and integration over the momentum label with measure d^3k. The 2- and 3-index u-tensors appearing here satisfy

$$u_{\alpha'\beta'}(\boldsymbol{x}) \equiv \delta(\boldsymbol{k}_\alpha - \boldsymbol{k}_\beta)u_{\alpha\beta}(\boldsymbol{x}) \tag{3.33a}$$

$$u_{\alpha'\beta'\gamma'}(\boldsymbol{x}) \equiv (2\pi)^{-3}\delta(\boldsymbol{k}_\alpha - \boldsymbol{k}_\beta - \boldsymbol{k}_\gamma)u_{\alpha\beta\gamma}(\boldsymbol{x}). \tag{3.33b}$$

Eq. (4.19) was given by Yokoyama et al. [14, 15] in real space, and used to obtain evolution equations for the momentum-independent Lyth–Rodríguez Taylor coefficients. We explore the relationship between our approaches in Appendix 3.A. However, Yokoyama et al. did not interpret $u_{\alpha\beta}$ as the expansion tensor of the flow or give the $\boldsymbol{k}$-space equations (3.32) and (3.33a)–(3.33b). As we will see, this $\boldsymbol{k}$-dependent information is necessary to obtain transport equations for the full set of coupled $\boldsymbol{k}$-space correlation functions.

One can arrive at the same conclusions using cosmological perturbation theory. Taking the background value of ϕ_α to be the average field over the μ-sized box, the perturbations within the box are $\delta\phi_\alpha(\boldsymbol{r})$. One should now interpret $\boldsymbol{r}$ as a coordinate relative to the box. Restricting attention to the infrared modes in $\delta\phi_\alpha(\boldsymbol{r})$, for which k/a is negligible, we recover Eqs. (3.32) and (3.33a)–(3.33b).

Correlation functions.—The full set of connecting vectors contains all information required to determine evolution of the bundle, and therefore the evolution of all statistical quantities. In Eq. (3.32) this data is carried by the u-tensors. The transport equations for correlation functions are simply a reorganization of this information. Therefore they must also be expressible purely in terms of u-tensors. Since (3.32) shows that these tensors

[8] In Eq. (3.32) we are keeping nonlinear terms in the evolution equation. We use the term "Jacobi field" to refer to infinitesimal connecting vectors, for which only the linear term need be kept.

can be obtained by the separate universe argument or traditional perturbation theory, it follows that they will make equivalent predictions.

There are multiple ways to organize the u-tensors to produce evolution equations. In Ref. [17, 18], transport equations were obtained after postulating a conservation equation for a probability density P,

$$\frac{\mathrm{d}P}{\mathrm{d}N} + \partial_\alpha(u_\alpha P) = 0. \tag{3.34}$$

Evolution equations for the moments of P were extracted using both a Gauss–Hermite expansion, and generating functions. Here we describe a third, simpler method. Provided the perturbations can be treated classically, we expect $\mathrm{d}\langle O\rangle/\mathrm{d}N = \langle \mathrm{d}O/\mathrm{d}N\rangle$ for any quantity O.[9]

Two-point function.—We write the two-point function as $\Sigma_{\alpha'\beta'} \equiv \langle \delta\phi_{\alpha'}\delta\phi_{\beta'}\rangle$. Eq. (3.32) implies

$$\begin{aligned}\frac{\mathrm{d}\Sigma_{\alpha'\beta'}}{\mathrm{d}N} &= \left\langle \frac{\mathrm{d}\delta\phi_{\alpha'}}{\mathrm{d}N}\delta\phi_{\beta'} + \delta\phi_{\alpha'}\frac{\mathrm{d}\delta\phi_{\beta'}}{\mathrm{d}N}\right\rangle \\ &= u_{\alpha'\gamma'}\Sigma_{\gamma'\beta'} + u_{\beta'\gamma'}\Sigma_{\gamma'\alpha'} + [\geq 3 \text{ p.f.}] \\ &\equiv \{u,\Sigma\}_{\alpha'\beta'} + [\geq 3 \text{ p.f.}]\end{aligned} \tag{3.35}$$

where $\{A, B\}$ is the matrix anticommutator of A and B, and $[\geq 3$ p.f.$]$ denotes terms including three-point functions or above which have been omitted. In general, the transport equations will couple correlation functions of all orders. They can be thought of as a limiting case of a Schwinger–Dyson hierarchy, applied to expectation values rather than the *in–out* amplitudes of scattering theory. Calzetta & Hu argued that the result could be interpreted as a Boltzmann hierarchy [70, 71].

As in any effective theory, the transport equations will be useful only if a reason can be found to systematically neglect an infinite number of terms. Applied to inflation, the statistical properties of the ensemble are nearly Gaussian: in the simplest models, an n-point function will typically be of order $H^{m(n)}$, where $m(n)$ is the smallest even integer at least as large as n [72]. This is suppressed compared to the natural scale M_{P} by $(H/M_{\mathrm{P}})^{m(n)} \ll 1$. However, this is not necessary; all that is required (or suggested by observation) for (4.21) to be valid is that the three- and higher n-point functions are substantially smaller than the two-point function.

Eq. (4.21) was given in Ref. [17, 18] for an arbitrary n-field model, but with $\Sigma_{\alpha'\beta'}$ interpreted as the real-space correlation function. The single-field case is discussed by

[9] This equation both implies and is implied by conservation of probability, Eq. (3.34)

Gardiner [73]. With the u-tensors given in (3.33a)–(3.33b), Eq. (4.21) applies for the full $\boldsymbol{k}$-dependent correlation function.

Three-point function.—We write the three-point function as $\alpha_{\alpha'\beta'\gamma'} \equiv \langle \delta\phi_{\alpha'}\delta\phi_{\beta'}\delta\phi_{\gamma'}\rangle$. Keeping contributions of order $\mathrm{O}(\Sigma^2)$ and $\mathrm{O}(\alpha)$, we conclude

$$\begin{aligned}\frac{\mathrm{d}\alpha_{\alpha'\beta'\gamma'}}{\mathrm{d}N} &= u_{\alpha'\lambda'}\alpha_{\lambda'\beta'\gamma'} + u_{\alpha'\lambda'\mu'}\Sigma_{\lambda'\beta'}\Sigma_{\mu'\gamma'} \\ &\quad + \text{cyclic } (\alpha' \to \beta' \to \gamma') + [\geq 4 \text{ p.f.}].\end{aligned} \tag{3.36}$$

In simple models, the scaling estimate $\langle \delta\phi^n\rangle \sim H^{m(n)}$ makes both terms the same order of magnitude. For (4.22) to be valid requires the 4-point function to be substantially smaller, which is also supported by observation [74, 75].

3.4 Evolution of correlation functions

3.4.1 Solution of the transport hierarchy by raytracing

The transport equations (4.21) and (4.22) can be solved using the machinery developed in §3.2. The key ingredients are the phase-space flows which describe evolution of individual "separate universes," and the Jacobi fields which connect them. The solution is formal and depends only on the structure described in §4.4. Therefore there is no requirement to impose the slow-roll approximation, and when written over the full phase-space our equations apply quite generally. When truncated to field-space they reproduce the slow-roll evolution.

Two-point function.—We write the two-point function $\Sigma_{\alpha'\beta'}$ in the form

$$\Sigma_{\alpha'\beta'} \equiv \Gamma_{\alpha'i'}\Gamma_{\beta'j'}\Sigma_{i'j'}, \tag{3.37}$$

where Γ is to be determined. This notation has been chosen because Γ will turn out to be the propagator matrix (3.15) for the primed indices. Indeed, (3.37) is a solution of the transport equation (4.21) if

$$\frac{\mathrm{d}\Gamma_{\alpha'i'}}{\mathrm{d}N} = u_{\alpha'\gamma'}\Gamma_{\gamma'i'} \tag{3.38a}$$

$$\frac{\mathrm{d}\Sigma_{i'j'}}{\mathrm{d}N} = \mathrm{O}(H^4) \approx 0. \tag{3.38b}$$

Eq. (3.38a) is the equation for a Jacobi field, Eq. (3.11).

In writing (3.38b) we have assumed approximate Gaussianity, so that contributions from higher-order correlation functions are suppressed by at least a power of H^2 compared to the terms which have been retained. Keeping these terms would yield the "loop corrections" of the Lyth–Rodríguez formalism [33, 35, 76–78]. To the order we are working, $\Sigma_{i'j'}$ should be identified as a constant: it is the value of the two-point function evaluated at $N = N_0$, where N_0 is the initial time which appears in the propagator (3.15). We write this constant value $\mathcal{S}_{i'j'}$.

The primed propagator satisfies

$$\Gamma_{\alpha' i'} = \delta(\boldsymbol{k}_\alpha - \boldsymbol{k}_i)\Gamma_{\alpha i}, \tag{3.39}$$

where $\Gamma_{\alpha i}$ is the flavour propagator (3.15). Therefore, written more explicitly, Eq. (3.37) becomes

$$\langle \delta\phi_\alpha(\boldsymbol{k}_\alpha)\delta\phi_\beta(\boldsymbol{k}_\beta)\rangle = \Gamma_{\alpha i}\Gamma_{\beta j}\langle \delta\phi_i(\boldsymbol{k}_\alpha)\delta\phi_j(\boldsymbol{k}_\beta)\rangle_0, \tag{3.40}$$

where our usual convention—that Latin indices denote evaluation of the correlation function at some initial time N_0—continues to apply. For the two point function, practical calculations usually simplify if this is taken to be the horizon-crossing time associated with scale $k = |\boldsymbol{k}_\alpha| = |\boldsymbol{k}_\beta|$. We have indicated this by attaching a subscript '0' to the correlation function. With this understanding, and recollecting the identification (3.16), Eq. (3.40) is the familiar "δN" result [5, 7, 11].

Three-point function.—Similar methods can be used to solve for the three- and four-point functions. We write $\alpha_{\alpha'\beta'\gamma'} \equiv \Gamma_{\alpha' i'}\Gamma_{\beta' j'}\Gamma_{\gamma' k'}\alpha_{i'j'k'}$. As for the two-point function, the propagator matrices absorb contributions from the $u_{\alpha\beta}$-tensors. In the case of $\Sigma_{\alpha'\beta'}$ there were no other terms, making the "kernel" $\Sigma_{i'j'}$ time independent. Here, the presence of terms involving u 3-tensors provides a source for $\alpha_{i'j'k'}$. We find[10]

$$\begin{aligned}\frac{\mathrm{d}\alpha_{i'j'k'}}{\mathrm{d}N} &= (\Gamma^{-1}_{i'\alpha'}u_{\alpha'\beta'\gamma'}\Gamma_{\beta' m'}\Gamma_{\gamma' n'})\mathcal{S}_{m'j'}\mathcal{S}_{n'k'} + \text{cyclic} \\ &\quad + \mathrm{O}(H^6),\end{aligned} \tag{3.41}$$

where, as above, $\mathcal{S}_{ij}$ is the initial value of the two-point function introduced in (3.37). The estimate $\mathrm{O}(H^6)$ for the truncation error, beginning with contributions from the four-point function, again assumes that the correlation functions order themselves in even powers

[10] We are allowing $\alpha_{i'j'k'}$ to be a function of N, which means our index convention must be interpreted more abstractly. The expressions for Γ-matrices to which Eq. (3.41) leads, such as Eqs. (3.50a)–(3.50b), can be interpreted in the original sense.

of H. We define the matrix $\Gamma^{-1}_{i'\alpha'}$ to be the left-inverse of the propagator, $\Gamma^{-1}_{i'\alpha'}\Gamma_{\alpha' j'} = \delta(\boldsymbol{k}_i - \boldsymbol{k}_j)\delta_{ij}$. Inspection of (3.39) shows that it can be written

$$\Gamma^{-1}_{i'\alpha'} = \delta(\boldsymbol{k}_i - \boldsymbol{k}_\alpha)\Gamma^{-1}_{i\alpha}, \tag{3.42}$$

where $\Gamma^{-1}_{i\alpha}$ is the conventional matrix inverse of the flavour propagator, Eq. (3.15). In what follows it is useful to define a projected u 3-tensor, $\tilde{u}_{i'j'k'}$, by

$$\tilde{u}_{i'j'k'} = \Gamma^{-1}_{i'\alpha'}u_{\alpha'\beta'\gamma'}\Gamma_{\beta' j'}\Gamma_{\gamma' k'}. \tag{3.43}$$

Combining (3.39) and (3.42), it follows that the explicit $\boldsymbol{k}$- and flavour-dependence can be written

$$\tilde{u}_{i'j'k'} = \delta(\boldsymbol{k}_i - \boldsymbol{k}_j - \boldsymbol{k}_k)\tilde{u}_{ijk}, \tag{3.44}$$

where the tensor $\tilde{u}_{ijk}$ is the obvious flavour projection of u_{ijk}, so that $\tilde{u}_{ijk} = \Gamma^{-1}_{i\alpha}u_{\alpha\beta\gamma}\Gamma_{\beta j}\Gamma_{\gamma k}$.

With these definitions, Eq. (3.41) can be solved by quadrature. Up to loop corrections, we find

$$\alpha_{i'j'k'} = \mathcal{A}_{i'j'k'} + \int_{N_0}^{N} \tilde{u}_{i'm'n'}(N')\mathcal{S}_{m'j'}\mathcal{S}_{n'k'}\,\mathrm{d}N' + \text{cyclic}, \tag{3.45}$$

where $\mathcal{A}_{i'j'k'}$ should be regarded as the value of the three-point function at $N = N_0$. The complete solution can be written (again up to loop corrections)

$$\begin{aligned}\alpha_{\alpha'\beta'\gamma'} &= \Gamma_{\alpha' i'}\Gamma_{\beta' j'}\Gamma_{\gamma' k'}\mathcal{A}_{i'j'k'} \\ &\quad + \Big(\Gamma_{\alpha' m'n'}\Gamma_{\beta' j'}\Gamma_{\gamma' k'}\mathcal{S}_{m'j'}\mathcal{S}_{n'k'} + \text{cyclic}\Big),\end{aligned} \tag{3.46}$$

where the cyclic permutations exchange $\alpha' \to \beta' \to \gamma'$.

One can regard Eqs. (3.38a)–(3.38b) and (3.45) as analogous to the "line of sight" integral which is used to obtain a formal solution to the Boltzmann equation in calculations of the cosmic microwave background anisotropies.

The quantity $\Gamma_{\alpha' m'n'}$ is defined by

$$\Gamma_{\alpha' m'n'} \equiv \Gamma_{\alpha' i'}\int_{N_0}^{N} \tilde{u}_{i'm'n'}(N')\,\mathrm{d}N'. \tag{3.47}$$

Observe that Eq. (3.47) is symmetric in the indices m' and n'. With our choices for the $\boldsymbol{k}$- and flavour-dependence of its constituent quantities, it can be written

$$\Gamma_{\alpha' m'n'} = \delta(\boldsymbol{k}_\alpha - \boldsymbol{k}_m - \boldsymbol{k}_n)\Gamma_{\alpha mn}, \tag{3.48}$$

where $\Gamma_{\alpha mn}$ is the flavour-only object obtained by exchanging primed for unprimed indices in (3.47). Comparing with (3.15), it follows that (up to matrix ordering ambiguities) $\Gamma_{\alpha mn}$ is the derivative of the propagator,

$$\frac{\partial^2\phi_\alpha}{\partial\phi_m\partial\phi_n} = \Gamma_{\alpha mn}. \tag{3.49}$$

Eq. (3.46) can now be recognized as the Lyth–Rodríguez formula for the three-point function [11].

3.4.2 Flow equations for "δN" coefficients

We conclude that the transport equations (4.21) and (4.22) are equivalent to the Taylor expansion algorithm of Lyth & Rodríguez for the three-point function. Also, because the u-tensors could equally well be derived using the methods of cosmological perturbation theory, all these methods will give answers which agree. Within this narrow reading, our analysis can be interpreted as a demonstration that these methods are interchangeable. Therefore we believe that statements to the effect that any particular method currently in use has an intrinsic drawback when compared with another, *as a matter of principle*, are wrong.

Nevertheless it *is* true that some approaches have advantages in practice, although no one approach outperforms the others in all applications. For example, as explained in §3.1, in some models the Taylor expansion algorithm leads to very simple analytic formulae. This property has encouraged a large literature studying models to which the method can be applied.

In this broader context our analysis is not simply a reformulation of existing results. First, as a byproduct of the raytracing method we have obtained explicit (but formal) expressions for the Lyth–Rodríguez Taylor coefficients,

$$\frac{\partial\phi_\alpha}{\partial\phi_i} = \Gamma_{\alpha i} = \mathcal{P}\exp\left(\int_{N_0}^{N} u_{\alpha\beta}(N')\,\mathrm{d}N'\right)\delta_{\beta i} \tag{3.50a}$$

$$\frac{\partial^2\phi_\alpha}{\partial\phi_i\partial\phi_j} = \Gamma_{\alpha ij} = \Gamma_{\alpha m}\int_{N_0}^{N}\tilde{u}_{mij}(N')\,\mathrm{d}N'. \tag{3.50b}$$

Analytically, the Taylor expansion method is useful only when a solution to (3.50a) can be found in closed form. This has been achieved only for a limited class of potentials obeying some form of separability criteria; a summary appears in Ref. [32] together with references to the original literature. Eq. (3.50a) clarifies the difficulty encountered in obtaining analytic formulae as the difficulty of computing closed-form expressions for a path-ordered exponential. A sophisticated theory is available [79] but explicit expressions can usually be obtained only in special cases, or where the expansion tensor commutes with itself at different times. It is possible that Eq. (3.50a) could be used to extend analytic progress beyond the separable cases, but we have not investigated this possibility in detail.

Eqs. (3.50a)–(3.50b) were given, in slightly different notation, by Yokoyama et al. [14, 15]. Because of its close relation to the present discussion we review and extend the Yokoyama et al. approach in Appendix 3.A.

Second, a naïve numerical implementation of the Taylor expansion formula is unfavourable. Beginning with fractionally displaced initial conditions one must evolve the equations of motion over many e-folds, during which numerical noise is accumulating. Taking differences between these evolved solutions requires high-accuracy integration in order that the small displacement in initial conditions is not swamped by noise. The explicit solutions (3.50a)–(3.50b) allow this naïve approach to be replaced by a simple system of ordinary differential equations for $\Gamma_{\alpha i}$ and $\Gamma_{\alpha ij}$. The $\Gamma_{\alpha i}$ equation is the Jacobi equation (3.38a), after dropping primes on indices. The initial condition is $\Gamma_{\alpha i} = \delta_{\alpha i}$. The $\Gamma_{\alpha ij}$ equation can be obtained by differentiation of (3.50b). It is

$$\frac{\mathrm{d}\Gamma_{\alpha ij}}{\mathrm{d}N} = u_{\alpha\beta}\Gamma_{\beta ij} + u_{\alpha\beta\gamma}\Gamma_{\beta i}\Gamma_{\gamma j}, \tag{3.51}$$

with initial condition $\Gamma_{\alpha ij} = 0$.

The same approach can be applied systematically to deduce transport equations for any of the Taylor coefficients. Yokoyama et al. wrote the transport equation (3.38a) for $\Gamma_{\alpha i}$, but did not write (3.51) for $\Gamma_{\alpha ij}$ which they computed directly from (3.50b). See Appendix 3.A for a comparison.

3.4.3 Transport of "shape" amplitudes

The results of §3.4.1 apply for arbitrary initial conditions $\mathcal{S}_{i'j'}$, $\mathcal{A}_{i'j'k'}$ for the two- and three-point functions. But for application to inflation, we will usually wish to apply them to the correlation functions produced in a specific model. In this case the fields ϕ_α will be a collection of light scalars for which $\mathcal{S}_{i'j'}$ and $\mathcal{A}_{i'j'k'}$ can be computed using the *in–in* formulation of quantum field theory [44]. These yield very specific $\boldsymbol{k}$-dependences whose amplitudes we wish to track.

In this section, our analysis remains general and continues to apply to the full phase space.

Two-point function.—The two-point function is straightforward. For a nearly scale-invariant spectrum we have

$$\Sigma_{\alpha'\beta'} \equiv (2\pi)^3\delta(\boldsymbol{k}_\alpha + \boldsymbol{k}_\beta)\frac{\Sigma_{\alpha\beta}}{k^3}, \tag{3.52}$$

where $k = |\boldsymbol{k}_\alpha| = |\boldsymbol{k}_\beta|$ and the flavour matrix $\Sigma_{\alpha\beta}$ should be nearly independent of k. Transport of $\Sigma_{\alpha\beta}$ can be accomplished using (3.40), or simply by solving the transport equation (4.21) with an appropriate initial condition after dropping primes on indices. That gives

$$\Sigma_{\alpha\beta} = \Gamma_{\alpha i}\Gamma_{\beta j}\mathcal{S}_{ij}, \tag{3.53}$$

where $\mathcal{S}_{ij}$ is the initial value of $\Sigma_{\alpha\beta}$. The mild k-dependence of (3.53) can also be obtained using transport techniques [80].

Three-point function.—Here, more possibilities exist. It is known that the $\mathrm{O}(\mathcal{S}^2)$ terms in (3.46) dominate whenever the bispectrum is large enough to be observed [50, 81]. Eq. (3.46) shows that these contributions add incoherently to the contribution from $\mathcal{A}_{ijk}$, so they can be studied separately. Using (3.52) and overall symmetry of the correlation function under exchange of indices, we can write

$$\alpha_{\alpha'\beta'\gamma'} \supseteq (2\pi)^3\delta(\boldsymbol{k}_\alpha + \boldsymbol{k}_\beta + \boldsymbol{k}_\gamma)\left(\frac{\alpha_{\alpha|\beta\gamma}}{k_\beta^3 k_\gamma^3} + \frac{\alpha_{\beta|\alpha\gamma}}{k_\alpha^3 k_\gamma^3} + \frac{\alpha_{\gamma|\alpha\beta}}{k_\alpha^3 k_\beta^3}\right), \tag{3.54}$$

where the notation "$\supseteq$" indicates that the three-point contribution contains this contribution among others. The amplitudes $a_{\alpha|\beta\gamma}$ are symmetric under exchange of β and γ, but not otherwise. Using Eqs. (3.33a), (3.33b), (4.22) and (3.52), we find the transport equation

$$\begin{aligned}\frac{\mathrm{d}\alpha_{\alpha|\beta\gamma}}{\mathrm{d}N} &= u_{\alpha\lambda}\alpha_{\lambda|\beta\gamma} + u_{\beta\lambda}\alpha_{\alpha|\lambda\gamma} + u_{\gamma\lambda}\alpha_{\alpha|\beta\lambda} \\ &\quad + u_{\alpha\lambda\mu}\Sigma_{\lambda\beta}\Sigma_{\mu\gamma}.\end{aligned} \tag{3.55}$$

If desired, we can apply the same method of formal solution described in §3.4.1. This yields

$$\alpha_{\alpha|\beta\gamma} = \Gamma_{\alpha mn}\Gamma_{\beta j}\Gamma_{\gamma k}\mathcal{S}_{mj}\mathcal{S}_{nk}. \tag{3.56}$$

In combination with (3.54) this reproduces our earlier formula (3.46), neglecting the initial contribution $\mathcal{A}_{i'j'k'}$.

3.4.4 Connections between the transport and other approaches

Up to this point we have shown that the Jacobi fields which connect "separate universe" trajectories in phase space can be used to solve the transport equations for the full set of $\boldsymbol{k}$-space correlation functions. But as we have explained, the transport hierarchy is just one of many techniques for handling correlation functions. We now pause to examine the connections between these approaches.

δN formalism.—In the Lyth–Rodríguez approach, or "δN formalism", one makes a Taylor expansion of the field values on a final hypersurface in terms of field values on some initial hypersurface. Following the discussion surrounding Eq. (4.19), and with the same meaning for the vectors $\boldsymbol{x}$ and $\boldsymbol{r}$, this can be written

$$\delta\phi_\alpha(\boldsymbol{r}) = \Gamma_{\alpha i}(\boldsymbol{x})\delta\phi_i(\boldsymbol{r}) + \frac{1}{2}\Gamma_{\alpha ij}(\boldsymbol{x})\left\{\delta\phi_i(\boldsymbol{r})\delta\phi_j(\boldsymbol{r}) - \langle\delta\phi_i(\boldsymbol{r})\delta\phi_j(\boldsymbol{r})\rangle\right\} + \dots . \tag{3.57}$$

Note that, despite appearances, we are making no assumption that the evolution of $\delta\phi$ is close to an attractor. Therefore there is no requirement to invoke the slow-roll approximation. It is true that the existence of an attractor would make the canonical momenta purely a function of the fields, yielding an equation with the appearance of Eq. (3.57). But as we have explained, by working in a first-order Hamiltonian formalism we can obtain expressions such as (3.57) without this limitation. Therefore we allow the $\delta\phi_i$ to include perturbations of the canonical momenta if necessary, in which case the indices α, i, etc. range over the $2M$ dimensions of phase space. Where slow-roll is a good approximation we can revert to a simpler formulation based on field space.

We have already remarked that the Γ-tensors are the derivatives (3.16) and (3.49). In Eq. (3.57) the $\delta\phi_\alpha$ are all defined on spatially flat hypersurfaces. More commonly, an analogous expansion is made for the total e-folding number N, measured from a flat slice to a final comoving slice; we give an explicit relation in §4.4.3. The choice of slicing simply corresponds to the gauge in which we wish to work [18].

For (3.57) to be useful, some means must be found to compute $\Gamma_{\alpha i}$ and $\Gamma_{\alpha ij}$.

Flow equations.—As a by-product of the raytracing solution, or "line of sight" integral, we obtained the evolution equations (3.38a) and (3.51). These allow the Γ-tensors to be computed easily. However, the same equations can be obtained directly from the separate universe formula, Eq. (3.57). Substituting (3.57) into both the right- and left-hand sides of (4.19) and separating the resulting expansion order-by-order, we immediately arrive at Eqs. (3.38a) and (3.51). This still does not require the slow-roll approximation.

Transfer matrices.—We have observed that Eq. (4.19) arises in the $k/aH \to 0$ limit of cosmological perturbation theory ("CPT"). Within that framework, at least in the first-order theory, it is common to introduce "transfer matrices" which relate field perturbations at different times [19]. Typically these are chosen to be the adiabatic and isocurvature directions, but in principle any basis can be used.

Restricting to first-order, the transfer matrix is determined precisely by the leading term of (3.57), or a gauge transformation of it. It follows that Eq. (3.57) represents the extension of the transfer matrix to second-order (and beyond), and Eqs. (3.38a) and (3.51) give the evolution of the transfer tensors $\Gamma_{\alpha i}$, $\Gamma_{\alpha ij}$. Therefore the transfer-matrix formalism is precisely equivalent to the separate universe picture and traditional cosmological perturbation theory. Note that if the perturbations are projected onto adiabatic and isocurvature modes this requires use of the correct u tensors at each time step.

CPT implies transport equations.—Finally, we show that cosmological perturbation theory implies the transport hierarchy with which we began. We write

$$\Sigma_{\alpha\beta} = \Gamma_{\alpha i}\Gamma_{\beta j}\mathcal{S}_{ij}, \tag{3.58}$$

which, neglecting "loops," follows from (3.57) and therefore either CPT or a transfer-matrix approach. Differentiating both sides with respect to time, recalling that $\mathcal{S}_{ij}$ is time-independent, and make use of (3.38a) we find

$$\frac{\mathrm{d}\Sigma_{\alpha\beta}}{\mathrm{d}N} = \left(u_{\alpha\mu}\Gamma_{\mu i}\Gamma_{\beta j} + u_{\beta\mu}\Gamma_{\alpha i}\Gamma_{\mu j}\right)\mathcal{S}_{ij}. \tag{3.59}$$

This gives the transport equation for $\Sigma_{\alpha\beta}$, Eq. (4.21). A similar procedure leads to the transport equation for $\alpha_{\alpha\beta\gamma}$, Eq. (4.21). It follows that each of these approaches implies and is implied by the others.

3.5 Gauge transformations

To this point, the formalism we have developed enables the correlation functions of fluctuations in the fields and their momenta, $\delta\phi_\alpha$ and δp_α, to be evolved along the bundle of trajectories picked out by an ensemble of smoothed regions. However, by themselves these fluctuations are not observable. Only specific combinations are observable, of which the most important is the primordial curvature fluctuation ζ. Therefore to proceed we require expressions for the gauge transformation between the $\delta\phi_\alpha$, δp_α and ζ.

In this section we impose the slow-roll approximation throughout, enabling us to work on field space and make use of the hypersurface-orthogonal property of the flow. We intend to return to the general case in a future publication.

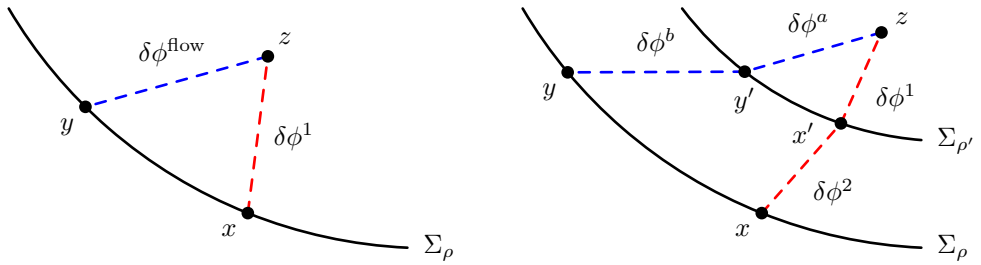

(a) First order **(b)** Second order

Figure 3.5: Gauge transformations in field space

3.5.1 Explicit transformations

In the slow-roll approximation there is no need to track the momentum fluctuations δp_α, which are purely determined by the field fluctuations $\delta\phi_\alpha$. Therefore ζ can be written purely in terms of the field fluctuations.

On superhorizon scales, the appropriate gauge transformation can be written as a Taylor expansion,

$$\zeta = N_\alpha \delta\phi_\alpha + \frac{1}{2} N_{\alpha\beta}(\delta\phi_\alpha \delta\phi_\beta - \langle \delta\phi_\alpha \delta\phi_\beta \rangle) + \cdots , \tag{3.60}$$

where all fields are evaluated at the same spatial position and a constant has been subtracted to set $\langle\zeta\rangle = 0$. The Taylor coefficients N_α and $N_{\alpha\beta}$ have been given by various authors [17, 82]. Working in field space, we give a purely geometrical derivation. This argument relies on the property that the flow is orthogonal to surfaces of constant density in field space, and therefore will not generalize directly to the full phase space.

Linear term.—Consider Fig. 3.5a. We wish to compute the coefficient N_α at a field-space point x, which can be taken to lie on a hypersurface of fixed energy density ρ. We denote this hypersurface Σ_ρ. According to the separate universe approximation, N_α can be computed from the number of e-folds required to flow back to Σ_ρ after making a generic ("off-shell") displacement from x. Anticipating the discussion of second-order contributions, we denote this displacement $\delta\phi^1$ and write $z = x + \delta\phi^1$.

The number of e-folds required to return to Σ_ρ must be computed along the inflationary trajectory which passes through z. In Fig. 3.5a, this trajectory intersects Σ_ρ at y. The tangent to the trajectory at y is the normal vector $\hat{n}(y)$. Therefore the ("on-shell") field-space displacement along this trajectory, to first order in $\delta\phi^1$, is $\delta\phi_\alpha^{\text{flow}} \approx -\hat{n}_\alpha \hat{n}_\beta \delta\phi^1_\beta$. The symbol '$\approx$' denotes equality up to higher-order terms in $\delta\phi^1$ which have been omitted, and

we have adopted a convention in which quantities evaluated at x—such as the unit vector $\hat{n}$—are written without an argument. Combining Eqs. (3.3) and (3.5), we conclude

$$\delta N \approx -\frac{1}{M_{\rm P}} \frac{\hat{n}_\alpha \delta\phi^1_\alpha}{\sqrt{2\epsilon}} \tag{3.61}$$

and therefore

$$\frac{\partial N}{\partial \phi^1_\alpha} = -\frac{1}{M_{\rm P}} \frac{\hat{n}_\alpha}{\sqrt{2\epsilon}} = -\frac{1}{M_{\rm P}} \frac{\hat{n}_\alpha}{\nu}. \tag{3.62}$$

where we have reintroduced the refractive index $\nu = \sqrt{2\epsilon}$ defined in §3.2.1. Eq. (3.62) is the term N_α in (3.60).

Quadratic term.—The quadratic Taylor coefficient can be obtained from the variation in $\partial N/\partial\phi^1_\alpha$ under a *second* generic displacement $\delta\phi^2$. Under this displacement the origin is shifted to $x' = x + \delta\phi^2$. Because the energy density at x' will typically differ from ρ, it lies on a displaced hypersurface $\Sigma_{\rho'}$. However, the definition of N is unchanged and must still be measured to the intersection with Σ_ρ at y. We should compute the flow along the trajectory passing through z. The path $z \to y' \to y$ is a discrete approximation to an integral along this flow. The calculation should be carried to linear order in $\delta\phi^1$ and $\delta\phi^2$ independently.

In Fig. 3.5b, the on-shell flow from $z = x' + \delta\phi^1$ back to $\Sigma_{\rho'}$ is $\delta\phi^a$. Repeating the analysis above, we find

$$\delta\phi^a_\alpha \approx -\hat{n}'_\alpha \hat{n}'_\beta \delta\phi^1_\beta, \tag{3.63}$$

where $\hat{n}'_\alpha \equiv \hat{n}_\alpha(x') \approx \hat{n}_\alpha + \delta\phi^2_\beta \partial_\beta \hat{n}_\alpha$. (It is only necessary to work to first order in $\delta\phi^2$, since (3.63) is proportional to $\delta\phi^1$.) The on-shell flow from y' back to Σ_ρ is

$$\delta\phi^b_\alpha \approx -\hat{n}''_\alpha \hat{n}''_\beta \Delta_\beta - \hat{n}''_\alpha \Big(\frac{K_{\beta\gamma}}{2} - \partial_\beta \hat{n}_\gamma \Big) \Delta_\beta \Delta_\gamma. \tag{3.64}$$

We have defined Δ_α to be the displacement to y',

$$\Delta_\alpha \equiv \delta\phi^1_\alpha + \delta\phi^2_\alpha + \delta\phi^a_\alpha, \tag{3.65}$$

and $\hat{n}''_\alpha \equiv \hat{n}_\alpha(y')$. The symmetric tensor $K_{\alpha\beta}$ is the extrinsic curvature of Σ_ρ, or "second fundamental form," and is defined by $K_{\alpha\beta} \equiv h_{\alpha\gamma} h_{\beta\delta} \partial_\gamma \hat{n}_\delta$ [40]. It is related to the dilation and shear of the expansion tensor via

$$K_{\alpha\beta} = \frac{1}{M_{\rm P}\nu} \left(\frac{\theta}{d} h_{\alpha\beta} + \sigma^{\rm iso}_{\alpha\beta} \right), \tag{3.66}$$

where $\sigma^{\rm iso}_{\alpha\beta}$ is the projection of the shear onto the isocurvature subspace, $\sigma^{\rm iso}_{\alpha\beta} \equiv h_{\alpha\gamma} h_{\beta\delta} \sigma_{\gamma\delta}$. The first term in (3.64) is a linear, trigonometric approximation. The second is a correction for the curvature of Σ_ρ. A similar construction could be used to obtain the Taylor coefficients at any desired order.

After computing all appropriate variations, we find

$$\begin{aligned}\frac{\partial^2 N}{\partial\phi^1_\alpha\partial\phi^2_\beta} &= -\frac{1}{M_\mathrm{P}}\left(\frac{K_{\alpha\beta}}{\sqrt{2\epsilon}} + \hat{n}_\alpha\partial_\beta(2\epsilon)^{-1/2} + \hat{n}_\beta\partial_\alpha(2\epsilon)^{-1/2} - \hat{n}_\alpha\hat{n}_\beta\hat{n}_\gamma\partial_\gamma(2\epsilon)^{-1/2}\right)\\ &= -\frac{1}{M_\mathrm{P}\nu}\Big(K_{\alpha\beta} - \hat{n}_\alpha\,\mathcal{D}_\beta\ln\nu - \hat{n}_\beta\,\mathcal{D}_\alpha\ln\nu - \frac{\hat{n}_\alpha\hat{n}_\beta}{M_\mathrm{P}}\frac{\eta}{2\nu}\Big),\end{aligned} \tag{3.67}$$

where $\eta = \mathrm{d}\ln\epsilon/\mathrm{d}N$ is the natural generalization of the single-field η-parameter. It measures the variation of ϵ along the adiabatic direction. To yield sufficient e-foldings, it must typically be small while observable scales are leaving the horizon. Defining $\mathcal{D}_\sigma \equiv \hat{n}_\alpha\partial_\alpha$ to be a derivative along $\hat{n}_\alpha$, it can be written

$$\eta \equiv \frac{2M_\mathrm{P}}{\nu}\,\mathcal{D}_\sigma\,\epsilon. \tag{3.68}$$

In addition, $\mathcal{D}_\alpha \equiv h_{\alpha\beta}\partial_\beta$ is a derivative in the plane tangent to Σ_ρ at x. This tangent space can be interpreted as the subspace of isocurvature modes. Only the η-component of (3.67) depends purely on the local behaviour of the adiabatic direction, and therefore the direction in field space restricted by the slow-roll approximation. The remaining terms all probe details of the isocurvature subspace.

Dropping the distinction between $\delta\phi^1$ and $\delta\phi^2$, Eq. (3.67) is equal to $N_{\alpha\beta}$. It is symmetric even though we have not treated the displacements $\delta\phi^1$ and $\delta\phi^2$ equally. This is a consequence of associativity of vector addition, which makes z the same no matter in which order we apply the displacements. The inflationary trajectory passing through z is unique, so $N_{\alpha\beta}$ can only depend on a symmetric combination of $\delta\phi^1$ and $\delta\phi^2$.

Eq. (3.67) shows that $N_{\alpha\beta}$ depends on the anisotropy of ϵ—or, in the optical interpretation, the refractive index ν. It also depends on the extrinsic curvature of Σ_ρ, which is a function of the shape of the hypersurfaces of constant energy density. In particular, because $\hat{n}_\alpha K_{\alpha\beta} = 0$, this term can be interpreted as a metric on the subspace of isocurvature modes.

3.5.2 Local mode f_NL

Two-point function.—These results can be combined to obtain the usual formulae for the amplitude of the local mode, f_NL. With our usual assumptions about the amplitude of those correlation functions we neglect, the two-point function of ζ satisfies

$$\begin{aligned}\langle\zeta(\boldsymbol{k}_1)\zeta(\boldsymbol{k}_2)\rangle = (2\pi)^3\delta(\boldsymbol{k}_1+\boldsymbol{k}_2)N_\alpha N_\beta\Gamma_{\alpha i}\Gamma_{\beta j}\frac{\mathcal{S}_{ij}}{k^3}\\ + \mathrm{O}\left(\frac{H^4}{M_\mathrm{P}^4}\right),\end{aligned} \tag{3.69}$$

where k is the common amplitude of $\boldsymbol{k}_1$ and $\boldsymbol{k}_2$ and N_α is the first-order component of the gauge transformation, Eq. (3.62). Application of the chain rule to the contractions in (3.69) allows the Lyth–Rodríguez Taylor coefficients to be identified,

$$N_i \equiv \frac{\partial N}{\partial \phi_i} = N_\alpha \Gamma_{\alpha i}. \tag{3.70}$$

It follows that (3.69) is the standard result [11].

Three-point function.—Neglecting the initial three-point function $\mathcal{A}_{i'j'k'}$, the bispectrum can be computed by similar methods. There is an added complication from second-order terms in the gauge transformation (3.60). Working from (3.46) (or (3.54) and (3.56)) gives

$$\begin{aligned}\langle \zeta(\boldsymbol{k}_1)\zeta(\boldsymbol{k}_2)\zeta(\boldsymbol{k}_3)\rangle = (2\pi)^3\delta(\boldsymbol{k}_1+\boldsymbol{k}_2+\boldsymbol{k}_3)(N_\alpha\Gamma_{\alpha mn} + N_{\alpha\beta}\Gamma_{\alpha m}\Gamma_{\beta n})N_i N_j \mathcal{S}_{mi}\mathcal{S}_{nk} \\ \times \left(\frac{1}{k_1^3 k_2^3} + \frac{1}{k_1^3 k_3^3} + \frac{1}{k_2^3 k_3^3}\right) + \mathrm{O}\left(\frac{H^6}{M_{\mathrm{P}}^6}\right).\end{aligned} \tag{3.71}$$

We can make the identification

$$N_{ij} \equiv \frac{\partial^2 N}{\partial\phi_i \partial\phi_j} = N_\alpha \Gamma_{\alpha ij} + N_{\alpha\beta}\Gamma_{\alpha i}\Gamma_{\beta j}, \tag{3.72}$$

where $N_{\alpha\beta}$ is the second-order term (3.67). The familiar approximation for the amplitude of the local mode, f_{NL}, follows immediately,

$$\begin{aligned}\frac{6}{5} f_{\mathrm{NL}} = \frac{N_{mn}N_j N_k \mathcal{S}_{mj}\mathcal{S}_{nk}}{(N_q N_r \mathcal{S}_{qr})^2} &= \frac{N_\alpha \Gamma_{\alpha mn} N_j N_k \mathcal{S}_{mj}\mathcal{S}_{nk}}{(N_q N_r \mathcal{S}_{qr})^2} + \frac{N_{\alpha\beta}\Gamma_{\alpha m}\Gamma_{\beta n} N_j N_k \mathcal{S}_{mj}\mathcal{S}_{nk}}{(N_q N_r \mathcal{S}_{qr})^2}. \\ &\equiv f_{\mathrm{NL}}^{\phi} + f_{\mathrm{NL}}^{\mathrm{gauge}}.\end{aligned} \tag{3.73}$$

In the final step we have divided the contributions into an *intrinsic* term, f_{NL}^{ϕ} (which contains $\Gamma_{\alpha mn}$), and a *gauge contribution* $f_{\mathrm{NL}}^{\mathrm{gauge}}$ (which does not). The intrinsic term depends on the bispectrum of the fluctuations $\delta\phi_\alpha$. Eq. (3.47) shows that it depends on $u_{\alpha\beta\gamma}$, and therefore has a memory of the *nonlinear* evolution of the connecting vectors along the trajectory. However, it has no dependence on the nonlinear part of the gauge transformation. *Vice versa*, the gauge term depends on the nonlinear part of the gauge transformation, and only on the *linear* evolution of the connecting vectors—that is, the Jacobi fields, in the guise of the van Vleck matrix (3.16).

This separation was first made in Ref. [17], where it was shown that the gauge contribution dominated in a class of models known to generate large $|f_{\mathrm{NL}}|$ [83, 84]. We will sharpen this division slightly in Eqs. (3.85a)–(3.85b) below.

The outcome of this discussion is that f_{NL} could be computed efficiently by decomposing (3.73) into the component gauge transformations and Γ-symbols, which can be

obtained using ordinary differential equations. An alternative approach is to work from the explicit formula (3.54), yielding

$$\begin{aligned}\langle\zeta(\boldsymbol{k}_1)\zeta(\boldsymbol{k}_2)\zeta(\boldsymbol{k}_3)\rangle = (2\pi)^3\delta(\boldsymbol{k}_1+\boldsymbol{k}_2+\boldsymbol{k}_3)\big(N_\alpha N_\beta N_\gamma \alpha_{\alpha|\beta\gamma} + N_{\alpha\beta}N_\gamma N_\delta \Sigma_{\alpha\gamma}\Sigma_{\beta\delta}\big)\\ \times\left(\frac{1}{k_1^3k_2^3}+\frac{1}{k_1^3k_3^3}+\frac{1}{k_2^3k_3^3}\right)+\mathrm{O}\left(\frac{H^6}{M_{\mathrm{P}}^6}\right).\end{aligned} \tag{3.74}$$

It then follows that

$$f_{\mathrm{NL}}^{\phi} = \frac{5}{6}\frac{N_\alpha N_\beta N_\gamma \alpha_{\alpha|\beta\gamma}}{(N_\lambda N_\mu \Sigma_{\alpha\beta})^2} = \frac{5}{18}\frac{N_\alpha N_\beta N_\gamma \alpha_{\alpha\beta\gamma}}{(N_\lambda N_\mu \Sigma_{\alpha\beta})^2}. \tag{3.75}$$

In the final equality we have defined $\alpha_{\alpha\beta\gamma}$ by symmetrization,

$$\alpha_{\alpha\beta\gamma} \equiv \alpha_{\alpha|\beta\gamma} + \alpha_{\beta|\alpha\gamma} + \alpha_{\gamma|\alpha\beta}. \tag{3.76}$$

Note that this combination is not normalized to give weight unity. Eq. (3.55) shows that it obeys the transport equation (4.22) for the three-point function after dropping primes on all indices. It was in this form that f_{NL} was quoted in Refs. [17, 18], although the derivation was given in real space and is not the same as the one given here.

Gauge contribution.—There is some interest in isolating the gauge contribution to $|f_{\mathrm{NL}}|$. As explained above, this is known to dominate in some models, including examples where large $|f_{\mathrm{NL}}|$ is generated during a turn in field space [32, 83, 84]. Comparison with (3.74) shows that it can be written

$$\frac{6}{5}f_{\mathrm{NL}}^{\mathrm{gauge}} = \frac{N_{\alpha\beta}N_\gamma N_\delta \Sigma_{\alpha\gamma}\Sigma_{\beta\delta}}{(N_\lambda N_\mu \Sigma_{\lambda\mu})^2}. \tag{3.77}$$

Combining (3.62) and (3.67) gives an explicit expression,

$$\frac{6}{5}f_{\mathrm{NL}}^{\mathrm{gauge}} = \frac{\eta}{2} - M_{\mathrm{P}}\nu\left(\frac{\langle\sigma\delta\phi_\alpha\rangle K_{\alpha\beta}\langle\delta\phi_\beta\sigma\rangle}{\langle\sigma\sigma\rangle^2} - 2\frac{\langle\sigma\delta\phi_\alpha\rangle\,\mathcal{D}_\alpha\ln\nu}{\langle\sigma\sigma\rangle}\right), \tag{3.78}$$

where we have defined $\langle\sigma\sigma\rangle = \hat{n}_\alpha\hat{n}_\beta\Sigma_{\alpha\beta}$, and $\langle\sigma\delta\phi_\alpha\rangle = \hat{n}_\beta\Sigma_{\alpha\beta}$. This expression is covariant under rotations of the isocurvature plane. However, its form suggests a natural coordinate basis in which its content is more transparent. Since $K_{\alpha\beta}$ is symmetric, it can be diagonalized. Its eigenvectors form an orthonormal basis directed along the *principal curvature directions* of the fixed energy-density hypersurface in field space. We label these eigenvectors with an index $\boldsymbol{m}$ and denote them $\zeta_\alpha^{\boldsymbol{m}}$, which can be considered as a vielbein. We can refer to the corresponding isocurvature directions as the *principal isocurvature modes*. The corresponding eigenvalues of the second fundamental form are the *principal curvatures* $k_{\boldsymbol{m}}$.

Next, we define a correlation coefficient $\rho_{\boldsymbol{m}}$ between the $\boldsymbol{m}^{\rm th}$ principal isocurvature mode and the adiabatic direction,

$$\zeta^{\boldsymbol{m}}_{\alpha}\langle\sigma\delta\phi_{\alpha}\rangle \equiv \langle\sigma\boldsymbol{m}\rangle = \rho_{\boldsymbol{m}}\langle\sigma\sigma\rangle^{1/2}\langle\boldsymbol{m}\boldsymbol{m}\rangle^{1/2}. \tag{3.79}$$

It is also useful to define analogues of the η-parameter for the isocurvature directions. It is a matter of convention how this is done. By analogy with our definition of η in the adiabatic direction we set

$$\eta_{\boldsymbol{m}} \equiv \frac{2M_{\rm P}}{\nu}\zeta^{\boldsymbol{m}}_{\alpha}\,\mathcal{D}_{\alpha}\,\epsilon. \tag{3.80}$$

Unlike the adiabatic η-parameter, these isocurvature $\eta_{\boldsymbol{m}}$-parameters need not be small even if slow-roll is an excellent approximation. In this basis we find

$$f_{\rm NL}^{\rm gauge} = \frac{\eta}{2} + \sum_{\boldsymbol{m}}\eta_{\boldsymbol{m}}\rho_{\boldsymbol{m}}\frac{\langle\boldsymbol{m}\boldsymbol{m}\rangle^{1/2}}{\langle\sigma\sigma\rangle^{1/2}} - M_{\rm P}\nu\sum_{\boldsymbol{m}}k_{\boldsymbol{m}}\rho^2_{\boldsymbol{m}}\frac{\langle\boldsymbol{m}\boldsymbol{m}\rangle}{\langle\sigma\sigma\rangle}. \tag{3.81}$$

As has been explained, these depend only on the Jacobi fields and geometrical quantities at the time of evaluation for $f_{\rm NL}$. We have not displayed the $\boldsymbol{k}$-modes associated with these objects. Eq. (3.81) strictly applies for roughly comparable $|\boldsymbol{k}|$.

There are three contributions. First, there is the adiabatic η-parameter. As explained above this will almost always be negligible. Second, there is a weighted sum of $\eta_{\boldsymbol{m}}$-parameters associated with the isocurvature directions. These may be individually large. Their contribution is suppressed by the correlation coefficient $\rho_{\boldsymbol{m}}$ between the adiabatic mode and fluctuations in the $\boldsymbol{m}^{\rm th}$ direction, and also by the "anisotropy factor" $(\langle\boldsymbol{m}\boldsymbol{m}\rangle/\langle\sigma\sigma\rangle)^{1/2}$ which measures their relative amplitude. Third, there is a weighted sum of the principal curvatures. These are weighted by the combination $\rho^2_{\boldsymbol{m}}\langle\boldsymbol{m}\boldsymbol{m}\rangle/\langle\sigma\sigma\rangle$. Therefore, this term is typically dominant when the bundle has exaggerated extent in at least one isocurvature direction.

In a two-field model, Eq. (3.81) becomes especially simple. There is only one principal isocurvature mode, and it is orthogonal to the adiabatic direction. Also, the second fundamental form $K_{\alpha\beta}$ has a null eigenvector and therefore the principal curvature k is simply its trace. Comparison with (3.66) shows that

$$k = \mathrm{tr}\,K_{\alpha\beta} = \frac{1}{M_{\rm P}\nu}\left(\frac{M-1}{M}\theta - \hat{n}_{\alpha}\hat{n}_{\beta}\sigma_{\alpha\beta}\right). \tag{3.82}$$

As in §3.2, we have set M to be the dimension of field space.

Non-Gaussianity at the adiabatic limit.—There has been considerable interest in the fate of non-Gaussianity if an adiabatic limit is reached during slow-roll inflation. Meyers &

Sivanandam [61, 62] studied a class of models in which $f_{\rm NL}$, $g_{\rm NL}$ and $\tau_{\rm NL}$ decay to negligible values when all isocurvature modes decay, and argued that this behaviour is generic. However, explicit examples exist in which an observable value of $f_{\rm NL}$ persists even after all isocurvature modes are extinguished [32, 65, 66, 85]. The separation of $f_{\rm NL}$ into intrinsic and gauge contributions allows us to shed further light on this issue.

At an adiabatic limit we expect $\langle \boldsymbol{mm} \rangle \to 0$, and therefore Eq. (3.81) implies $f_{\rm NL}^{\rm gauge} \approx \eta/2$. The same conclusion can be obtained from (3.78) because any tensor projected onto the isocurvature plane (such as $K_{\alpha\beta}$ or $\mathcal{D}_\alpha$) is orthogonal to $\Sigma_{\alpha\beta}$ in this limit. This is an advantage of the tensorial approach we have described, based on associating isocurvature modes with the tangent plane to surfaces of constant energy density in phase space.

One can also show that the intrinsic $f_{\rm NL}$ satisfies

$$f_{\rm NL}^{\phi} = f_{\rm NL}^{\phi,{\rm AL}} + \frac{\eta_{\rm AL}}{2} - \frac{\eta}{2}, \tag{3.83}$$

where 'AL' denotes evaluation just after the adiabatic limit is reached. In the language of §3.2.5 this may coincide with the onset of an inflow trajectory. We conclude that, at any subsequent time, $f_{\rm NL}$ has value

$$f_{\rm NL} = f_{\rm NL}^{\phi,{\rm AL}} + \frac{\eta_{\rm AL}}{2}, \tag{3.84}$$

which is constant as we expect. If the adiabatic limit is reached during slow-roll inflation, where $\eta_{\rm AL}$ must be small, this enables us to give a more precise formulation of Meyers & Sivanandam's argument: if $f_{\rm NL}$ is large in the adiabatic limit, it must be because a large *intrinsic* three-point function is developed during the evolution. This is indeed the case in known examples where a large $f_{\rm NL}$ is reached in the "horizon-crossing approximation" [32, 64, 65].

Eqs. (3.81), (3.83) and (3.84) also enable us to sharpen the division between "gauge" and "intrinsic" contributions. We define

$$f_{\rm NL}^{A} = f_{\rm NL}^{\phi} + \frac{\eta}{2} \tag{3.85a}$$

$$f_{\rm NL}^{B} = f_{\rm NL}^{\rm gauge} - \frac{\eta}{2}. \tag{3.85b}$$

The advantage of this redefinition is that the A- and B-type contributions are constant at an adiabatic limit; indeed, $f_{\rm NL}^{B}$ is zero there because it captures only transient effects caused by the evolving isocurvature modes. However, when $|f_{\rm NL}|$ is large the A- and B-type terms approximately correspond to the intrinsic and gauge $f_{\rm NL}$.

This division is not unique, because a total derivative can always be added to the time integral in $\Gamma_{\alpha ij}$. However, the division in Eqs. (3.85a)–(3.85b) seems phenomenologically useful because all models (of which we are aware) which generate large non-gaussianity do so in one of two ways: *either* f_{NL}^{A} becomes large at the adiabatic limit, *or* f_{NL}^{B} is large some time before the adiabatic limit is reached. As the following examples show, the underlying reason seems to be that the B-type term responds immediately to strong distortions of the shape of bundle, whereas the A-type term does not.

Example: Byrnes et al. model.—We illustrate Eqs. (3.78), (3.81) and (3.85a)–(3.85b) using examples drawn from the literature.

Consider the model $V = V_0\phi^2 \mathrm{e}^{-\lambda\chi^2}$ introduced by Byrnes et al. [83]. We follow their choices, setting $\lambda = 0.05 M_{\mathrm{P}}^{-2}$ and fixing initial conditions $\phi = 16 M_{\mathrm{P}}$ and $\chi = 0.001 M_{\mathrm{P}}$. The first phase of evolution is descent from a ridge, during which a large spike in f_{NL} is generated by the gauge term. An interpretation of this contribution was given in Ref. [32].

In Fig. 3.6a we plot f_{NL} during the inflationary phase. For most of the evolution it is dominated by $f_{\mathrm{NL}}^{\mathrm{gauge}}$. In turn $f_{\mathrm{NL}}^{\mathrm{gauge}}$ is dominated by the extrinsic curvature term $K_{\alpha\beta}$. In Fig. 3.6b we plot the difference between the full f_{NL} and the $K_{\alpha\beta}$-term, demonstrating explicitly that it is small.

In Figs. 3.6c–3.6f we plot the bundle parameters which determine the $K_{\alpha\beta}$-term and the other contributions to $f_{\mathrm{NL}}^{\mathrm{gauge}}$. The correlation constant is initially zero but approaches -1, making the curvature and isocurvature mode (anti-) correlated, as first discussed by Langlois [39]. The principal curvature k and isocurvature η-parameter exhibit only modest evolution over the entire range of e-folds. In comparison, the anisotropy factor $(\langle \boldsymbol{mm} \rangle / \langle \sigma\sigma \rangle)^{1/2}$ grows dramatically. Its evolution is the dominant factor which determines the evolution of f_{NL}. A large f_{NL} arises because the ensemble of separate universes becomes highly anisotropic, with nearly twenty-five times as much power in the isocurvature direction as in the adiabatic direction. Evidently this must arise from a large contribution to the integrated shear in the propagator matrix.

Note that, although $f_{\mathrm{NL}}^{B} \approx f_{\mathrm{NL}}^{\mathrm{gauge}}$ responds immediately to this strong anisotropy factor, there is no corresponding significant enhancement of the intrinsic three-point function.

In Fig. 3.6g and 3.6h we plot the bundle dilation, θ, and the focusing Θ. The dilation is always positive, so the bundle cross-section grows monotonically. Hence the total power in the isocurvature mode also grows monotonically. Evidently, the spike in f_{NL} is not due to the *total* isocurvature power, but to its relative growth compared with the adiabatic power. The large Θ implies that this model does not reach an adiabatic limit, and some other

mechanism must be invoked to end inflation and determine the value of each observable. In Ref. [83] it was assumed that sudden destabilization of a waterfall field could play this role.

Example: axion quadratic model.—A similar phenomenon occurs in the axion–quadratic model discussed above. We plot the evolution of $f_{\rm NL}$ in Fig. 3.7a. It exhibits three distinct components. The first is a negative spike, generated by the axion rolling off its hilltop. The second is a smaller positive spike produced by the axion rolling into its minimum. These two spikes come from the gauge contribution to $f_{\rm NL}$, as clearly shown in Fig. 3.7b. Fig. 3.7c shows that each spike is inherited from a spike in the anisotropy factor. This is consistent with the analysis of Elliston et al. [32], in which the spikes were interpreted as due to strong deformations in the shape of the bundle. In the present interpretation, the differing signs arise because the principal curvature changes sign in the intermediate evolution.

As for the Byrnes et al. model, the intrinsic term $f_{\rm NL}^A \approx f_{\rm NL}^\phi$ does not respond immediately to this strong anisotropy, growing only later on approach to the adiabatic limit. The anisotropy is due to a strong shearing effect arising near the turn from dominantly ϕ-evolution to dominantly χ-evolution. Near the deep negative spike in $f_{\rm NL}$, there is an enhancement in the shear oriented parallel to the principal isocurvature mode. This enhances the fluctuations in the isocurvature direction.

The third feature is the flat plateau at late times, associated with the adiabatic limit. Fig. 3.7b shows that this comes from growth in the intrinsic term $f_{\rm NL}^\phi$; see the discussion in Refs. [32, 65, 66].

3.6 Summary

In this paper we have developed an analogy between inflationary perturbation theory and geometrical optics. Here we summarize the main steps in the discussion.

Background.—In inflationary perturbation theory, we are interested in following the statistical properties—as measured by the correlation functions—of an ensemble of spacetime regions. This ensemble can be constructed equally well within the separate universe picture or traditional cosmological perturbation theory.

The ensemble picks out a cloud of points in phase space. In the limit $k/aH \ll 0$,

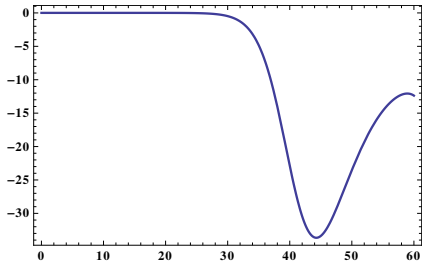

(a) f_{NL}

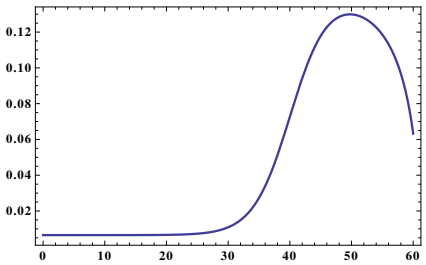

(b) difference between full f_{NL} and curvature contribution

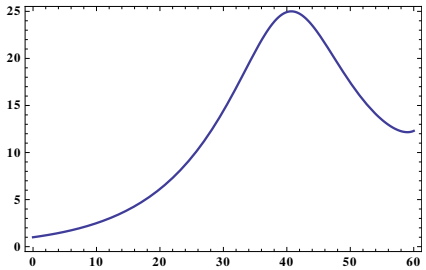

(c) anisotropy factor $(\langle \boldsymbol{mm} \rangle / \langle \sigma\sigma \rangle)^{1/2}$

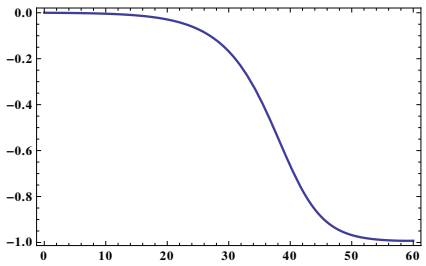

(d) correlation coefficient $\rho_{\boldsymbol{m}}$

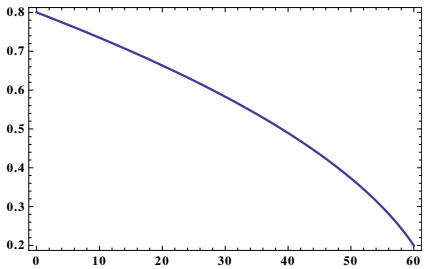

(e) principal curvature $k_{\boldsymbol{m}}$

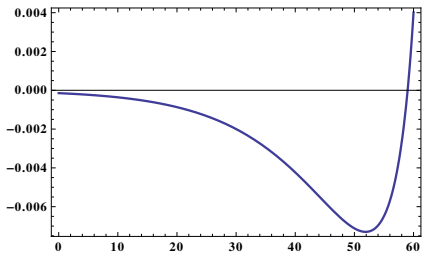

(f) isocurvature $\eta_{\boldsymbol{m}}$

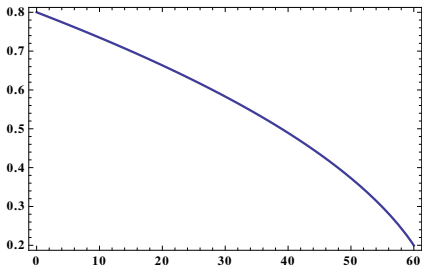

(g) dilation θ

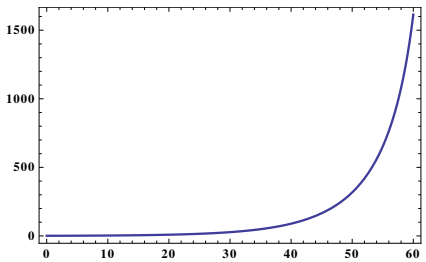

(h) focusing $\exp \int \theta \, \mathrm{d}N$

Figure 3.6: Bundle parameters for the Byrnes et al. model $V = V_0 \phi^2 \mathrm{e}^{-\lambda\chi^2}$. The initial conditions are $\phi = 16 M_{\mathrm{P}}$ and $\chi = 0.001 M_{\mathrm{P}}$, and $\lambda = 0.05 M_{\mathrm{P}}^{-2}$. All plots are against the e-folding number N, measured from horizon exit of the mode in question.

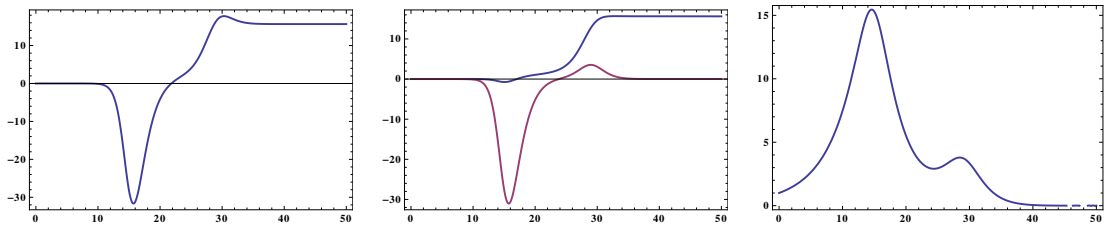

(a) $f_{\rm NL}$ **(b)** $f_{\rm NL}^{\phi}$ (blue curve) and $f_{\rm NL}^{\rm gauge}$ (red curve) **(c)** anisotropy factor $(\langle \boldsymbol{mm} \rangle / \langle \sigma\sigma \rangle)^{1/2}$

Figure 3.7: Bundle parameters for the axion–quadratic model; for the potential and initial conditions, see Fig. 3.4. All plots are against the e-folding number N, measured from horizon exit of the mode in question.

interactions between members of the ensemble are suppressed and each point moves along a phase space orbit of the unperturbed system. Therefore the ensemble traces out a narrowly-collimated "spray" or bundle of trajectories. Where slow-roll applies, the momenta are determined in terms of the fields and we can work in terms of a simplified flow on field space.

Optical quantities.—Geometrical properties of the bundle of trajectories can be used to describe its evolution and determine its statistical properties. The quantities of principal importance are obtained by decomposing the expansion tensor, yielding the dilation, shear and twist. These are well-known from the description of light rays in general relativity.

Jacobi fields and van Vleck matrix.—The dilation, shear and twist determine the evolution of *Jacobi fields*, which describe infinitesimal vectors connecting nearby trajectories. At any point in the flow, the van Vleck matrix aggregates the linearly independent Jacobi fields. The Jacobi fields themselves are measured from a fiducial trajectory, which can be thought of as the eikonal of geometrical optics. This analogy is exact within the slow-roll approximation.

We have argued that different implementations of the separate universe assumption—such as the Lyth–Rodríguez Taylor expansion, or the transport equations of §4.4—can be thought of as different methods to compute the Jacobi fields, in the form of the van Vleck matrix (3.16). More generally, the same is true for all approaches to perturbation theory in the limit $k/aH \to 0$. The most familiar implementation of the separate universe assumption, the "δN formalism" or Taylor expansion approach, follows from Jacobi's method of varying a solution with respect to its constants of integration. Conversely, the transport equations arise more naturally from Jacobi's differential equation.

On approach to a caustic, some number of Jacobi fields decay. At an *adiabatic caustic*, defined in §3.2.4, all but one of the Jacobi fields decay. The single remaining field represents fluctuations along the caustic. In inflation this mode is the adiabatic fluctuation. The other Jacobi fields represent isocurvature fluctuations between the spacetime regions which make up the ensemble. Therefore, focusing at an adiabatic caustic can be interpreted as decay of isocurvature modes, or approach to an adiabatic limit in the sense of Elliston et al. [32].

Transport equations.—The "u-tensors" encode evolution of the connecting vector fields. We have argued that these tensors can be computed using either cosmological perturbation theory or the separate universe approximation. More generally, any formalism which can reproduce the $\boldsymbol{k}$-space deviation equation (3.32) will reproduce the correct correlation functions, because the u-tensors uniquely determine the transport equations. Therefore the u-tensors may be used as an objective way to compare competing formalisms.

The transport equations obtained in this way are generalizations of the transport equations previously introduced in Ref. [17, 18]. Because they are expressed in terms of u-tensors, it follows that they can be integrated in terms of the Jacobi fields and their derivatives. Therefore the correlation functions can be expressed using the van Vleck matrix and its derivatives. (Technically it is the inverse of the van Vleck matrix which appears, in the form of the propagator matrix (3.15).)

In turn the van Vleck matrix can be expressed in terms of the integrated dilation, shear and twist. This makes it possible to diagnose regions where the flow may become adiabatic by tracking the behaviour of the focusing parameter Θ, defined in Eq. (5.13), and the behaviour of the shear and twist.

Working within the slow-roll approximation we have argued that $\Theta \gtrsim 1$ implies the presence of remaining isocurvature modes. To be compatible with experiment, these must almost certainly decay before the surface of last scattering. The consequent transfer of power into the adiabatic mode can change the value of ζ.

Flow equations.—The Jacobi fields yield a formal solution for each correlation function, analogous to the "line of sight" used to simplify integration of the Boltzmann equation in CMB codes.

This formal solution demonstrates explicitly that the transport equations reproduce the Taylor expansion algorithm of Lyth & Rodríguez. In doing so we also obtain explicit expressions for the Taylor coefficients $\Gamma_{\alpha i}$ and $\Gamma_{\alpha ij}$ in terms of integrals of the expansion tensor and its derivatives along the flow. Similar expressions had previously been obtained

by Yokoyama et al. [14, 15].

These explicit expressions can be manipulated to obtain a closed set of evolution equations for the Taylor coefficients. These are Eqs. (3.38a) and (3.51). Such equations are extremely helpful in practice, because it means the Taylor coefficients can be obtained without the challenging problem of extracting a variational derivative after numerical integration: without a sufficiently accurate integration algorithm, the small variation of interest can be swamped by numerical noise.

Transport of shape coefficients.—Even after obtaining the Taylor coefficients, it is necessary to extract coefficients for each type of momentum dependence (or "shape," in inflationary terminology) which occurs in a correlation function. An alternative is to return to the full $\boldsymbol{k}$-space transport equations and derive evolution equations for these coefficients directly. The first nontrivial case is the three-point function, whose shape coefficients are determined by Eq. (3.55).

Gauge transformations.—Specializing to the slow-roll approximation, where the flow can be described in field space, ray-tracing techniques can be used to obtain the gauge transformation to ζ. In this way the gauge transformation is expressed using geometrical quantities in field space, rather than merely derivatives of the potential.

In models where a large f_{NL} is obtained from the gauge transformation, this gives a geometrical interpretation of its magnitude. The contributory factors are: (1) the η-parameters of the adiabatic and principal isocurvature modes; (2) the principal curvatures of uniform-density hypersurfaces in field space; (3) the correlation coefficient between the adiabatic fluctuations and the fluctuations in each principal isocurvature mode; and (4) an anisotropy factor which measures distortions in the cloud of field-space points representing the ensemble.

In two cases where a large, transient contribution to f_{NL} has been observed, we show this principally arises from a strong enhancement in the anisotropy factor.

Comparison with other geometrical formulations.—In common with all other approaches to the evolution of correlation functions, the interpretation described in §§4.4–4.4.3 is a reformulation of perturbation theory. All approaches carry the same physical content. Therefore, aside from practical considerations, the merit of each reformulation arises from the insight gained by emphasis on different structures.

The formulation we have given emphasizes the background phase space manifold, which encodes the structure of the theory in its geometry. This geometrical structure is mapped

out by the behaviour of the trajectories flowing over it. Globally, this connection is made precise by the methods of Morse theory. Locally, it is encoded in the Jacobi fields whose role we have highlighted.

Attempts to reformulate perturbation theory in terms of geometrical objects have already attracted attention by various authors. Gordon et al. [86] and Nibbelink & van Tent [20] formulated perturbation theory for the two-point function in terms of the Frenet basis, which they called the "kinematical basis." (See also Achúrcarro et al. [25].) Peterson & Tegmark later extended this approach to the three-point function [22–24]. A Frenet basis can be defined for each trajectory, and the Frenet–Serret equation describes how this basis is transported along the trajectory. In Refs. [20, 22–25, 86] these equations are used to describe transfer between the adiabatic and isocurvature modes.

In the Frenet formulation, the isocurvature modes are identified with the normal, binormal, ..., vectors. In our formulation these modes arise from the eigenvectors of the extrinsic curvature, $K_{\alpha\beta}$, which we have described as the principal isocurvature modes. The tangent plane spanned by the Frenet normal, binormal, ..., is the same as the subspace spanned by the eigenvalues of $K_{\alpha\beta}$, so the physical content of these formulations is the same. More generally, in our formulation the properties of the isocurvature modes are expressed using the familiar mathematical apparatus used to describe hypersurfaces—normal vectors, first and second fundamental forms, and so on.

In addition, we explicitly separate a "local" contribution to each ζ correlation function, arising from a gauge transformation and depending on the precise orientation of the Frenet basis, from the "integrated" contributions, obtained by solving the transport equations. Although it is clear that one can equally well express the integrated contributions in *any* suitable basis, it requires extra effort to rotate to the Frenet basis at each step in the integration. We feel it is preferable to express the evolution equations of perturbation theory in terms of the original basis on field space.

Future directions.—This formalism can be extended in several directions.

First, at some points in the discussion we specialized to the slow-roll approximation, to take advantage of certain simplifications—such as the twist-free and hypersurface-orthogonal character of flow. However, as we have presented it, the underlying formalism is independent of slow-roll. It can be used to evolve both field and momentum perturbations. This is desirable because future data from microwave background or galaxy surveys will be highly accurate, demanding commensurate accuracy in our theoretical calculations.

Second, in this paper we have interpreted the decay of isocurvature modes, and approach to an adiabatic limit, as focusing of the bundle to an "adiabatic" caustic. Our detailed discussion was restricted to field space. It should also be possible to study focusing and decay of isocurvature modes on the full phase space, providing a framework for the study of *kinetically* dominated scenarios, such as descent through the waterfall of hybrid inflation, where focusing may also occur.

Third, the existence of explicit expressions for the Taylor coefficients $\Gamma_{\alpha i}$ and $\Gamma_{\alpha ij}$ may enable new analytic solutions to be found.

Finally, the entire formalism can be extended to higher n-point functions. The case of principal interest is the four-point function. In contrast to the three-point function, this requires two shape parameters which determine $\tau_{\rm NL}$ and $g_{\rm NL}$.

3.A Appendix: Yokoyama et al. backwards formalism

In §3.4.2 we presented integral formulae for the "δN" coefficients, Eqs. (3.50a)–(3.50b), and noted that essentially identical expressions had been presented by Yokoyama et al. [14–16]. (However, Yokoyama et al. obtained their results by very different means.) Since their work is closely related to our own in content and outlook, we take this opportunity to review and extend their results.

Their aim is to develop evolution or "transport" equations (in our terminology) for objects closely related to observation, such as the derivatives N_i—defined in section §4.4.3—and the f_{NL} parameter. They proceed as we do, first fixing a flat initial hypersurface. In our notation this is distinguished with lower case Roman indices. Unlike us, they also fix the final slice to be the precise time at which we wish to know the value of each observable quantity. In our notation this slice is labelled with Greek letters, and we obtain the matrices $\Gamma_{\alpha i}$ and $\Gamma_{\alpha ij}$ as a function of it. Observables can be obtained after evaluating these functions at the time of interest. Instead, Yokoyama et al. consider intermediate flat slices *between* the initial and final slices, and express their answers as a function of the intermediate time. As we now explain, observables are to be obtained by setting this intermediate slice equal to the *initial* hypersurface.

For convenience we extend our index notation, and label quantities evaluated on the intermediate slice with upper case Roman indices. Yokoyama et al. introduce the quantity

$$N_I = N_\alpha \Gamma_{\alpha I}, \tag{3.86}$$

where N_α was defined in §4.4.3. N_I is the derivative of the number of e-folds between an intermediate flat hypersurface and the final uniform density hypersurface, with respect to the field values on the intermediate slicing. Yokoyama et al. introduce a further quantity $\Theta_I = \Gamma_{Ii} N_i$. Note that Θ_I is not to be confused with the focusing parameter Θ defined in the text, which is the exponential of the integrated dilation. N_I and Θ_I obey the autonomous transport equations

$$\frac{\mathrm{d}N_I}{\mathrm{d}N} = -u_{JI} N_J, \tag{3.87}$$

$$\frac{\mathrm{d}\Theta_I}{\mathrm{d}N} = u_{IJ} \Theta_J, \tag{3.88}$$

Evaluating N_I at the final hypersurface gives N_α, which provides a boundary condition for the differential equation. One can then evolve *backwards* in time until we reach the initial

slice. At this point N_I will equal N_i, which is the Taylor coefficient we set out to calculate. After this has been done, Θ_I can be evolved *forwards* from the initial hypersurface with boundary condition $\Theta_i = N_i$.

We describe this as the "backwards" formalism, to be contrasted with the "forwards" formalism we have described in the text.

The introduction of these quantities is ingenious. Employing Eq. (3.72) together with Eq. (3.50b) yields

$$N_{ij} = N_\alpha \Gamma_{\alpha l} \int_{N*}^{N} \Gamma^{-1}_{l\sigma} u_{\sigma\beta\gamma} \Gamma_{\beta i} \Gamma_{\gamma j} dN' + N_{\alpha\beta} \Gamma_{\alpha i} \Gamma_{\beta j}, \tag{3.89}$$

In turn this leads to

$$N_i N_{ij} N_j = \int_{N*}^{N} N_I u_{IJK} \Theta_J \Theta_k dN' + \Theta_\alpha \Theta_\beta N_{\alpha\beta}. \tag{3.90}$$

Therefore, $f_{\rm NL}$ can be evaluated with knowledge only of N_I, Θ_I and u_{IJK}.

In performing this calculation, Yokoyama et al. traded a three-index object (either $\Gamma_{\alpha ij}$ or $\alpha_{\alpha|\beta\gamma}$, depending which formulation is in use) for two one-index objects, N_I and Θ_I. This involves fewer equations and therefore can be numerically advantageous.

Nevertheless, the backwards formalism has some disadvantages. First, because it computes only the Taylor coefficients, information about isocurvature modes is discarded. The evolution equations for $\Sigma_{\alpha\beta}$ and $\alpha_{\alpha|\beta\gamma}$, or $\Gamma_{\alpha i}$ and $\Gamma_{\alpha ij}$, allow the isocurvature modes to be retained.

Second, to obtain information about the time-evolution of any observable it is necessary to recalculate N_I and Θ_I with multiple *final* times. Although the method yields N_I, which is apparently related to the gauge transformation at an intermediate time, this is not quite correct. N_I is defined for a fixed *future* rather than past boundary condition, and therefore gives information about a range of scales at a fixed time of observation, rather than a fixed scale at a range of final times. The past-defined objects required for the latter are automatically provided by the forwards formalism, meaning that multiple integrations are not required.

If the time of observation is known then the backwards formalism gives an efficient means to treat multiple scales at once.

To extend the backwards formalism to the trispectrum, one needs to separate the observables $\tau_{\rm NL}$ and $g_{\rm NL}$. For this purpose N_{ij} and N_{ijk} themselves would be required. Therefore, given the potential utility of this method, we conclude by extending it to include a backwards evolution equation for N_{IJ}. As for the spectrum, this can be used to obtain

information about $f_{\rm NL}$ and $\tau_{\rm NL}$ over a range of scales at a fixed time of observation. It still requires the solution for only a two-index object. The transport equation for N_{IJ} can be shown to be

$$\frac{\mathrm{d}N_{JK}}{\mathrm{d}N} = -u_{IJK}N_I - u_{IJ}N_{IK} - u_{IK}N_{IJ}. \tag{3.91}$$

This is to be solved backwards from the final hypersurface where N_{IJ} is equal to $N_{\alpha\beta}$.

References

[1] E. Komatsu et al. "Seven-Year Wilkinson Microwave Anisotropy Probe (WMAP) Observations: Cosmological Interpretation". In: *Astrophys.J.Suppl.* 192 (2011), p. 18. arXiv:1001.4538 [astro-ph.CO] (cit. on p. 86).

[2] "The scientific programme of Planck". 2006 (cit. on p. 86).

[3] P.A.R. Ade et al. "Planck Early Results: The Planck mission". In: (2011). arXiv:1101.2022 [astro-ph.IM] (cit. on p. 86).

[4] Vincent Desjacques and Uros Seljak. "Primordial non-Gaussianity from the large scale structure". In: *Class.Quant.Grav.* 27 (2010), p. 124011. arXiv:1003.5020 [astro-ph.CO] (cit. on p. 86).

[5] Alexei A. Starobinsky. "Multicomponent de Sitter (Inflationary) Stages and the Generation of Perturbations". In: *JETP Lett.* 42 (1985), pp. 152–155 (cit. on pp. 86, 108).

[6] D. H. Lyth. "Large Scale Energy Density Perturbations and Inflation". In: *Phys.Rev.* D31 (1985), pp. 1792–1798 (cit. on p. 86).

[7] Misao Sasaki and Ewan D. Stewart. "A General analytic formula for the spectral index of the density perturbations produced during inflation". In: *Prog.Theor.Phys.* 95 (1996), pp. 71–78. arXiv:astro-ph/9507001 (cit. on pp. 86, 108).

[8] D. S. Salopek and J. R. Bond. "Nonlinear evolution of long wavelength metric fluctuations in inflationary models". In: *Phys. Rev.* D42 (1990), pp. 3936–3962 (cit. on p. 86).

[9] Misao Sasaki and Takahiro Tanaka. "Superhorizon scale dynamics of multiscalar inflation". In: *Prog.Theor.Phys.* 99 (1998), pp. 763–782. arXiv:gr-qc/9801017 [gr-qc] (cit. on p. 86).

[10] David Wands et al. "A New approach to the evolution of cosmological perturbations on large scales". In: *Phys.Rev.* D62 (2000), p. 043527. arXiv:astro-ph/0003278 [astro-ph] (cit. on p. 86).

[11] David H. Lyth and Yeinzon Rodríguez. "The inflationary prediction for primordial non-gaussianity". In: *Phys.Rev.Lett.* 95 (2005), p. 121302. arXiv:astro-ph/0504045 (cit. on pp. 86, 94, 108, 110, 118).

[12] Gerasimos I. Rigopoulos and E. P. S. Shellard. "Non-linear inflationary perturbations". In: *JCAP* 0510 (2005), p. 006. arXiv:astro-ph/0405185 (cit. on p. 86).

[13] G. I. Rigopoulos, E. P. S. Shellard and B. J. W. van Tent. "Non-linear perturbations in multiple-field inflation". In: *Phys.Rev.* D73 (2006), p. 083521. arXiv:astro-ph/0504508 (cit. on p. 86).

[14] Shuichiro Yokoyama, Teruaki Suyama and Takahiro Tanaka. "Primordial Non-Gaussianity in Multi-Scalar Slow-Roll Inflation". In: *JCAP* 0707 (2007), p. 013. arXiv:0705.3178 [astro-ph] (cit. on pp. 86, 94, 105, 111, 127, 130).

[15] Shuichiro Yokoyama, Teruaki Suyama and Takahiro Tanaka. "Primordial Non-Gaussianity in Multi-Scalar Inflation". In: *Phys.Rev.* D77 (2008), p. 083511. arXiv:0711.2920 [astro-ph] (cit. on pp. 86, 105, 111, 127, 130).

[16] Shuichiro Yokoyama, Teruaki Suyama and Takahiro Tanaka. "Efficient diagrammatic computation method for higher order correlation functions of local type primordial curvature perturbations". In: *JCAP* 0902 (2009), p. 012. arXiv:0810.3053 [astro-ph] (cit. on pp. 86, 130).

[17] David J. Mulryne, David Seery and Daniel Wesley. "Moment transport equations for non-Gaussianity". In: *JCAP* 1001 (2010), p. 024. arXiv:0909.2256 [astro-ph.CO] (cit. on pp. 87, 106, 115, 118, 119, 126).

[18] David J. Mulryne, David Seery and Daniel Wesley. "Moment transport equations for the primordial curvature perturbation". In: *JCAP* 1104 (2011), p. 030. arXiv:1008.3159 [astro-ph.CO] (cit. on pp. 87, 106, 113, 119, 126).

[19] Luca Amendola et al. "Correlated perturbations from inflation and the cosmic microwave background". In: *Phys.Rev.Lett.* 88 (2002), p. 211302. arXiv:astro-ph/0107089 [astro-ph] (cit. on pp. 87, 113).

[20] S. Groot Nibbelink and B.J.W. van Tent. "Scalar perturbations during multiple field slow-roll inflation". In: *Class.Quant.Grav.* 19 (2002), pp. 613–640. arXiv:hep-ph/0107272 [hep-ph] (cit. on pp. 87, 128).

[21] Z. Lalak et al. "Curvature and isocurvature perturbations in two-field inflation". In: *JCAP* 0707 (2007), p. 014. arXiv:0704.0212 [hep-th] (cit. on p. 87).

[22] Courtney M. Peterson and Max Tegmark. "Testing Two-Field Inflation". In: *Phys.Rev.* D83 (2011), p. 023522. arXiv:1005.4056 [astro-ph.CO] (cit. on pp. 87, 128).

[23] Courtney M. Peterson and Max Tegmark. "Non-Gaussianity in Two-Field Inflation". In: *Phys.Rev.* D84 (2011), p. 023520. arXiv:1011.6675 [astro-ph.CO] (cit. on pp. 87, 128).

[24] Courtney M. Peterson and Max Tegmark. "Testing Multi-Field Inflation: A Geometric Approach". In: (2011). arXiv:1111.0927 [astro-ph.CO] (cit. on pp. 87, 128).

[25] Ana Achúcarro et al. "Features of heavy physics in the CMB power spectrum". In: *JCAP* 1101 (2011), p. 030. arXiv:1010.3693 [hep-ph] (cit. on pp. 87, 128).

[26] Anastasios Avgoustidis et al. "The Importance of Slow-roll Corrections During Multi-field Inflation". In: *JCAP* 1202 (2012), p. 038. arXiv:1110.4081 [astro-ph.CO] (cit. on p. 87).

[27] Jean-Luc Lehners and Sebastien Renaux-Petel. "Multifield Cosmological Perturbations at Third Order and the Ekpyrotic Trispectrum". In: *Phys.Rev.* D80 (2009), p. 063503. arXiv:0906.0530 [hep-th] (cit. on p. 87).

[28] Christophe Ringeval. "The exact numerical treatment of inflationary models". In: *Lect.Notes Phys.* 738 (2008), pp. 243–273. arXiv:astro-ph/0703486 [astro-ph] (cit. on p. 87).

[29] Jerome Martin and Christophe Ringeval. "Inflation after WMAP3: Confronting the Slow-Roll and Exact Power Spectra to CMB Data". In: *JCAP* 0608 (2006), p. 009. arXiv:astro-ph/0605367 [astro-ph] (cit. on p. 87).

[30] Ian Huston and Karim A. Malik. "Numerical calculation of second order perturbations". In: *JCAP* 0909 (2009), p. 019. arXiv:0907.2917 [astro-ph.CO] (cit. on p. 87).

[31] Ian Huston and Karim A. Malik. "Second Order Perturbations During Inflation Beyond Slow-roll". In: *JCAP* 1110 (2011), p. 029. arXiv:1103.0912 [astro-ph.CO] (cit. on p. 87).

[32] Joseph Elliston et al. "Evolution of fNL to the adiabatic limit". In: *JCAP* 1111 (2011), p. 005. arXiv:1106.2153 [astro-ph.CO] (cit. on pp. 87, 88, 96, 103, 110, 119, 121–123, 126).

[33] Lotfi Boubekeur and David.H. Lyth. "Detecting a small perturbation through its non-Gaussianity". In: *Phys.Rev.* D73 (2006), p. 021301. arXiv:astro-ph/0504046 [astro-ph] (cit. on pp. 87, 108).

[34] David H. Lyth. "Non-gaussianity and cosmic uncertainty in curvaton-type models". In: *JCAP* 0606 (2006), p. 015. arXiv:astro-ph/0602285 [astro-ph] (cit. on p. 87).

[35] David Seery. "Infrared effects in inflationary correlation functions". In: *Class.Quant.Grav.* 27 (2010), p. 124005. arXiv:1005.1649 [astro-ph.CO] (cit. on pp. 87, 108).

[36] David Polarski and Alexei A. Starobinsky. "Isocurvature perturbations in multiple inflationary models". In: *Phys.Rev.* D50 (1994), pp. 6123–6129. arXiv:astro-ph/9404061 [astro-ph] (cit. on pp. 88, 102).

[37] Juan García-Bellido and David Wands. "Metric perturbations in two field inflation". In: *Phys.Rev.* D53 (1996), pp. 5437–5445. arXiv:astro-ph/9511029 [astro-ph] (cit. on pp. 88, 102).

[38] David Wands and Juan García Bellido. "Density perturbations from two field inflation". In: *Helv.Phys.Acta* 69 (1996), pp. 211–214. arXiv:astro-ph/9608042 [astro-ph] (cit. on pp. 88, 97).

[39] David Langlois. "Correlated adiabatic and isocurvature perturbations from double inflation". In: *Phys.Rev.* D59 (1999), p. 123512. arXiv:astro-ph/9906080 [astro-ph] (cit. on pp. 88, 102, 122).

[40] S.W. Hawking and G.F.R. Ellis. *The Large scale structure of space-time*. Cambridge University Press, 1973 (cit. on pp. 89, 93, 95, 99, 116).

[41] Fernando de Felice and C.J.S. Clarke. *Relativity on curved manifolds*. Cambridge University Press, 1990 (cit. on p. 89).

[42] Raquel H. Ribeiro and David Seery. "Decoding the bispectrum of single-field inflation". In: *JCAP* 1110 (2011), p. 027. arXiv:1108.3839 [astro-ph.CO] (cit. on p. 89).

[43] Thorsten Battefeld and Jan Grieb. "Anatomy of bispectra in general single-field inflation – modal expansions". In: *JCAP* 1112 (2011), p. 003. arXiv:1110.1369 [astro-ph.CO] (cit. on p. 89).

[44] David Seery and James E. Lidsey. "Primordial non-Gaussianities from multiple-field inflation". In: *JCAP* 0509 (2005), p. 011. arXiv:astro-ph/0506056 [astro-ph] (cit. on pp. 93, 111).

[45] R.K. Sachs. "Gravitational waves in general relativity. 6. The outgoing radiation condition". In: *Proc.Roy.Soc.Lond.* A264 (1961), pp. 309–338 (cit. on p. 94).

[46] R. Penrose. In: *Perspectives in Geometry and Relativity*. Ed. by B.H. Hoffman. Bloomington, Indiana: Indiana University Press, 1966, p. 259 (cit. on p. 94).

[47] H.M. Fried. *Green's functions and ordered exponentials*. Cambridge University Press, 2002. ISBN: 9780521443906. URL: http://books.google.co.uk/books?id=eDH3X1vpM7EC (cit. on p. 94).

[48] G.I. Rigopoulos, E.P.S. Shellard and B.J.W. van Tent. "Large non-Gaussianity in multiple-field inflation". In: *Phys.Rev.* D73 (2006), p. 083522. arXiv:astro-ph/0506704 [astro-ph] (cit. on pp. 94, 102).

[49] G.I. Rigopoulos, E.P.S. Shellard and B.J.W. van Tent. "Quantitative bispectra from multifield inflation". In: *Phys.Rev.* D76 (2007), p. 083512. arXiv:astro-ph/0511041 [astro-ph] (cit. on pp. 94, 102).

[50] Filippo Vernizzi and David Wands. "Non-gaussianities in two-field inflation". In: *JCAP* 0605 (2006), p. 019. arXiv:astro-ph/0603799 [astro-ph] (cit. on pp. 95, 102, 112).

[51] Thorsten Battefeld and Richard Easther. "Non-Gaussianities in Multi-field Inflation". In: *JCAP* 0703 (2007), p. 020. arXiv:astro-ph/0610296 [astro-ph] (cit. on p. 95).

[52] David Seery and James E. Lidsey. "Non-Gaussianity from the inflationary trispectrum". In: *JCAP* 0701 (2007), p. 008. arXiv:astro-ph/0611034 [astro-ph] (cit. on p. 95).

[53] Matt Visser. "van Vleck determinants: Geodesic focusing and defocusing in Lorentzian space-times". In: *Phys.Rev.* D47 (1993), pp. 2395–2402. arXiv:hep-th/9303020 [hep-th] (cit. on p. 95).

[54] C. DeWitt-Morette. "The Semiclassical Expansion". In: *Annals Phys.* 97 (1976), pp. 367–399 (cit. on p. 95).

[55] C. DeWitt-Morette and T.R. Zhang. "PATH INTEGRALS AND CONSERVATION LAWS". In: *Phys.Rev.* D28 (1983), pp. 2503–2516 (cit. on p. 95).

[56] C. DeWitt-Morette, T.R. Zhang and B. Nelson. "CAUSTIC PROBLEMS IN QUANTUM MECHANICS WITH APPLICATIONS TO SCATTERING THEORY". In: *Phys.Rev.* D28 (1983), pp. 2526–2546 (cit. on p. 95).

[57] David H. Lyth, Karim A. Malik and Misao Sasaki. "A General proof of the conservation of the curvature perturbation". In: *JCAP* 0505 (2005), p. 004. arXiv:astro-ph/0411220 [astro-ph] (cit. on p. 96).

[58] G.I. Rigopoulos and E.P.S. Shellard. "The separate universe approach and the evolution of nonlinear superhorizon cosmological perturbations". In: *Phys.Rev.* D68 (2003), p. 123518. arXiv:astro-ph/0306620 [astro-ph] (cit. on p. 96).

[59] Steven Weinberg. "Non-Gaussian Correlations Outside the Horizon". In: *Phys.Rev.* D78 (2008), p. 123521. arXiv:0808.2909 [hep-th] (cit. on p. 96).

[60] Steven Weinberg. "Non-Gaussian Correlations Outside the Horizon II: The General Case". In: *Phys.Rev.* D79 (2009), p. 043504. arXiv:0810.2831 [hep-ph] (cit. on p. 96).

[61] Joel Meyers and Navin Sivanandam. "Non-Gaussianities in Multifield Inflation: Superhorizon Evolution, Adiabaticity, and the Fate of fnl". In: *Phys.Rev.* D83 (2011), p. 103517. arXiv:1011.4934 [astro-ph.CO] (cit. on pp. 96, 121).

[62] Joel Meyers and Navin Sivanandam. "Adiabaticity and the Fate of Non-Gaussianities: The Trispectrum and Beyond". In: *Phys.Rev.* D84 (2011), p. 063522. arXiv:1104.5238 [astro-ph.CO] (cit. on pp. 96, 121).

[63] S. Dimopoulos et al. "N-flation". In: *JCAP* 0808 (2008), p. 003. arXiv:hep-th/0507205 [hep-th] (cit. on p. 100).

[64] Soo A Kim and Andrew R Liddle. "Nflation: multi-field inflationary dynamics and perturbations". In: *Phys.Rev.* D74 (2006), p. 023513. arXiv:astro-ph/0605604 [astro-ph] (cit. on pp. 100, 121).

[65] Soo A. Kim, Andrew R. Liddle and David Seery. "Non-gaussianity in axion Nflation models". In: *Phys.Rev.Lett.* 105 (2010), p. 181302. arXiv:1005.4410 [astro-ph.CO] (cit. on pp. 100, 103, 121, 123).

[66] Soo A. Kim, Andrew R. Liddle and David Seery. "Non-gaussianity in axion N-flation models: detailed predictions and mass spectra". In: *Phys.Rev.* D85 (2012), p. 023532. arXiv:1108.2944 [astro-ph.CO] (cit. on pp. 100, 103, 121, 123).

[67] John L. Cardy. *Scaling and renormalization in statistical physics*. Cambridge University Press, 1996 (cit. on p. 102).

[68] Joseph Silk and Michael S. Turner. "Double Inflation". In: *Phys.Rev.* D35 (1987), p. 419 (cit. on p. 102).

[69] Laila Alabidi and David H. Lyth. "Inflation models and observation". In: *JCAP* 0605 (2006), p. 016. arXiv:astro-ph/0510441 [astro-ph] (cit. on p. 102).

[70] E. Calzetta and B-L. Hu. "Stochastic behavior of effective field theories across threshold". In: *Phys.Rev.* D55 (1997), pp. 3536–3551. arXiv:hep-th/9603164 [hep-th] (cit. on p. 106).

[71] Esteban Calzetta and B.L. Hu. "Stochastic dynamics of correlations in quantum field theory: From Schwinger-Dyson to Boltzmann-Langevin equation". In: *Phys.Rev.* D61 (2000), p. 025012. arXiv:hep-ph/9903291 [hep-ph] (cit. on p. 106).

[72] Philip R. Jarnhus and Martin S. Sloth. "de Sitter limit of inflation and nonlinear perturbation theory". In: *JCAP* 0802 (2008), p. 013. arXiv:0709.2708 [hep-th] (cit. on p. 106).

[73] Crispin W. Gardiner. *Handbook of stochastic methods: for physics, chemistry and the natural sciences*. Springer Series in Synergetics, 13. Springer, Nov. 2002. ISBN: 3540616349 (cit. on p. 107).

[74] Joseph Smidt et al. "CMB Constraints on Primordial non-Gaussianity from the Bispectrum ($f_{\rm NL}$) and Trispectrum ($g_{\rm NL}$ and $\tau_{\rm NL}$) and a New Consistency Test of Single-Field Inflation". In: *Phys.Rev.* D81 (2010), p. 123007. arXiv:1004.1409 [astro-ph.CO] (cit. on p. 107).

[75] J.R. Fergusson, D.M. Regan and E.P.S. Shellard. "Optimal Trispectrum Estimators and WMAP Constraints". In: (2010). arXiv:1012.6039 [astro-ph.CO] (cit. on p. 107).

[76] David H. Lyth and David Seery. "Classicality of the primordial perturbations". In: *Phys.Lett.* B662 (2008), pp. 309–313. arXiv:astro-ph/0607647 [astro-ph] (cit. on p. 108).

[77] David Seery. "One-loop corrections to a scalar field during inflation". In: *JCAP* 0711 (2007), p. 025. arXiv:0707.3377 [astro-ph] (cit. on p. 108).

[78] David Seery. "One-loop corrections to the curvature perturbation from inflation". In: *JCAP* 0802 (2008), p. 006. arXiv:0707.3378 [astro-ph] (cit. on p. 108).

[79] C.S. Lam. "Decomposition of time ordered products and path ordered exponentials". In: *J.Math.Phys.* 39 (1998), pp. 5543–5558. arXiv:hep-th/9804181 [hep-th] (cit. on p. 110).

[80] Mafalda Dias and David Seery. "Transport equations for the inflationary spectral index". In: *Phys.Rev.* D85 (2012), p. 043519. arXiv:1111.6544 [astro-ph.CO] (cit. on p. 112).

[81] David H. Lyth and Ignacio Zaballa. "A Bound concerning primordial non-Gaussianity". In: *JCAP* 0510 (2005), p. 005. arXiv:astro-ph/0507608 [astro-ph] (cit. on p. 112).

[82] Karim A. Malik and David Wands. "Cosmological perturbations". In: *Phys.Rept.* 475 (2009), pp. 1–51. arXiv:0809.4944 [astro-ph] (cit. on p. 115).

[83] Christian T. Byrnes, Ki-Young Choi and Lisa M.H. Hall. "Conditions for large non-Gaussianity in two-field slow-roll inflation". In: *JCAP* 0810 (2008), p. 008. arXiv:0807.1101 [astro-ph] (cit. on pp. 118, 119, 122, 123).

[84] Christian T. Byrnes, Ki-Young Choi and Lisa M.H. Hall. "Large non-Gaussianity from two-component hybrid inflation". In: *JCAP* 0902 (2009), p. 017. arXiv:0812.0807 [astro-ph] (cit. on pp. 118, 119).

[85] David Mulryne, Stefano Orani and Arttu Rajantie. "Non-Gaussianity from the hybrid potential". In: *Phys.Rev.* D84 (2011), p. 123527. arXiv:1107.4739 [hep-th] (cit. on p. 121).

[86] Christopher Gordon et al. "Adiabatic and entropy perturbations from inflation". In: *Phys.Rev.* D63 (2001), p. 023506. arXiv:astro-ph/0009131 [astro-ph] (cit. on p. 128).

Paper 4

Multifield consequences for D-brane inflation

Mafalda Dias, Jonathan Frazer and Andrew Liddle

We analyse the multifield behaviour in D-brane inflation when contributions from the bulk are taken into account. For this purpose, we study a large number of realisations of the potential; we find the nature of the inflationary trajectory to be very consistent despite the complex construction. Inflation is always canonical and occurs in the vicinity of an inflection point. Extending the transport method to non-slow-roll and to calculate the running, we obtain distributions for observables. The spectral index is typically blue and the running positive, putting the model under moderate pressure from WMAP7 constraints. The local $f_{\rm NL}$ and tensor-to-scalar ratio are typically unobservably small, though we find approximately 0.5% of realisations to give observably large local $f_{\rm NL}$. Approximating the potential as sum-separable, we are able to give fully analytic explanations for the trends in observed behaviour. Finally we find the model suffers from the persistence of isocurvature perturbations, which can be expected to cause further evolution of adiabatic perturbations after inflation. We argue this is a typical problem for models of multifield inflation involving inflection points and renders models of this type technically unpredictive without a description of reheating.

4.1 Motivation

Inflation (for recent reviews see Ref. [1–3]) is widely viewed as the most elegant paradigm to understand the very early universe, but despite being a simple set-up, it is hard to

fully describe it within an ultra-violet complete theory. The main reason for this is that its dynamics are highly sensitive to Planck-scale physics. Generally speaking, Planck-suppressed contributions arise by integrating out heavy fields, which are present as extra degrees of freedom necessary for the ultra-violet completion of a theory. Unless protected by some specific symmetry, the inflaton will couple to these heavy fields, which results in a radiative instability of its mass and of the flatness of the potential. It is therefore of enormous interest to try to study inflation in an effective action that takes into account contributions of high energy physics.

In string theory, the important degrees of freedom to take into consideration are the heavy moduli that arise from stabilized compactifications of the extra dimensions. To compute the detailed contributions that their coupling to the inflaton induces in the effective action requires full knowledge of the stabilized compactification, which is rarely possible. In this sense, it is important to identify and work with string set-ups that present a sufficient level of computability. This is the main motivation to look at inflation arising from the dynamics of D3-branes in warped throats. This scenario is not expected to be generic but it allows some major simplifications that make the task of building the effective action more achievable.

The flux compactification causes warping of the manifold, giving rise to regions of the bulk with warped throats. Inflation can occur in this scenario when a D3-brane, corresponding to our four-dimensional space-time, is Coulomb attracted to an anti-D3-brane that sits at the infra-red tip of the throat, where it minimizes its energy. Inflation is driven by the dynamics of the D3-brane, and it behaves like a multi scalar field system, where the fields can be viewed as the physical coordinates separating the branes. The inflationary epoch ends when the branes collide and annihilate.

What is special about these warped throat regions is that they can be approximated by a finite region of a non-compact conifold geometry, for which the metric and background fluxes are well known. This finite segment is then glued to the compact bulk at some ultra-violet scale. Corrections to this non-compact approximation will arise from the effect of fields on the throat, like stabilized moduli of the compact bulk, and are clearly examples of the Planck-suppressed contributions to the effective action mentioned above.

Even working in this 'simple' set-up, the effective action cannot be fully computed. At most, it is possible to calculate the form of the Planck-suppressed contributions, but they will come necessarily with an unknown Wilson coefficient. For this reason, to study the inflationary potential that arises from the D-brane scenario one needs to sample over

a lot of realisations of random Wilson coefficients. Observational predictions need to be understood in the light of this statistical nature.[1]

Another issue to keep in mind is that the conifold approximation for the throat does not hold at the infra-red tip. This implies that, if using such an approximation, the dynamics can only be analysed before the tip, ignoring everything that occurs around and just before the collision of the branes. One can hope that this regime will not significantly affect the curvature perturbation ζ, otherwise the predictions made are useless for comparisons with observations at decoupling time or after. To check if this is a reasonable assumption, it is necessary to keep track of isocurvature modes as they transfer power to the curvature perturbations. If they have not completely decayed by the end of the analysis, the curvature perturbation will continue to evolve as the brane moves into the tip. The inflationary trajectory is said to have not yet reached its 'adiabatic limit'. The observable properties of ζ will then depend on unknown details of the tip, including reheating, making the model incomplete.

In this paper, our aim is to exhaustively study the possible D-brane dynamics above the tip and understand the consequent inflationary behaviour. For this purpose, we follow the most sophisticated set-up in the literature [4]. This includes the sampling over Wilson coefficients and assumptions like the ones described above. The throat is approximated by a conifold parameterized by one radial and five angular directions that can be effectively viewed as the scalar fields driving inflation; this approximation only holds for a fixed range in the radial direction and it can be shown that within it DBI effects can be neglected. The framework and details of the construction of the potential are reviewed in §4.2.

Since the potential that describes the motion of the D-brane is sensitive to all 6 coordinates, multifield effects have a profound impact on the dynamics of the inflationary trajectory and consequent curvature perturbations ζ. To compute observables within this multifield superhorizon dynamics, we use the *transport equations* method originally introduced in Refs. [5, 6] along with an extension to non-slow-roll that will be described fully in a forthcoming paper [7]. This technique is a realisation of the separate universe assumption in which the values of correlation functions of ζ and their tilts can be directly transported

[1] This issue is analogous to the challenge of making predictions in models of the string landscape. In order to compare predictions from this model with observation we must assume we are a typical observer. Of what class of observer we are typical is however a very difficult question to address and brings with it an inherent measure problem. We make no attempt to address this interesting challenge here, but it should be noted that a resolution of this problem will add a weighting to the distributions we present in this work.

from horizon-crossing to the desired time of evaluation, as described in §4.4. Since this is framed in terms of ordinary differential equations, it allows for a clean and efficient numerical implementation as well as a means of explicitly keeping track of the evolution of isocurvature modes.

As a consequence of our analysis, we obtain the probability of getting inflation, found to be in agreement with Ref. [4], and the statistical distributions of observables predicted by our set-up. But the most interesting results of this work come from our understanding of the peculiarities of the multifield dynamics of the D-brane potential. By looking in detail at the resulting inflationary trajectories, we are able to map trends in the distributions of observables to generic features of the potential. Moreover, we can see if these features allow the trajectories to reach their adiabatic limit. The outcome of our work is then more than the computation of predictions, being an investigation on the limitations of our set-up as a predictive and useful toy model for the D-brane scenario.

4.2 D-brane inflation

4.2.1 D-branes in a warped throat

As mentioned earlier, in the D-brane inflation scenario, our Universe lives in a D3-brane and experiences inflation due to its dynamics in a warped throat region of a stabilized compact space; the D3-brane is attracted by an anti-D3-brane that sits at the tip of the throat where its energy is minimized. When the two branes collide, they annihilate, inflation ends and reheating occurs [8, 9].

The throat region, excluding the tip, can be well approximated by a non-compact conifold geometry; the conical singularity that would arise at the tip is smoothed by fluxes such that the radial coordinate at this point is finite. For the purpose of this work, only the region above the tip will be considered. In this case, and ignoring logarithmic corrections to the warp factor, the background geometry can be approximated by:

$$ds^2 = \left(\frac{R}{r}\right)^2 g_{ij} d\phi^i d\phi^j = \left(\frac{R}{r}\right)^2 \left(dr^2 + r^2 ds^2_{T^{1,1}}\right), \tag{4.1}$$

where r is the radial conical coordinate and $T^{1,1}$ is the coset space $(SU(2) \times SU(2))/U(1)$ that describes the angular directions of the cone. The radius R is approximately $r_{\rm UV}$, the coordinate at which the throat is glued to the compact bulk, as illustrated in Fig. 4.1.

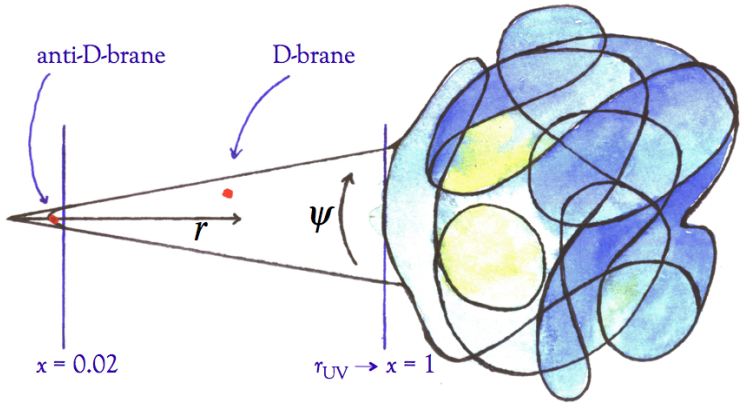

Figure 4.1: The non-compact conifold approximation for the warped throat. This approximation holds between $x = 1$, where the throat is glued to the compact bulk, and $x = 0.02$, where the tip that cannot be described by our approximated geometry starts.

In agreement with Ref. [4] we use the value $r_{\rm UV} = 1$ throughout this work. It is useful to define a rescaled radial coordinate as $x \equiv r/r_{\rm UV}$ that in the cone region is always $0 \ll x < 1$. To ensure that the non-compact approximation always holds, we restrict our analysis to the regime comfortably above the tip, where $0.02 < x < 1$. The value $x = 0.02$ was chosen in agreement with Ref. [4].

The $T^{1,1}$ space is parameterized by 5 angles $\Psi = \{\theta_1, \theta_2, \varphi_1, \varphi_2, \psi\}$ where $0 \leq \theta_1 \leq \pi$, $0 \leq \theta_2 \leq \pi$, $0 \leq \varphi_1 < 2\pi$, $0 \leq \varphi_2 < 2\pi$ and $0 \leq \psi < 4\pi$.

Throughout this paper we will use units $M_{\rm Pl}^{-2} = 8\pi G = 1$. Also, in agreement with Ref. [4], we use the value $r_{\rm UV} = 1$. In this throat the D3-brane experiences a DBI inflationary Lagrangian like

$$\mathcal{L} = a^3 \left(-T(\phi)\sqrt{1 - \frac{T_3 g_{ij}\dot{\phi}^i\dot{\phi}^j}{T(\phi)}} - V(\phi) + T(\phi) \right), \tag{4.2}$$

where a is the scale factor, T_3 is a constant representing the brane tension and, within the approximation where the logarithmic corrections to the warp factor can be ignored, $T(\phi) = T_3 x^4$. The value of the warp factor at the tip is determined by the parameter a_0 such that $T(\phi)|_{\rm tip} \equiv T_3 a_0^4$. Some physical arguments concerning the consistency of the set-up enforce a limit on how small $T(\phi)$ can get [10]; in this work, following Ref. [4], we use the values $T_3 = 10^{-2}$ and $a_0 = 10^{-3}$.

As mentioned in Ref. [4], for our specific realisations of the D-brane action, the brane velocity is always very small compared to $T(\phi)$, making

$$\frac{T_3 g_{ij}\dot{\phi}^i\dot{\phi}^j}{T(\phi)} \ll 1. \tag{4.3}$$

This is equivalent to saying that DBI effects are negligible, as we can rewrite the Lagrangian as

$$\mathcal{L} = a^3 \left(\frac{1}{2} T_3 g_{ij} \dot{\phi}^i \dot{\phi}^j - V(\phi) \right) \tag{4.4}$$

and identify the canonical kinetic term rescaled by the constant T_3.

The fact that this simplification can be made is related not only to the choice of T_3 and a_0 but also to the fact that our analysis only includes the throat region above the tip. Condition (4.3) breaks if $T(\phi)$ gets very small and, in fact, $T(\phi)$ decreases with x. Possible DBI inflation in this regime can have strong repercussions in the value of observables at the end of inflation; the inclusion of the whole throat in the computation of perturbations is then potentially very interesting but beyond the scope of this work.

4.2.2 D-brane potential

In the simplest form of this scenario, the potential that induces inflation has two contributions [9]. First, there is the Coulomb interaction between the pair of branes, which is a multipole expansion where high-multipole terms are suppressed by powers of a_0. The leading terms are:

$$V_C = D_0 \left(1 - \frac{27 D_0}{64 \pi^2 T_3^2 r_{\rm UV}^4} \frac{1}{x^4} \right) \tag{4.5}$$

where the parameter $D_0 \equiv 2 T_3 a^4$ determines the overall scale of inflation.

Second, the coupling to the curvature induces, at leading order, a mass term like:

$$V_M = \frac{1}{3} \mu^4 x^2 \tag{4.6}$$

where the scale $\mu^4 \equiv D_0 T_3 r_{\rm UV}^2 / M_{\rm Pl}^2$.

In this basic picture, inflation would actually be single-field, with the inflaton being the radial separation between brane and anti-brane, x. However, if the dynamics was determined by these two terms only, sufficient inflation couldn't be achieved [8]. Such a potential has a single inflection point; this feature will be shown in the next sections to have strong consequences for the phenomenology of the full model.

This simplified picture ignores some important contributions to the potential experienced by the D-brane. One needs to take into account that the throat is finite and glued to a compact manifold, and as such, moduli stabilization from the bulk will necessarily have an impact on the throat geometry. These contributions can be viewed as corrections to the non-compact approximation, and will be denoted by $V_{\rm bulk}$.

Ideally, one would like to have the full knowledge of the 4-dimensional potential induced by the compactification flux on the brane dynamics, but this is not possible to achieve for a general Calabi–Yau bulk. However, it is known [10] that such a potential, in the non-compact background of the conifold, respects the Laplace equation:

$$\nabla^2 V_{\text{bulk}} = 0. \tag{4.7}$$

Since we know completely the geometry of the conifold, this equation can be explicitly solved. We refer to these contributions, following the notation of Ref. [10], as the homogeneous contributions to V_{bulk}.

Deviations from this expression, which holds for the non-compact background, can be obtained by allowing a source from the bulk. In this case, the Poisson equation looks like [10]

$$\nabla^2 V_{\text{bulk}} = \frac{g_s}{96} |\Lambda|^2 , \tag{4.8}$$

where g_s is the string coupling constant and Λ is proportional to the imaginary anti-self-dual three-form flux from the bulk. We will refer to these contributions as the inhomogeneous contributions to V_{bulk}. To solve this equation, a simplification can be used. Since these contributions are perturbations to the non-compact approximation, they can be assumed, up to a good approximation, to have the same structure as the homogeneous contributions. So the idea is to express them as an expansion of harmonic terms from the homogeneous solution. In other words, the solutions to the Laplace equation dictate the structure of the bulk contribution to the potential.

Homogeneous contributions: The Laplace equation (4.7) for our non-compact conifold can be written in the form of the expansion [11]:

$$V_{\text{hom bulk}}(x, \Psi) = \mu^4 \sum_{LM} C_{LM} x^{\Delta(L)} Y_{LM}(\Psi) \tag{4.9}$$

where C_{LM} are constant coefficients, $Y_{LM}(\Psi)$ are the angular eigenfunctions of the Laplacian of the $T^{1,1}$ space and the subscripts $L \equiv \{l_1, l_2, R\}$ and $M \equiv \{m_1, m_2\}$ represent the quantum numbers under the $T^{1,1}$ isometries. The powers $\Delta(L)$ are related to the eigenvalues of the Laplacian and are given by

$$\Delta(L) \equiv -2 + \sqrt{6l_1(l_1+1) + 6l_2(l_2+1) - 3R/4 + 4}. \tag{4.10}$$

The magnitudes of C_{LM} are highly dependent on details of specific compactifications, so they need to be considered unknown parameters. Using the scale μ^4, considerations of

Ref. [12] suggest that $C_{LM} \sim \mathcal{O}(1)$, so a way to deal with this lack of knowledge is to scan randomly over values in this range. To take the leading contributions of this term, one needs to consider the lower values of $\Delta(L)$. The maximum value desired for $\Delta(L)$ determines the truncation of the summation.

INHOMOGENEOUS CONTRIBUTIONS: To solve Eq. (4.8) as an expansion of the type of Eq. (4.9), one needs to identify the radial scaling of the flux Λ in terms of the quantum numbers L and M of $T^{1,1}$. It is possible to classify the flux in 3 different series, I, II and III, regarding their different radial scaling [10]. The radial scaling of $|\Lambda|^2$ is given by [2]

$$\Delta(L_\alpha, L_\beta)_{\text{inhom bulk}} \equiv \Delta_\alpha(L_\alpha) + \Delta_\beta(L_\beta) - 4 \tag{4.11}$$

where α and β run over the 3 different series I, II and III and

$$\Delta_I(L) \equiv -1 + \sqrt{6l_1(l_1+1) + 6l_2(l_2+1) - 3R/4 + 4}, \tag{4.12}$$

$$\Delta_{II}(L) \equiv \sqrt{6l_1(l_1+1) + 6l_2(l_2+1) - 3R/4 + 4}, \tag{4.13}$$

$$\Delta_{III}(L) \equiv 1 + \sqrt{6l_1(l_1+1) + 6l_2(l_2+1) - 3R/4 + 4}. \tag{4.14}$$

It is then possible to write the inhomogeneous contributions as:

$$V_{\text{inhom bulk}}(x,\Psi) = \mu^4 \sum_{L_\alpha M_\alpha, L_\beta M_\beta} C_{L_\alpha M_\alpha L_\beta M_\beta} x^{\Delta(L_\alpha, L_\beta)} Y_{L_\alpha M_\alpha}(\Psi) Y_{L_\beta M_\beta}(\Psi). \tag{4.15}$$

To write this expression with the same structure as Eq. (4.9), the angular part needs to be expanded in terms of Y_{LM} of $T^{1,1}$ as

$$Y_{L_\alpha M_\alpha}(\Psi) Y_{L_\beta M_\beta}(\Psi) = \sum_{LM} A_{\alpha\beta} Y_{LM}(\Psi) \tag{4.16}$$

such that finally,

$$V_{\text{inhom bulk}}(x,\Psi) = \mu^4 \sum_{L_\alpha, L_\beta} \sum_{LM} C_{LM} x^{\Delta(L_\alpha, L_\beta)} A_{\alpha\beta} Y_{LM}(\Psi). \tag{4.17}$$

The constants C_{LM} correspond to the random parameters associated to each Y_{LM} from the homogeneous contribution, and, just as in that case, the maximum value desired for $\Delta(L_\alpha, L_\beta)$ determines the truncation of the summation.

[2] Some contractions of flux series vanish following the considerations of Ref. [10].

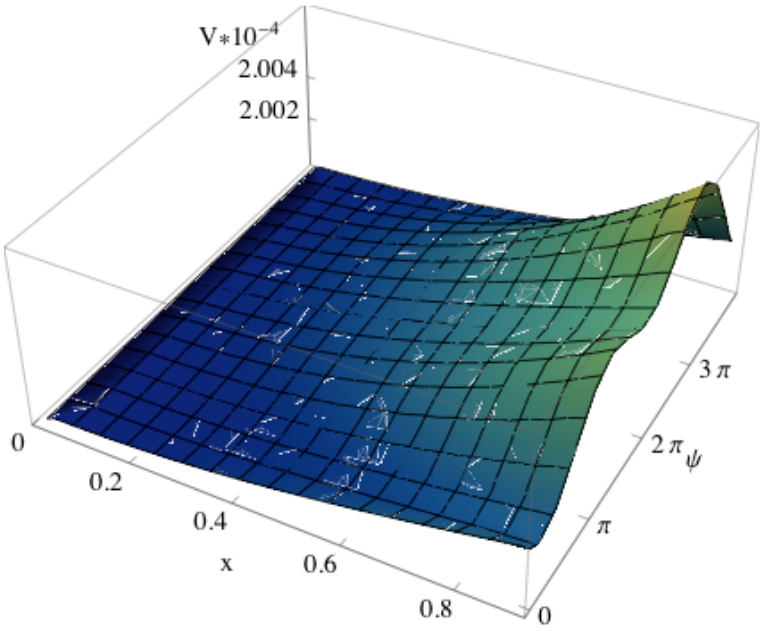

Figure 4.2: A typical realisation of the D-brane potential with only one angular direction, ψ, active.

The total potential experienced by the D-brane in the throat is then

$$\begin{aligned} V(x,\Psi) &= V_C + V_M + V_{\text{hom bulk}} + V_{\text{inhom bulk}} \\ &= D_0\left(1 - \frac{27D_0}{64\pi^2 T_3^2 r_{\text{UV}}^4}\frac{1}{x^4}\right) + \frac{1}{3}\mu^4 x^2 \\ &+ \mu^4 \sum_{LM} C_{LM} x^{\Delta(L)} Y_{LM}(\Psi) + \mu^4 \sum_{L_\alpha, L_\beta} \sum_{LM} C_{LM} x^{\Delta(L_\alpha, L_\beta)} A_{\alpha\beta} Y_{LM}(\Psi) \end{aligned} \tag{4.18}$$

A specific realisation of this potential, with only one angular direction being taken into account, is shown in Fig. 4.2.

4.3 Experimental procedure

Having established that the brane potential necessarily has a level of randomness to be able to encompass complex contributions, it is important to construct a useful sample of realisations for the study of the emergent inflationary behaviour.

The first thing to specify is the maximum values of $\Delta(L)$ and $\Delta(L_\alpha, L_\beta)$ in the potential. Since the mass term has power $\propto x^2$, it makes sense to include at least all terms with $\Delta \leq 2$. For computational reasons, and in accordance with Ref. [4], we looked at potentials with $\Delta \leq 3$ and with $\Delta \leq \sqrt{28} - 3/2$. This corresponds to a total of 121 and 390 independent

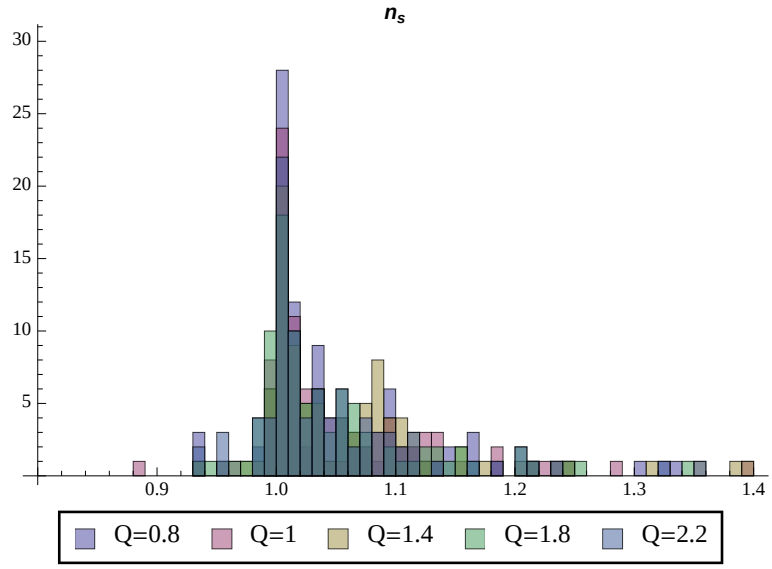

Figure 4.3: Distributions for the scalar spectral index for the model with 2 active fields. The distributions were taken with different values of Q and show very similar behaviours ($\Delta_{\rm MAX} = 3$ in all distributions).

terms in the potential, respectively.[3] The values taken by Δ are: $1, 3/2, 2, 5/2, \sqrt{28} - 5/2, 3, \sqrt{28} - 2, 7/2, \sqrt{28} - 3/2$.

The second thing to decide is how to generate the random C_{LM} coefficients. Following Ref. [4], we define $C_{LM} \equiv Q\hat{C}_{LM}$ such that $\hat{C}_{LM}$ is a distribution with unit variance, encapsulating the information on the distribution, and Q is the root mean square size of C_{LM}, encapsulating the information on its magnitude.

Drawing conclusion on the predictions of the model would be problematic if the inflationary behaviour emerging from our sample was dependent on the type of distribution of $\hat{C}_{LM}$. Fortunately, as shown in Ref. [4], this is not the case. In this work, we use a Gaussian distributed $\hat{C}_{LM}$.

Regarding the choice of Q, a similar argument could be invoked. As mentioned in the previous section $Q \sim \mathcal{O}(1)$, but the probability of inflation is very sensitive to its precise value [4]. If the emergent behaviour, given that inflation occurs, was also sensitive to this choice of Q, it would be hard to make general predictions. To ensure that no issue would arise from this effect, we tested the dependence of the inflationary phenomenology on the choice of Q and found it to be independent. This is demonstrated in Fig. 4.3, where, as an illustrative example, the distribution of the spectral index for a two-field sample is plotted for five different values of Q.

The last thing to fix before constructing the sample is the choice of initial conditions, for

[3] Note that these numbers differ slightly from those of Ref. [4]. The origin of this discrepancy lies in details of the expansions performed on $V_{\rm bulk}$.

which we follow Ref. [4] precisely. Since the potential is statistically invariant under angular translation in $T^{1,1}$, generating multiple realisations starting always at the same angular coordinate automatically encompasses the statistical effect of varying initial conditions within a single realization. We hence consider just one initial condition per realization, arbitrarily taken as the angular coordinates being $\Psi_0 = \{1, 1, 1, 1, 1\}$. Regarding the initial radial direction, and following arguments from Ref. [4], we chose $x_0 = 0.9$. We set all the initial velocities to zero, $\dot{x}_0 = \dot{\Psi}_0 = 0$, leaving the study of the possible impact of initial velocities on inflationary phenomenology for future work.

We can now present our experimental procedure for the building of a statistical sample of inflationary trajectories. This procedure was first used in Ref. [13] and more recently in Refs. [4, 14, 15]:

1. Generate a random potential $V(x, \Psi)$ starting at $(x_0, \Psi_0) = (0.9, 1, 1, 1, 1, 1)$ and evolve to find the field trajectory.

2. If the model gets stuck in eternal inflation, *i.e.* does not reach $x = 0.02$, reject.

3. If the brane gets ejected from the throat, *i.e.* x gets larger than 1, reject.

4. Once the brane has reached $x = 0.02$, if the number of e-folds of inflation $N < 60$, reject, as insufficient inflation occurred, otherwise calculate observables.

5. Repeat steps 1-4 many times to obtain a statistical sample.

Several sets of samples were generated by changing some parameter, either $\Delta_{\rm MAX}$, Q or the number of active fields. When mentioning two-field samples, we are referring to a model with the radial direction and one angular direction active. When we discuss more active fields, we are referring to models with additional angular directions.

The probability of achieving successful inflation in this set-up is in agreement with Ref. [4]. If Q is too small, most of the trajectories do not produce 60 e-folds of inflation; if Q is too large, most of the trajectories lead to an ejection of the brane. The optimum value of Q lies between these two regimes. As the number of active fields increases, just as when $\Delta_{\rm MAX}$ increases, $P(N > 60)$ becomes more sensitive to the choice of Q, and decreases slightly. Illustrative values are shown in Table 4.1. It is interesting to note that even for the optimum Q, more than half of the rejections are due to the brane being ejected from the throat, in agreement with Ref. [4].

Regarding the value of $\Delta_{\rm MAX}$, we noticed that the inflationary phenomenology does not depend strongly on the chosen value. An illustrative example is shown in Fig. 4.4, for

Fields	2	2	3	3	4	6
$\Delta_{\rm MAX}$	3	$\sqrt{28}-3/2$	3	$\sqrt{28}-3/2$	3	3
$P(N>60)$	3×10^{-4}	3×10^{-4}	2×10^{-4}	9×10^{-5}	6×10^{-5}	3×10^{-5}

Table 4.1: Probability of getting successful trajectories ($N > 60$) as a function of the number of active fields and $\Delta_{\rm MAX}$.

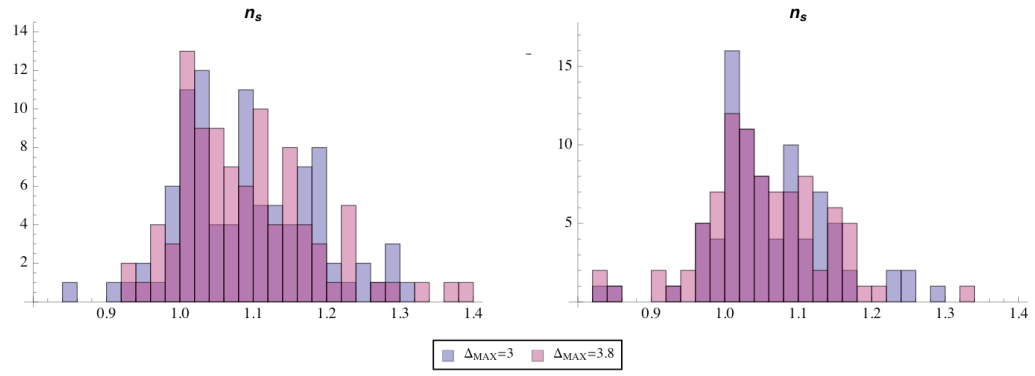

Figure 4.4: Distributions for the scalar spectral index for the model with 2 active fields, left, and 3 active fields, right. The distributions were taken with $\Delta_{\rm MAX} = 3$ and $\Delta_{\rm MAX} = \sqrt{28} - 3/2 \approx 3.8$ and show very similar behaviours (Q=1.4 in all distributions).

the spectral index of models with two and three fields. For this reason, in what follows, we concentrate on distributions with $\Delta_{\rm MAX} = 3$.

In the next section, we present the techniques used for the computation of observables.

4.4 Computing the curvature perturbation

A central feature of any model of inflation with more than one active scalar field is that the primordial curvature perturbation ζ evolves on superhorizon scales. To compute this, almost all methods in the literature to date make use of some variant of the separate universe assumption [16–18]. The idea is to understand the final curvature perturbation as the result of the scatter of a collection of equal size space-time patches, within which the field values at a given time are constant. Let us make this more precise.

4.4.1 The separate universe assumption is a geometrical optics approximation

The separate universe assumption states that, when smoothed on some physical scale L much larger than the horizon scale, the average evolution of each L-sized patch can be computed using the background equations of motion and initial conditions taken from smoothed quantities local to the patch. The evolution of ζ can be understood as the variation in the expansion of these patches. Since each smoothed patch corresponds to a position in phase space, the evolution of ζ can be determined by the evolution of an ensemble of points in the classical phase space. These points are subject to the laws of statistical physics and hence evolve according to the Liouville equation.

Under the separate universe assumption, interactions between patches are negligible and therefore all that is required is a mapping of the initial conditions to a final state. The final distribution in phase space can then be viewed as an *image* of the initial conditions. This mapping simply follows a flow generated by the background theory and can be calculated in precisely the same way as geometrical optics enables us to calculate the image generated by a source of light rays. This optical description was made precise in Ref. [19], which we briefly summarise in this section, referring the reader to Ref. [19] for a more detailed discussion.

4.4.2 Transport equations

Since slow-roll approximations are not valid in general, we are required to work in a $2N_{\rm F}$-phase space. This consists of $N_{\rm F}$ fields ϕ_i as well as their momenta $p_i \equiv \phi_i'$, where primes represent differentiation with respect to the number of e-folds N. The fields ϕ_i and p_i are treated on an equal footing, so from now on we will denote a point in phase space by $\varphi_\alpha \equiv \{\phi_i, p_i\}$ where α runs from 1 to $2N_{\rm F}$.

In canonical models of inflation, if we set initial conditions near horizon-crossing, the initial distribution of field perturbations will be close to Gaussian [20]. Furthermore, typical spacing between arbitrarily selected members of the ensemble is of order the quantum scatter. It follows that the trajectories traversed by the ensemble trace out a narrowly-collimated spray or 'bundle' of rays in phase space with an initial Gaussian distribution. This scenario is well studied in the optics literature since many lasers have this character-

istic.

Cross-sections within the bundle of trajectories may be focused, sheared or rotated by refraction. It is ultimately through these distortions that any evolution in ζ occurs. To describe these distortions quantitatively, it is only necessary to know how some basis which spans the cross-section is transported from slice to slice. Denoting the difference between two field values at equal-time positions $\mathbf{x}$ and $\mathbf{x}+\mathbf{r}$ by $\delta\varphi_\alpha(\mathbf{r})$, we have an appropriate basis. This basis evolves along the beam as [19]

$$\frac{d\delta\varphi_\alpha(\mathbf{r})}{dN} = u_{\alpha\beta}[\varphi(\mathbf{x})]\delta\varphi_\beta(\mathbf{r}) + \frac{1}{2}u_{\alpha\beta\gamma}[\varphi(\mathbf{x})]\delta\varphi_\beta(\mathbf{r})\delta\varphi_\gamma(\mathbf{r}) + \cdots . \tag{4.19}$$

where $u_{\alpha\beta} \equiv \partial_\beta u_\alpha$ is the expansion tensor defined as the derivative with respect to the fields of the background flow $u_\alpha[\varphi(\mathbf{x})] \equiv \varphi'_\alpha(\mathbf{x})$ and similarly $u_{\alpha\beta\gamma} \equiv \partial_\gamma u_{\alpha\beta}$. For clarity, we will drop the explicit $\varphi(\mathbf{x})$ dependence from now on.

The expansion tensor can be decomposed as a dilation $\theta = \operatorname{tr} u_{\alpha\beta}$, a traceless symmetric shear $\sigma_{\alpha\beta}$, and an antisymmetric twist $\omega_{\alpha\beta}$,

$$u_{\alpha\beta} \equiv \frac{\theta}{M}\delta_{\alpha\beta} + \sigma_{\alpha\beta} + \omega_{\alpha\beta}, \tag{4.20}$$

Dilation describes a rigid, isotropic rescaling of $\delta\varphi_\alpha$ by $1+\theta$, representing a global tendency of the light rays to focus or defocus. The shear σ_{ij} represents a tendency for some light rays within the beam to propagate faster than others. The twist $\omega_{\alpha\beta}$ describes a tendency of neighbouring trajectories to braid around each other.

The observables of interest, like the power spectrum of ζ, its spectral index n_s, the local non-Gaussianity parameter $f_{\rm NL}$, etc, are related to the correlators $\langle\zeta\zeta\rangle$ and $\langle\zeta\zeta\zeta\rangle$. So to compute the evolution of these quantities we need to know the evolution of the correlators of $\delta\varphi_\alpha$. The full set of basis vectors contains all information required to determine the evolution of the bundle, encoded in Eq.(4.19) by the u-tensors. To obtain transport equations for the correlation functions simply requires reorganisation of this information. As was shown in Refs [5, 6, 19] this can be done in a number of ways. A particularly quick method is to acknowledge that provided the perturbations can be treated classically, we expect $d\langle O\rangle/dN = \langle dO/dN\rangle$ for any quantity O. We can therefore immediately arrive at expressions for the two-point and three-point functions. Writing the two-point function as $\Sigma_{\alpha\beta} \equiv \langle\delta\varphi_\alpha\delta\varphi_\beta\rangle$, Eq. (4.19) implies

$$\frac{d\Sigma_{\alpha\beta}}{dN} = \left\langle \frac{d\delta\varphi_\alpha}{dN}\delta\varphi_\beta + \delta\varphi_\alpha\frac{d\delta\varphi_\beta}{dN} \right\rangle = u_{\alpha\gamma}\Sigma_{\gamma\beta} + u_{\beta\gamma}\Sigma_{\gamma\alpha} + [\geq 3 \text{ p.f.}] \tag{4.21}$$

Similarly, writing the three-point function as $\alpha_{\alpha\beta\gamma} \equiv \langle\delta\varphi_\alpha\delta\varphi_\beta\delta\varphi_\gamma\rangle$, we get

$$\frac{d\alpha_{\alpha\beta\gamma}}{dN} = u_{\alpha\lambda}\alpha_{\lambda\beta\gamma} + u_{\alpha\lambda\mu}\Sigma_{\lambda\beta}\Sigma_{\mu\gamma} + \text{cyclic } (\alpha\to\beta\to\gamma) + [\geq 4 \text{ p.f.}]. \tag{4.22}$$

This forms a coupled set of ordinary differential equations which can in principle be extended to any n-point correlation function (see Ref. [21] for an implementation of this technique for the trispectrum). In the context of this work we only care about the power spectrum and bispectrum of ζ, so this set of equations encodes all the information we need for the understanding of superhorizon evolution of our observables.

4.4.3 Gauge tranformations

Having seen how to compute the evolution of the field perturbations, now we need to relate these to the primordial curvature perturbation ζ. This can be done by realizing that the curvature perturbation ζ evaluated at some time $t = t_c$ is equivalent on large scales to the perturbation of the number of e-foldings $N(t_c, t_*, x)$ from an initial flat hypersurface at $t = t_*$, to a final uniform-density hypersurface at $t = t_c$ [22–25],

$$\zeta(t_c, x) \simeq \delta N(t_c, t_*, x) \equiv N(t_c, t_*, x) - N(t_c, t_*) \tag{4.23}$$

where $N(t_c, t_*) \equiv \int_*^c H dt$. In the transport method, the hypersurfaces at $t = t_*$ and $t = t_c$ are chosen to be infinitesimally separated. Expanding δN in terms of the initial field perturbations to second order, one obtains

$$\zeta(t_c, x) = \delta N(t_c, t_*, x) = N_{,\alpha}\, \delta\varphi_\alpha^* + \frac{1}{2} N_{,\alpha\beta}\, (\delta\varphi_\alpha^* \delta\varphi_\beta^* - \langle \delta\varphi_\alpha^* \delta\varphi_\beta^* \rangle), \tag{4.24}$$

where repeated indices should be summed over, and $N_{,\alpha}$, $N_{,\alpha\beta}$ represent first and second derivatives of the number of e-folds with respect to the fields φ_α^*.[4] The N derivatives are simply a gauge transformation from field perturbations to curvature perturbations. This gauge transformation only needs to be performed at the time of evaluation of ζ. The fact that it does not need to be transported through superhorizon evolution is a great numerical advantage of this technique.

It is straightforward to express the observables of interest at the time of evaluation within this formalism. The power spectrum is just related to the two-point correlation function of ζ and can be obtained by [5, 6]

$$P_{\zeta\zeta} = N_{,\alpha} N_{,\beta} \Sigma_{\alpha\beta}. \tag{4.25}$$

[4] The subtraction of the correlation function in the second term is due to the fact that this covariance matrix corresponds to the contribution from disconnected diagrams which gives the vacuum energy. In Fourier space one only considers connected diagrams from the outset and thus the subtraction is already implicitly taken care of.

To obtain initial conditions at horizon-crossing, we set all the fields to be effectively massless. We tested the consistency of this assumption and found it to be valid in every realisation.[5] The scalar spectral index, which expresses how the power spectrum changes with scale, is defined as

$$n_s - 1 \equiv \left.\frac{d\ln P_{\zeta\zeta}}{d\ln k}\right|_{k=k_*} \tag{4.26}$$

where k_* is the pivot scale. This can be rewritten as

$$n_s - 1 = \frac{N_{,\alpha}N_{,\beta}}{P_{\zeta\zeta}}\frac{d\Sigma_{\alpha\beta}}{d\ln k} = \frac{N_{,\alpha}N_{,\beta}n_{\alpha\beta}}{N_{,\lambda}N_{,\mu}\Sigma_{\lambda\mu}}, \tag{4.27}$$

where we have introduced the matrix $n_{\alpha\beta} \equiv d\Sigma_{\alpha\beta}/d\ln k$. Since the gauge-transformation factors $N_{,\alpha}$ and the expansion tensors $u_{\alpha\beta}$ are k-independent (they depend only on the typical trajectory followed by the smoothed fields at each time) we can understand how the spectral index evolves on superhorizon scales [26]. The only necessary ingredient is a transport equation for the object $n_{\alpha\beta}$ which is:

$$\frac{dn_{\alpha\beta}}{dN} = \frac{d}{d\ln k}\frac{d\Sigma_{\alpha\beta}}{dN} = u_{\alpha\lambda}n_{\lambda\beta} + u_{\beta\lambda}n_{\lambda\alpha}. \tag{4.28}$$

In this work, for the first time, we apply an equivalent method to evaluate the running of the spectral index, which estimates how n_s itself changes with scale. It is defined as

$$\left.\frac{d(n_s-1)}{d\ln k}\right|_{k=k_*} = \frac{d}{d\ln k}\left(\frac{N_{,\alpha}N_{,\beta}n_{\alpha\beta}}{P_{\zeta\zeta}}\right) = \frac{N_{,\alpha}N_{,\beta}r_{\alpha\beta}}{P_{\zeta\zeta}} - (n_s-1)^2 \tag{4.29}$$

where we have introduced the matrix $r_{\alpha\beta} \equiv dn_{\alpha\beta}/d\ln k$. Again, to have the evolution of the running, we just need to specify the transport equation for $r_{\alpha\beta}$ which is:

$$\frac{dr_{\alpha\beta}}{dN} = \frac{d}{d\ln k}\frac{dn_{\alpha\beta}}{dN} = u_{\alpha\lambda}r_{\lambda\beta} + u_{\beta\lambda}r_{\lambda\alpha}. \tag{4.30}$$

The horizon-crossing initial condition for this expression can be obtained by calculating the derivative with respect to $\ln k$ of the horizon-crossing value of $n_{\alpha\beta}$ given in Ref. [26].[6] This derivative is to be evaluated at equal times. To do so, we first compute how the $n_{\alpha\beta}$ associated to the pivot scale k_* changes with a variation in scale like $k_* + \delta\ln k$. This is

$$\left.\frac{dn_{\alpha\beta}}{d\ln k}\right|_{\rm h.c.} = (-2\epsilon'_{\rm h.c.}+4\epsilon^2_{\rm h.c.})\Sigma_{\alpha\beta}|_{\rm h.c.} - \left.\left(\frac{du_{\alpha\gamma}}{dN}\Sigma_{\gamma\beta} + \frac{du_{\beta\gamma}}{dN}\Sigma_{\gamma\alpha}\right)\right|_{\rm h.c.} + 2\epsilon_{\rm h.c.}(u_{\alpha\gamma}\Sigma_{\gamma\beta}+u_{\beta\gamma}\Sigma_{\gamma\alpha})|_{\rm h.c.} \tag{4.31}$$

where $\epsilon' = d\epsilon/dN$.

The k_* and $k_* + \delta\ln k$ modes cross the horizon at different times but we are looking for the change at *equal* times. When compared at the same time the longer mode experiences

[5] We would like to thank Sebastien Renaux-Petel for pointing out this possible issue.

[6] We would like to thank David Seery for discussions on this topic.

slightly more evolution. For this reason, we then need to include an extra contribution that corresponds to this $n_{\alpha\beta}$ displacement. Remembering that at horizon crossing $d\ln k \sim dN$, this is just $dn_{\alpha\beta}/dN$. The total expression is then

$$r_{\alpha\beta}|_{\rm h.c.} = (-2\epsilon'_{\rm h.c.} + 4\epsilon^2_{\rm h.c.})\Sigma_{\alpha\beta}|_{\rm h.c.} - \left(\frac{du_{\alpha\gamma}}{dN}\Sigma_{\gamma\beta} + \frac{du_{\beta\gamma}}{dN}\Sigma_{\gamma\alpha}\right)\Big|_{\rm h.c.} \\ +2\epsilon_{\rm h.c.}(u_{\alpha\gamma}\Sigma_{\gamma\beta} + u_{\beta\gamma}\Sigma_{\gamma\alpha})|_{\rm h.c.} - (u_{\alpha\gamma}n_{\gamma\beta} + u_{\beta\gamma}n_{\gamma\alpha})|_{\rm h.c.}. \tag{4.32}$$

The local non-gaussianity parameter $f_{\rm NL}$ is defined as [27–29]

$$f_{\rm NL} \equiv \frac{5}{18}\frac{B_{\zeta\zeta\zeta}}{(P_{\zeta\zeta})^2} \tag{4.33}$$

where $B_{\zeta\zeta\zeta}$ is the bispectrum of curvature perturbations, related to the three-point function of ζ. It is useful to decompose it as $B_{\zeta\zeta\zeta} = B_{\zeta\zeta\zeta 1} + B_{\zeta\zeta\zeta 2}$, where

$$B_{\zeta\zeta\zeta 1} = N_{,\alpha}\, N_{,\beta}\, N_{,\gamma}\, \alpha_{\alpha\beta\gamma}, \tag{4.34}$$

and

$$B_{\zeta\zeta\zeta 2} = \frac{3}{2} N_{,\alpha}\, N_{,\beta}\, N_{,\gamma\rho}\left[\Sigma_{\alpha\gamma}\Sigma_{\beta\rho} + \Sigma_{\alpha\rho}\Sigma_{\beta\gamma}\right]. \tag{4.35}$$

Eq. (4.34) is the intrinsic non-linearity among the fields, while Eq. (4.35) encodes the non-Gaussianity resulting from the gauge transformation to ζ [5, 6].

Given these expressions for the observables, it is now only necessary to specify the gauge transformation expressed by the N derivatives. Following the procedure developed in Ref. [7], the expansion of Eq. (5.3), can be understood in two steps. First, δN can be written as an expansion in terms of $\delta\rho$, where δ refers to a change from an initial flat hypersurface to a final uniform-density hypersurface:[7]

$$\delta N = \frac{dN}{d\rho}\delta\rho + \frac{1}{2}\frac{d^2N}{d\rho^2}\delta\rho^2 + \cdots, \tag{4.36}$$

where $\rho = 3H^2$. To obtain the derivatives of N as desired, one just needs to perturb each term of the above expansion in terms of the fields. The result is [7]

$$N_{,\phi_i} = \frac{V_{,i}}{2H^2\epsilon(3-\epsilon)}, \tag{4.37}$$

$$N_{,p_i} = \frac{VTp_i}{2H^2\epsilon(3-\epsilon)^2}, \tag{4.38}$$

$$N_{,\phi_i\phi_j} = \frac{V_{,ij}}{2H^2\epsilon(3-\epsilon)} - \frac{V_{,i}V_{,j}}{4H^4\epsilon^2(3-\epsilon)^2}\left(\frac{Tp_kp'^k}{\epsilon} + 2\epsilon\right), \tag{4.39}$$

[7] We particularly thank David Mulryne for this result and discussions around this topic.

$$N_{,p_i p_j} = \frac{T\delta_{ij}}{2\epsilon(3-\epsilon)} - \frac{T^2 p_i p_j}{4\epsilon^2(3-\epsilon)^2}\left(\frac{T p_k p'^k}{\epsilon} - 6\epsilon + 12\right), \tag{4.40}$$

$$N_{,\phi_i p_j} = -\frac{T V_i p_j}{4H^2\epsilon^2(3-\epsilon)^2}\left(\frac{T p_k p'^k}{\epsilon} - 2\epsilon + 6\right), \tag{4.41}$$

where the derivatives are taken explicitly with respect to ϕ_i and p_i rather than the combined φ_α, the objects $V_{,i}$ and $V_{,ij}$ refer to the derivatives of the potential with respect to the fields ϕ_i and ϕ_j and $p_i' = dp_i/dN = d^2\phi_i/d^2N$.

4.4.4 The adiabatic limit

This section has been dedicated to the understanding of superhorizon evolution of the curvature perturbations. What is yet to be addressed is at what point ζ ceases to evolve. This happens when the trajectory has effectively reached its adiabatic limit, *i.e.* the model has become effectively single-field (see Ref. [30–32] for early discussions on this topic).

One needs to ensure that the adiabatic limit is reached before the time of computation of observables, which generally is taken to be at the end of inflation. If isocurvature modes are still present at that point, the curvature perturbations will continue to evolve through an epoch of reheating, for which there is no precise knowledge. This would mean that the conclusions reached at the time of estimation would necessarily be incomplete, and the model not predictive.

In the D-brane case, the situation is even more delicate, since the validity of the approximations of the set-up breaks down as one approaches the tip of the conifold, or, for practical purposes, at $x = 0.02$. If ζ continues to evolve after that point, it will suffer changes due not only to reheating, but also an unknown background geometry and potential.

Formally, the approach to an adiabatic limit can be understood via the parameter $\theta = \mathrm{tr}\ u_{\alpha\beta}$ of Eq. (4.20) which describes the tendency for the bundle of trajectories to focus or dilate. The factor by which the bundle's cross-section has grown (or decayed) from its horizon-crossing value at N_0 to the time N is given by:

$$\Theta(N, N_0) \equiv \exp\left[\int_{N_0}^{N} \theta(n) dn\right]. \tag{4.42}$$

In a slow-roll two-field case, where the phase space is simply ϕ_i, when $\Theta \to 0$, or equivalently $\theta \to -\infty$, the trajectory is becoming effectively single-field [19]. However, since we are working with more than two fields and in a phase space composed by ϕ_i and p_i the situation is more subtle, and the relation not so direct [7, 19].

In the full phase space, it is instructive to understand how the bundles of ϕ_i and p_i individually behave. In particular, let us identify $p_i = p_i^{\rm SR}(\phi_i) + s_i$, where $p_i^{\rm SR}$ is the slow-roll attractor for the momenta p_i and a function of ϕ_i only and s_i are the momenta isocurvature modes. With these new variables, we can write [7]

$$\theta = \theta^{\rm SR}(\phi_i) + \theta^s(s_i) \tag{4.43}$$

where $\theta^{\rm SR}$ describes the dilation of the field bundle and θ^s describes the dilation of the s modes, *i.e.* how the momenta converge to their slow-roll attractor. We can also define $\Theta^{\rm SR}$ and Θ^s in analogy with Eq. (4.42).

The interpretation of when the adiabatic limit has been adequately reached from the above quantities is not straightforward [7], but to infer when it has not been is often simple. For the purpose of this work it will be sufficient to know that if $\Theta^{\rm SR} \gtrsim 1$ then an adiabatic limit certainly has not been reached.

4.5 Distributions for observables

We now present the results obtained from computing the curvature perturbations for different samples of inflationary trajectories. The outcomes are distributions for the values of the cosmological parameters presented in the previous section: amplitude $P_{\zeta\zeta}$, spectral index n_s and running of the spectral index of the scalar power spectrum, tensor-to-scalar ratio r, and local non-gaussianity parameter $f_{\rm NL}$. We compare these with constraints from observations; all constraint contours are 95% confidence limits using the WMAP 7 year data release combined with baryonic acoustic oscillations and supernov data [33–35]. We use as pivot the scale that crossed the horizon 55 e-folds before the end of inflation.

4.5.1 Field number dependence

Regarding the dependence of the inflationary behaviour on the number of active fields, we found that the effect of increasing the number of angular directions is negligible for the trajectories and consequent observables. Fig. 4.5 shows how the increase in angular directions changes the distributions of the tensor-to-scalar ratio and spectral index. We can identify a slight suppression in r as the number of active fields increases, as one would

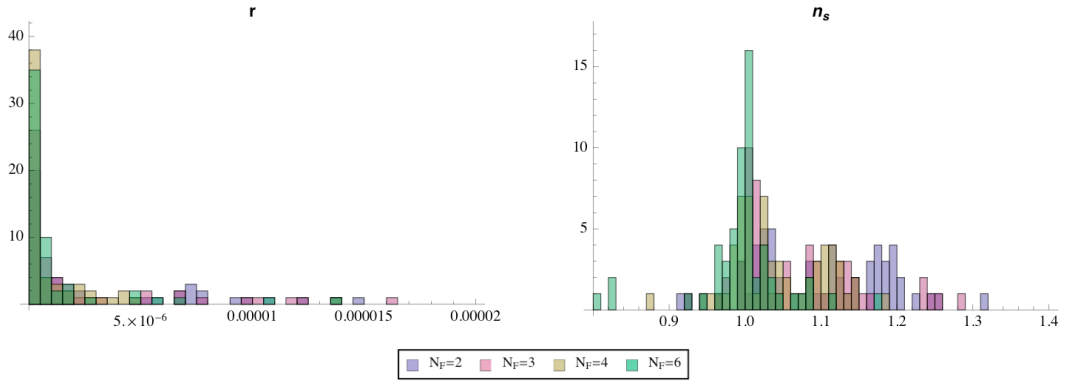

Figure 4.5: Distributions for the tensor-to-scalar ratio r, left, and scalar spectral index n_s, right. The distributions were taken for different numbers of active fields. It is possible to identify a small suppression in r and a tendency towards redder values of n_s (keeping the peak at $n_s = 1$) as $N_{\rm F}$ increases.

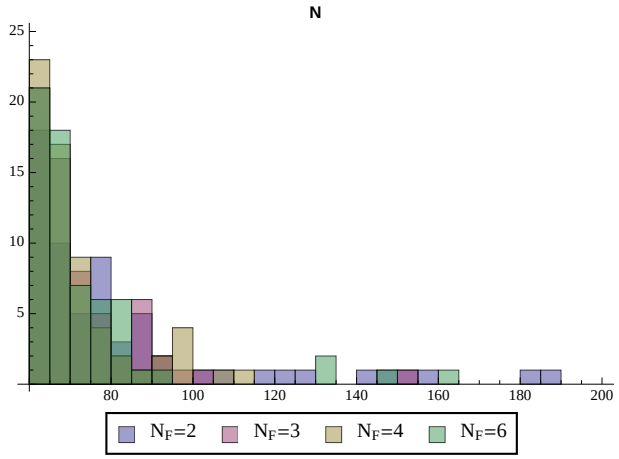

Figure 4.6: Number of e-folds of inflation for different number of active fields. We can see that this distribution is unchanged by varying $N_{\rm F}$.

expect since more directions allow for more turns in field space which fuel the scalar power spectrum. The spectral index, which consistently peaks at 1, gets a shift towards red values as the number of fields increases. This is not the consequence of a change in the inflationary trajectories and it can be readily understood, as will be shown shortly.

Interestingly, although an increase in the number of fields allows in principle a wider range of trajectories, we did not encounter any difference in the distribution for the total number of e-folds when varying $N_{\rm F}$, as can be seen in Fig. 4.6.

In the remainder of this paper, we will concentrate mainly on the results for two active fields for which our sample is constituted of 1086 inflationary trajectories, using the sample for the full six-field case, composed of 93 trajectories, for comparison.

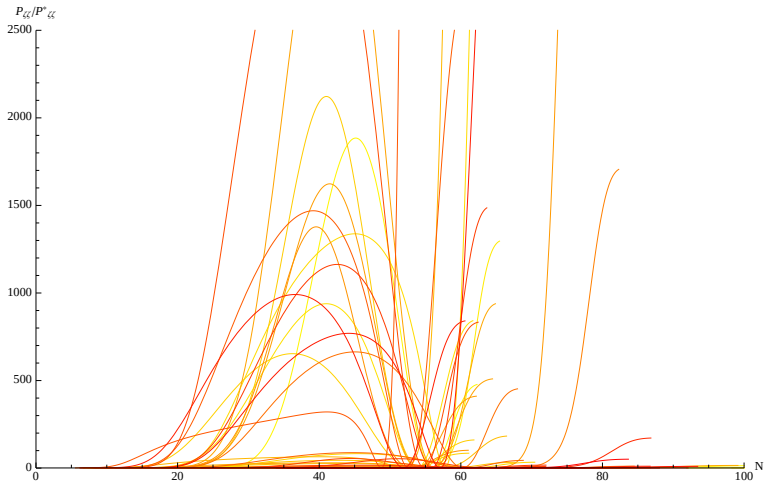

Figure 4.7: Superhorizon evolution of the amplitude of the scalar power spectrum $P_{\zeta\zeta}$ for 50 trajectories with 2 active fields, coloured at random. The evolutions show a consistent non-monotonic growth that we refer as 'caterpillar' shaped. It is impractical to show the full evolution of all the trajectories due to the large range in scales even for this reduced sample; for this reason the plot has been cut-off.

4.5.2 Observables

The amplitude of the power spectrum, as can be seen in Fig. 4.7, consistently undergoes a superhorizon evolution that we refer to as 'caterpillar' shaped, *i.e.* non-monotonic. This is interesting as this sort of evolution is very rare in purely random generated potentials [15] and so indicative of a dynamical trait common to all of our inflation realisations. The next section will explore its origin. As can be seen in Fig. 4.16, the histogram of $P_{\zeta\zeta}$ has a smooth maximum at around 10^{-9}, in agreement with observations (the WMAP value is $\sim 2.5 \times 10^{-9}$ [34]). This is not surprising as the overall magnitude of the potential is determined by the scale μ^4, which in turn is set by our choice of the throat length $r_{\rm UV}$. The important fact is that the distribution does not sharply peak at a precise value of $P_{\zeta\zeta}$, indicating that there is no fine-tuning issue around this parameter.

The spectral index shows a much clearer peak at $n_s = 1$, as seen in Fig. 4.16. Actually, the spread in n_s is not well approximated by a Gaussian; instead, two different populations can be identified, one with $n_s \geq 1$ and one with $n_s < 1$. For the two-field ensemble, these correspond to $\sim 84\%$ and $\sim 16\%$ of the trajectories, respectively. As seen previously, an increase in the number of active fields enhances the number of red trajectories; the respective ratios, for the six-field sample are then $\sim 50\%$ each. In the next section we will address the dynamical characteristics of these two populations and the changes with the number of fields.

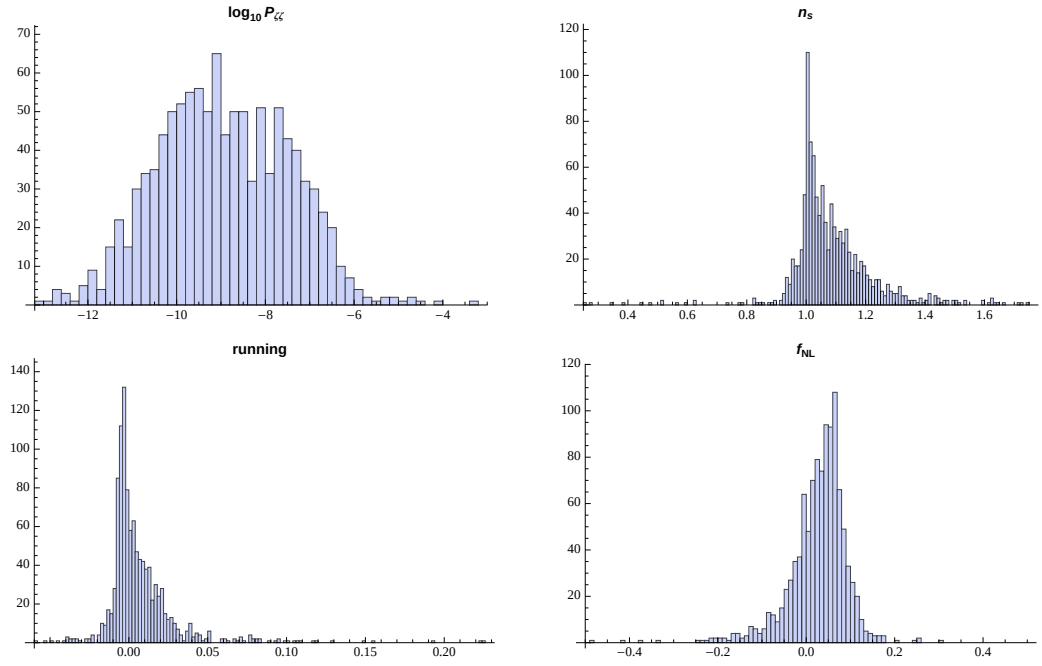

Figure 4.8: Distributions for the amplitude of the power spectrum $P_{\zeta\zeta}$, top left, scalar spectral index n_s, top right, running of the spectral index, bottom left, and local non-gaussianity parameter $f_{\rm NL}$, bottom right. All distributions were taken for the sample with 2 active fields.

A very interesting result comes from the computation of the running of the spectral index. Fig. 4.16 shows that the running tends to be positive and that it can take large values. This outcome, as will be discussed shortly, is extremely constraining. One could think that, since the running can take large values, the value of the spectral index changes a lot with the choice of pivot scale. Our approach is to think that sampling over a large number of inflationary potentials reproduces the effect of sampling over different choices of pivot scales, such that the final distributions for different pivot scales are actually identical. We tested this assumption and found it to be the case.

The tensor-to-scalar ratio is always extremely small, as it is related to the slow-roll parameter ϵ that remains $\ll 1$ throughout the calculation. This can be clearly seen in Fig. 4.9. Furthermore, the usual single-field result for the brane case would be the relation

$$r = 16\frac{\epsilon}{T_3} \tag{4.44}$$

which corresponds to the green line. We can see how multifield effects change this result, by weakening this expression to an inequality.

The local non-gaussianity parameter $f_{\rm NL}$, as can be seen in Fig. 4.16, is almost always too small to possibly be detected by any anticipated observation. In the full two-field ensemble only five trajectories yielded values of $|f_{\rm NL}| > 1$. Although these are highly

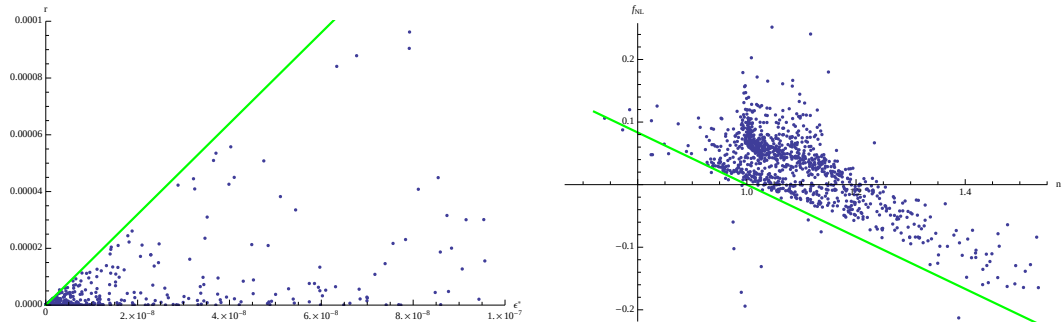

Figure 4.9: Plot of the values of ϵ at horizon-crossing versus r, left, and n_s versus $f_{\rm NL}$, right, for the sample with 2 active fields. The green lines represent the single-field predictions, $r = 16\epsilon/T_3$ and $f_{\rm NL} = -5(n_s - 1)/12$, respectively.

unlikely, any case presenting interesting observational signatures can be informative in its own right; we leave a detailed analysis of these cases for future work. When plotted against n_s, this parameter also shows the deviation from the single-field prediction $f_{\rm NL} = -5(n_s - 1)/12$ [36] represented by the green line in Fig. 4.9. Once again, multifield effects break this degeneracy.

4.5.3 Constraints from WMAP

We now impose the observational constraints on the distributions.

As can be seen in Fig. 4.17, the majority of the trajectories gives rise to values of running and spectral index that lie outside the observational bounds. From the running versus n_s plot alone, one could think that the trajectories giving rise to the peak around $n_s = 1$ would be in agreement with observations. Actually, a stronger constraint for n_s is imposed by the fact that the model predicts a negligible tensor-to-scalar ratio. Constraints on the n_s versus r plot shown in Fig. 4.17 exclude all the trajectories which result in $n_s > 0.995$. These constraints alone result in only $\sim 10\%$ of the total two-field sample, and $\sim 50\%$ of the six-field sample, of trajectories being in agreement with observations.

A further constraint is imposed by requiring the correct amplitude of the scalar power spectrum, $(2.5\pm0.1)\times10^{-9}$ [34]. Combining all constraints we obtained only two realisations in total concordance with observations in the full sample of 1086 cases of two-field inflation, and one realisation in the sample of 93 cases of six-field inflation. As discussed in the previous subsection, this is not a worrying result as the distribution of $P_{\zeta\zeta}$ does not show a sharp peak.

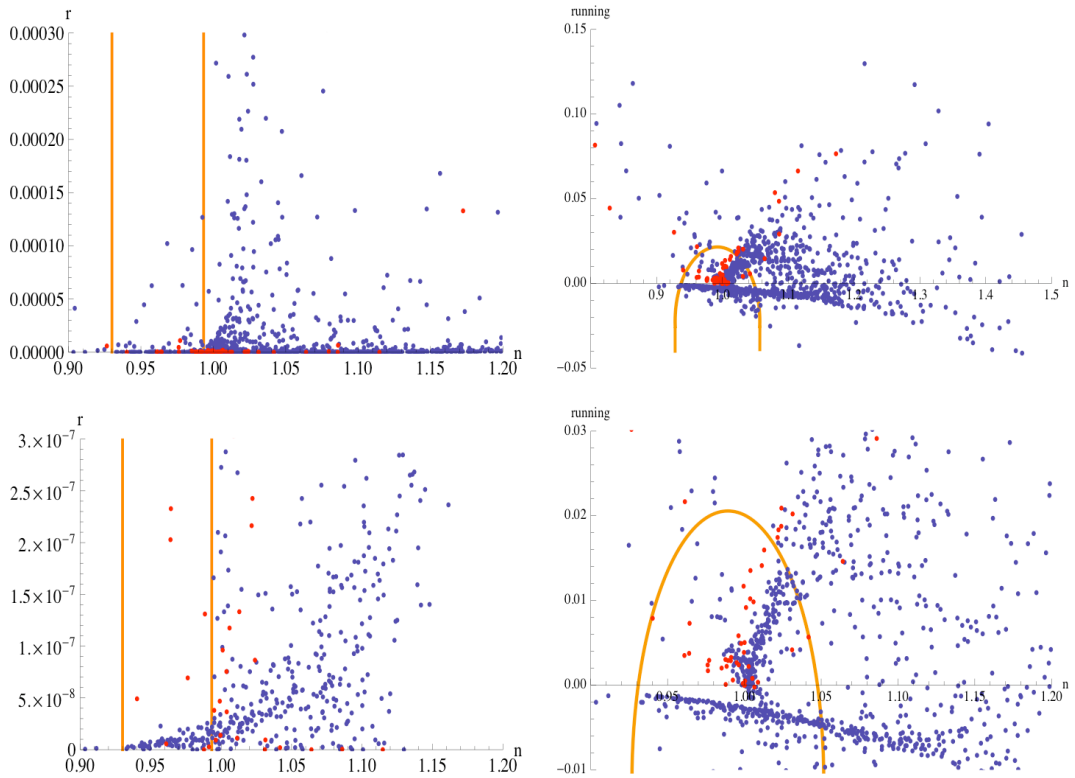

Figure 4.10: Plot of the values of n_s versus r, left, and n_s versus running, right, for the model with 2 active fields, blue points, and 6 active fields, red points. The lower panels greatly expand the vertical scales. The orange lines represent the 95% confidence limits using WMAP data. When running is allowed to be $\neq 0$ it is important to know what is the best scale with which to make comparisons with observations. In Ref. [35] this issue was explored; following their conclusions, we look at the constraints for $k^* = 0.017\,\mathrm{Mpc}^{-1}$ which is not the same choice made in Ref. [34].

4.6 A CLOSE LOOK AT TRAJECTORIES

In this section we describe in detail the dynamics of individual trajectories and how they give rise to the distributions seen in the previous section.

A remarkable feature of this model is that all inflationary trajectories encountered were essentially of the same type, inflection-point inflation with a wiggle in the trajectory. It turns out that while in principle inflation could occur at any location within the throat (above the tip), at least the last 60 e-folds of inflation always occur in a small sub-region (typically $0.02 < x < 0.09$) in the vicinity of the inflection point discussed in §§4.2.2. While the inflection-point contribution to the potential, $V_C + V_M$, alone could not give enough inflation, the contributions from the bulk can alter the potential in such a way that sufficient inflation *can* occur. The range of contributions capable of giving inflation is limited so in practice the result is a very consistent dynamical behaviour.

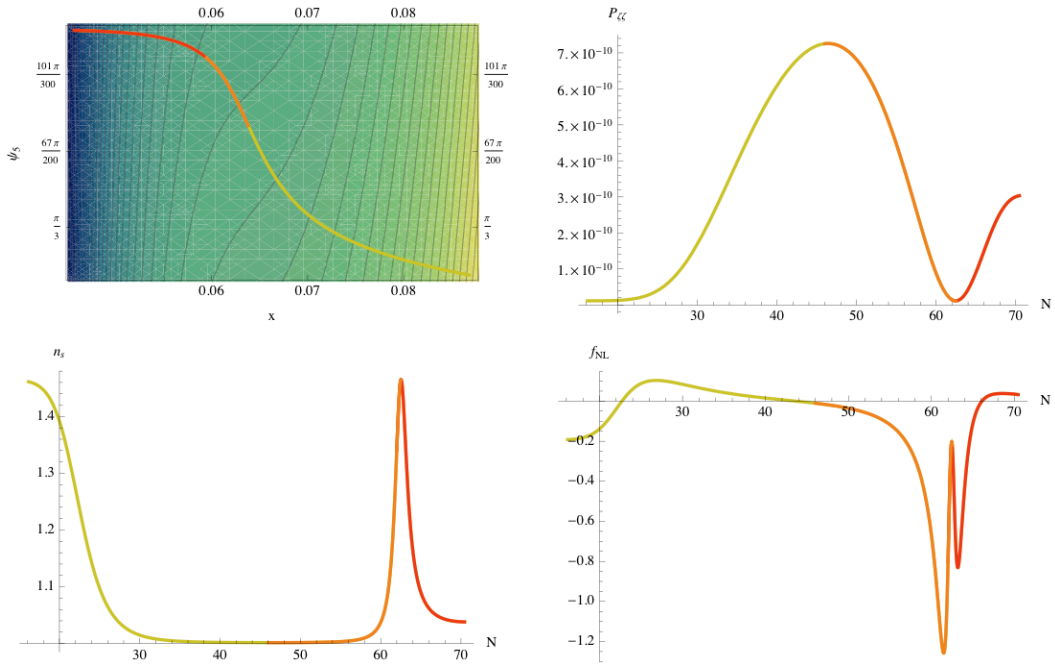

Figure 4.11: The dynamical behaviour of Verse 20277, for the region of the trajectory where inflation occurred. The top left plot shows the trajectory in field space plotted on top of the potential contours. The evolution of the amplitude of the power spectrum, top right, spectral index, bottom left, and running, bottom right, show different colours regarding the position in the potential; yellow represents evolution before the inflection point, orange between the inflection point and the fall of the ledge and red after the starting falling off the ledge. For the region represented in red, $|\eta| > 1$.

4.6.1 One inflationary trajectory to explain them all

A typical inflationary realisation in our $N_{\rm F} = 2$ set-up is the affectionately-named Verse 20277. Fig. 4.18 shows the inflationary trajectory superimposed on a contour plot of the potential, together with the evolution of the observable quantities we investigated. The trajectory evolves from right to left, passing an inflection point in the radial direction but also experiencing a slope in the angular direction, causing a wiggle in what would otherwise be standard single-field inflection-point inflation (see for example Ref. [37]). As will be shown, this behaviour explains the non-monotonic evolution of $P_{\zeta\zeta}$, which we saw to be so common. Verse 20277, as $\sim 84\%$ of our realisations, has a blue spectral index, $n_s > 1$, which can also be understood by its inflationary dynamics. It also presents the most common evolution of $f_{\rm NL}$ we encountered, giving rise to an unobservably small value of $f_{\rm NL}$, as seen consistently across our distributions.

Another interesting characteristic of the dynamics of Verse 20277, which again is representative of the whole sample, is that the process of falling off the ledge after the inflection point gives rise to a prolonged period of non-slow-roll inflation, often leading to $\mathcal{O}(10)$

e-folds. This regime is shown in red in Fig. 4.18. While the slow-roll parameter ϵ remains much smaller than 1 throughout all the analysis, the parameter $|\eta|$ increases significantly, getting to values of ~ 35. The consequences of this effect will be discussed in what follows.

4.6.2 A separable potential approximation

A simple explanation for all of the above evolutionary traits presents itself if we approximate the inflationary region as a separable potential of the type.[8]

$$W(\phi) \equiv W(x, \Psi) = U(x) + \sum_{i=2}^{N_{\rm F}} V_i(\Psi_i) \tag{4.45}$$

where $U(x)$ possesses an inflection point in the radial direction

$$U(x) \equiv V_1(\phi_1) = \alpha_0 + \alpha_1(x - x_0) + \alpha_3(x - x_0)^3 \tag{4.46}$$

and $V(\Psi)$ are slopes in the angular directions

$$V_i(\Psi_i) = \beta_i \Psi_i. \tag{4.47}$$

As already mentioned, for the majority of inflation, the evolution sits well within the slow-roll regime. During this period, we can write the number of e-folds of inflation as

$$N(t_c, t_*) = -T_3 \int_*^c \sum_{i=1}^{N_{\rm F}} \frac{V_i}{V_{,i}} d\phi_i. \tag{4.48}$$

For this section we take the flat surface to be at horizon-crossing and the constant density surface to be at our time of evaluation. This allows us to write down the total derivative as

$$dN = T_3 \sum_{j=1}^{N_{\rm F}} \left[\left(\frac{V_j}{V_{,j}} \right) - \sum_{i=1}^{N_{\rm F}} \frac{\partial \phi_i^c}{\partial \phi_j^*} \left(\frac{V_i}{V_{,i}} \right) \right] d\phi_j^*. \tag{4.49}$$

Following the procedure in Ref. [39, 40] one can obtain an expression for the partial derivative in the previous expression as

$$\frac{\partial \phi_i^c}{\partial \phi_j^*} = -\frac{W_c}{W_*} \sqrt{\frac{\epsilon_i^c}{\epsilon_j^*}} \left(\frac{\epsilon_j^c}{\epsilon^c} - \delta_{ij} \right) \tag{4.50}$$

where the slow-roll parameters associated with each field are defined as

$$\epsilon_i \equiv \frac{1}{2T_3} \left(\frac{V_{,i}}{W} \right)^2, \quad \eta_i \equiv \frac{1}{T_3} \frac{V_{,ii}}{W}, \quad \xi_i \equiv \frac{V_{,i} V_{,iii}}{T_3^2 W^2} \tag{4.51}$$

[8] Approximating small regions of potentials as separable is a very useful technique which can be applied quite generally. See Ref. [38] for another recent and rather nice example of this.

such that $\epsilon = \sum \epsilon_i$. Finally, we arrive at an expression for the derivatives of N

$$\frac{\partial N}{\partial \phi_i^*} = \sqrt{\frac{T_3}{2\epsilon_i^*}} \frac{V_i^* + Z_i}{W^*}, \tag{4.52}$$

where we have the, rather important for the following discussion, term

$$Z_i \equiv \frac{1}{\epsilon^c} \sum_{j=1}^{N_{\rm F}} V_j^c (\epsilon_i^c - \epsilon^c \delta_{ij}) \tag{4.53}$$

which contains all the information about the constant density surface at the time of evaluation. All other terms are determined by horizon-crossing values. Note that due to assuming slow-roll, we have reduced our phase space to the $N_{\rm F}$ fields ϕ_i and that by approximating the potential as sum-separable, this expression no longer requires the 'c' and '*' surfaces to be infinitesimally separated.

The second derivatives are given by [39, 40]

$$\frac{\partial^2 N}{\partial \phi_i^* \partial \phi_j^*} = \delta_{ij} T_3 \left(1 - \frac{\eta_j^*}{2\epsilon^*} \frac{V_j^* + Z_j}{W_*}\right) + \frac{1}{W_*} \sqrt{\frac{T_3}{2\epsilon_j^*}} \frac{\partial Z_j}{\partial \phi_i^*}. \tag{4.54}$$

Having obtained expressions for the first and second derivatives of N, it is now possible to write down analytical expressions for the desired observable quantities. This is done by using the expressions from §§4.4.3 and using the horizon-crossing values for the correlation functions of $\delta\phi$. The amplitude of the power spectrum is given by

$$P_{\zeta\zeta} = \frac{T_3 W_*}{24\pi^2} \sum_{i=1}^{N_{\rm F}} \frac{u_i^2}{\epsilon_i^*} \tag{4.55}$$

where

$$u_i \equiv \frac{V_i^* + Z_i}{W_*}. \tag{4.56}$$

The spectral index is given by [9]

$$n_s - 1 = -2\epsilon_* - 4 \frac{\left(1 - \sum_{i=1}^{N_{\rm F}} \frac{\eta_i^* u_i^2}{2\epsilon_i^*}\right)}{\sum_{i=1}^{N_{\rm F}} \frac{u_i^2}{\epsilon_i^*}} \tag{4.57}$$

Differentiating with respect to $\ln k$ we also obtain a new expression for the running. We find it to be

$$n' = -8\epsilon^{*2} + 4 \sum_{i=1}^{N_{\rm F}} \epsilon_i^* \eta_i^* - 16 \frac{\left(1 - \sum_i \frac{\eta_i^* u_i^2}{2\epsilon_i^*}\right)^2}{\left(\sum_i \frac{u_i^2}{\epsilon_i^*}\right)^2} - 8 \frac{\sum_i \eta_i^* u_i \left(1 - \frac{\eta_i^* u_i}{2\epsilon_i^*}\right)}{\sum_i \frac{u_i^2}{\epsilon_i^*}} + 4\epsilon^* \frac{\sum_i \frac{\eta_i^* u_i^2}{\epsilon_i^*}}{\sum_i \frac{u_i^2}{\epsilon_i^*}} - 2 \frac{\sum_i \frac{\xi_i^* u_i^2}{\epsilon_i^*}}{\sum_i \frac{u_i^2}{\epsilon_i^*}} \tag{4.58}$$

[9] Here we have used the fact that $d/d\ln k \approx d/dN = (\phi_i/H)\partial/\partial\phi_i$ and continually made use of the substitutions $N_{,i}V_{,i} = -VT_3$ and $\dot{\phi}_i N_{,ij}/H = V_{,j}/V + V_{,ij}N_{,i}/VT_3$.

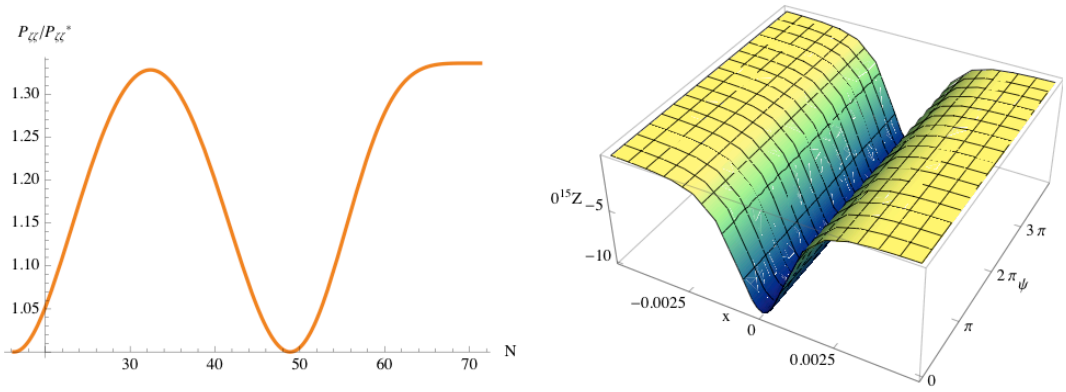

Figure 4.12: Example of evolution of the power spectrum $P_{\zeta\zeta}$ and the form of Z_i giving rise to it for the separable potential. The power spectrum appears to stop evolving in the last few e-folds despite the bundle dilating in this region.

Finally, the local non-Gaussianity is

$$-\frac{5}{6}f_{\rm NL} = 2\frac{\sum_{i=1}^{N_{\rm F}}\frac{u_i^2}{\epsilon_i^*}\left(1-\frac{\eta_i^*}{2\epsilon_i^*}\right)+\sum_{i,j=1}^{N_{\rm F}}\frac{u_iu_j}{\epsilon_i^*\epsilon_j^*}A_{ji}}{\left(\sum_{i=1}^{N_{\rm F}}\frac{u_i^2}{\epsilon_i^*}\right)^2}, \tag{4.59}$$

where as a result of differentiating Z_i, another term A_{ji} containing contributions from the 'c' surface is required [39, 40];

$$\begin{aligned}\frac{\partial Z_j^c}{\partial\phi_i^*} &= -\frac{W_c^2}{W_*}\sqrt{\frac{2}{\epsilon_i^*}}\left[\sum_{k=1}^{N_{\rm F}}\epsilon_k\left(\frac{\epsilon_j}{\epsilon}-\delta_{jk}\right)\left(\frac{\epsilon_i}{\epsilon}-\delta_{ik}\right)\left(1-\frac{\eta_k}{\epsilon}\right)\right]_c \\ &\equiv \sqrt{\frac{2}{\epsilon_i^*}}W_*\mathcal{A}_{ji}\,.\end{aligned} \tag{4.60}$$

All of the above expressions can be shown to reduce to the standard single-field formula by setting $u_i = 1$.

With these expressions from the separable potential approximation, the phenomenology described at the beginning of this section becomes clear. We now discuss each of the trends encountered in the results individually.

4.6.3 WHY SO MANY CATERPILLARS?

First, we would like to address the question of why non-monotonic evolution in the amplitude of the power spectrum is so common.

Under the separable approximation, all superhorizon behaviour is encapsulated in the Z_i terms. This must go to zero in the adiabatic limit since, as there is no evolution in this

limit, the result must be independent of our choice of the time of evaluation. However this is not a sufficient condition for reaching the adiabatic limit; as we will see, it is possible for Z_i to become negligible towards the end of inflation even when an adiabatic limit has not been reached. Before this limit is reached, Z_i demonstrates significant variation. The extent to which Z_i varies over the course of the last 55 e-folds of inflation changes between inflationary realisations according to both the realisation of the random coefficients and the path the inflationary trajectory takes in field space, but an example of the form of the variation is given in Fig. 4.12, where the fields have been redefined such that the inflection point is at the origin.

As the trajectory crosses the inflection point, Z_i has a trough, then increases to zero as the trajectory leaves the plateau. As can be seen in Eq. (4.55), a peaking in $|Z_i|$ corresponds to a peak in $P_{\zeta\zeta}$, though the precise shape will also depend on the angular component which determines for how long the trajectory stays on the corresponding ridge in Z_i. The peak in $|Z_i|$ occurs due to ϵ^c in the denominator of Eq. (5.8) reaching a minimum value and as such non-monotonic evolution is an inevitable consequence of the inflationary trajectory crossing an inflection point. The form of Z_i also accounts for the final rise (the caterpillar's head) in the evolution of $P_{\zeta\zeta}$ since Z_i turns up as a sum of quadratic terms in Eq. (4.55). This stage of the evolution is non-slow-roll but when comparing the evolution as given by Z_i with our non-slow-roll transport code we found them to be in good agreement.

4.6.4 Why so blue?

Recognising that all inflationary trajectories take place in the vicinity of an inflection point also tells us about the spectral index. Remembering that $Z_i \to 0$ towards the end of inflation, Eq. (5.9) states that the final value of the spectral index (along with the other observables we discuss) will be determined purely in terms of horizon-crossing values. This is what is often referred to as 'the horizon-crossing approximation' [41]. Unless very close to the inflection point, η_x dominates Eq. (5.9). When horizon-crossing takes place prior to the inflection point, $\eta_x > 0$, the horizon-crossing approximation says that n_s will necessarily be larger than 1. However if the situation arises where horizon-crossing takes place after the inflection point, $\eta_x < 0$ and a red spectral index can be expected. This is what we find to be the case for approximately 16% of our trajectories (for $N_{\rm F} = 2$). The reason they are so rare is that 60 e-folds of inflation still need to take place and this is difficult to achieve

before falling off the ledge. It turns out that for the red cases, the total number of e-folds was always at least $\mathcal{O}(100)$.

Fig. 4.5 shows a sensitivity to the number of fields $N_{\rm F}$, where additional angular terms appear to act to redden the spectral index. This is not due to a larger proportion of trajectories with horizon-crossing occurring after the inflection point. If this was the case then there would also be an increase in the number of e-folds. Instead, the increased redness seems to be a direct result of the geometry of the conifold and can be accounted for by the separable approximation. Writing Eq. (5.9) in a more suggestive form

$$n_{\rm s} - 1 = -2\sum_{i=1}^{N_{\rm F}} \epsilon_i^* - \frac{4}{\sum_{i=1}^{N_{\rm F}} \frac{u_i^2}{\epsilon_i^*}} + 2\frac{\frac{\eta_x^*}{\epsilon_x^*}u_x^2}{\sum_{i=1}^{N_{\rm F}} \frac{u_i^2}{\epsilon_i^*}}, \tag{4.61}$$

it is clear that additional angular terms act solely to redden the spectral index by suppressing the contribution from η_x as well as increasing ϵ.

4.6.5 Trends in the running

Fig. 4.17 shows a lower bound in the plot of the running against the spectral index. This bound turns out to be parabolic and approximately proportional to $-(n_s-1)^2$, suggesting that there could be a dominant term in η_x^2 among the contributions for the running. Interestingly, in the single-field case, terms in η^2 do not contribute to the running, $n' = -24\epsilon^2 + 16\epsilon\eta - 2\xi$. However, as can be seen by following Eq. (4.58), in the multifield case the situation changes. The terms from Eq. (4.58) in η_x^2 are:

$$n' \supset -4\left(\frac{\sum_i \frac{\eta_i^* u_i^2}{\epsilon_i^*}}{\sum_i \frac{u_i^2}{\epsilon_i^*}}\right)^2 + 4\frac{\sum_i \frac{\eta_i^{*2} u_i^2}{\epsilon_i^*}}{\sum_i \frac{u_i^2}{\epsilon_i^*}} = -4\frac{\frac{\eta_x^{*2}u_x^4}{\epsilon_x^{*2}}}{\left(\sum_i \frac{u_i^2}{\epsilon_i^*}\right)^2} + 4\frac{\frac{\eta_x^{*2}u_x^2}{\epsilon_x^*}\sum_j \frac{u_j^2}{\epsilon_j^*}}{\left(\sum_i \frac{u_i^2}{\epsilon_i^*}\right)^2}, \tag{4.62}$$

which means that there is a residual η_x^2 cross term which dominates the expression. The parabolic lower bound is therefore intrinsically multifield.

4.6.6 Evolution in $f_{\rm NL}$

The separable approximation fares less well in reproducing the behaviour seen for $f_{\rm NL}$. The radial acceleration parameter η_x is the dominant contribution to Eq. (4.59), so the horizon-crossing approximation gives $f_{\rm NL} < 0$ for horizon-crossing prior to the inflection point and $f_{\rm NL} > 0$ for post inflection-point horizon-crossing. Bringing this together with

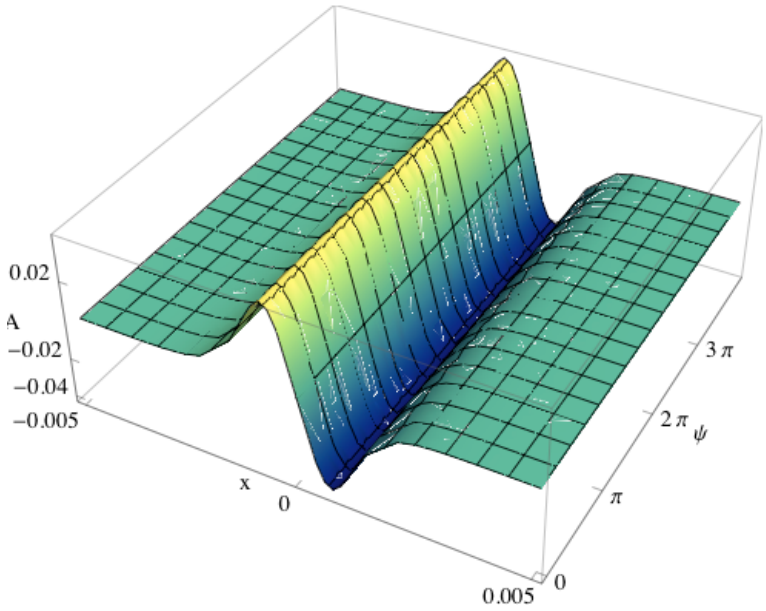

Figure 4.13: Example of the form of A_{ji} for the separable model.

the previous discussion for the spectral index implies there should be a correlation between n_s and $f_{\rm NL}$ such that a blue spectral index is accompanied by $f_{\rm NL} < 0$ and vice versa. This is in fact the relation from single-field inflation, $f_{\rm NL} = -5(n_s - 1)/12$ [36]. While Fig. 4.9 clearly shows this line, it is also clear that the majority of points deviate from this trend. In fact, the histogram for $f_{\rm NL}$ shows a tendency for $f_{\rm NL} > 0$, while the discussion until now would imply the opposite.

Looking closely at particular evolutions of $f_{\rm NL}$, like the one in Fig. 4.18, what we see is that during the non-slow-roll period at the end of inflation, the evolution of $f_{\rm NL}$ experiences a rise, that typically forces the final value to be > 0. This behaviour is not predicted by the separable approximation. This discrepancy could be the result of modelling the inflection point as being cubic when in fact the ledge in the D-brane potential tends to be much more severe, or more interestingly it could be an intrinsically non-slow-roll effect.

However, the slow-roll phase of the evolution does seem to be captured by the separable approximation. In addition to Z_i, there is contribution to the evolution A_{ji} which, as shown in Fig. 4.13, has a peak and a trough. While the precise form varies between trajectories, this contribution gives rise to a peak and a trough in $f_{\rm NL}$, one above and one below the value $f_{\rm NL}$ takes towards the end of inflation.

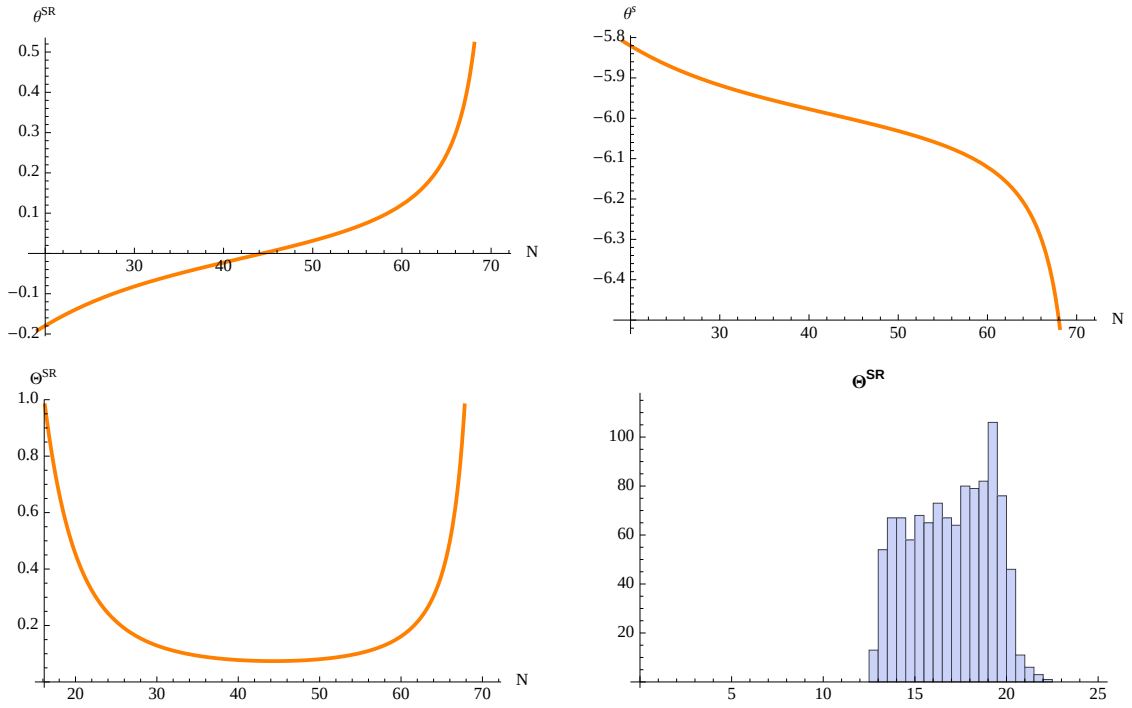

Figure 4.14: Evolution of $\theta^{\rm SR}$ top left, $\theta^{\rm s}$ top right, and the dilation of the field bundle $\Theta^{\rm SR}$ bottom left for verse 20277. Bottom right is the histogram of the final field bundle widths for our two-field sample. The fields initially go through a region of focussing but all is undone as the trajectory falls off the ledge, resulting the persistence of isocurvature modes at the end of inflation. The histogram shows this to be true for all 1086 realisations, leading us to conclude the model is unpredictive without a description of reheating.

4.7 How predictive?

A consideration of paramount importance in any model of inflation is at what point does ζ cease to evolve. In single-field models, ζ does not evolve on superhorizon scales but for any model with more than one field this tends not be the case. As we have already discussed, the criteria for whether or not evolution can persist is whether or not isocurvature modes are present. The limit in which these decay is referred to as the adiabatic limit.

As already mentioned, one way to keep track of isocurvature modes is to monitor the dilation of the bundle of trajectories using Eq. (4.42). In the adiabatic limit the bundle is a caustic, for which a necessary but not sufficient condition is $\theta \to -\infty$, or equivalently $\Theta \to 0$. Strictly speaking this limit cannot be reached during the slow-roll regime [19] but we can at least hope that isocurvature modes are exponentially suppressed. More generally $\theta^{\rm SR} < 0$ corresponds to a region of focussing and $\theta^{\rm SR} > 0$ to dilation, while $\theta^{\rm s} > 0$ and $\theta^{\rm s} < 0$ represent divergence and convergence to the momenta slow-roll attractor

respectively.

It is interesting to note that our results show exceedingly consistent behaviour. As shown by the histogram in Fig. 4.20, in not one realisation did we find focussing to be occurring at the end of inflation. Rather, the process of falling off the ledge results in dilation of the bundle. This result is still present in the separable approximation and indeed we expect this result to apply to any model where inflation is terminated by falling off a ledge if sufficient focussing has not taken place previously.

The downside of a lack of focussing at the end of inflation is that the model is technically unpredictive without knowledge of what takes place at the tip and the details of reheating. The plus side is that one should expect interesting evolution during subsequent periods. Since reheating is a non-linear process, this could give rise to interesting observational signatures. This is however beyond the scope of this paper.

4.8 Summary

In this paper we explored the multifield effects in D-brane inflation. To do this we made use of a particularly sophisticated model, originally developed in Ref. [4], to include contributions from the bulk containing random coefficients. These contributions make the multifield nature of D-brane inflation explicit. Our aim was to use the transport equations [5–7, 19] to study a large number of realisations of the potential, their resulting inflationary behaviours, and the consequent properties of ζ. We had two main objectives with this endeavour, first to present distributions for the observable predictions of this specific model and second to analyse how the isocurvature modes behave towards the end of inflation to understand how reliable those predictions are.

Despite the random contributions, the inflationary behaviour was very consistent across different realisations. Inflation was always found to have canonical kinetic behaviour and to take place in the vicinity of the inflection point, which constitutes a very small region of field space. We also always found a break of the slow-roll condition $|\eta| < 1$ when the inflationary trajectory falls off the ledge after the inflection point. This particular characteristic led to the extension of transport methods to non-slow-roll cases [7]. We also extended this method to compute the running of the spectral index.

Regarding the predictions for observables, the amplitude of the power spectrum was

found to be consistent with observation but unpredictive in so much as the spread in values was vast compared with the observational constraints. The spectral index tended to be blue but less so in the full six-field case. This fact, together with the negligible values found for the tensor-to-scalar ratio and the large spread in values of the spectral index running, moderately constrains the model given WMAP7 data. Without a reason to believe we are an atypical observer in our distribution, the soon-to-arrive data from Planck has the potential to put this model under considerable pressure.

The non-Gaussianity parameter $f_{\rm NL}$ was found to be consistently small. In over 1000 inflationary realisations we found only 5 examples of potentially observable $f_{\rm NL}$. This further supports the recent discussions in Refs. [15, 38, 42] which suggests canonical multifield inflation is not expected to produce observable $f_{\rm NL}$.

Due to the remarkable consistency in the inflationary behaviour, it was possible to approximate the inflationary region of the potential as a sum-separable potential consisting of a polynomial inflection point in the radial direction and linear slopes in the angular directions. With this description all the observed characteristics of this model could be accounted for analytically except the final evolution in $f_{\rm NL}$. It was shown that the evolution of the amplitude of the power spectrum undergoes non-monotonic evolution whenever the trajectory traverses the inflection point and this will typically give rise to a blue tilt which, along with all other observable quantities of interest, can be calculated purely in terms of horizon-crossing values. It was also shown that additional angular terms act to make the tilt more red.

Regarding the reliability of these predictions, we made first steps towards a means of efficiently tracking isocurvature modes in non-slow-roll multifield models. Though we leave a complete description of this to a separate publication, we nevertheless found the bundle width to be exceedingly informative. Extending the ideas on the adiabatic limit discussed in Ref. [19] to non-slow roll constitutes a considerable increase in complexity. We found it helpful to consider two distinct bundles, one for the fields and a second for the momenta. With this we were able to conclude that in not a single realisation was an adiabatic limit reached. We expect this result to hold for any model where inflation is terminated by falling off a ledge, provided sufficient focussing does not occur prior to this. This result renders the model technically unpredictive, since subsequent events such as reheating can modify the characteristics of ζ.

References

[1] David H. Lyth and Antonio Riotto. "Particle physics models of inflation and the cosmological density perturbation". In: *Phys.Rept.* 314 (1999), pp. 1–146. arXiv:hep-ph/9807278 [hep-ph] (cit. on p. 141).

[2] Daniel Baumann and Liam McAllister. "Advances in Inflation in String Theory". In: *Ann.Rev.Nucl.Part.Sci.* 59 (2009), pp. 67–94. arXiv:0901.0265 [hep-th] (cit. on p. 141).

[3] Anupam Mazumdar and Jonathan Rocher. "Particle physics models of inflation and curvaton scenarios". In: *Phys.Rept.* 497 (2011), pp. 85–215. arXiv:1001.0993 [hep-ph] (cit. on p. 141).

[4] Nishant Agarwal et al. "Universality in D-brane Inflation". In: *JCAP* 1109 (2011), p. 002. arXiv:1103.2775 [astro-ph.CO] (cit. on pp. 143–145, 149–151, 173).

[5] David J. Mulryne, David Seery and Daniel Wesley. "Moment transport equations for non-Gaussianity". In: *JCAP* 1001 (2010), p. 024. arXiv:0909.2256 [astro-ph.CO] (cit. on pp. 143, 154, 155, 157, 173).

[6] David J. Mulryne, David Seery and Daniel Wesley. "Moment transport equations for the primordial curvature perturbation". In: *JCAP* 1104 (2011), p. 030. arXiv:1008.3159 [astro-ph.CO] (cit. on pp. 143, 154, 155, 157, 173).

[7] Mafalda Dias et al. "A general computation of the primordial curvature perturbation by transport: A how to". In: (In preperation) (cit. on pp. 143, 157–159, 173).

[8] Shamit Kachru et al. "Towards inflation in string theory". In: *JCAP* 0310 (2003), p. 013. arXiv:hep-th/0308055 [hep-th] (cit. on pp. 144, 146).

[9] C.P. Burgess et al. "The Inflationary brane anti-brane universe". In: *JHEP* 0107 (2001), p. 047. arXiv:hep-th/0105204 [hep-th] (cit. on pp. 144, 146).

[10] Daniel Baumann et al. "D3-brane Potentials from Fluxes in AdS/CFT". In: *JHEP* 1006 (2010), p. 072. arXiv:1001.5028 [hep-th] (cit. on pp. 145, 147, 148).

[11] Igor R. Klebanov and Arvind Murugan. "Gauge/Gravity Duality and Warped Resolved Conifold". In: *JHEP* 0703 (2007), p. 042. arXiv:hep-th/0701064 [hep-th] (cit. on p. 147).

[12] Daniel Baumann et al. "Holographic Systematics of D-brane Inflation". In: *JHEP* 0903 (2009), p. 093. arXiv:0808.2811 [hep-th] (cit. on p. 148).

[13] Max Tegmark. "What does inflation really predict?" In: *JCAP* 0504 (2005), p. 001. arXiv:astro-ph/0410281 [astro-ph] (cit. on p. 151).

[14] Jonathan Frazer and Andrew R. Liddle. "Exploring a string-like landscape". In: *JCAP* 1102 (2011), p. 026. arXiv:1101.1619 [astro-ph.CO] (cit. on p. 151).

[15] Jonathan Frazer and Andrew R. Liddle. "Multi-field inflation with random potentials: field dimension, feature scale and non-Gaussianity". In: *JCAP* 1202 (2012), p. 039. arXiv:1111.6646 [astro-ph.CO] (cit. on pp. 151, 161, 174).

[16] Gerasimos I. Rigopoulos and E. P. S. Shellard. "Non-linear inflationary perturbations". In: *JCAP* 0510 (2005), p. 006. arXiv:astro-ph/0405185 (cit. on p. 152).

[17] G. I. Rigopoulos, E. P. S. Shellard and B. J. W. van Tent. "Non-linear perturbations in multiple-field inflation". In: *Phys.Rev.* D73 (2006), p. 083521. arXiv:astro-ph/0504508 (cit. on p. 152).

[18] Shuichiro Yokoyama, Teruaki Suyama and Takahiro Tanaka. "Primordial Non-Gaussianity in Multi-Scalar Inflation". In: *Phys.Rev.* D77 (2008), p. 083511. arXiv:0711.2920 [astro-ph] (cit. on p. 152).

[19] David Seery et al. "Inflationary perturbation theory is geometrical optics in phase space". In: *JCAP* 1209 (2012), p. 010. arXiv:1203.2635 [astro-ph.CO] (cit. on pp. 153, 154, 158, 172–174).

[20] David Seery and James E. Lidsey. "Primordial non-Gaussianities from multiple-field inflation". In: *JCAP* 0509 (2005), p. 011. arXiv:astro-ph/0506056 [astro-ph] (cit. on p. 153).

[21] Gemma J. Anderson, David J. Mulryne and David Seery. "Transport equations for the inflationary trispectrum". In: *JCAP* 1210 (2012), p. 019. arXiv:1205.0024 [astro-ph.CO] (cit. on p. 155).

[22] Alexei A. Starobinsky. "Multicomponent de Sitter (Inflationary) Stages and the Generation of Perturbations". In: *JETP Lett.* 42 (1985), pp. 152–155 (cit. on p. 155).

[23] D. H. Lyth. "Large Scale Energy Density Perturbations and Inflation". In: *Phys.Rev.* D31 (1985), pp. 1792–1798 (cit. on p. 155).

[24] Misao Sasaki and Ewan D. Stewart. "A General analytic formula for the spectral index of the density perturbations produced during inflation". In: *Prog.Theor.Phys.* 95 (1996), pp. 71–78. arXiv:astro-ph/9507001 (cit. on p. 155).

[25] David H. Lyth and Yeinzon Rodríguez. "The inflationary prediction for primordial non-gaussianity". In: *Phys.Rev.Lett.* 95 (2005), p. 121302. arXiv:astro-ph/0504045 (cit. on p. 155).

[26] Mafalda Dias and David Seery. "Transport equations for the inflationary spectral index". In: *Phys.Rev.* D85 (2012), p. 043519. arXiv:1111.6544 [astro-ph.CO] (cit. on p. 156).

[27] David Wands. "Local non-Gaussianity from inflation". In: *Class.Quant.Grav.* 27 (2010), p. 124002. arXiv:1004.0818 [astro-ph.CO] (cit. on p. 157).

[28] David Langlois, Filippo Vernizzi and David Wands. "Non-linear isocurvature perturbations and non-Gaussianities". In: *JCAP* 0812 (2008), p. 004. arXiv:0809.4646 [astro-ph] (cit. on p. 157).

[29] Christian T. Byrnes and David Wands. "Curvature and isocurvature perturbations from two-field inflation in a slow-roll expansion". In: *Phys.Rev.* D74 (2006), p. 043529. arXiv:astro-ph/0605679 [astro-ph] (cit. on p. 157).

[30] David Polarski and Alexei A. Starobinsky. "Isocurvature perturbations in multiple inflationary models". In: *Phys.Rev.* D50 (1994), pp. 6123–6129. arXiv:astro-ph/9404061 [astro-ph] (cit. on p. 158).

[31] Juan García-Bellido and David Wands. "Metric perturbations in two field inflation". In: *Phys.Rev.* D53 (1996), pp. 5437–5445. arXiv:astro-ph/9511029 [astro-ph] (cit. on p. 158).

[32] David Wands and Juan García Bellido. "Density perturbations from two field inflation". In: *Helv.Phys.Acta* 69 (1996), pp. 211–214. arXiv:astro-ph/9608042 [astro-ph] (cit. on p. 158).

[33] E. Komatsu et al. "Seven-Year Wilkinson Microwave Anisotropy Probe (WMAP) Observations: Cosmological Interpretation". In: *Astrophys.J.Suppl.* 192 (2011), p. 18. arXiv:1001.4538 [astro-ph.CO] (cit. on p. 159).

[34] E. Komatsu et al. "Five-Year Wilkinson Microwave Anisotropy Probe (WMAP) Observations: Cosmological Interpretation". In: *Astrophys.J.Suppl.* 180 (2009), pp. 330–376. arXiv:0803.0547 [astro-ph] (cit. on pp. 159, 161, 163, 164).

[35] Marina Cortes, Andrew R Liddle and Pia Mukherjee. "On what scale should inflationary observables be constrained?" In: *Phys.Rev.* D75 (2007), p. 083520. arXiv:astro-ph/0702170 [astro-ph] (cit. on pp. 159, 164).

[36] Juan Martin Maldacena. "Non-Gaussian features of primordial fluctuations in single field inflationary models". In: *JHEP* 0305 (2003), p. 013. arXiv:astro-ph/0210603 [astro-ph] (cit. on pp. 163, 171).

[37] Shaun Hotchkiss, Anupam Mazumdar and Seshadri Nadathur. "Inflection point inflation: WMAP constraints and a solution to the fine-tuning problem". In: *JCAP* 1106 (2011), p. 002. arXiv:1101.6046 [astro-ph.CO] (cit. on p. 165).

[38] Joseph Elliston et al. "Evolution of fNL to the adiabatic limit". In: *JCAP* 1111 (2011), p. 005. arXiv:1106.2153 [astro-ph.CO] (cit. on pp. 166, 174).

[39] Filippo Vernizzi and David Wands. "Non-gaussianities in two-field inflation". In: *JCAP* 0605 (2006), p. 019. arXiv:astro-ph/0603799 [astro-ph] (cit. on pp. 166–168).

[40] Thorsten Battefeld and Richard Easther. "Non-Gaussianities in Multi-field Inflation". In: *JCAP* 0703 (2007), p. 020. arXiv:astro-ph/0610296 [astro-ph] (cit. on pp. 166–168).

[41] Soo A. Kim and Andrew R. Liddle. "Nflation: Non-Gaussianity in the horizon-crossing approximation". In: *Phys.Rev.* D74 (2006), p. 063522. arXiv:astro-ph/0608186 [astro-ph] (cit. on p. 169).

[42] Joel Meyers and Navin Sivanandam. "Non-Gaussianities in Multifield Inflation: Superhorizon Evolution, Adiabaticity, and the Fate of fnl". In: *Phys.Rev.* D83 (2011), p. 103517. arXiv:1011.4934 [astro-ph.CO] (cit. on p. 174).

Erratum

4.9 Curved field-space metric and massive modes

In the analysis presented in our paper 'Multifield consequences for D-brane inflation', we considered the field-space metric in Eq. (2.4) to be the flat trivial metric, $g_{ij} = \delta_{ij}$. However, the inclusion of the curved conifold metric has several implications on the inflationary dynamics, and as such should be incorporated in our calculations. We thank Liam McAllister and Sebastien Renaux-Petel for pointing out this issue.

In this case, the Lagrangian experienced by the D-brane is

$$\mathcal{L} = a^3 \left(\frac{1}{2} T_3 G_{ij} \dot{\phi}^i \dot{\phi}^j - V(\phi) \right) \tag{4.63}$$

where a is the scale factor and T_3 is the brane tension. For simplicity, the vector composed of the 6 brane coordinates in the throat — radial and Ψ — is represented by ϕ and the vector Ψ refers to the 5 angular dimensions, $\Psi = \theta_1, \theta_2, \phi_1, \phi_2, \psi$.

The field-space metric G_{ij} corresponds to the Klebanov–Witten geometry in which the non-compact conifold geometry is built over the five-dimensional $(SU(2) \times SU(2))/U(1)$ coset space $T^{1,1}$. In this case [1],

$$G_{ij} d\phi^i d\phi^j = dr^2 + r^2 ds^2_{T^{1,1}}. \tag{4.64}$$

where r is the radial conical coordinate and

$$ds^2_{T^{1,1}} = \frac{1}{9} \left(d\psi + \cos\theta_1 d\phi_1 + \cos\theta_2 d\phi_2 \right)^2 + \frac{1}{6} \left(d\theta_1^2 + \sin^2\theta_1 d\phi_1^2 \right) + \frac{1}{6} \left(d\theta_1^2 + \sin^2\theta_1 d\phi_1^2 \right). \tag{4.65}$$

With this new Lagrangian we repeated the experimental procedure described in §3, and collected over 500 trajectories, with 6 active fields and $\Delta_{\mathrm{MAX}} = 3$, which give rise to at least 63 e-folds of inflation.

It is usual that models with curved field-space metrics present massive modes around horizon crossing. To verify if this was the case in our model, we calculated the eigenvalues

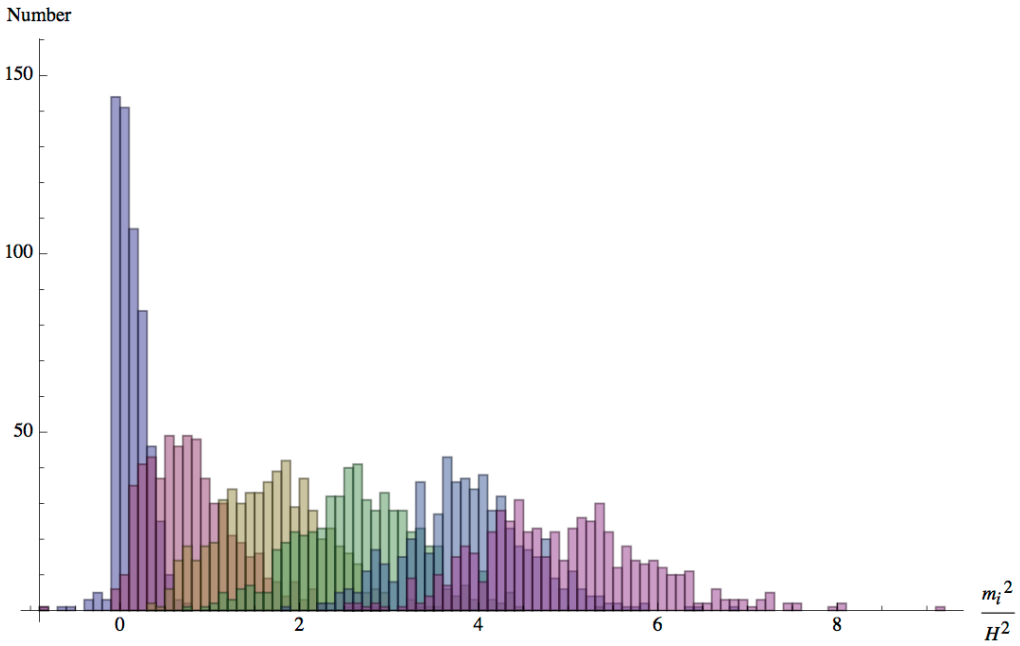

Figure 4.15: The eigenvalues of the mass matrix at horizon crossing for all the successful realisations. We can see that there is consistently one light quantum mode while all the others are heavy.

of the mass matrix. The mass matrix can be determined from the second-order perturbed action:

$$S_{(2)} = \int dt d^3x a^3 \left(G_{ij}\mathcal{D}_t Q^i \mathcal{D}_t Q^j - \frac{1}{a^2} G_{ij}\partial_\mu Q^i \partial^\mu Q^j - M_{ij} Q^i Q^j \right), \tag{4.66}$$

where $\mathcal{D}_t$ are covariant cosmic time derivatives, Q^i are the covariant field perturbations and

$$M_{ij} = V_{;ij} - R_{iklj}\dot{\phi}^k\dot{\phi}^l - \frac{1}{a^3}\mathcal{D}_t\left[\frac{a^3}{H}\dot{\phi}_i\dot{\phi}_j\right] \tag{4.67}$$

with semicolon referring to covariant derivatives. From this action we can recover the Klein–Gordon equation for the field perturbations Q^i

$$\mathcal{D}_t^2 Q^i + 3H\mathcal{D}_t Q^i + \frac{k^2}{a^2}Q^i + M^i_j Q^j = 0. \tag{4.68}$$

For our sample of trajectories we consistently found one of the directions to be light while the other quantum modes have masses of order of the Hubble scale at horizon exit, in agreement with Ref. [2]. The results are shown in Fig. 4.15. The presence of heavy modes required the development of a new computational tool for the calculation of ζ. The problem relates to the initial condition at horizon exit necessary for implementing the separate universe assumption. In our previous analysis, the standard light-field Gaussian approximation at horizon exit was sufficient — $\Sigma^{\phi\phi} = G_{ij}H^2/(2\pi)^2$. But now this approximation does not hold. An analytic solution of the full Klein–Gordon equation is impossible to

achieve and for this reason we developed with our collaborators David Mulryne and David Seery an efficient method to deal with this issue numerically [3, 4]. Here, we only present the analysis for the two-point function of ζ, leaving a detailed study of the three-point function for a future publication.

4.10 New techniques

In this section, our aim is to sketch the extensions to the transport method (§4 of our paper) used in the new analysis of the D-brane model. First, we will briefly present the argument of Elliston *et al.* [5] applied to a non-slow-roll setup, and then we will introduce the idea of quantum transport on subhorizon scales. We will not develop these descriptions in great detail here; we refer the reader to Refs. [3, 4] for a complete description.

If inflation is driven by a system of several scalar fields whose field-space metric G_{ij} is different from δ_{ij}, the field perturbations $\delta\phi$ of §4 are no longer covariant objects. To use the transport method in this case, we need to reformulate it in terms of the above covariant perturbations Q^i. In the same spirit as §4 we can define a vector $\mathcal{Q}^\alpha \equiv \{Q^i, \mathcal{D}_N Q^i\} \equiv \{Q^i, P^i\}$. The foundation of the transport formulation is the deviation equation which determines the evolution of perturbations according to background expansion tensors. For the new covariant perturbations this looks like

$$\mathcal{D}_N \mathcal{Q}^\alpha = w^\alpha{}_\beta \mathcal{Q}^\beta + \frac{1}{2} w^\alpha{}_{\beta\gamma} \mathcal{Q}^\beta \mathcal{Q}^\gamma + \cdots \tag{4.69}$$

For the computation of the two-point function, the first-order term is sufficient. The expansion tensor $w^\alpha{}_\beta$ can be read off directly from the Klein–Gordon equation for Q^i given above by taking the superhorizon limit $k^2/a^2 \ll 1$. If we change the time coordinate to be N rather than cosmic time, and assuming that we are well outside the horizon,

$$\mathcal{D}_N Q^i = P^i \tag{4.70}$$

$$\begin{aligned} \mathcal{D}_N P^i = &\left[-\frac{V_{;}{}^i{}_j}{H^2} + \frac{V_{,}{}^i V_{,j}}{H^3 V} + R^i{}_{lmj} p^l p^m \right] Q^j \\ &+ \left[\frac{V_{,}{}^i p_j}{(3-\epsilon)H^2} + p^i p_j + (\epsilon - 3)\delta^i_j \right] P^j. \end{aligned} \tag{4.71}$$

The expansion tensor $w^\alpha{}_\beta$ contains all the information on the superhorizon evolution of the power spectra $\Sigma^{\alpha\beta}$ associated to $\langle \mathcal{Q}^\alpha \mathcal{Q}^\beta \rangle$

$$\mathcal{D}_N \Sigma^{\alpha\beta} = w^\alpha{}_\mu \Sigma^{\mu\beta} + w^\beta{}_\mu \Sigma^{\mu\alpha} + \cdots \tag{4.72}$$

The power spectra $\Sigma^{\alpha\beta}$ relate to the power spectrum of ζ by the usual gauge transformations described in §4.

This method describes the transport of field perturbations on superhorizon scales using the separate universe assumption. The question to ask now is what are the initial conditions for this method at horizon exit. Since it is impossible to deal with this question analytically, correlation functions need to be transported from subhorizon scales up to the end of inflation, so that the full evaluation is numerical. Usually, a numerical implementation of perturbation theory is computationally very intensive. This is related to the oscillatory nature of the perturbations as wave functions. However, by only keeping track of the evolution of correlators, the calculation becomes much lighter.

In order to do this, we extended the transport technique to a quantum era on subhorizon scales. In this case, if the evaluation is chosen to start early enough, such that the perturbations are much smaller than the horizon, one can assume that the initial conditions are established in flat Minkowski space-time, where correlation functions are well known.

To quantise transport, the field perturbations and their momenta should be interpreted as operators in Fourier space related by the usual commutation relations. In k space it is helpful to use a DeWitt notation where indices are primed to indicate the Fourier space scale dependence:

$$\widehat{\mathcal{Q}}^{\alpha'} = \widehat{\mathcal{Q}}^{\alpha}(k_\alpha) \tag{4.73}$$

where k_α is the scale associated with the perturbation of index α (with no sum on α). This operator has an evolution equation like

$$\mathcal{D}_N \widehat{\mathcal{Q}}^{\alpha'} = w^{\alpha'}{}_{\beta'} \widehat{\mathcal{Q}}^{\beta'} + \frac{1}{2} w^{\alpha'}{}_{\beta'\gamma'} \widehat{\mathcal{Q}}^{\beta'} \widehat{\mathcal{Q}}^{\gamma'} + \cdots \tag{4.74}$$

where

$$w^{\alpha'}{}_{\beta'} = (2\pi)^3 w^{\alpha}{}_{\beta}\, \delta(k_\alpha - k_\beta). \tag{4.75}$$

For the quantum subhorizon evolution the expansion tensor is not determined by the background only. It can be recovered by looking at the second-order perturbed action computed above. In this case, the quantum expansion tensor $w^{\alpha}{}_{\beta}$ only gets modified by the extra term containing information on the (comoving) scale k of the perturbations:

$$w^{\alpha}{}_{\beta} \supset -\frac{k^2}{a^2 H^2} \delta^{\alpha}_{\beta}. \tag{4.76}$$

The evolution equation for $\Sigma^{\alpha\beta}$ follows from the Ehrenfest theorem

$$\frac{d\langle \widehat{O} \rangle}{dt} = \Big\langle -i \Big[\widehat{O}, \widehat{H} \Big] \Big\rangle, \tag{4.77}$$

which is the direct equivalent to the evolution of classical expectation values. For simplicity, one can choose to work with the symmetrised $\Sigma^{\alpha\beta}$, which corresponds to the real part of the two-point correlator; as perturbations become classical, the imaginary part decays which means that only the evolution of the real part is necessary to compute observables. The transport equation for this symmetrised $\Sigma^{\alpha\beta}$ is equivalent to the one on superhorizon scales:

$$\mathcal{D}_N \Sigma^{\alpha\beta} = w^{\alpha}{}_{\mu} \Sigma^{\mu\beta} + w^{\beta}{}_{\mu} \Sigma^{\mu\alpha} + \cdots \tag{4.78}$$

With these equations we were able to compute the perturbations for our sample of trajectories. We started our computation 8 e-folds of inflation before horizon exit, which is early enough to find the perturbations well inside the horizon where Minkowski initial conditions hold. We computed the observables for the perturbation associated with the scale which crossed the horizon 55 e-folds before the end of inflation.

4.11 Results

4.11.1 Observables

We now present the results from our new analysis. The outcome is distributions for the values of the cosmological parameters associated to the two-point function of perturbations: amplitude $P_{\zeta\zeta}$, spectral index n_s, and tensor-to-scalar ratio r. We compared these with constraints from observations; all constraint contours are 95% confidence limits using the WMAP 7-year data release combined with baryonic acoustic oscillations and supernovæ data [6].

We concluded that the inclusion of the curved field-space metric, even though it induces large masses in 5 of the 6 quantum modes active during inflation, does not qualitatively change the results for observables that we obtained with a trivial field-space metric.

As can be seen in Fig. 4.16, the histogram of $P_{\zeta\zeta}$ has a smooth maximum at around 10^{-9}, in agreement with observations (the WMAP value is $\sim 2.5 \times 10^{-9}$ [6]) and with our original computation. This is not surprising as the overall magnitude of the potential is determined by the scale μ^4, which in turn is set by our choice of the throat length $r_{\rm UV}$.

The spectral index still presents a peak around $n_s = 1$ but it is less dramatic than in our previous computation, as seen in Fig. 4.16. As before, two different populations can

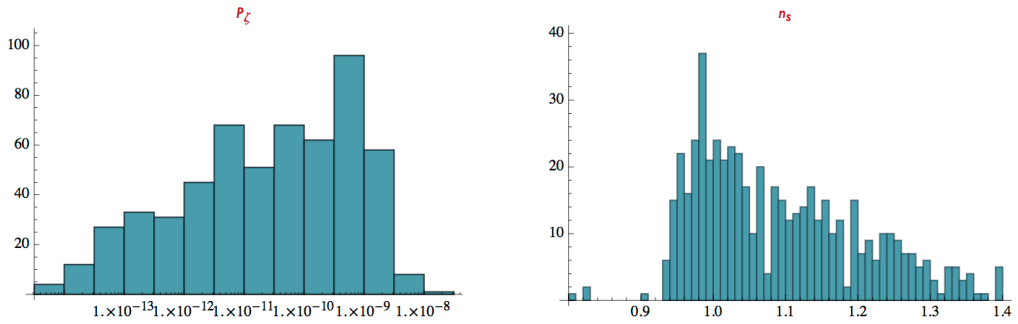

Figure 4.16: Distributions for the amplitude of the power spectrum $P_{\zeta\zeta}$, left and scalar spectral index n_s, right.

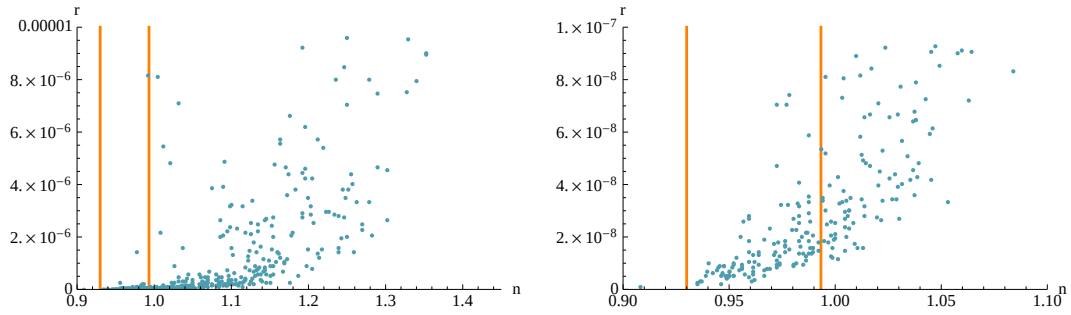

Figure 4.17: Plot of the values of n_s versus r. The right panel greatly expands the vertical scale. The orange lines indicate the 95% confidence limits using WMAP data.

be identified, 73% of the realisations with $n_s \geq 1$ and 27% with $n_s < 1$.

The tensor-to-scalar ratio is always extremely small, as it is related to the slow-roll parameter ϵ that remains $\ll 1$ throughout inflation. This can be clearly seen in Fig. 4.17.

Imposing observational constraints on the distributions, as can be seen in Fig. 4.17, excludes the majority of the trajectories. Almost all the realisations with red tilt are in accordance with observational constraints, such that $\sim 20\%$ of the total sample is in agreement with data. A further constraint is imposed by requiring the correct amplitude of the scalar power spectrum, $(2.5 \pm 0.1) \times 10^{-9}$ [6]. Combining all constraints we obtained only three realisations in total concordance with observations in the full sample of 564 cases. As discussed in the original article, this is not a worrying result as the distribution of $P_{\zeta\zeta}$ does not show a sharp peak.

As in our original computation, all trajectories are essentially of the same type — inflection-point inflation. Most of the inflation occurs in a small sub-region of the conifold (typically $0.02 < x < 0.09$) in the vicinity of an inflection point in the radial direction. Looking closely at one particular representative trajectory, Verse 79856, this is evident.

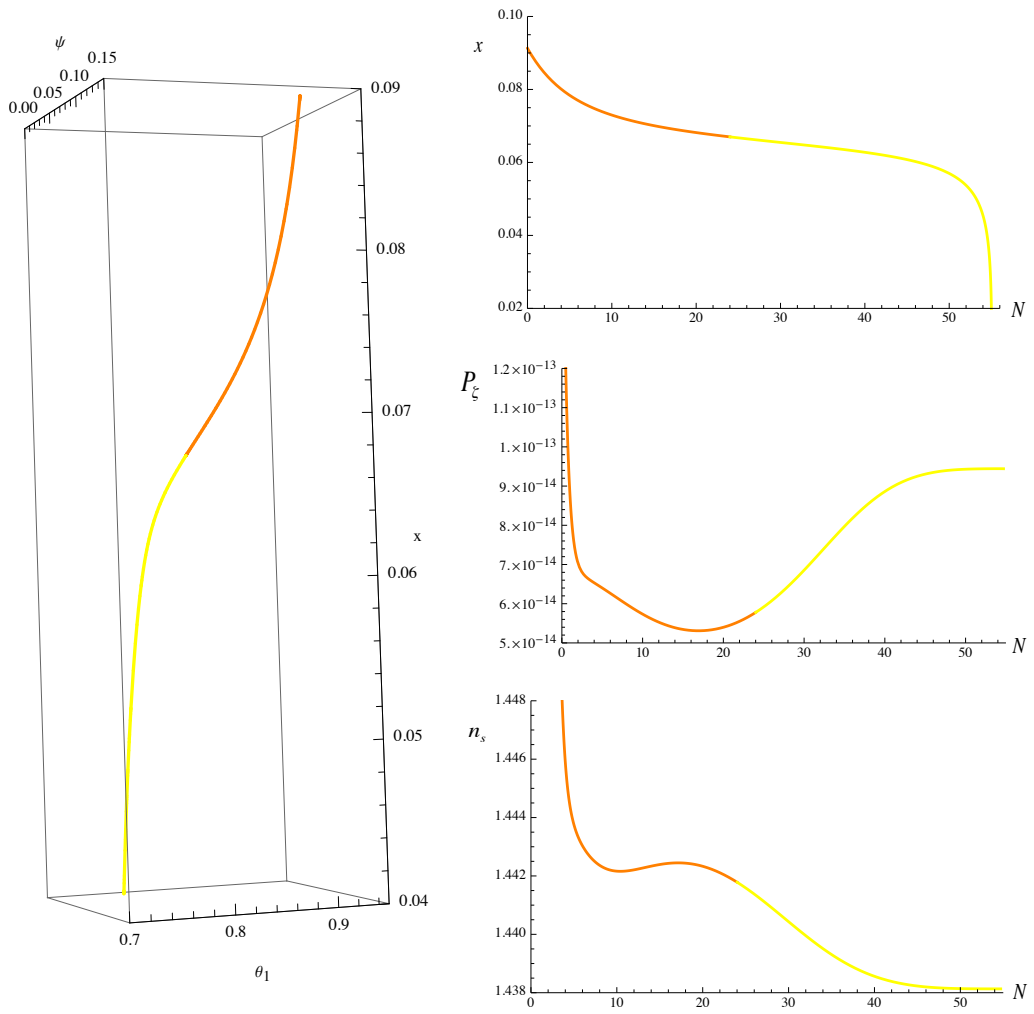

Figure 4.18: The dynamical behaviour of Verse 79856. The left plot shows the projection of the trajectory across x, θ_1 and ψ. The top-right panel shows the trajectory in x, whereas the middle and bottom panel show the superhorizon evolutions of $P_{\zeta\zeta}$ and n_s. Orange and yellow approximately indicates before and after the inflection point, respectively.

In the top right panel of Fig. 4.18, the trajectory in the radial coordinate is plotted in two different colours to highlight the approximate position of the inflection-point – orange before and yellow after it. The left panel shows the inflationary trajectory projected over three of the six directions – radial, θ_1 and ψ. The trajectory evolves from top to bottom and it is easy to see that around the inflection point it undertakes turns in the angular directions. The turns distinguish this trajectory from single-field inflection-point inflation and, as discussed, have consequences in the statistics of ζ. In fact, it is possible to see in Fig. 4.18 — right middle and bottom panels — that the values of $P_{\zeta\zeta}$ and n_s undergo superhorizon evolution around these turns in field space.

As in our previous analysis, the populations with red and blue spectral index could be understood by the position of horizon crossing relative to the inflection point. In fact,

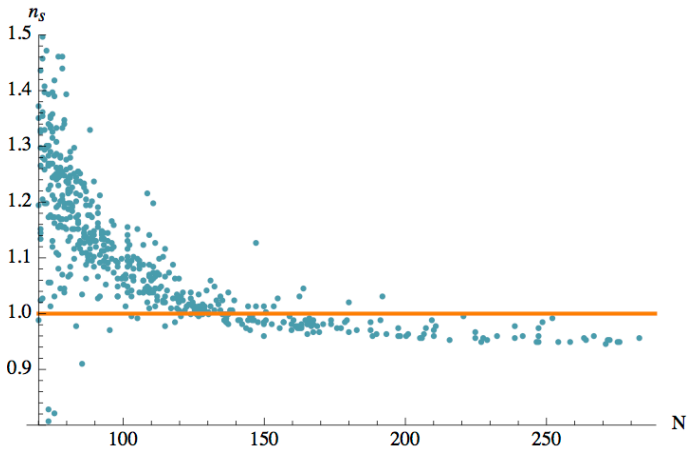

Figure 4.19: The value of the spectral index plotted against the total number of e-folds. The orange line represents the $n_s = 1$ cut. It is possible to see how $n_s < 1$ implies $N \gtrsim 120$.

it is straightforward to see that whenever horizon exit occurs before the inflection point, the spectral index is bigger than one. For the spectral index to be smaller than one, a dominant negative η contribution is required, which implies horizon exit after the inflection point. The latter is harder to achieve, which explains the small proportion of inflationary trajectories with red tilt; a trajectory that gives rise to 55 e-folds in the yellow region needs to have a much larger total number of e-folds. Roughly, one would expect it to give rise to at least twice 55. Indeed, this rough estimation is confirmed by Fig. 4.19, where the value of the spectral index is plotted against the total number of e-folds.

4.11.2 How predictive?

The biggest discrepancy between our two analyses concerns the approach to an adiabatic limit. As stated in §7, one way to keep track of isocurvature modes is to monitor the dilation of the bundle of trajectories.

When the number of fields is larger than one, the bundle of trajectories is a tensor of rank $n > 1$. In this case, the condition $\theta^{\rm SR} \to -\infty$ is not sufficient to ensure the bundle is reaching a caustic, becoming an object of rank 0. In fact, $\theta^{\rm SR}$ would experience this behaviour whenever the bundle becomes a tensor of rank $n-1$. In other words, a 'spherical' bundle could focus to a 'sheet' rather than a point; if this happens, isocurvature modes are not suppressed [7]. Therefore it is hard to make absolute statements.

In the D-brane model, as can be seen in Fig. 4.20, we consistently found across all the trajectories and throughout the full inflationary period $\theta^{\rm SR} < 0$, which means the bundle

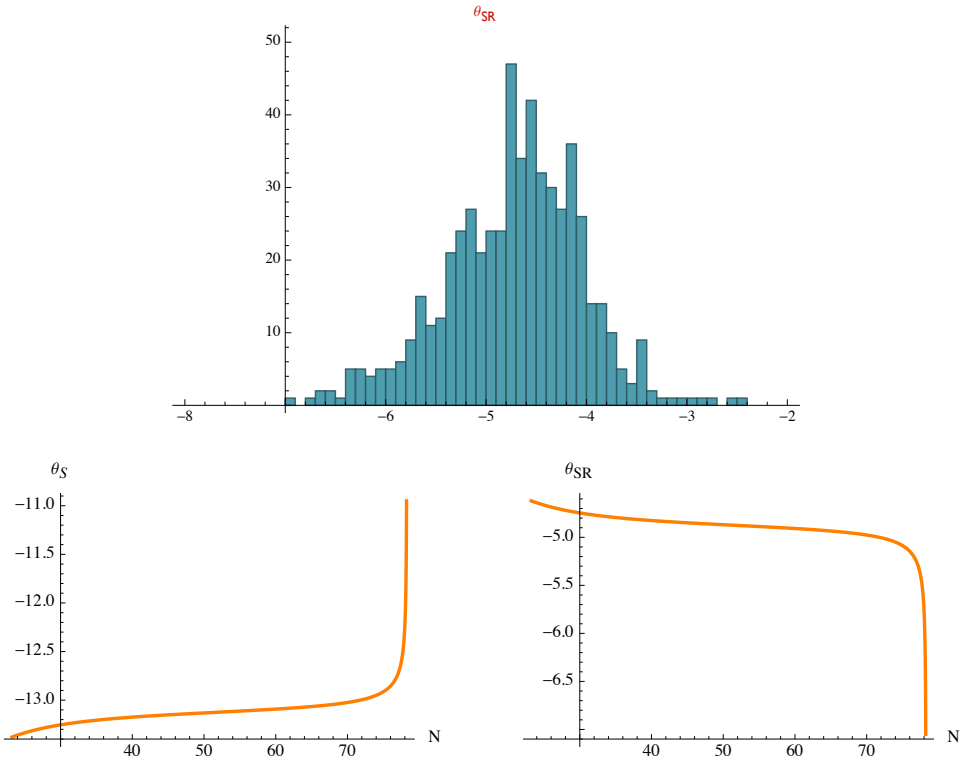

Figure 4.20: On top, histogram of the final field bundle widths for our sample. On the bottom, evolution of θ^s left and $\theta^{\rm SR}$ right for verse 79856.

of trajectories is focusing. To ensure this corresponds to reaching an adiabatic limit we have to make sure the bundles are reaching caustics. In this model, where we are near what can be considered quasi-single-field inflation, with one direction light and all the others heavy, there is no dynamical reason for the bundle to be focusing in any other way than by exponentially suppressing the isocurvature modes. Therefore we can consider that this model does not raise problems of predictiveness related to persistence of isocurvature through reheating, in agreement with Ref. [2].

4.12 Conclusions

In this erratum we repeat our calculations for the predictions of the D-brane model presented in 'Multifield consequences for D-brane inflation' taking into account the curved field-space metric in the conifold. We performed this analysis for the power spectrum of curvature perturbations only, leaving the study of bispectrum for a future publication. The inclusion of curvature induces large masses in 5 of our 6 active quantum modes, in

agreement with Ref. [2], which has consequences for the dynamics of inflation. To perform this computation we used extensions of the transport method which allow for curved field space metrics and quantum subhorizon evolution.

The results of our new analysis are in agreement with Ref. [2] and qualitatively identical to our original discussion, except regarding the suppression of isocurvature modes before the end of inflation, or, in other words, the reaching of an adiabatic limit. Our original conclusion, that the adiabatic limit was commonly not achieved, is not supported by our corrected analysis, where we find that the adiabatic limit is approached in all cases studied.

References

[1] Philip Candelas and Xenia C. de la Ossa. "Comments on Conifolds". In: *Nucl.Phys.* B342 (1990), pp. 246–268 (cit. on p. 179).

[2] Liam McAllister, Sebastien Renaux-Petel and Gang Xu. "A Statistical Approach to Multifield Inflation: Many-field Perturbations Beyond Slow Roll". In: *JCAP* 1210 (2012), p. 046. arXiv:1207.0317 [astro-ph.CO] (cit. on pp. 180, 187, 188).

[3] Mafalda Dias et al. "A general computation of the primordial curvature perturbation by transport: A how to". In: (In preperation) (cit. on p. 181).

[4] David J. Mulryne. "Transporting non-Gaussianity from sub to super-horizon scales". In: (2013). arXiv:1302.3842 [astro-ph.CO] (cit. on p. 181).

[5] Joseph Elliston, David Seery and Reza Tavakol. "The inflationary bispectrum with curved field-space". In: *JCAP* 1211 (2012), p. 060. arXiv:1208.6011 [astro-ph.CO] (cit. on p. 181).

[6] E. Komatsu et al. "Seven-Year Wilkinson Microwave Anisotropy Probe (WMAP) Observations: Cosmological Interpretation". In: *Astrophys.J.Suppl.* 192 (2011), p. 18. arXiv:1001.4538 [astro-ph.CO] (cit. on pp. 183, 184).

[7] David Seery et al. "Inflationary perturbation theory is geometrical optics in phase space". In: *JCAP* 1209 (2012), p. 010. arXiv:1203.2635 [astro-ph.CO] (cit. on p. 186).

Paper 5

Predictions in multifield models of inflation

Jonathan Frazer

This paper presents a method for obtaining an analytic expression for the density function of observables in multifield models of inflation with sum-separable potentials. The most striking result is that the density function in general possesses a sharp peak and the location of this peak is only mildly sensitive to the distribution of initial conditions. A simple argument is given for why this result holds for a more general class of models than just those with sum-separable potentials and why for such models, it is possible to obtain robust predictions for observable quantities. As an example, the joint density function of the spectral index and running in double quadratic inflation is computed. For scales leaving the horizon 55 e-folds before the end of inflation, the density function peaks at $n_s = 0.967$ and $\alpha = 0.0006$ for the spectral index and running respectively.

5.1 Introduction

The observable consequences of the simplest models of inflation with only one canonical field are quite well understood but ideas from fundamental physics seem to motivate models with more than one active field.[1] Models involving more than one light field, often referred to as “multifield models" allow for much richer inflationary behaviour and consequently making a prediction for observables in models of this kind is more complex. Although the

[1] As described in Ref. [1], although it remains difficult in string theory to achieve a sufficiently light scalar to give rise to inflation, once this is managed, the mechanism which gives rise to one light scalar, tends to give rise to many.

phenomenology of these models is well studied, and the search for observational signatures such as local non-Gaussianity is an active area of research, at present it is not clear what even the simplest multifield models actually predict.

One characteristic which makes computing observables more challenging is the fact that the primordial curvature perturbation evolves on superhorizon scales. In order to understand the possible signatures of multifield inflation it is essential to be able to precisely track the evolution after horizon crossing. Fortunately this is well studied and a number of techniques exist [2–28]. However, there is another important distinction between single field models of inflation and models with multiple active fields which is the sensitivity to initial conditions.

Models involving only one field are essentially insensitive to initial conditions; some minimum number of e-folds of inflation is required to solve cosmological problems such as the flatness and homogeneity, but provided the total amount of inflation is a few e-folds more than this, the observational consequences are independent of how much inflation actually takes place.[2] The primordial curvature perturbation on a given scale is uniquely determined by the value of the inflaton at the moment that scale left the horizon. If we take the largest scales we observe to have left the horizon say 55 e-folds before the end of inflation, our observations are generally insensitive to what happened before then, be it another 20 e-folds of inflation or 200.

When there is more than one active field the situation changes. As illustrated in Fig. 5.1, if the model involves $N_{\rm f}$ inflationary fields, instead of there being only one possible value of the inflaton at horizon crossing, now there is an infinite set of possible locations in field space forming an $N_{\rm f}-1$ dimentional hypersurface.[3] Without specifying initial conditions, it is not possible to say which inflationary trajectory corresponds to our observable universe and since different trajectories will in general give rise to different values for observables, the model is only as predictive as the volume in the space of observables permitted by the model. If we are to seriously confront multifield models of inflation with observation, then it is of paramount importance that this problem is overcome.

The obvious question then is whether a description of initial conditions can be derived within the framework of the model. One can hope that an ultraviolet complete theory of

[2] An important exception is the situation where there is more than one metastable vacuum. This situation certainly is sensitive to initial conditions. The discussion in this paper applies when only one minimum is relevant.

[3] Discussed in more detail in section §5.2, this assumes only one trajectory passes through a given point in field space.

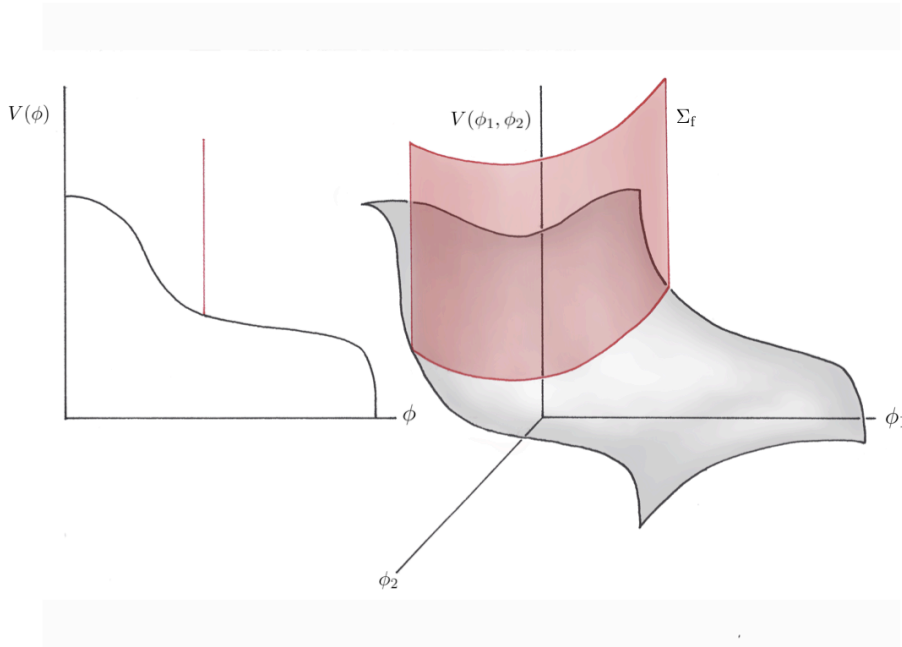

Figure 5.1: Sketch showing the horizon crossing surface in a single field inflationary potential and a two-field model. For a single field model, the horizon crossing surface is a single point, meaning that observables are approximately insensitive to inflationary dynamics prior to crossing this point. For the case of the two-field model, without knowledge of initial conditions one can not identify a single inflationary trajectory that corresponds to what we observe. One must therefore consider all possible inflationary trajectories.

inflation will provide information on the initial state but calculations along this line are clearly well beyond our current understanding of fundamental physics. A more promising approach is to consider how chaotic inflation populates the potential. Although this issue has received some attention in the past for the case of single field inflation (see for instance Refs. [29, 30] and references therein), a general description for the multifield case currently does not exist.

Ultimately the most problematic aspect of this question is what is often referred to as the measure problem (see Ref. [31] for a recent review). Often described in the context of tunnelling between metastable vacua but nevertheless still of critical importance even to much simpler models [32], the issue is that one must choose a measure when addressing what proportion of an infinite space-time corresponds to a particular choice of an infinite set of initial conditions.

Despite the significant challenge of computing initial conditions, the aim of this paper is to show that at least for some models it is still possible to make robust predictions for observables. A general method is not given here. Instead, by considering the subclass of multifield models where there is no couplings between the fields, it is shown that the density

function for observables can be computed analytically given an initial density function on field space. It turns out that under mild assumptions, the density function of observables is strongly peaked. This characteristic is largely determined by the geometry of the potential and can be comparatively insensitive to the initial density function on field space. This makes clear how the prediction for observables is (marginally) affected by the choice of measure, leading one to conclude that only certain choices will significantly change the result in comparison to the resolution of current and future observations such as Planck.

The approach taken in this paper utilises the fact that for sum-separable potentials, provided isocurvature modes have decayed before the end of inflation, observables o may be expressed solely in terms of quantities evaluated at horizon crossing. As is often the case, in what follows this will be referred to as the horizon crossing approximation [33]. The use of this approximation means that all the information required to compute observables for *all* possible inflationary trajectories is contained in a single hypersurface $\Sigma_{\rm f}$ parameterised by $N_{\rm f}-1$ variables $\{\theta_1,..,\theta_{N_{\rm f}-1}\}$. The idea then is that by specifying the density function $f(\theta_1,..,\theta_{N_{\rm f}-1})$ on the hypersurface, conservation of probability implies it is possible to compute the resulting density function for observables $p(o_1,...,o_n)$. For instance, consider the case where the hypersurface is 1-dimensional: Let θ be a continuous random variable with probability density $f(\theta)$. Defining $o\equiv o(\theta)$, provided the function is bijective, the probability density of o is given by $p(o)$ where

$$p(o)|do| = f(\theta)|d\theta|. \tag{5.1}$$

The density function $f(\theta)$ will depend on details of the theory as well as whatever the resolution of the measure problem may be, but even at this point Eq. (5.1) shows that a stationary point in $o(\theta)$ will give rise to a spike in $p(o)$ and so, with only mild assumptions as to the form of $f(\theta)$, one can obtain a sharp prediction for the model. Furthermore, if the surface of evaluation is closed, then $o(\theta)$ will be periodic and hence the existence of stationary points is guaranteed!

With regard to relevant work existing in the literature, there seems to be little seeking to directly address the issue of predictions in multifield models. In Refs. [32, 34] a toy model of inflation in the landscape was investigated. By using a method equivalent to taking a flat distribution over initial conditions, distributions for observables were computed. However, the presence of multiple minima meant that the results were clearly sensitive to the choice of distribution of initial conditions yet it was not clear how to asses the impact of this choice on results. A similar approach was taken in Refs. [35–37] to study 6-field D-brane

inflation but this model suffered from much the same problem. Here, drastically simpler models are considered and the approach taken to studying these models is very different. The most important difference is that here the role of the initial density function is explicit.

Despite not being directly about inflation, it is interesting to note the recent work of Sumitomo and Tye on the cosmological constant [38–40]. The mechanism by which they argue for the smallness of the cosmological constant is closely related to why a spike in the density function of observables is argued to be generic here.

The rest of this paper is structured as follows. §5.2 briefly reviews the relevant expressions for observable quantities in sum-separable potentials and discusses the conditions under which the method sketched above is applicable. §5.3 is dedicated to a more thorough explanation of the use of Eq. (5.1). §5.4 is a detailed discussion of the prediction of quadratic inflation; as well as being an interesting model in its own right, the spherical symmetry of the model makes calculating predictions exceptionally straightforward and hence will serve as a transparent demonstration of the method. §5.5 briefly discusses why the results should hold for a more general class of models than just the class of sum-separable models and §5.6 concludes this paper.

5.2 Sum-Separable Potentials and the Horizon Approximation

This section briefly introduces the expressions for observables in canonical models of inflation with sum-separable potentials and then discusses the conditions necessary for the proposed method to be applicable.

5.2.1 Expressions for Observables

The curvature perturbation may be related to perturbations in the fields by realising that on large scales ζ is equivalent to the perturbation of the number of e-foldings from an initial flat hypersurface at $t = t_*$, to a final uniform-density hypersurface at $t = t_c$ [2–4, 8]

$$\zeta(t_c, x) \simeq \delta N(t_c, t_*, x) \equiv N(t_c, t_*, x) - N(t_c, t_*). \tag{5.2}$$

where $N(t_c, t_*) \equiv \int_*^c H dt$. Expanding δN in terms of the initial field perturbations to second order, one obtains

$$\zeta(t_c, x) = \delta N(t_c, t_*, x) = N_{,\alpha}\, \delta\phi_\alpha^* + \frac{1}{2} N_{,\alpha\beta}\, \delta\phi_\alpha^* \delta\phi_\beta^*, \tag{5.3}$$

where repeated indices should be summed over, and $N_{,\alpha}$, $N_{,\alpha\beta}$ represent first and second derivatives of the number of e-folds with respect to the fields ϕ_α^*.

Observables of interest are related to the correlation functions of ζ and hence may be expressed in terms of field correlation functions multiplied by derivatives of N. In general computing the N derivatives require numerical techniques but a useful exception is the case of sum-separable potentials

$$W(\phi_1, .., \phi_{N_\mathrm{f}}) = \sum_i^{N_\mathrm{f}} V_i(\phi_i). \tag{5.4}$$

Models of this kind have the appealing characteristic that observables such as the power spectrum, spectral index, running, non-Gaussianity parameter f_NL etc. may be computed analytically. It should be noted however that there is no particularly good reason to believe that these models are well motivated from an effective field theory perspective; one in general should expect couplings between the fields. Although a more general approach is not given here, in later sections it will be argued that the main result of this paper applies to a broader class of models than just those with sum-separable potentials.

This paper focusses on quantities relating to the two-point statistics of ζ, particularly the spectral index n_s and running α, however all techniques used throughout this work are just as easily applied to higher order statistics. The reader is referred to Refs. [36, 41, 42] for derivations of the expressions. For this paper it will suffice to quote the results. Setting $M_\mathrm{PL} = 1$, the power spectrum is given by

$$\mathcal{P}_\zeta = \frac{W_*}{24\pi^2} \sum_{\alpha=1}^{N_\mathrm{F}} \frac{u_\alpha^2}{\epsilon_\alpha^*} \tag{5.5}$$

where

$$u_\alpha \equiv \frac{V_\alpha^* + Z_\alpha}{W_*}, \tag{5.6}$$

and ϵ_α is the first slow-roll parameter

$$\epsilon_\alpha \equiv \frac{1}{2}\left(\frac{V_\alpha'}{W}\right)^2, \tag{5.7}$$

such that $\epsilon = \sum \epsilon_\alpha$. Also, rather importantly for what follows, the term

$$Z_\alpha \equiv \frac{1}{\epsilon^c} \sum_{\beta=1}^{N_\mathrm{F}} V_\beta^c (\epsilon_\alpha^c - \epsilon^c \delta_{\alpha\beta}) \tag{5.8}$$

contains all the information about the constant density surface at the time of evaluation and all other terms are evaluated at horizon-crossing.

By differentiating with respect to $\ln k$, the spectral index is found to be

$$n_s - 1 = -2\epsilon_* - 4\frac{\left(1 - \sum_{\alpha=1}^{N_{\rm F}} \frac{\eta_\alpha^* u_\alpha^2}{2\epsilon_\alpha^*}\right)}{\sum_{\alpha=1}^{N_{\rm F}} \frac{u_\alpha^2}{\epsilon_\alpha^*}}, \tag{5.9}$$

where η_α is the second slow-roll parameter

$$\eta_\alpha \equiv \frac{V_\alpha''}{W}. \tag{5.10}$$

Differentiating with respect to $\ln k$ once again, the running is found to be [36]

$$\begin{aligned}\alpha = & -8\epsilon^{*2} + 4\sum_{\alpha=1}^{N_{\rm F}} \epsilon_\alpha^* \eta_\alpha^* - 16\frac{\left(1 - \sum_\alpha \frac{\eta_\alpha^* u_\alpha^2}{2\epsilon_\alpha^*}\right)^2}{\left(\sum_\alpha \frac{u_\alpha^2}{\epsilon_\alpha^*}\right)^2} - 8\frac{\sum_\alpha \eta_\alpha^* u_\alpha \left(1 - \frac{\eta_\alpha^* u_\alpha}{2\epsilon_\alpha^*}\right)}{\sum_\alpha \frac{u_\alpha^2}{\epsilon_\alpha^*}} \\ & + 4\epsilon^* \frac{\sum_\alpha \frac{\eta_\alpha^* u_\alpha^2}{\epsilon_\alpha^*}}{\sum_\alpha \frac{u_\alpha^2}{\epsilon_\alpha^*}} - 2\frac{\sum_\alpha \frac{\xi_\alpha^* u_\alpha^2}{\epsilon_\alpha^*}}{\sum_\alpha \frac{u_\alpha^2}{\epsilon_\alpha^*}},\end{aligned} \tag{5.11}$$

where ξ_α is the third slow-roll parameter

$$\xi_\alpha \equiv \frac{V_\alpha' V_\alpha'''}{W^2}. \tag{5.12}$$

All of the above expressions can be shown to reduce to the standard single-field formula by setting $u_\alpha = 1$.

5.2.2 The horizon crossing approximation and the adiabatic limit

As already discussed, the method proposed here for mapping a density function in field space to a density function for observables makes use of the horizon crossing approximation. The above expressions for the power spectrum (5.5), tilt (5.9) and running (5.11), are all composed of slow-roll terms evaluated at horizon crossing "*" and one other term u_α, of which the only contribution not evaluated on "*" is Z_α. It follows that in order for this approach to be appropriate two requirements must be satisfied:

1. The slow-roll approximations $\epsilon \ll 1$, $\eta \ll 1$, $\xi \ll 1$ must be valid.

2. Observables must stop evolving within the realm of validity of the model.

The first requirement is necessary for a number of reasons. The method proposed here seeks to map the density function on an $N_{\rm f} - 1$ hypersurface in field space to a density

function for observables. The very fact that the objective is phrased this way already implicitly assumes that (up to a time shift) there is a unique trajectory passing through each point in field space. A simple way to ensure this is the case is to stipulate that the slow-roll conditions are satisfied. If one does not wish to place any constraints on momenta then the situation is drastically more complicated. In principle an infinite number of both inflationary and non-inflationary trajectories may pass through any given point in field space. To handle such a situation is well beyond the scope of this approach.

Another reason for the first requirement is that the expressions for observables given above are obtained by assuming slow-roll. In practice it can well be the case that these expressions are valid even when the slow-roll approximations start to break down but this range of validity is clearly model-dependant.

The second requirement refers to the fact that for the model to be predictive, the primordial curvature perturbation must become conserved before the end of inflation. Otherwise a description of reheating is required. In order for the curvature perturbation to become conserved, isocurvature modes must have exponentially decayed by the end of inflation such that the model approaches the adiabatic limit [32, 36, 43–45]. Although it is difficult to say with certainty when isocurvature modes are sufficiently decayed, an intuitive method to test that this requirement has been satisfied is to track the evolution of the width of the bundle of perturbed inflationary trajectories in field space. The reader is referred to Ref. [45] for detailed discussion but an expression for the bundle width can be found to be

$$\Theta(N, N_0) = \exp\left\{-\sum_\alpha \int_{\phi_*}^{\phi_c} (-\eta_\alpha + 2\epsilon_\alpha)\frac{V_\alpha}{V'_\alpha} d\phi_\alpha\right\}, \tag{5.13}$$

where the expression given here differs from that given in Ref. [45] slightly since this has been written for the case of sum-separable potentials and made use of $dN = -\sum_\alpha V_\alpha/V'_\alpha d\phi_\alpha$. For an adiabatic limit to be reached, a necessary (but not sufficient if $N_\mathrm{f} > 2$) condition is that $\Theta \to 0$. By inspection of Eq. (5.13), a period of focusing requires

$$\sum_\alpha \eta_\alpha > 2\epsilon, \tag{5.14}$$

though how much focussing is required is a model dependant statement.

Satisfaction of the second requirement guarantees Z_α will be exponentially close to a constant at the end of inflation but does not guarantee that it is negligible. Satisfaction of both the first and the second requirement does however guarantee that to a good approximation one can express observables solely in terms of quantities evaluated at horizon

crossing. This is what is referred to as the horizon crossing approximation.[4] In practice, it is often the case that $Z_\alpha \to 0$ in the approach to the adiabatic limit but even in the situations where this is not the case, provided the first requirement is satisfied, it will be possible to map a given location on the final surface to a unique location on the horizon crossing surface. For the example of quadratic inflation given in this paper $Z_\alpha \to 0$ at the end of inflation.

5.3 Computing the density function of observables

The objective is to obtain an expression for $p(o_1, .., o_n)$ where o_i are the observables of interest such as the spectral index, running etc. If the model consists of $N_{\rm f}$ fields, then the horizon crossing contour is an $(N_{\rm f}-1)$-dimensional hypersurface in field space and hence, under the horizon crossing approximation, each observable may be expressed in terms of $N_{\rm f}-1$ parameters $\theta_{\alpha'}$. Latin indices label the observables, greek indices label coordinates on field space and primed greek indices label coordinates on the horizon crossing hypersurface in field space. The choice of parameterisation is arbitrary. Describing the horizon crossing hypersurface parametrically such that $\phi_\alpha = \phi_\alpha(\theta_1, .., \theta_{N_{\rm f}-1})$, the volume element on the horizon crossing hypersurface can be expressed in terms of the parameters $\theta_{\alpha'}$ in the usual way. Constructing basis vectors

$$e^\alpha_{\alpha'} \equiv \frac{\partial \phi_\alpha}{\partial \theta_{\alpha'}}, \tag{5.15}$$

assuming flat field space, the induced metric is then

$$g^{\Sigma_{\rm f}}_{\alpha'\beta'} = \sum_\alpha^{N_{\rm f}} e^\alpha_{\alpha'} e^\alpha_{\beta'} \tag{5.16}$$

so remembering that the volume of the corresponding parallelepiped is given by $\sqrt{\det g^{\Sigma_{\rm f}}}$, the volume element $d\theta$ in Eq. (5.1) can now be written more explicitly as

$$d\theta \to \sqrt{\det g^{\Sigma_{\rm f}}} d\theta_1 \cdots d\theta_{N_{\rm f}-1}, \tag{5.17}$$

If $n \leq N_{\rm f}$ then a similar picture holds for the left hand side of Eq. (5.1). $o_i(\theta_1, .., \theta_{N_{\rm f}-1})$ are the parametric equations of a surface in the space of observables and so one can construct the volume element in the same way. The induced metric in "observables space"

[4] N.B this is not the same as evaluating the expression for a given observable at horizon crossing!

is

$$g^{o}_{\alpha'\beta'} = \sum_{i}^{n} \frac{\partial o_i}{\partial \theta_{\alpha'}} \frac{\partial o_i}{\partial \theta_{\beta'}} \tag{5.18}$$

and so Eq. (5.1) becomes

$$p(o_1, .., o_n) = f[\phi_1(\theta_1, .., \theta_{N_{\rm f}-1}), .., \phi_{N_{\rm f}}(\theta_1, .., \theta_{N_{\rm f}-1})] \sqrt{\frac{\det g^{\Sigma_{\rm f}}}{\det g^{\Sigma_{\rm o}}}}. \tag{5.19}$$

Although it will always be possible to compute this expression when the horizon crossing approximation is valid and $n \leq N_{\rm f}$, clearly some sacrifices are made to achieve this generality. Ideally what one would like to do is perform the inverse mapping and express $\theta_{\alpha'}(o_1, ..., o_n)$ such that $p(o_1, .., o_n)$ can be written explicitly in terms of the observables. Whether this is practical is a model dependant statement and the difficulty in doing so will also depend on the number of observables under consideration. For instance if $n > N_{\rm f}$, then one either needs to compute the cumulative distribution function or construct enough dummy variables such that $n = N_{\rm f}$. To give an explicit example, consider the case of 1 observable $n = 1$ and a 2-dimensional horizon crossing surface $N_{\rm f} - 1 = 2$. One would essentially need to compute

$$p(o) = \frac{d}{do} \iint f \sqrt{det g^{\theta}} d\theta_1 d\theta_2, \tag{5.20}$$

which in general one probably would prefer to avoid in favour of numerical techniques.

However Eq. (5.19) does have some advantages. As already mentioned, it is simple to compute and still allows one to locate and compare peaks in the density function. In some cases, it is sufficient to construct the full density function and even make a sensible estimate of confidence limits. The main advantage as far as this paper is concerned is that Eq. (5.19) makes manifest the relationship between the geometry of the potential and the initial density function. One potentially valuable application of this is in understanding the sensitivity of the model to the choice of measure. This will be discussed in the context of the example in the following section.

5.4 Quadratic Inflation

In this section an explicit example is given of the method outlined in §5.3. Double quadratic inflation is a good example for a number of reasons. Explicitly shown in Ref. [45] for an arbitrary number of fields approaching a quadratic minimum, all isocurvature modes

are exponentially decaying before the end of inflation and so the horizon crossing approximation is valid. The spherical symmetry of the horizon crossing surface also makes it a particularly simple example.

The potential for double quadratic inflation is [46]

$$V_1 = \frac{1}{2}m_1^2\phi_1^2 \qquad\qquad V_2 = \frac{1}{2}m_2^2\phi_2^2, \tag{5.21}$$

such that $W = V_1 + V_2$. An expression for the horizon crossing contour may be obtained by writing the number of e-folds as

$$N(t_c, t_*) = -\int_*^c \sum_{\alpha=1}^{N_{\rm F}} \frac{V_\alpha}{V'_\alpha} d\phi_\alpha \tag{5.22}$$

and so

$$N = \frac{1}{4}(\phi_{1*}^2 + \phi_{2*}^2) - \frac{1}{4}(\phi_{1c}^2 + \phi_{2c}^2). \tag{5.23}$$

A well known [42, 46] and rather helpful choice of parameterisation is to move into polar coordinates. By neglecting the contribution from the "c" surface one can write

$$\phi_1 = 2\sqrt{N}\cos\theta \qquad\qquad \phi_2 = 2\sqrt{N}\sin\theta, \tag{5.24}$$

where here and what follows, unless explicitly written otherwise, fields only lie on the surface $\Sigma_{\rm f}$ and so the "*" label has been dropped. For quadratic inflation, the observables (5.5), (5.9) and (5.11) become

$$\mathcal{P}_\zeta(\theta, N) = \frac{H^2}{4\pi^2}N, \tag{5.25}$$

$$n_s(\theta, N) - 1 = -2\epsilon - \frac{1}{N}, \tag{5.26}$$

$$\alpha(\theta, N) = -8\epsilon^2 - \frac{2}{N^2} + 4\left(\epsilon_1\eta_1 + \epsilon_2\eta_2\right). \tag{5.27}$$

The amplitude of the power spectrum is in a sense less interesting than the other observables since it may always be adjusted by a pre-factor on the potential which does not affect the inflationary dynamics. Other observables one might want to consider are the non-Gaussianity parameter $f_{\rm NL}$ and the tensor-to-scalar ratio r. For the case of double quadratic inflation, it was shown in Ref. [42] that $-\frac{6}{5}f_{\rm NL} = 1/N$. Since $\Sigma_{\rm f}$ is defined as being at a fixed number of e-folds before the end of inflation, $f_{\rm NL}$ is single valued over Σ_f which is why it has not been part of the discussion until now (the same is true for the tensor-to-scalar ratio). Hence, for this example, the objective is to calculate $p(n_s, \alpha)$. Fig. 5.2 shows plots of the spectral index and running evaluated 55 e-folds before the end of inflation. As mentioned previously, an important characteristic to bear in mind for what

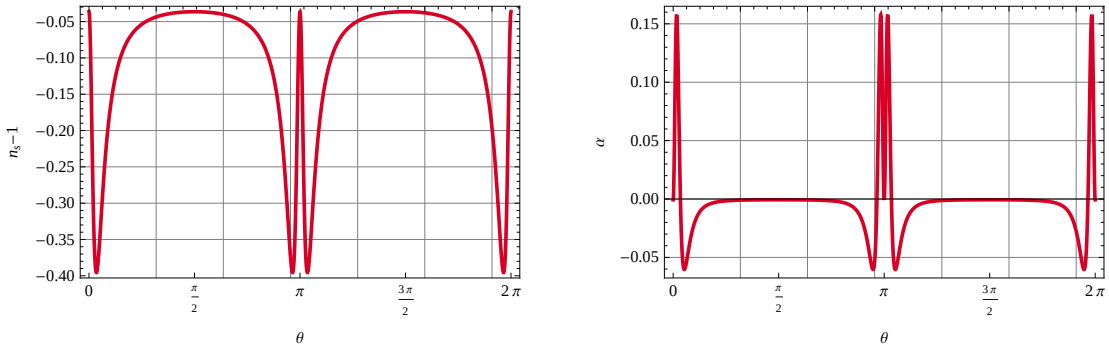

Figure 5.2: Example plots of $n_s(\theta)$ and $\alpha(\theta)$ for scales leaving the horizon 55 e-folds before the end of inflation in double quadratic inflation with masses $m_2/m_1 = 9$.

follows is that these observables are periodic in θ. This is simply a consequence of the fact that θ represents coordinates on a closed surface. It is also worth noting that the stationary points at $\theta = \pi i/2$, where i is an integer, occur at the same values for n_s and α.

5.4.1 Regarding the field space density function f_{Σ_f}

It is necessary to specify the density function f_{Σ_f}. As already mentioned, this is dependant on the details of the model as well as the choice of measure. For the purposes of this paper the distribution is chosen to be flat

$$f_{\Sigma_\mathrm{f}} = c = \frac{1}{\int_{\Sigma_\mathrm{f}} d\Sigma_\mathrm{f}}. \tag{5.28}$$

Following Ref. [47], this choice is a statement of ignorance. We simply adopt the distribution requiring the least additional assumptions. No further justification will be given at this stage, however in §5.5.1 the implications of this choice will be discussed.

The physics in each quadrant of field space is the same, so without loss of generality consider just the first quadrant where both fields are positive. The density function over the contour is then

$$f_{\Sigma_\mathrm{f}} = \frac{1}{\pi\sqrt{N}}. \tag{5.29}$$

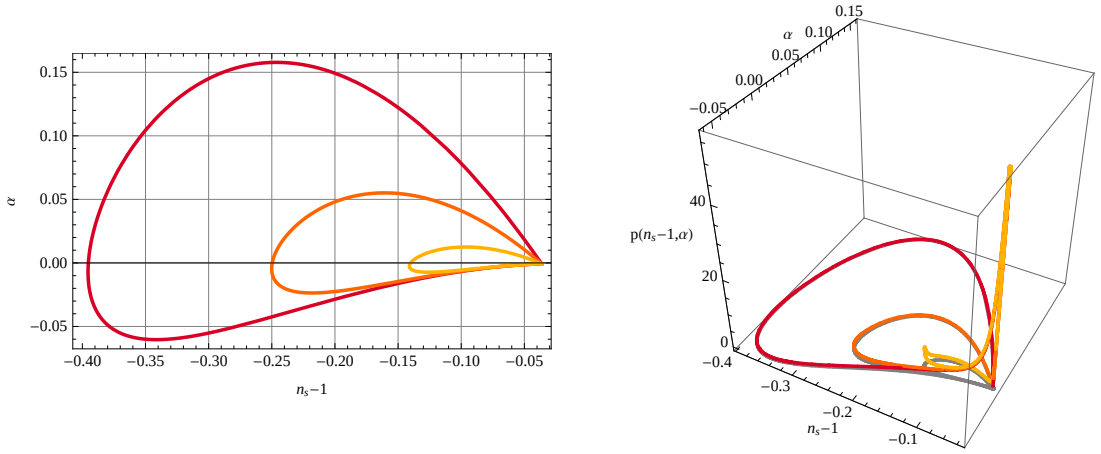

Figure 5.3: Example plots for double quadratic potential with masses $m_2/m_1 = 9$ (red), $m_2/m_1 = 7$ (orange), $m_2/m_1 = 5$ (gold). The plot on the left shows the set of possible values of $\{n_s, \alpha\}$. The right hand plot additionally includes $p(n_s, \alpha)$. The density function for all examples shown peak at $n_s - 1 = -\frac{1}{30}$ and $\alpha = -\frac{1}{1800}$ and are divergent and so the full plot range is not shown. The grey lines are the projections onto the $p(n_s, \alpha) = 0$ plane.

5.4.2 THE JOINT DENSITY FUNCTION $p(n_s, \alpha)$

As mentioned, it is convenient to parameterise in terms of polar coordinates $\{N, \theta\}$. Pythagorus and Eq. (5.24) give $d\Sigma_{\rm f} = 2\sqrt{N}d\theta$ and so the right hand side of Eq. (5.1) becomes

$$f_{\Sigma_{\rm f}} d\Sigma_{\rm f} = \frac{2}{\pi} d\theta. \tag{5.30}$$

Since for this model the observables of interest are $o = \{n_s, \alpha\}$, using Eq. (5.15) and Eq. (5.16) the element do may be rewritten as

$$do = \sqrt{\left(\frac{dn_s}{d\theta}\right)^2 + \left(\frac{d\alpha}{d\theta}\right)^2}\, d\theta \tag{5.31}$$

and hence combing Eq. (5.1) with Eq. (5.30) and Eq. (5.31),

$$p(n_s, \alpha) = \frac{2}{\pi} \frac{1}{\sqrt{\left(\frac{dn_s}{d\theta}\right)^2 + \left(\frac{d\alpha}{d\theta}\right)^2}}. \tag{5.32}$$

The right hand plot of Fig. 5.3 shows $p(n_s, \alpha)$ for the case of double quadratic inflation with masses $m_2/m_1 = 9$, $m_2/m_1 = 7$, $m_2/m_1 = 5$ shown in red, orange and gold respectively. The left plot shows the contours of possible values in the $n_s - \alpha$ plane. There is a strong peak in the density function which corresponds $\theta = \pi i/2$, where i is a member of the integers. Comparing with Fig. 5.2, this is exactly what should be expected. Fig. 5.2 shows that for a large range of θ, the tilt and running are slowly varying. Since a large proportion

of the contour maps to a relatively small proportion of the possible range of values of the tilt and running, this will give rise to a very sharp spike in the density function.

It is interesting to note that the peak occurs at the same point for each mass ratio. i.e the prediction of the model is not as sensitive to the mass hierarchy as the space of possible values for observables might suggest.

5.5 Discussion

In computing the density function for observables in the previous section, two important assumptions were made. One was that the density function on field space was taken to be a flat distribution over the horizon crossing contour. The second was that the potential was sum-separable. In this section the significance of these assumptions is assessed.

5.5.1 The choice of a flat density function at horizon crossing

Following the procedure in Ref. [46], an expression for the evolution of θ from some initial surface Σ_i to the horizon crossing surface Σ_* can be obtained by substituting Eq. (5.24) into the slow-roll equations of motion for the fields and integrating

$$\frac{N_*}{N_i} = \left(\frac{\sin\theta_*}{\sin\theta_i}\right)^{\frac{2m_1^2}{m_2^2-m_1^2}} \left(\frac{\cos\theta_*}{\cos\theta_i}\right)^{\frac{2m_2^2}{m_2^2-m_1^2}} . \tag{5.33}$$

As shown by the example plots in Fig. 5.4, there is a dynamical attractor causing the field trajectories to converge on $\theta = 0$ or $\theta = \pi$. This means that a flat distribution chosen on some $N > N_*$ contour will evolve to give rise to a density function at horizon crossing with peaks at $\theta = 0$ and $\theta = \pi$. As shown in Fig. 5.4, the result of this is to sharpen the peak in the density function of observables. In this sense choosing a flat distribution at horizon crossing can be considered to result in a lower bound on the strength of the peak sourced by dynamical effects.

As mentioned previously, one advantage of computing the density function as given by Eq. (5.19), is that it makes clear the role of the density function on field space and so in turn, the choice of measure. Since field space dynamics act to strengthen the peak in $p(o)$, in order for the prediction of the model to be changed significantly, one would require a choice of measure that acts to counter this dynamical effect.

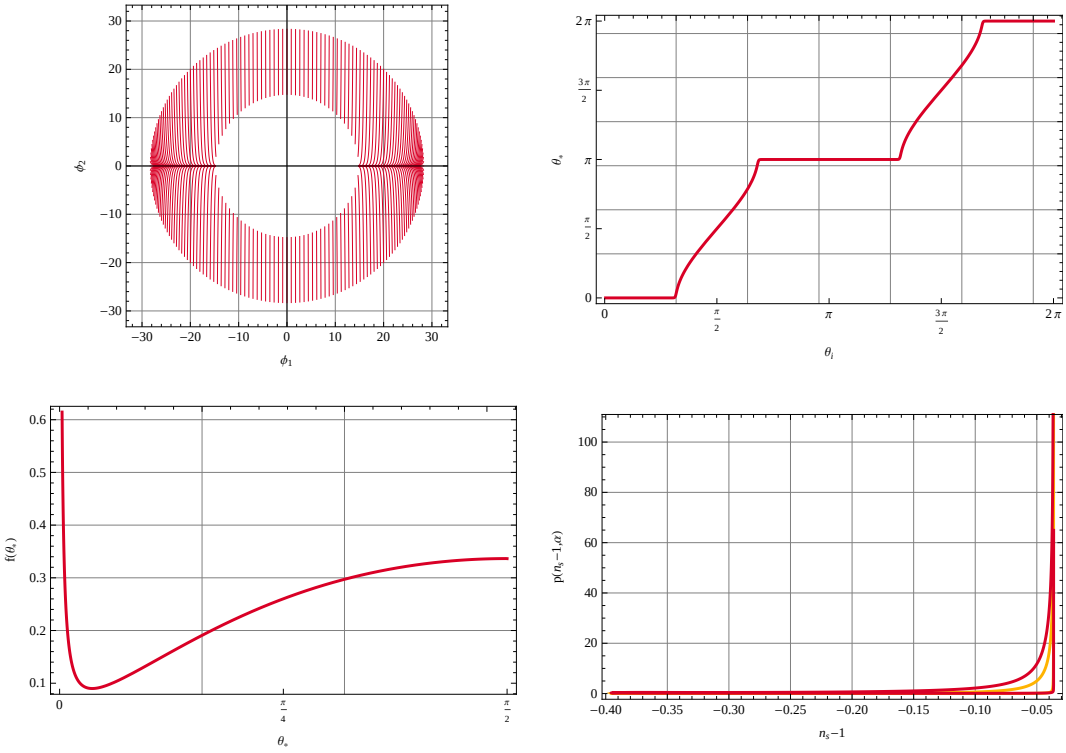

Figure 5.4: Example plots showing the effect on $p(n_s - 1, \alpha)$ if a flat distribution is taken at 200 e-folds before the end of inflation instead of at horizon crossing, for the case of double quadratic inflation with mass ratio $m_2/m_1 = 9$. The top left plot shows the evolution of example trajectories from 200 e-folds before the end of inflation up until horizon crossing. The plot shows a significant proportion of the trajectories converge at $\theta = 0$ and $\theta = \pi$. The top right plot shows the relation of θ_i, the parameterisation of the initial contour, to θ_*, the parameterisation of the horizon crossing contour. The plot shows once again that trajectories over a significant range of θ_i converge onto $\theta_* = 0$ and $\theta_* = \pi$. The bottom left hand plot shows the resulting density function over one quadrant of the horizon crossing surface with a strong peak at $\theta = 0$. Finally, the bottom right plot shows the result on $p(n_s - 1, \alpha)$ in gold compared to $p(n_s - 1, \alpha)$ for a flat distribution at horizon crossing shown in red. The red plot is the same as that shown in the right hand plot of Fig. 5.3 but projected onto the $p(n_s - 1, \alpha) - n_s - 1$ plane. The effect of the evolution is to sharpen the peak in $p(n_s - 1, \alpha) - n_s - 1$.

5.5.2 The use of sum-separable potentials

Central to the approach taken in this paper is the use of sum-separable potentials. It is therefore important to understand to what extent the results are special to this class of models. The reason the analysis performed here was restricted to this class was that it enabled the use of the horizon crossing approximation and hence provided a simple method of mapping a density function on field space to a density function for observables. The most striking result is that the functional form of Eq. (5.19) seems to imply that the density function of observables will be strongly peaked and this is indeed the case for the example of double quadratic inflation that was explored. If a strong peak turns out to be a generic

feature of multifield models this is advantageous on two fronts. Most importantly it means that a given multifield model may be significantly more predictive than considering just the range of possible values of observables allowed within the model and hence one can be much more optimistic about the prospect of constraining such models. Secondly, if sharp peaks in the density function exist, then knowing the location of these peaks can be very advantageous to numerical approaches to computing the density function.

Although the use of the horizon crossing approximation provides a simple map from field space to observables, it is argued here that it is not the cause of the peak in $p(o)$. It may not be very efficient but clearly there already exists a method of computing the density function of observables for a much broader class inflationary models than the method given here. For example, consider the class of all inflationary models where the slow-roll approximation is valid at horizon crossing and also reach an adiabatic limit before the end of inflation.[5] For this class one could perform the following procedure:

1. Perform a Monte Carlo search for the horizon crossing surface Σ_*.

2. Draw initial field space positions from a given density function f_{Σ_*}.

3. For each set of initial field space positions, starting with momenta given by the slow-roll equations, evolve each trajectory until the end of inflation.

4. For each inflationary trajectory, using one of the methods given in Refs. [2–28], compute relevant observables.

In doing this, one would numerically obtain a map from the $N_{\rm f}-1$ dimensional surface on which inflation ends to observables which may, as before, be parameterised by $N_{\rm f}-1$ variables $\{\theta_1,..,\theta_{N_{\rm f}-1}\}$. Once this map is obtained, Eq. (5.19) is once again applicable.

If the surface in field space is closed there are only two options for the mapping. Either the observable is independent of $\{\theta_1,..,\theta_{N_{\rm f}-1}\}$, or it is periodic in $\{\theta_1,..,\theta_{N_{\rm f}-1}\}$. If the observable is independent of $\{\theta_1,..,\theta_{N_{\rm f}-1}\}$ then (as was the case here for $f_{\rm NL}$ and r) that observable is single valued. If the observable is periodic in $\{\theta_1,..,\theta_{N_{\rm f}-1}\}$, then stationary points are guaranteed.

If the surface in field space is not closed then it is not possible to say anything so concrete. Nevertheless, the conditions for a peak in the density function to occur are clear. As illustrated in Fig. 5.5, a peak in $p(o)$ occurs when $do/d\theta$ is small. If the surface in field

[5]The method proposed here is straightforward to adapt to other models of inflation but some details may vary and so in pursuit of being a little more concrete, discussion has been restricted to this class.

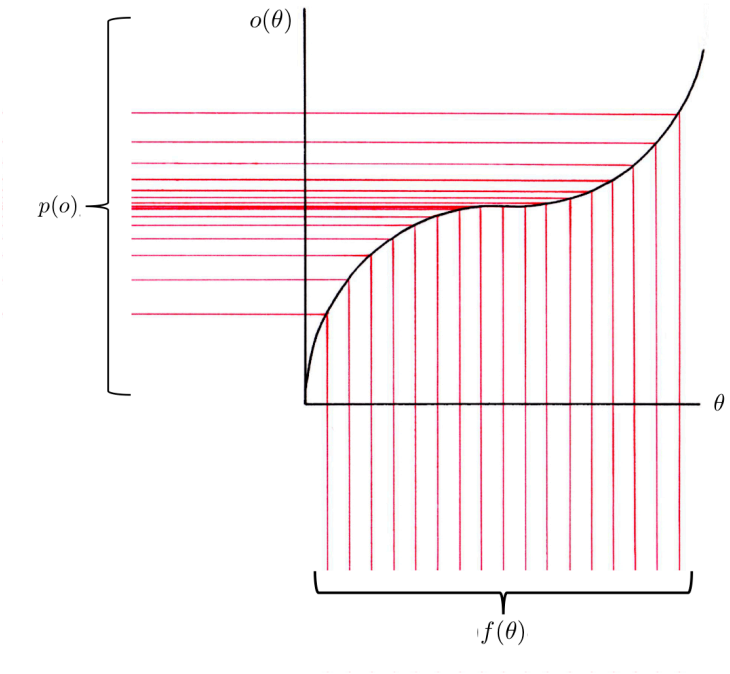

Figure 5.5: Sketch of why a stationary point in the functional form of $o(\theta)$ will give rise to a divergence in the density function $p(o)$. The spacing of the red lines represents the density function $f(\theta)$ and how it is distorted under a change of variable to give $p(o)$.

space is not closed, then this requirement can not be guaranteed but it is certainly still permitted.

5.6 Conclusion

If multifield models of inflation are to be confronted with data, it is essential that we understand what the prediction of a given model actually is. As has been discussed, there is essentially two parts to this problem:

1. Computing the density function on field space.

2. Mapping the density function on field space to the density function of observables.

Progress with the first part is stymied by the measure problem. This issue has received considerable attention recently and a number of authors have proposed various possible solutions. At present however, the problem remains open. The second part has received comparatively little attention but it is hoped that this paper represents steps towards rectifying this.

As an attempt at making progress with the second issue, here a solution for the case of sum-separable potentials was proposed. Although it is useful to have analytic examples, clearly this is not sufficient and a more general approach is urgently needed if we are to compare multifield models with the soon to arrive data from Planck. As discussed, in principle a numerical approach is already available. However it is inefficient, meaning that a thorough analysis of models with a large number of active fields, or models with complicated Lagrangians may still be computationally unaccessible.

The main point this work is trying to make is that a strongly peaked density function for observables is expected to be generic for a broad class of models. This means that some models may be relatively insensitive to the density function on field space and hence for such models it should be possible to make robust predictions with the knowledge we already have available to us.

References

[1] M. Cicoli et al. "Modulated Reheating and Large Non-Gaussianity in String Cosmology". In: *JCAP* 1205 (2012), p. 039. arXiv:1202.4580 [hep-th] (cit. on p. 190).

[2] Alexei A. Starobinsky. "Multicomponent de Sitter (Inflationary) Stages and the Generation of Perturbations". In: *JETP Lett.* 42 (1985), pp. 152–155 (cit. on pp. 191, 194, 205).

[3] D. H. Lyth. "Large Scale Energy Density Perturbations and Inflation". In: *Phys.Rev.* D31 (1985), pp. 1792–1798 (cit. on pp. 191, 194, 205).

[4] Misao Sasaki and Ewan D. Stewart. "A General analytic formula for the spectral index of the density perturbations produced during inflation". In: *Prog.Theor.Phys.* 95 (1996), pp. 71–78. arXiv:astro-ph/9507001 (cit. on pp. 191, 194, 205).

[5] D. S. Salopek and J. R. Bond. "Nonlinear evolution of long wavelength metric fluctuations in inflationary models". In: *Phys. Rev.* D42 (1990), pp. 3936–3962 (cit. on pp. 191, 205).

[6] Misao Sasaki and Takahiro Tanaka. "Superhorizon scale dynamics of multiscalar inflation". In: *Prog.Theor.Phys.* 99 (1998), pp. 763–782. arXiv:gr-qc/9801017 [gr-qc] (cit. on pp. 191, 205).

[7] David Wands et al. "A New approach to the evolution of cosmological perturbations on large scales". In: *Phys.Rev.* D62 (2000), p. 043527. arXiv:astro-ph/0003278 [astro-ph] (cit. on pp. 191, 205).

[8] David H. Lyth and Yeinzon Rodríguez. "The inflationary prediction for primordial non-gaussianity". In: *Phys.Rev.Lett.* 95 (2005), p. 121302. arXiv:astro-ph/0504045 (cit. on pp. 191, 194, 205).

[9] Gerasimos I. Rigopoulos and E. P. S. Shellard. "Non-linear inflationary perturbations". In: *JCAP* 0510 (2005), p. 006. arXiv:astro-ph/0405185 (cit. on pp. 191, 205).

[10] G. I. Rigopoulos, E. P. S. Shellard and B. J. W. van Tent. "Non-linear perturbations in multiple-field inflation". In: *Phys.Rev.* D73 (2006), p. 083521. arXiv:astro-ph/0504508 (cit. on pp. 191, 205).

[11] Shuichiro Yokoyama, Teruaki Suyama and Takahiro Tanaka. "Primordial Non-Gaussianity in Multi-Scalar Slow-Roll Inflation". In: *JCAP* 0707 (2007), p. 013. arXiv:0705.3178 [astro-ph] (cit. on pp. 191, 205).

[12] Shuichiro Yokoyama, Teruaki Suyama and Takahiro Tanaka. "Primordial Non-Gaussianity in Multi-Scalar Inflation". In: *Phys.Rev.* D77 (2008), p. 083511. arXiv:0711.2920 [astro-ph] (cit. on pp. 191, 205).

[13] Shuichiro Yokoyama, Teruaki Suyama and Takahiro Tanaka. "Efficient diagrammatic computation method for higher order correlation functions of local type primordial curvature perturbations". In: *JCAP* 0902 (2009), p. 012. arXiv:0810.3053 [astro-ph] (cit. on pp. 191, 205).

[14] David J. Mulryne, David Seery and Daniel Wesley. "Moment transport equations for non-Gaussianity". In: *JCAP* 1001 (2010), p. 024. arXiv:0909.2256 [astro-ph.CO] (cit. on pp. 191, 205).

[15] David J. Mulryne, David Seery and Daniel Wesley. "Moment transport equations for the primordial curvature perturbation". In: *JCAP* 1104 (2011), p. 030. arXiv:1008.3159 [astro-ph.CO] (cit. on pp. 191, 205).

[16] Luca Amendola et al. "Correlated perturbations from inflation and the cosmic microwave background". In: *Phys.Rev.Lett.* 88 (2002), p. 211302. arXiv:astro-ph/0107089 [astro-ph] (cit. on pp. 191, 205).

[17] S. Groot Nibbelink and B.J.W. van Tent. "Scalar perturbations during multiple field slow-roll inflation". In: *Class.Quant.Grav.* 19 (2002), pp. 613–640. arXiv:hep-ph/0107272 [hep-ph] (cit. on pp. 191, 205).

[18] Z. Lalak et al. "Curvature and isocurvature perturbations in two-field inflation". In: *JCAP* 0707 (2007), p. 014. arXiv:0704.0212 [hep-th] (cit. on pp. 191, 205).

[19] Courtney M. Peterson and Max Tegmark. "Testing Two-Field Inflation". In: *Phys.Rev.* D83 (2011), p. 023522. arXiv:1005.4056 [astro-ph.CO] (cit. on pp. 191, 205).

[20] Courtney M. Peterson and Max Tegmark. "Non-Gaussianity in Two-Field Inflation". In: *Phys.Rev.* D84 (2011), p. 023520. arXiv:1011.6675 [astro-ph.CO] (cit. on pp. 191, 205).

[21] Courtney M. Peterson and Max Tegmark. "Testing Multi-Field Inflation: A Geometric Approach". In: (2011). arXiv:1111.0927 [astro-ph.CO] (cit. on pp. 191, 205).

[22] Ana Achúcarro et al. "Features of heavy physics in the CMB power spectrum". In: *JCAP* 1101 (2011), p. 030. arXiv:1010.3693 [hep-ph] (cit. on pp. 191, 205).

[23] Anastasios Avgoustidis et al. "The Importance of Slow-roll Corrections During Multi-field Inflation". In: *JCAP* 1202 (2012), p. 038. arXiv:1110.4081 [astro-ph.CO] (cit. on pp. 191, 205).

[24] Jean-Luc Lehners and Sebastien Renaux-Petel. "Multifield Cosmological Perturbations at Third Order and the Ekpyrotic Trispectrum". In: *Phys.Rev.* D80 (2009), p. 063503. arXiv:0906.0530 [hep-th] (cit. on pp. 191, 205).

[25] Christophe Ringeval. "The exact numerical treatment of inflationary models". In: *Lect.Notes Phys.* 738 (2008), pp. 243–273. arXiv:astro-ph/0703486 [astro-ph] (cit. on pp. 191, 205).

[26] Jerome Martin and Christophe Ringeval. "Inflation after WMAP3: Confronting the Slow-Roll and Exact Power Spectra to CMB Data". In: *JCAP* 0608 (2006), p. 009. arXiv:astro-ph/0605367 [astro-ph] (cit. on pp. 191, 205).

[27] Ian Huston and Karim A. Malik. "Numerical calculation of second order perturbations". In: *JCAP* 0909 (2009), p. 019. arXiv:0907.2917 [astro-ph.CO] (cit. on pp. 191, 205).

[28] Ian Huston and Karim A. Malik. "Second Order Perturbations During Inflation Beyond Slow-roll". In: *JCAP* 1110 (2011), p. 029. arXiv:1103.0912 [astro-ph.CO] (cit. on pp. 191, 205).

[29] David H. Lyth. "Non-gaussianity and cosmic uncertainty in curvaton-type models". In: *JCAP* 0606 (2006), p. 015. arXiv:astro-ph/0602285 [astro-ph] (cit. on p. 192).

[30] David Seery. "A parton picture of de Sitter space during slow-roll inflation". In: *JCAP* 0905 (2009), p. 021. arXiv:0903.2788 [astro-ph.CO] (cit. on p. 192).

[31] Ben Freivogel. "Making predictions in the multiverse". In: *Class.Quant.Grav.* 28 (2011), p. 204007. arXiv:1105.0244 [hep-th] (cit. on p. 192).

[32] Jonathan Frazer and Andrew R. Liddle. "Multi-field inflation with random potentials: field dimension, feature scale and non-Gaussianity". In: *JCAP* 1202 (2012), p. 039. arXiv:1111.6646 [astro-ph.CO] (cit. on pp. 192, 193, 197).

[33] Soo A. Kim and Andrew R. Liddle. "Nflation: Non-Gaussianity in the horizon-crossing approximation". In: *Phys.Rev.* D74 (2006), p. 063522. arXiv:astro-ph/0608186 [astro-ph] (cit. on p. 193).

[34] Jonathan Frazer and Andrew R. Liddle. "Exploring a string-like landscape". In: *JCAP* 1102 (2011), p. 026. arXiv:1101.1619 [astro-ph.CO] (cit. on p. 193).

[35] Nishant Agarwal et al. "Universality in D-brane Inflation". In: *JCAP* 1109 (2011), p. 002. arXiv:1103.2775 [astro-ph.CO] (cit. on p. 193).

[36] Mafalda Dias, Jonathan Frazer and Andrew R. Liddle. "Multifield consequences for D-brane inflation". In: *JCAP* 1206 (2012), p. 020. arXiv:1203.3792 [astro-ph.CO] (cit. on pp. 193, 195–197).

[37] Liam McAllister, Sebastien Renaux-Petel and Gang Xu. "A Statistical Approach to Multifield Inflation: Many-field Perturbations Beyond Slow Roll". In: *JCAP* 1210 (2012), p. 046. arXiv:1207.0317 [astro-ph.CO] (cit. on p. 193).

[38] Yoske Sumitomo and S.-H. Henry Tye. "A Stringy Mechanism for A Small Cosmological Constant". In: *JCAP* 1208 (2012), p. 032. arXiv:1204.5177 [hep-th] (cit. on p. 194).

[39] Yoske Sumitomo and S.-H. Henry Tye. "A Stringy Mechanism for A Small Cosmological Constant - Multi-Moduli Cases -". In: *JCAP* 1302 (2013), p. 006. arXiv:1209.5086 [hep-th] (cit. on p. 194).

[40] Yoske Sumitomo and S.-H. Henry Tye. "Preference for a Vanishingly Small Cosmological Constant in Supersymmetric Vacua in a Type IIB String Theory Model". In: (2012). arXiv:1211.6858 [hep-th] (cit. on p. 194).

[41] Thorsten Battefeld and Richard Easther. "Non-Gaussianities in Multi-field Inflation". In: *JCAP* 0703 (2007), p. 020. arXiv:astro-ph/0610296 [astro-ph] (cit. on p. 195).

[42] Filippo Vernizzi and David Wands. "Non-gaussianities in two-field inflation". In: *JCAP* 0605 (2006), p. 019. arXiv:astro-ph/0603799 [astro-ph] (cit. on pp. 195, 200).

[43] Juan García-Bellido and David Wands. "Metric perturbations in two field inflation". In: *Phys.Rev.* D53 (1996), pp. 5437–5445. arXiv:astro-ph/9511029 [astro-ph] (cit. on p. 197).

[44] Joseph Elliston et al. "Evolution of fNL to the adiabatic limit". In: *JCAP* 1111 (2011), p. 005. arXiv:1106.2153 [astro-ph.CO] (cit. on p. 197).

[45] David Seery et al. "Inflationary perturbation theory is geometrical optics in phase space". In: *JCAP* 1209 (2012), p. 010. arXiv:1203.2635 [astro-ph.CO] (cit. on pp. 197, 199).

[46] David Polarski and Alexei A. Starobinsky. "Spectra of perturbations produced by double inflation with an intermediate matter dominated stage". In: *Nucl.Phys.* B385 (1992), pp. 623–650 (cit. on pp. 200, 203).

[47] P.S.M. De Laplace, F.W. Truscott and F.L. Emory. *A Philosophical Essay on Probabilities*. Cosimo, Incorporated, 2007. ISBN: 9781602063280. URL: `http://books.google.co.uk/books?id=QLCUcR6dZD4C` (cit. on p. 201).

Conclusion

At the time of writing of this thesis, it seems that we live in a time of transition. Perhaps this is a feeling common to many students at the end of their PhD. Perhaps this is feeling that is common to many people active in research, independent of time or position. In any case, I would like to reflect on the work done in this thesis, while trying to keep in mind the more general situation in cosmology and particle physics.

The current status of inflation

As of a few days ago the Large Hadron Collider (LHC) in Geneva completed the first run and has been shut down for upgrades estimated to take two years to complete. A Higgs-like particle was discovered at approximately 125 GeV. The discovery of what may be the first scalar particle is certainly reassuring for the theory of inflation but it is somewhat disconcerting that as yet there is no evidence of supersymmetry.

In less than a month it is expected that first data from the Planck satellite will be released. This data is likely to have a profound impact on the study inflation in years to come. For instance, if evidence of primordial non-Gaussianity is found, then the study of these non-Gaussian statistics will provide an incredibly rich source of information about the effective Lagrangian of inflation. Not only from Planck data itself; there are arguments to say that in such circumstances data on large scale structure from future missions such as Euclid will become of great interest to the study of inflation. It does not seem too much of a stretch to say that such a detection would herald a new era for particle physics.

If the LHC discovers no new physics, and Planck only tightens current constraints, then it is not clear how best to proceed. This situation could potentially be quite problematic in so much as perhaps we are simply "running out" of observables. Then again, to overcome

this issue would surely be an exciting pursuit, likely to send the study of fundamental physics in new unforeseen directions.

The status of this work

As outlined in the introduction, the work done in this thesis could be summarised as seeking to address the question

How does one compute predictions when there is more than one field?

Here I will reflect on the progress made over the course of this work and how I plan on continuing this pursuit.

To account for the superhorizon evolution of ζ, over the course of this work, a computationally efficient and highly versatile method for evolving the statistics of ζ was developed. The method works by numerically solving a hierarchy of first order differential equations for the correlation functions of the field perturbations. Apart from the numerical efficiency of such an approach, another significant benefit is that the method can essentially be applied whenever the problem can be expressed in terms of evolving a probability distribution. Utilising this versatility, the original slow-roll superhorizon method developed by Mulryne, Seery and Wesley was extended, to include non-slow-roll effects, a non-trivial field space metric and evolution on subhorizon scales. This work is still ongoing but as demonstrated in this thesis, the method has now reached a level of maturity where it is now possible to compute the statistics of ζ in more sophisticated models than was previously possible. Having reached this status, we are now in the final stages of preparing code for public release.

Another important characteristic of the transport method is the new perspective it lends to building a better intuition of the evolution of correlation functions. The method evolves correlation functions in field space which can be related to geometrical optics and the analogy becomes precise in the slow-roll limit. This new perspective can be useful in a number of circumstances. One such situation is tracking evolution to the adiabatic limit. Once an adiabatic limit is reached ζ become conserved and so tracking such a characteristic is essential in computing the prediction of the model.

The most problematic feature of multifield models of inflation is that the probabilistic nature of the prediction is highly non-trivial. Any given multifield model possesses an uncountable infinite set of inflationary trajectories which necessarily gives rise to a probability distribution for observables. This challenge is exacerbated in models where the potential contains more than one minimum, such as in models of inflation in the string landscape. Here I addressed both cases to a varying degree.

For the case of models possessing multiple minima, we explored in detail two models. A toy model of the landscape there the potential was a Fourier series with random coefficients and a D-brane model where the contribution from the bulk was modelled using spherical harmonics with random coefficients. For such models, the primary question to address is how the random coefficients affect the ability to make a prediction. For the case of the Fourier potential, we showed that while varying the number of fields did not significantly affect the distribution of observables, varying the typical length-scale of features in the potential had a very significant effect. A well known signature of multifield inflation is a non-zero $f_{\rm NL}$. It is therefore important not just to address if a given model can give rise to an observably large $f_{\rm NL}$ but also to know if it is in any sense generic. We found not a single inflationary realisation that gave rise to an observably large $f_{\rm NL}$. Although it is hard to make robust predictions in models of this kind due to an unknown weighting from the choice of measure, a detection of $f_{\rm NL}$ seems likely to rule out the model.

The D-brane model represented a considerable step up in complexity. In order to compute observables in this model required considerable extensions to the transport method. Some of which we did not fully appreciate at first and hence in addition to the paper, an erratum is also included in this work. The key challenge with this model was accounting for the large mass spectrum present at horizon crossing that comes about as a result of the metric on the conifold. To account for this, we evolved correlations functions from subhorizon scales which required a quantum extension to the transport method. We saw new kinds of evolution including a range of non-monotonic behaviours in the power spectrum and spectral index. Understanding this behaviour and its implications for higher order correlation functions is part of our present work. Little-to-nothing is currently known about the inflationary behaviour in models with non-trivial field space metrics but equipped with the tools developed during this work, now we are in a position to explore this uncharted territory. This is exciting because models of this kind are expected to be generic in supergravity.

We found the distribution for the spectral index to be in some tension with current

observations and quite likely to be under considerably more tension with the release of the Planck data. As with the Fourier model, there is an unknown weighting related to the choice of measure. In this case, there was a clear relation between the spectral index and the number of e-folds of inflation. Inflationary realisations with more e-folds of inflation tended to have a redder spectrum. This implies that imposing a measure that favours more inflation would shift the distribution we obtained to be in better agreement with observation.

When the potential only has one minimum the situation is much simpler. In the last paper of this thesis, I showed that for the class of sum-separable potentials, it is possible to obtain analytic expressions for the density function of observables. In contrast to the previous papers, this provided an explicit means of understanding the role of the initial field space distribution. It turns out that under quite general conditions, the density function of observables will be strongly peaked and that the strength and location of this peak is remarkably insensitive to the field space distribution. Although this paper worked with a very special class of models, this result appears to apply more generally. This is very encouraging as it means that for single minimum models, it should be possible to place strong constraints.

Clearly it is important to understand how to make predictions for any model of interest but in lieu of detecting a straightforward signature distinguishing broad classes of models, it may turn out that the best we can do is constrain models on a case by case basis. If this turns out to be the situation, then a good understanding of how to compute predictions in multifield models will becomes all the more critical.

Ultimately the goal is to unite inflation with fundamental theory. Particle physics is in desperate need of a means of being confronted with observation. We await future data from the LHC but for many, it seems that the future progress of particle physics will rely on cosmological tests. Meanwhile inflation severely lacks a foundation in particle physics, requiring better observations and considerable theoretical development. It is my sincere hope that this contribution will help, be it in some very small way, in bringing us one step closer to achieving this union.